FOREWORD

This volume of the Pressurization Systems Design Guide has been prepared under Contract NAS7-548 "Liquid Propellant Gas Absorption Study." The work was administered under the direction of the Jet Propulsion Laboratory; Mr. Howard B. Stanford of JPL served as Technical Manager and Mr. Frank E. Compitello of NASA Washington, Liquid Propulsion Systems, was Project Manager.

This volume is an expansion of Section VI-D, Volume II-B of the report originally prepared by Aerojet General under Contract NAS7-169 (September 1964, Revised December 1965 and July 1966).

The technical effort at Astropower Laboratory, McDonnell Douglas Corporation was directed by Dr. W. David English, Chief, Propellant Compatibility Section. Experimental studies that developed new data for the report were carried out by Mr. W. A. Cannon and Dr. J. H. Robson. Program supervision was carried out by Dr. D. R. Mash, succeeding Dr. N. A. Tiner.

In preparing this volume, extensive use has been made of the data available in the literature, handbooks and textbooks. Acknowledgments and credit are given throughout the volume for the use of this material.

The technical details of the experimental work carried out on this contract are reported separately in a Final Summary Technical Report, "The Solubility of Gases in Liquid Propellants," Report Number DAC-60510-F2, July 1968.

This report was prepared by J. H. Robson, W. A. Cannon and W. D. English.

ABSTRACT

This volume of the Pressurization Systems Design Guide is a compendium of information on the solubility of pressurant gases in liquid propellants. Two main sections are presented: first, a theoretical discussion of the nature of gas-liquid, two-component systems; second, a compilation of available numerical data about the equilibrium solubility of pressurant gases in liquid propellants. Data on rates of solution and evolution of the gases are not available.

ACKNOWLEDGMENT

This volume is based on the report originally prepared by Aerojet-General Corporation under the direction of William J. Flaherty. Much of the theoretical presentation and discussion in this report was originally presented in the Aerojet-General report. The compilation of experimental data, too, bears heavily on the compilation and style of presentation developed by Aerojet-General. We gladly acknowledge their pioneering presentation.

However, this acknowledgment does not remove responsibility from our own shoulders, and Astropower Laboratory, McDonnell Douglas Corporation, is solely responsible for misstatements, errors, and omissions in the current volume.

PRESSURIZATION SYSTEMS DESIGN GUIDE

VOLUME III

PRESSURANT GAS SOLUBILITY IN LIQUID PROPELLANTS

CONTENTS

		Page
I.	INTRODUCTION	I-1
II.	THEORY OF GAS SOLUBILITY	II-1
	A. Literature Available	II-1
	B. Ideal Solutions	II-1
	C. Gas Solubility in Nonideal Solutions	II-2
	D. Prediction of Solubilities	II-4
	1. Basic Concepts	II-4
	2. Criteria for Equilibrium	II-5
	3. Pure Liquid Phase in Equilibrium With Vapor	II-7
	4. The Virial Equation Of State	II-8
	5. Solubility In The Liquid Phase	II-9
	6. Comparison Of Theory With Experimental Data	II-10
	7. Obtaining Virial Coefficients And P-V-T Data	II-13
	E. Gas Solution and Evolution – Nonequilibrium Systems	II-14
	1. Introduction	II-14
	2. Rate of Solution	II-14
	3. Experimental Studies	II-18
	4. Rate of Evolution	II-22
	5. Certain System Effects Under Nonequilibrium Conditions	II-23

CONTENTS (cont.)

		Page
III.	MEASUREMENT OF GAS SOLUBILITY	III-1
	A. Methods of Solubility Measurement	III-1
	B. Graphical Representation of Pressure, Temperature, and Composition Relations	III-1
	C. Illustrative Phase Equilibria Data for the System Normal Hydrogen-Helium	III-8
	D. Studies at McDonnell Douglas	III-12
IV.	PRESSURANT SOLUBILITIES IN PROPELLANTS	IV-1
	A. Introduction	IV-1
	B. Pressurant Gases	IV-2
	C. Solubility Data for Pressurant Gases in Propellant Oxidizers	IV-5
	1. Chlorine Pentafluoride-Helium	IV-5
	2. Chlorine Pentafluoride-Nitrogen	IV-5
	3. Chlorine Trifluoride-Helium	IV-9
	4. Chlorine Trifluoride-Nitrogen	IV-9
	5. Dioxygen Difluoride-Helium	IV-14
	6. 70% FLOX-Helium	IV-20
	7. Fluorine-Helium	IV-20
	8. MON-10-Helium	IV-23
	9. Nitrogen Tetroxide-Argon	IV-23
	10. Nitrogen Tetroxide-Helium	IV-23
	11. Nitrogen Tetroxide-Oxygen	IV-27
	12. Nitrogen Tetroxide-Nitrogen	IV-27

CONTENTS (cont.)

		Page
13.	Nitrogen Trifluoride-Helium	IV-27
14.	Nitrogen Trifluoride-Nitrogen	IV-27
15.	Nitryl Fluoride-Helium	IV-35
16.	Nitryl Fluoride-Nitrogen	IV-35
17.	Oxygen-Helium	IV-36
18.	Oxygen-Nitrogen	IV-45
19.	Oxygen Difluoride-Helium	IV-45
20.	Oxygen Difluoride-Nitrogen	IV-45
21.	Perchloryl Fluoride-Helium	IV-56
22.	Perchloryl Fluoride-Nitrogen	IV-56
23.	Tetrafluorohydrazine-Helium	IV-61
24.	Tetrafluorhydrazine-Nitrogen	IV-61
D.	Solubility Data for Pressurant Gases in Propellant Fuels	IV-66
1.	Aerozine 50-Ammonia	IV-66
2.	Aerozine 50-Helium	IV-66
3.	Aerozine 50-Nitrogen	IV-66
4.	Ammonia-Helium	IV-66
5.	Ammonia-Nitrogen	IV-66
6.	Diborane-Helium	IV-75
7.	Diborane-Nitrogen	IV-75
8.	Diborane-Hydrogen	IV-80
9.	Ethane-Helium	IV-80
10.	Ethane-Nitrogen	IV-80

CONTENTS (cont.)

		Page
11.	Ethane-Hydrogen	IV-83
12.	Ethylene-Helium	IV-83
13.	Ethylene-Nitrogen	IV-83
14.	Ethylene-Hydrogen	IV-96
15.	Hydrazine-Argon	IV-96
16.	Hydrazine-Helium	IV-96
17.	Hydrazine-Nitrogen	IV-96
18.	Hydrogen (Normal)-Helium	IV-105
19.	Hydrogen (Equilibrium)-Helium	IV-105
20.	Methane-Helium	IV-114
21.	Methane-Hydrogen	IV-114
22.	Methane-Nitrogen	IV-114
23.	Monomethylhydrazine-Argon	IV-114
24.	Monomethylhydrazine-Helium	IV-123
25.	Monomethylhydrazine-Nitrogen	IV-123
26.	Monomethylhydrazine Hydrate-Helium	IV-123
27.	Pentaborane-Helium	IV-123
28.	Pentaborane-Hydrogen	IV-132
29.	Pentaborane-Nitrogen	IV-132
30.	Propane-Helium	IV-132
31.	Propane-Nitrogen	IV-132
32.	Propane-Hydrogen	IV-137
33.	Trimethylborane-Helium	IV-146

CONTENTS (cont.)

		Page
34.	Trimethylborane-Nitrogen	IV-146
35.	Unsymmetrical Dimethylhydrazine (UDMH)-Argon	IV-151
36.	Unsymmetrical Dimethylhydrazine (UDMH)-Helium	IV-151
37.	Unsymmetrical Dimethylhydrazine (UDMH)-Nitrogen	IV-151
V. REFERENCES		V-1

Table		Page
II-1	Rate of Solution of N_2 In N_2O_4	II-19
IV-1	Properties of Selected Pressurant Gases	IV-2
IV-2	Physical Properties of Propellant Oxidizers	IV-4
IV-3	Solubility of Helium and Nitrogen in Liquid Chlorine Pentafluoride	IV-5
IV-4	Solubility of Helium and Nitrogen in Liquid Chlorine Trifluoride	IV-9
IV-5	Solubility of Helium in Liquid Dioxygen Difluoride	IV-14
IV-6	Solubility of Helium in Liquid 70-FLOX	IV-20
IV-7	Solubility of Helium in Liquid Fluorine	IV-23
IV-8	Solubilities of He, N_2, O_2, and Ar in Liquid N_2O_4	IV-28
IV-9	Solubility of Helium and Nitrogen in Liquid Nitrogen Tetroxide	IV-29
IV-10	Solubility of Helium and Nitrogen in Liquid Nitrogen Trifluoride	IV-29
IV-11	Solubility of Helium and Nitrogen in Liquid Nitryl Fluoride	IV-35

CONTENTS (cont.)

Table		Page
IV-12	Solubility of Helium in Liquid Oxygen	IV-36
IV-13	Solubility of Helium and Nitrogen in Liquid Oxygen Difluoride	IV-51
IV-14	Solubility of Helium and Nitrogen in Liquid Perchloryl Fluoride	IV-56
IV-15	Solubility of Helium and Nitrogen in Liquid Tetrafluorohydrazine	IV-61
IV-16	Physical Properties of Propellant Fuels	IV-67
IV-17	Solubility of Ammonia, Helium and Nitrogen in Aerozine 50	IV-68
IV-18	Solubility of Helium and Nitrogen in Liquid Ammonia	IV-68
IV-19	Solubility of Helium and Nitrogen in Liquid Diborane	IV-75
IV-20	Solubility of Helium and Nitrogen in Liquid Ethane	IV-80
IV-21	Liquid-Vapor Equilibrium Constants for the System Ethane-Hydrogen	IV-88
IV-22	Solubility of Helium and Nitrogen in Liquid Ethylene	IV-88
IV-23	Liquid-Vapor Equilibrium Constants for the System Ethylene-Hydrogen	IV-98
IV-24	Solubilities of Argon, Helium and Nitrogen in Liquid Hydrazine	IV-98
IV-25	Solubility of Helium in Normal Hydrogen	IV-106
IV-26	Experimental Liquid-Vapor Equilibrium Data for the System Helium-Methane	IV-115
IV-27	Solubilities of Argon, Helium and Nitrogen in Liquid Monomethylhydrazine	IV-124
IV-28	Solubility of Helium and Nitrogen in Liquid Propane	IV-137
IV-29	Liquid-Vapor Equilibrium Constants for the System Propane-Hydrogen	IV-142

CONTENTS (cont.)

Table		Page
IV-30	Solubility of Helium and Nitrogen in Liquid Trimethylborane	IV-146
IV-31	Solubilities of Argon, Helium and Nitrogen in Liquid Unsymmetrical Dimethylhydrazine	IV-151
IV-32	Solubility of Helium and Nitrogen in UDMH	IV-152

SYMBOLS

Subscripts

c	critical property
f	interface between two films
g	gas phase
i, j, k	component
L	liquid phase
m	indicates property for a mixture
s	saturated condition for property indicated
int.	initial

Superscripts

–	property in a mixture, such as $\bar{f}_i$ = fugacity of i in a mixture
o	indicates pure component, such as p_i^o
vap, liq	indicates component as vapor, liquid

Latin

A	gas-liquid
B	second virial coefficient
b	$U\frac{W}{V_L}$
C	third virial coefficient
c	mass concentration of gas dissolved in liquid phase
c_p	gas specific heat
D	fourth virial coefficient
E	enhancement factor, P_y/p_s, also energy of vaporization in Hildebrand solubility parameter equation
F	film thickness
f	fugacity
G	initial rate of solution
H	Henry's constant in equation $p_i = Hx_i$
K	y/x = equilibrium constant
L	liquid

M	average mass velocity
n	empirical constant (in Equation 27)
P	pressure, total (= gas concentration)
p	partial pressure, of component designated
R	ideal gas law constant
r	system radius
S	solid
T	temperature, absolute scale
U	coefficient of escape of gas from liquid
V	volume
v	bubble radius
W	weight of solute
x	mole fraction in liquid phase
y	mole fraction in vapor phase
Z	compressibility factor

Greek

γ	liquid phase activity coefficient
δ	Hildebrand solubility parameter, see Equation 22
φ	vapor phase fugacity coefficient
$\varkappa$	diffusion coefficient
θ	time
η	viscosity
π	3.1416
ρ	gas density

I. INTRODUCTION TO VOLUME III

The purpose of this volume is to present some considerations of gas solubility in liquid propellants as a guide to the designer of propellant handling systems. A discussion of the behavior of two-phase, two-component systems as they have been correlated theoretically and empirically is presented. This supplies some guide lines for use of the data, and supplies background for predicting solubilities under new conditions or in systems for which measurements are unavailable.

The solubility data presentations are primarily in the form of isothermal and isobaric graphs. Solubility figures on the ordinates are in terms of both mole percent concentration of dissolved gas and STP volume of dissolved gas per unit weight of liquid solution. This latter relation is of interest in considering problems of gas evolution downstream of the propellant tank.

The gas solubility data presented in this volume are for equilibrium conditions. It is recognized that rate data would be very valuable to designers, since most processes on a rocket vehicle occur under nonequilibrium conditions. However, accurate rate data have not been reported for liquid propellants. Solution and evolution rates for gases are very system-dependent; they are effected by factors such as surface/volume ratio, speed of mixing, suspended solid particles in the liquid, etc.

In practice, the use of nitrogen to pressurize liquid oxygen presents a special case of the problem of rate of gas solution. It is possible to pressurize liquid oxygen tanks with nitrogen for very short times, perhaps 10 minutes, without exceeding the oxygen dilution limits (References 1-4), and this procedure is commonly followed. However, phase equilibria data (Reference 1) show that at 20 psia and -297°F liquid phase temperature the nitrogen could comprise 32 weight percent (35 mole percent), the equilibrium composition of this system. It is evident that one condition that permits the pressurization of oxygen propellant tanks for limited short times (e.g., as can be acceptably employed in some static test stand work) is the use of relatively warm nitrogen gas. The nitrogen gas delivered from a storage

pressure bottle system usually is above -100°F, even with the cooling of expansion, due to system heating effects. The nitrogen gas will rapidly cool to its condensation temperature and go into solution in the liquid oxygen when left pressurized for moderate-to-long periods. The rate of solution can be minimized if desired, and is a function of the characteristics of the pressurization system (e.g., the extent of circulation and mixing of the gas in the ullage volume, the surface area, temperature and mass of the tank walls, etc.). Conversely, pressurization of liquid oxygen propellant tanks with gaseous nitrogen for long periods is generally unacceptable, because of condensation and solution of the nitrogen.

Pressurization design techniques are treated quantitatively in Section III of Volume I, so that conclusions based on calculation can be made, for example, on when acceptable performance can be expected with a given pressurant or pressurizing system. Volume III is primarily concerned with the equilibrium concentrations of various pressurants in propellants rather than the rates of solution. Information on equilibrium solubility will show the maximum solubility to be expected, and will also provide some of the essential data needed for estimating pressure rise or fall in propellant tanks over extended periods of operation. (Methods of estimating the pressure rise or fall in propellant tanks are presented in Section III of Volume I; methods for comparing pressurization systems are presented in Section II of Volume I.)

Generalizations can be made about the solubility of gases in liquids. One approximation found to be true over some temperature ranges is that, for highly soluble gases, the solubility tends to decrease with rise in system temperature, the reverse of the general trend for solubility of solids. However, even this generalization on gas solubility is found not to be applicable for gases with low solubility or for many of the systems at the temperatures and pressures of interest to the pressurization designer. For instance, most helium systems and many other propellant-pressurant systems exhibit reverse-order solubility. Further comments on gas solubilities, trends and the phenomena that significantly determine solubility are presented in the next sections.

II. THEORY OF GAS SOLUBILITY

A. LITERATURE AVAILABLE

There are several treatises and reviews dealing with various aspects of the subject of gas solubility. A very valuable article is that by Battino and Clever, "The Solubility of Gases in Liquids" in Chemical Reviews (Reference 5). Hildebrand and Scott wrote an excellent book dealing with many facets of solubility (Reference 6). Glasstone's well known "Text Book of Physical Chemistry" also has useful discussions (Reference 7).

B. IDEAL SOLUTIONS

The gas solubility in ideal solutions can be estimated, but first an ideal solution must be defined. Consideration of ideal solutions is worthwhile to establish approximate relations; also, very dilute solutions approach the behavior of ideal solutions. An ideal solution is defined as one in which the heat of mixing of the pure components is zero and there is no change in total volume (Reference 6).

For such solutions, the relationship known as Raoult's Law (i.e., the vapor pressure p_i of component i equals the vapor pressure p_i^o of that pure component times its liquid mole fraction x_i) holds.

$$p_i = p_i^o x_i$$

Since vapor pressure increases as temperature increases, for an ideal solution gas solubility decreases as the temperature increases.

Another relationship known as Henry's Law is then followed: that is, the solubility of a gas is proportional to its gaseous phase partial pressure.

At any one temperature a gas with a higher critical temperature and boiling point is more soluble than one with a lower critical temperature, since p^o is smaller for the former. (This approximation also is found to be generally followed for solutions not following Raoult's Law.)

When these relationships are not followed for any reasons, the liquid solution or the gas phase, or both, do not behave ideally. Departures from ideality are due to a number of reasons, including the nature of the molecules of the two components; their relative size, shape and intermolecular forces; and tendencies for chemical compound formation. It is evident then that the nature and magnitude of the atomic and molecular bonds play a significant role in solubility values. Qualitatively, the equilibrium solubility can be looked at as a balance between those forces encouraging solution and those opposing it.

C. GAS SOLUBILITY IN NONIDEAL SOLUTIONS

The generalizations that may be made on the solubility of gases in solutions with nonideal behavior can be related to departures from Raoult's Law. In Figure II-1, the vapor pressure is plotted as a function of the mol fraction; the ideal situation is curve B, where Raoult's Law holds; deviations are either positive as in curve A, or negative as in curve C. The solubility of a gas exhibiting a positive deviation from Raoult's Law is seen to be less at a given partial vapor pressure, here assumed to be 1 atm, for a saturated solution of component, y. Conversely for a negative deviation from Raoult's Law, curve C, the solubility is greater than if the system behaved ideally.

Much effort has resulted in establishing methods for predicting solubilities from thermodynamic reasoning using expressions that consider the forces believed to influence solubility, see References 6, 8 and 9. Polarity, formation of hydrogen bonds, any ionic tendencies of the components or tendency for chemical compound formation can be taken into account providing enough basic data are available. Correlations of solubilities have been made mostly of gases in solvents at or near normal atmospheric conditions on earth. The trends have been as predicted by theory, see for example Table 4, page 243 of Reference 6 showing the solubility of ten nonpolar gases in 15 different liquids at atmospheric pressure and temperature. Helium is noted to be least soluble in each case. These results are mainly of theoretical interest here because none of the liquids are propellants. The accuracy of prediction, using the methods described by Hildebrand and Scott, approaches

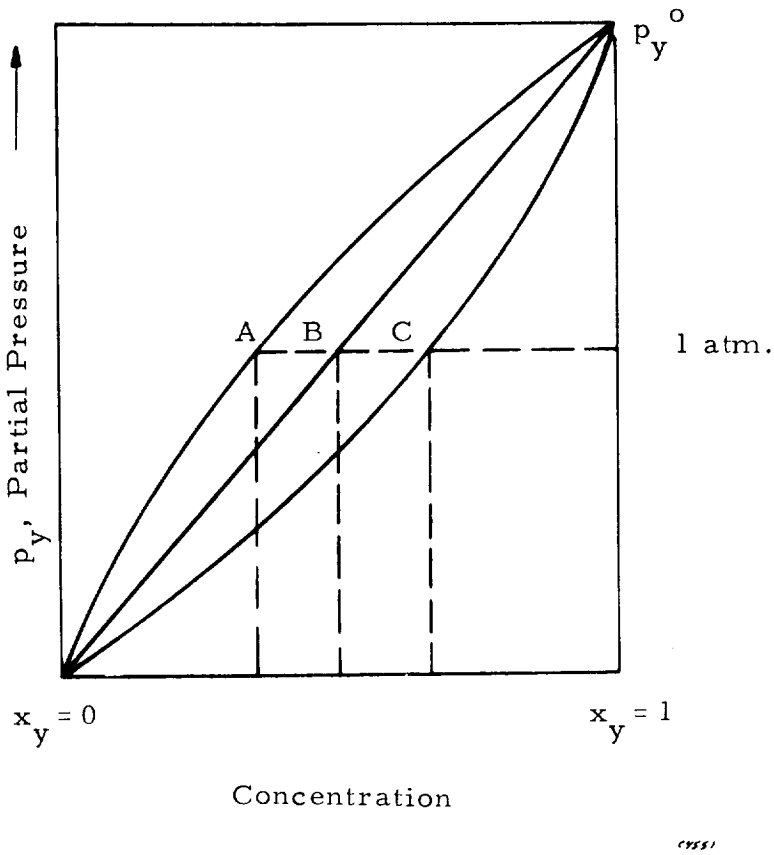

Figure II-1. Deviations from Raoult's Law (Reference 6)

10% of the measured values, particularly when data are known for several analagous systems (Reference 6). Application of these predictions to some representative cryogenic liquids are described in the next section. It should be noted that available solubility data and theory predicts the tendency for CO_2 and NO_2 to have high solubilities in some solvents due to specific chemical interactions (e.g., compounds containing carbonyl groups, etc.). It is considered worthwhile to estimate solubilities by theoretical techniques when no experimental data can be obtained, e.g., by using the Hildebrand solubility parameter, δ, described in Reference 6. Corrections for nonideality in the gas phase can also be made but accuracies of solubility predictions thus obtainable seldom approach the desired goal of 10% of the measured values, for reasons to be made more evident in the next section.

D. PREDICTION OF SOLUBILITIES

1. Basic Concepts

Vapor-liquid equilibrium data can be predicted with a degree of accuracy for purposes of engineering calculations by the use of virial equations of state for the vapor-phase fugacity coefficient (References 8 and 9) and Hildebrand's equations for liquid-phase activity coefficients (Reference 6). Such calculations are illustrated for the hydrogen-carbon monoxide-propane system in Reference 10. The conditions were such that the virial equation, truncated after the second virial coefficient, sufficed to describe the vapor phase nonidealities, and the liquid phase was essentially pure. Reference 8 illustrates the use of the foregoing relations in the calculation of equilibrium concentration of oxygen in hydrogen at 100 psig and -370°F.

The two-parameter Redlich-Kwong equation has been found to represent P-V-T data in the gas phase with good precision, even at high gas densities. The application of the Redlich-Kwong equation of state to correlations of methane-nitrogen and helium-hydrogen systems is shown in Reference 11. (Comparisons of calculated and measured solubilities for the hydrogen-helium system are discussed in References 12 and 13, the measured data are presented in Section III-C following.)

Raoult's Law states that the partial pressure p_i of component i in the gas phase is directly proportional to the concentration of component i in the liquid phase, and that the proportionality factor is the vapor pressure of the pure component i at the temperature: $p_i = p_i^o x_i$. At low pressures, where the gas phase is approximately ideal, the partial pressure of component i, p_i, is equal to the mole fraction of i in the gas phase, y_i, times the total pressure P. Thus

$$y_i P = x_i p_i^o \tag{1}$$

or

$$\frac{y_i}{x_i} = \frac{p_i^o}{P} \tag{2}$$

The equilibrium ratio y_i/x_i is frequently identified and used as the constant K. (Note: K more properly should be referred to as a ratio because it is single valued only at each single value of pressure and temperature, thus having a range of values.)

When the liquid and gas phases cannot be considered as ideal, this most simple expression must be modified. Henry's Law is one modification.

$$\text{Raoult's Law} \qquad p_i = p_i^o x_i \tag{3}$$

$$\text{Henry's Law} \qquad p_i = H x_i \tag{4}$$

In effect, Henry's "constant" is an adjusted vapor pressure for component i at a given temperature.

2. Criteria for Equilibrium

It is a criterion for equilibrium between phases that at a given temperature and pressure the fugacity or escaping tendency of a constituent will be the same in each phase. The expression of equilibrium between a liquid and a gas phase

$$y_i P = x_i p_i^{o} \tag{5}$$

may be made more precise through use of fugacities.* The fugacities of component i in the two phases are equal.

$$f_i^{vap} = f_i^{liq} \tag{6}$$

the fugacity of i in the vapor phase may be expressed as a product of the fugacity coefficient, the concentration, and the total pressure.

$$f_i^{vap} = \varphi_i y_i P \tag{7}$$

The fugacity coefficient of a given component, φ_i, is a function of temperature, pressure, and the concentrations of each of the components in the vapor phase, that is to say, it is essentially a function of the interactions between the given component and all of the components of the system. For the liquid phase, the fugacity may be expressed as a product of the liquid phase activity coefficient, the concentration, and the fugacity of the pure liquid at the same temperature and at the total pressure of the mixture.

$$f_i^{liq} = \gamma_i x_i f_i^{oliq} \tag{8}$$

Since the fugacity of i in the two phases is the same at equilibrium,

$$\varphi_i y_i P = \gamma_i x_i f_i^{oliq} \tag{9}$$

or

$$K = \frac{y_i}{x_i} = \frac{\gamma_i f_i^{oliq}}{\varphi_i P} \tag{10}$$

which is the equilibrium ratio discussed above (also called K constant or K-factor).

---

*Fugacity is a special function which simplified the treatment of cases in which the ideal-gas and ideal-solution laws do not apply. (For extremely dilute solutions the fugacity of a component very nearly equals its pressure.)

Equilibrium "constants" can thus be computed from such expressions if the activity coefficient of i, the fugacity of pure component i at the temperature and pressure of interest, and the fugacity coefficient of component i in the vapor phase can be evaluated.

3. Pure Liquid Phase In Equilibrium With Vapor

The computation of the concentration of component i in the vapor phase may be made through use of Equation 10 for the simplified case when the liquid phase is essentially pure. In this case, $x_i \cong 1.0$ and $\gamma \cong 1.0$. And

$$y_i = \frac{f_i^{oliq}}{\varphi_i P} \tag{11}$$

In this expression, with y_i being the sought after concentration of i in the vapor phase and P the total system pressure it is now necessary to evaluate f_i^{oliq} and φ_i.

The value f_i^{oliq} is the fugacity of the pure liquid component i at the temperature of interest and at the total pressure of the system. This pressure of the pure component, increases the fugacity of component i. The increase of fugacity with pressure may be determined from

$$\left(\frac{\partial \ln f_i}{\partial P}\right)_T = \frac{V_i}{RT} \tag{12}$$

if V_i, the molal volume in the liquid state, is known as a function of pressure

$$RT \ln \frac{f_i^{P_2}}{f_i^{p_i\,oliq}} = \int_{p_i^{oliq}}^{P_2} V_i \, dP \tag{13}$$

and if V_i is relatively noncompressible, its average molal volume between p_i^{oliq} and P_2 and at temperature T may be used to obtain

$$RT \ln \frac{f_i^{P_2}}{f_i^{oliq}} = V_i (P_2 - p_i^{oliq}) \qquad (14)$$

All is known except $f_i^{P_2}$, which can now be calculated.

The fugacity coefficient, φ, in Equation 11 is defined as the ratio of that component's fugacity in the mixture to its partial pressure

$$\ln \varphi_i \equiv \ln \frac{f_i^{oliq}}{y_i P} \qquad (15)$$

$$= \frac{1}{RT} \int_o^P (\overline{V}_i - \frac{RT}{p}) \, dP \qquad (16)$$

Calculation of the fugacity coefficient from this equation requires a volume-explicit equation of state.

4. The Virial Equation Of State

The virial equation of state, a power series in volume (or in pressure or in density), may be used for evaluation of the fugacity coefficient (Equation 17).

$$Z_m = \frac{PV}{RT} = 1 + \frac{B_m}{V} + \frac{C_m}{V^2} + \frac{D_m}{V^3} + * \; * \qquad (17)$$

B, C, and D, the second, third, and fourth virial coefficients, are functions of temperature. The equation of state for a mixture requires the use of virial coefficients for the mixed gases. The second virial coefficient of a mixture, B_m, is a quadratic function of the mole fraction

$$B_m = \sum_i^n \sum_j^n y_i y_j B_{ij} \qquad (18)$$

and the third virial coefficient of a mixture C_m is a cubic function

$$C_m = \sum_i^n \sum_j^n \sum_k^n y_i\, y_j\, y_k\, C_{ijk} \qquad (19)$$

It can be shown that using the fundamental equation relating fugacity to P-V-T properties, use of the virial equation of state to describe these properties through use of the preceding mixing coefficients, and limiting the expression to the second and third virial coefficients, that

$$\ln \varphi_i = \frac{Z}{V_m} \sum_j^n y_i\, B_{ij} + \frac{3}{2\, V_m^2} \sum_j^n \sum_k^n y_i y_k\, C_{ijk} - \ln Z_m \qquad (20)$$

The restriction of using only the second and third virial coefficients limits the expression to use in the pressure range up to about the critical density. When terminated after the secondvirial coefficient, the expression is reliable to about half the critical density.

5. Solubility In The Liquid Phase

It has been pointed out that the fugacity of a component in the liquid phase may be written as the product of its activity coefficient, its concentration, and its fugacity in the pure liquid state at the same temperature and total pressure in Equation 8.

$$f_i^{liq} = \gamma_i\, x_i\, f_i^{oliq}$$

The liquid-phase activity coefficient, γ_i may be calculated from Hildebrand's equation for regular solutions (Reference 6)

$$\ln \gamma_i = \frac{V_i^{liq}}{RT} \left(\delta_i - \sum_i^n \varphi_i\, \delta_i \right)^2 \qquad (21)$$

The solubility parameter δ_i is defined by

$$\delta_i = \left(\frac{\Delta E_i}{V_i^{liq}} \right)^{1/2} \qquad (22)$$

where ΔE_i is the energy of vaporization to the gas at zero pressure (i.e., infinite separation of the molecules) and V_i^{liq} is the liquid molal volume of component i.

Using Equations 21 and 14, expression 8 may be evaluated and equated to the fugacity of i in the gas phase or to the fugacity of the pure solid or pure liquid.

It should be noted that the logarithm of the activity coefficient varies with the square of the difference between the solubility parameters of the component and of the solution, and that for moderate differences in solubility parameters, the activity coefficients are sensitive to slight variations in thermal data.

6. Comparison Of Theory With Experimental Data

Comparison of experimental data with theoretical calculations shows that although solubilities can be predicted by analytical techniques, it is best to measure solubilities when accuracies within 10% are desired.

Calculated and experimental vapor-liquid equilibrium ratios for a ternary system, hydrogen-carbon monoxide-propane, at 340°F and 475 psia (Reference 10) are shown in Figure II-2.

Figures II-3 and II-4 show comparisons of calculated and measured py/x equilibria values for hydrogen and helium. The correlations for vapor-liquid equilibrium were obtained by means of a modified Redlich-Kwong equation of state (Reference 11).

It is interesting to note that the unusual decreases of py/x of helium with increasing temperature is correctly predicted by the correlation. Most materials show an increase of py/x with increasing temperature. This representation of the special behavior of helium lends considerable confidence to this correlation method.

A comparison of methods of predicting equilibrium gas phase compositions in pressurized binary systems containing an essentially pure condensed phase is given in Reference 9. Four methods were used to calculate

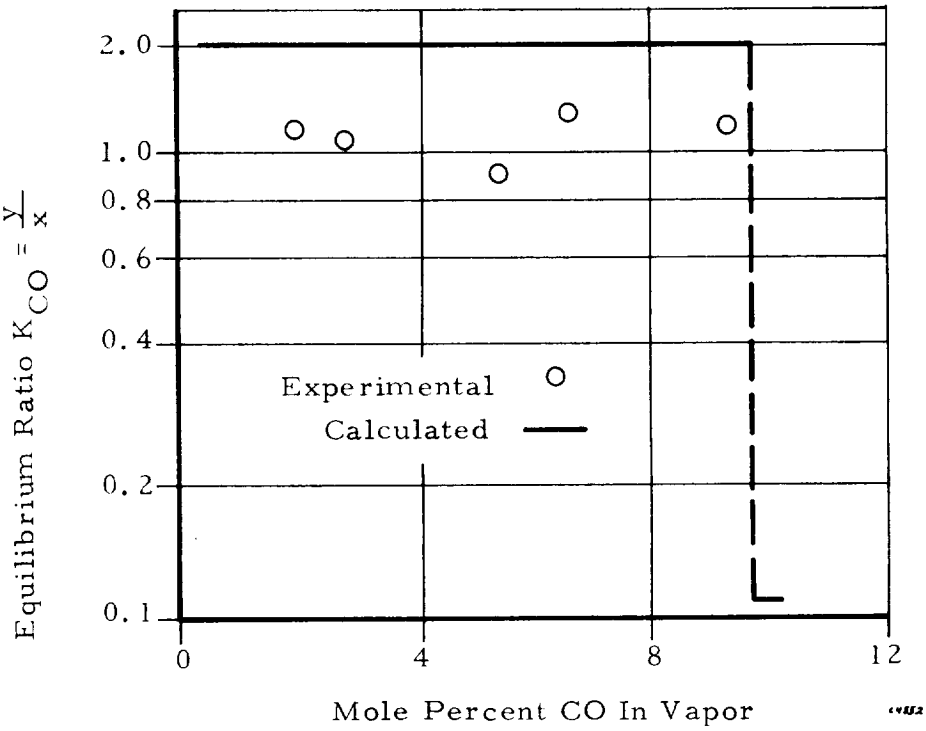

Figure II-2. Vapor-Liquid Equilibrium Ratios in H_2-CO-C_3H_8 (Reference 10)

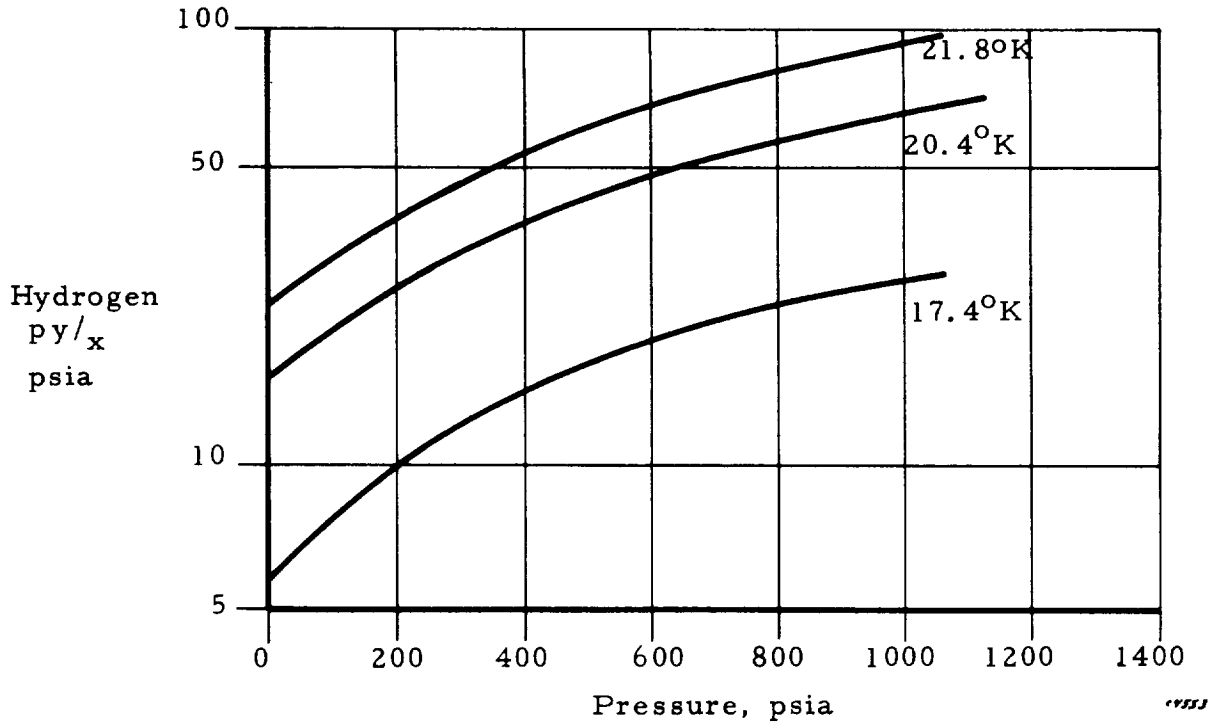

Figure II-3. Comparison of Calculated and Measured py/x of Hydrogen (Ref. 11)

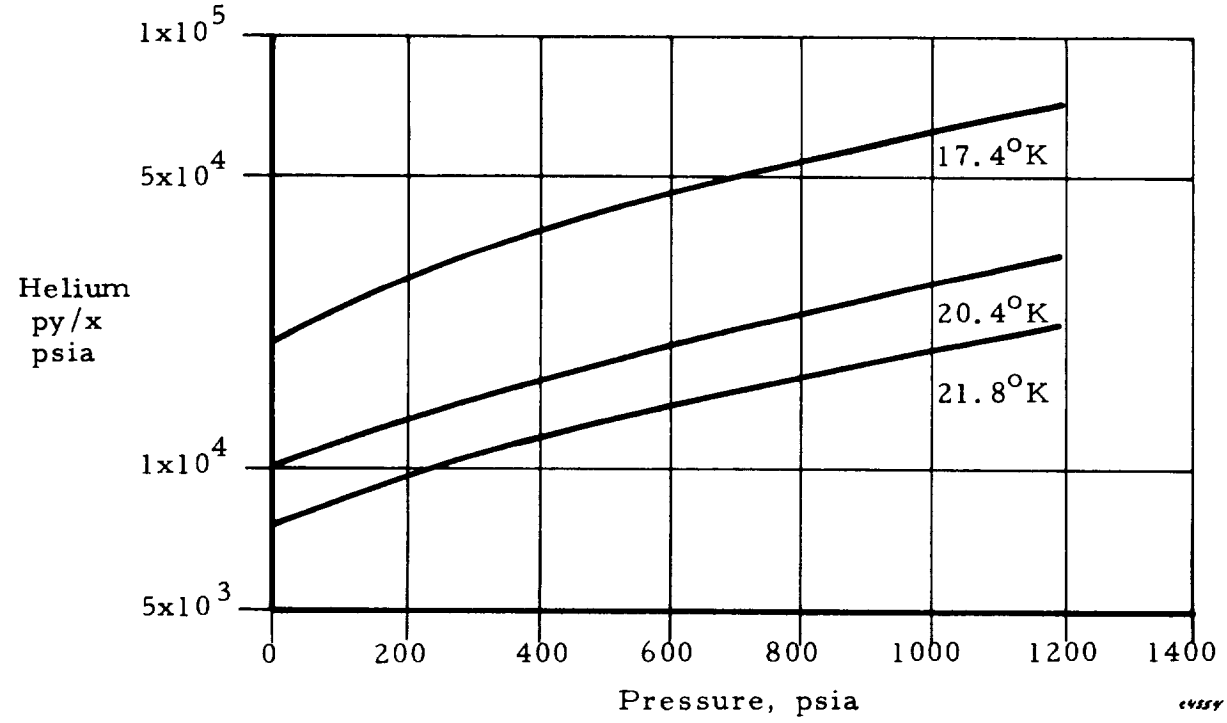

Figure II-4. Comparison of Calculated and Measured py/x of Helium (Reference 11).

phase equilibrium for methane-hydrogen. Comparison with experimental data shows that the enhancement factor can be predicted within 25%. No single equation agrees closely with the experimental data over the entire pressure range considered (675 to 3000 psia, 25 to 200 atm).

7. Obtaining Virial Coefficients And P-V-T Data

Attention is called to various experimental methods that have been used for direct measurement of phase equilibria and also to methods for the related virial coefficient and P-V-T measurements.

The virial coefficient equation of state is such a powerful theoretical tool in phase equilibria work that much attention is given to the improvement of virial coefficient data. The virial coefficients are functions of temperature and of composition of mixtures. The coefficients for the pure components and appropriate combining rules are required for treatment of the binary or multicomponent mixture. Prausnitz and Gunn (Reference 14) discuss the virial equation and make an analysis of second virial coefficient data for many systems. Prausnitz and Meyers (Reference 15) apply the Kihara parameters to the calculation of second virial coefficients for 16 cryogenic fluids. Beenakker and Varekamp (Reference 16) describe an apparatus for the differential determination of the second virial coefficient working with hydrogen and its isotopes and experimentally measuring the difference between hydrogen and helium. Thomaes and Van Steenwinkel (Reference 17) describe a very accurate apparatus for measuring small differences in the second virial coefficient of gases at low temperatures. The principle of the experimental method consists of measuring the difference in volume expansions of two gases subjected simultaneously to the same change in pressure.

Kurata and Kohn (Reference 18) describe a glass cell apparatus that can be used at pressures up to 3000 psi for P-V-T measurements. Known increments of gas are injected into the cell and the pressure rise noted.

White et al (Reference 19) measured the compressibility of gaseous helium over a wide temperature and pressure range, and from the resulting 22 experimental isotherms developed a virial equation of state.

Mueller et al (Reference 20) obtained second virial coefficients from about 600 experimental points for the volumetric behavior of methane and methane-hydrogen mixtures as obtained in a Burnett-type apparatus. Byrne and Thedos (Reference 21) have used the critical compressibility factor for the correlation of P-V-T behavior of several diatomic gases. Nelson and Obert (Reference 22) present a comprehensive bibliography of P-V-T data for 30 gases and generalized compressibility charts.

E. GAS SOLUTION AND EVOLUTION – NONEQUILIBRIUM SYSTEMS

1. Introduction

In normal practice, most of the functioning of pressurized liquid propellant systems is at nonequilibrium conditions. Two main departures from equilibrium occur:

The fluid is unsaturated relative to the pressurant conditions (solution still occurring).

The fluid is supersaturated relative to the pressurant conditions (evolution may be occurring).

In real systems, these conditions may occur at the same time; in the fluid tank saturation may not have been reached, but fluid is being withdrawn and downstream of the tank, where the pressurant is not present in the gas phase, the fluid is supersaturated and gas evolution can occur.

When systems are not at equilibrium and so are undergoing changes, the most important way to characterize the condition is the rate of change as a function of the operating variables.

2. Rate of Solution

A number of papers have been published on the rate of solution of gases in liquids; however, no adequate reviews of the reports seem to exist. The most important reference is a series of papers presented at an "Absorption Symposium" of the American Chemical Society in 1924, and published in Industrial and Engineering Chemistry that year (Reference 23). At that meeting,

a paper by Lewis and Whitman (Reference 24) presented a theoretical treatment which has come to be called the "Two Film Theory." Almost all the papers at the symposium and subsequent research have been found to confirm this theory, and extend the definition of the parameters that enter it. However, it may be mentioned that most of the reported studies do not relate to conditions similar to those in propellant pressurization; instead the studies relate to falling liquid films, bubbling gas mixtures through the liquid, and other dynamic systems. This is not to say that the Two Film Theory is not applicable, but only that most of the parameters that have been defined closely are not those which are important in tank pressurization.

The Two Film Theory can be summarized in the following fashion:

At a gas-liquid interface, on both the gas and liquid sides, there are surface layers of gas and liquid that are effectively stationary, since each is relatively free from mixing by convection or mechanical processes. Generally, it can be assumed that the concentrations in the bulk gas and liquid phases are essentially uniform, but this is not necessarily true in the liquid phase if the bulk of the liquid is stagnant (Reference 25), a condition which tends to be true in propellant pressurization. Since the surface films are quiescent, all mass transfer through the two films must occur by diffusion. The diffusion rates in each film are functions of the concentration gradient across them and the film thicknesses. An equation for the rate across the two films is

$$\frac{d\,W}{A\,d\,\theta} = \varkappa_g (P_g - P_f) = \varkappa_L (c_f - c_L) \tag{23}$$

In systems where the gas is very soluble, P_f is negligible relative to P_g. Then

$$\frac{d\,W}{A\,d\,\theta} = \varkappa_g P_g \tag{24}$$

and the liquid film is unimportant.

If the gas is relatively insoluble, $P_g = P_f$, and

$$\frac{d W}{A d \theta} = \varkappa_L (c_f - c_L) \tag{25}$$

and since c_f is obviously the concentration in a film saturated at pressure P_g, it is c_g

$$\frac{d W}{A d \theta} = \varkappa_L (c_g - c_L) \tag{26}$$

and the gas film can be neglected.

For intermediate solubility, the full equation must be considered.

The physical existence of the stationary film was discussed by Davis and Crandall (Reference 26), who measured it on quiet water at room temperature, and found it 0.04 cm thick. When the water was stirred at 1000 rpm but the film was not broken, the thickness dropped to 0.004 cm. Bubbles rising through water have a film thickness of 0.002 cm; presumably this is the minimum that can be obtained.

Davis and Crandall explain the mechanism as follows: "When a pure gas, oxygen for example, is suddenly admitted at atmospheric pressure into contact with pure water from which all gases have been removed, the very surface layer, perhaps monomolecular in thickness, instantaneously becomes very nearly saturated with oxygen. This must be true, because an oxygen pressure is at once exerted from the surface equal to the partial pressure against it, which is the condition necessary for a saturated solution.

"The oxygen now begins to diffuse into the film at a tremendous rate, for although the solubility of oxygen in water is small, 0.0012 M, the gradient from the surface is very steep. We wish to stress this point because of its bearing on the rapid rates at which some olefinic gases are absorbed by sulfuric acid, although they are quite insoluble therein.

"As diffusion proceeds the magnitude of this gradient quickly grows less and the absorption slows down, soon reaching a constant value

(initial absorption rate). At this stage the gradient is uniform and the same quantity of oxygen is passed from the surface through each unit cross section of the film into the main body of the liquid which is still practically free from dissolved oxygen."

Hanks and McAdams (Reference 27) studied the gas film by using very soluble gases. They showed that the film thickness determined in heat transfer studies was the same as that for mass transfer (gas diffusion), and that an equation for deriving film thickness is

$$F = 2br \left(\frac{\eta_g}{2rM_g} \right)^n \tag{27}$$

The above discussions implicitly assume infinite reservoirs of gas and liquid, and saturation of the liquid is not considered. This is because most of the work relates to chemical process plants in which absorption of a continuously supplied gas to a continuously renewed liquid is of prime interest.

In typical pressurization systems, the liquid cannot be regarded as an infinite reservoir, and so the rate of absorption of gas at any time must be affected by the concentration already present. Adeny and Becker (Reference 28) did consider this condition, and derived the equation

$$\frac{d\,W}{A\,d\,\theta} = G\,P - U\frac{W}{V_L} \tag{28}$$

This can be simplified to the form

$$\frac{W_\theta}{W_s} = \left(100 - \frac{W_{int}}{W_s}\right)\left(1 - e^{-b\theta}\right) \tag{29}$$

This equation predicts a logarithmic curve. Studies by Becker (Reference 25) with a large number of gases dissolving in water substantiated the equation. However another effect showed up which is not accounted for. The initial rates for some gases fell off along a logarithmic curve, but the asymptotic portion was well below the saturation concentration. It appears

that these gases form saturated upper layers and affect the viscosity and density of these layers to reduce diffusion rates. The layers in effect become thick liquid films. Gases that behaved in this fashion in water solution included carbon dioxide, hydrogen, and hydrogen sulfide. Nitrous oxide, nitric oxide and chlorine did not form such barrier films on water.

3. Experimental Studies

Only a few studies of the rate of solution of pressurant gases in rocket propellants have been reported.

a. Nitrogen Tetroxide – Nitrogen

In some undisclosed experiments carried out by M. M. Calvert (Reference 29), the rate of pressure drop in a calibrated closed system of nitrogen over undisturbed N_2O_4 was measured. From the pressure decay, the amount of nitrogen dissolved in the propellant was calculated. The experiments gave data of suprising consistency. A summary of the results of four of the experiments is presented in Table II-1 and Figure II-5. In another experiment with only 1/3 the volume of N_2O_4 in the same container, the absorption levelled off at about 55% of saturation, and a brief shaking after three hours caused completed saturation.

b. Ethane – Helium

A brief study of the rate of solution of helium in ethane at $-50^{\circ}F$ was conducted (Reference 30). Samples of the liquid phase were withdrawn periodically for analysis after helium was admitted to the system. The helium pressure was maintained constant. The eductor probe to withdraw the specimens was located 5 cm below the surface of the liquid ethane, at the bottom of the liquid phase.

The data are presented in graphic form in Figure II-6. They were fitted to Equation 29, and b was calculated to be 0.485. The value for $\theta = 0$ was also calculated from the equation. It was 0.99 hours after the experiment started. This probably corresponds to the time necessary for the first molecules of helium to reach the eductor probe opening.

TABLE II-1

RATE OF SOLUTION OF N_2 IN N_2O_4

(Initial N_2 Pressure, 290 psig. System Volume, 512 ml)

Time (Minutes)	Test Conditions, Nitrogen Pressure (psig)			
	327 ml N_2O_4 71°F	320 ml N_2O_4 74°F	330 ml N_2O_4 78°F	309 ml N_2O_4 96°F
0	0	0	0	0
1	214	236	186	179
2	227	242	236	193
3	240	249	236	207
4	–	–	248	–
5	240	249	248	–
8	–	–	–	207
10	–	–	248	–
13	–	–	–	221
17	240	–	–	–
18	–	–	–	235
35	–	–	248	–
44	240	–	–	–
58	–	–	–	262
66	–	262	–	–
70	–	–	248	–
82	–	–	–	276
119	253	–	–	–
205	–	–	332*	–

*Agitated slightly.

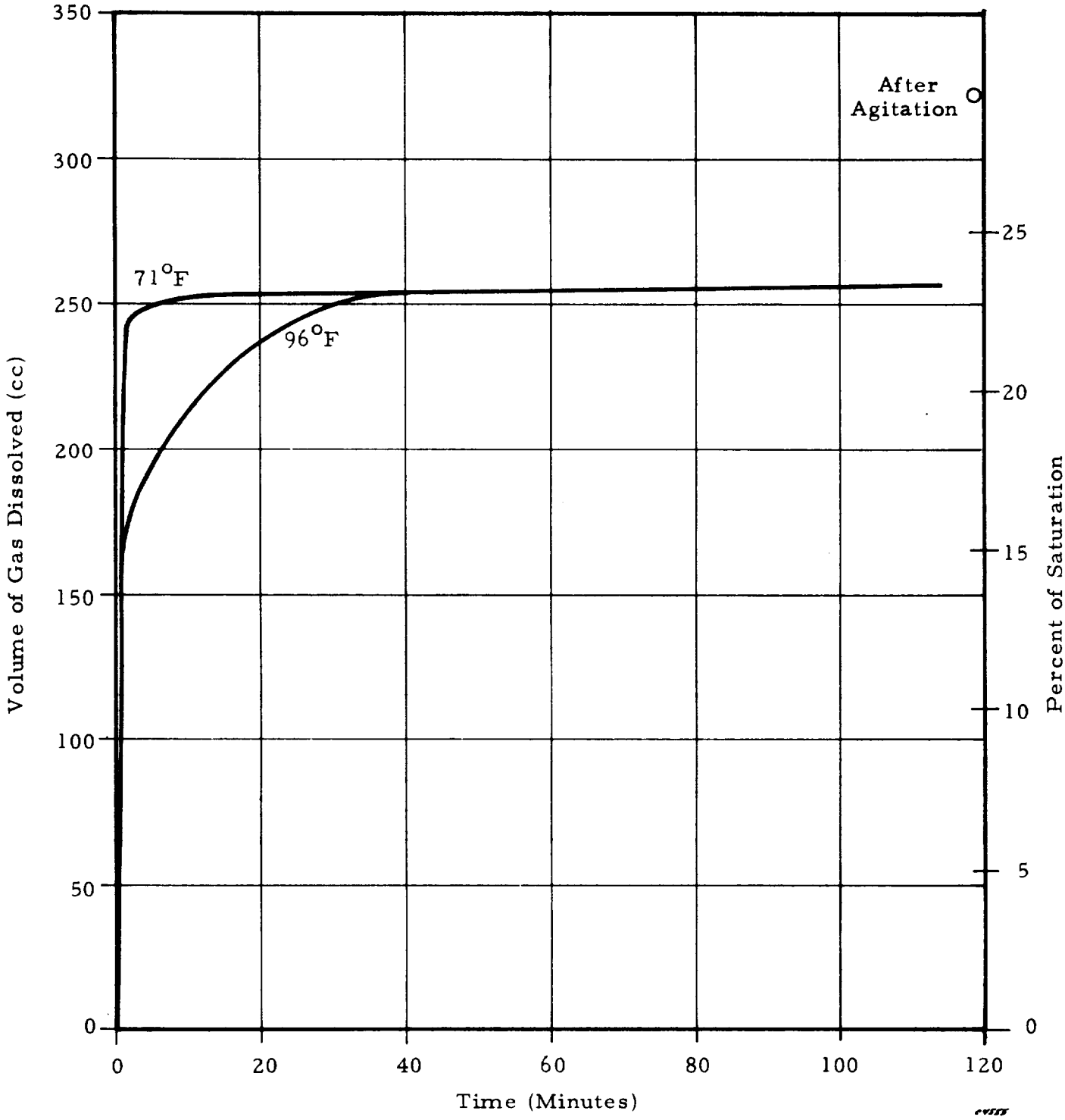

Figure II-5. Rate of Solution of Nitrogen in Nitrogen-Tetroxide

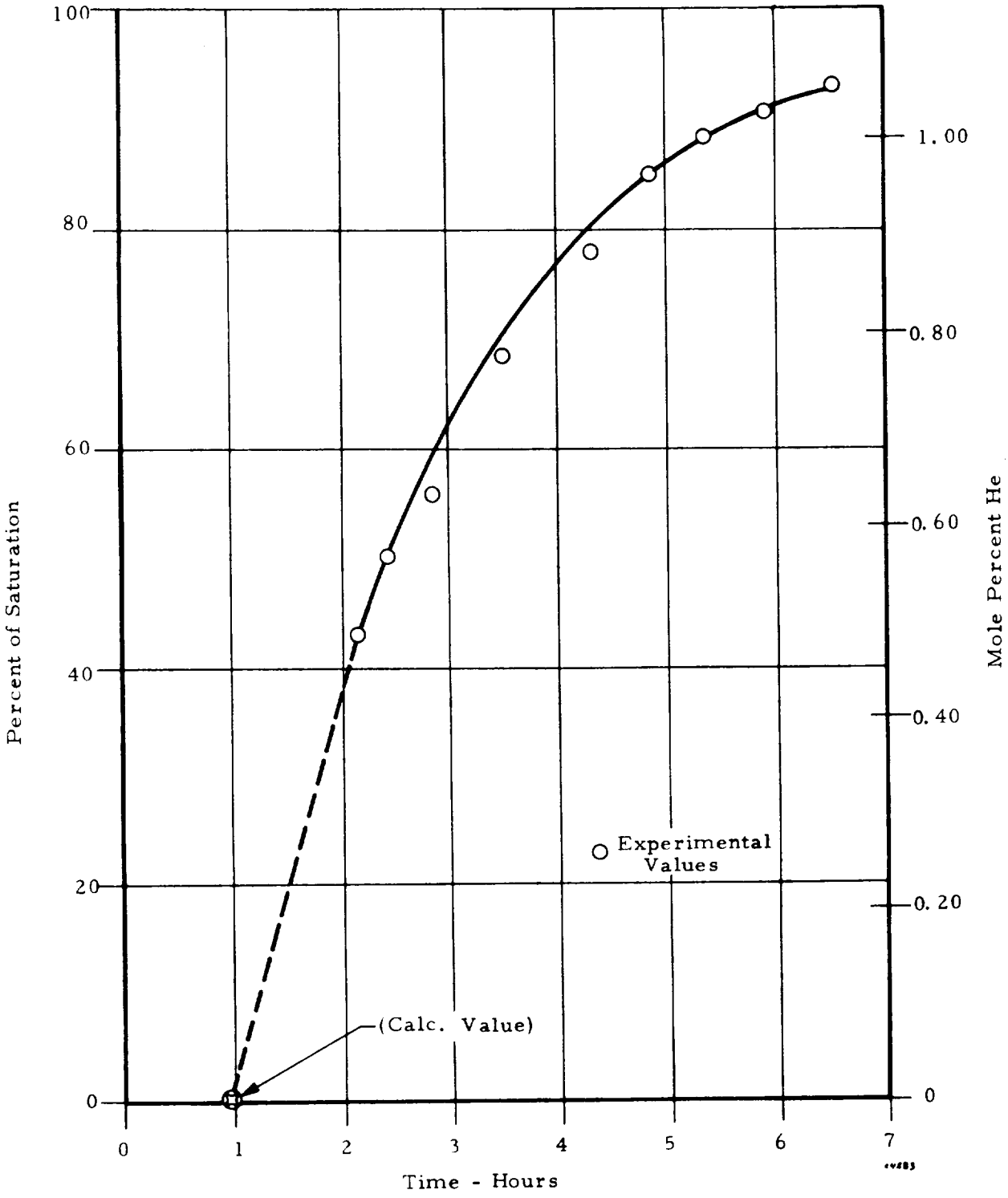

Figure II-6. Rate of Solution of Helium in Liquid Ethane at -50°F and 720 Psi

c. Monomethylhydrazine – Helium

The Marquardt Corporation has experienced difficulty in tests at certain of its facilities, and these were traced to problems in insuring complete saturation of propellant with helium in the run tanks. The problems were much greater with MMH. A complex procedure was developed to insure complete saturation, but the approach was specific to the particular facilities involved (Reference 31). Since the tank geometries and conditions at the facility are not detailed in the reference, general solubility rates cannot be calculated.

4. Rate of Evolution

The equations presented for solution of gases should be equally valid for evolution, since the concentration gradients can be in either direction. Under conditions of vigorous stirring and mixing of gas and liquid phases this assumption was shown to be true by Lewis and Whitman (Reference 24), using the data of Perman (Reference 32), and also of Whitman and Davis (Reference 33).

Again, these studies were in infinite systems, and do not relate directly to a propellant pressurization system. The rate of gas evolution from a relatively quiescent fluid depends on a number of other factors.

Gases frequently evolve from supersaturated liquids by forming bubbles within the bulk of the fluid and at the container walls, in a manner reminiscent of a liquid boiling. Thus nucleation phenomena must be considered. However, no analyses or experiments relating nucleation to gas evolution have been found. Epstein and Plesset (Reference 34) have analyzed the behavior of bubbles once they are formed, relating growth, shrinkage, and translation of bubbles to various system parameters. In this article, the volume growth rate of bubbles immersed in a supersaturated solution is shown to be

$$\frac{dv}{d\theta} = \left(c_{int} - c_s\right)\left(\frac{1}{v} + \frac{1}{(\pi \varkappa \theta)^{1/2}}\right) \qquad (30)$$

5. Certain System Effects Under Nonequilibrium Conditions

Many of the problems in liquid propellant systems that arise from dissolved gases have not been carefully studied, and some have only been cursorily identified. But information is available on analagous situations that arise in hydraulic systems. Such systems are frequently designed to have very long service lives, and many types of interactions that can cause service problems have been identified and evaluated.

An article by V. G. Magorien (Reference 35) includes both a review of known factors and new experimental data. Among the information presented by Magorien is the fact that 0.17 Vol % entrained gas (air) reduces the bulk modulus of a liquid by 50% (Figure II-7). A completely dissolved gas has no effect on the bulk modulus. Another important observation is that the presence of dissolved gases accelerates erosion and cavitation corrosion. And dissolved air is released as bubbles which do not redissolve when the liquid lineal velocity through a constriction is greater than 100 feet a second. The drastic reduction in bulk modulus is one possible explanation for pressure fluctuations and chugging in blowdown N_2O_4 – UDMH ACS engines in several rocket vehicles.

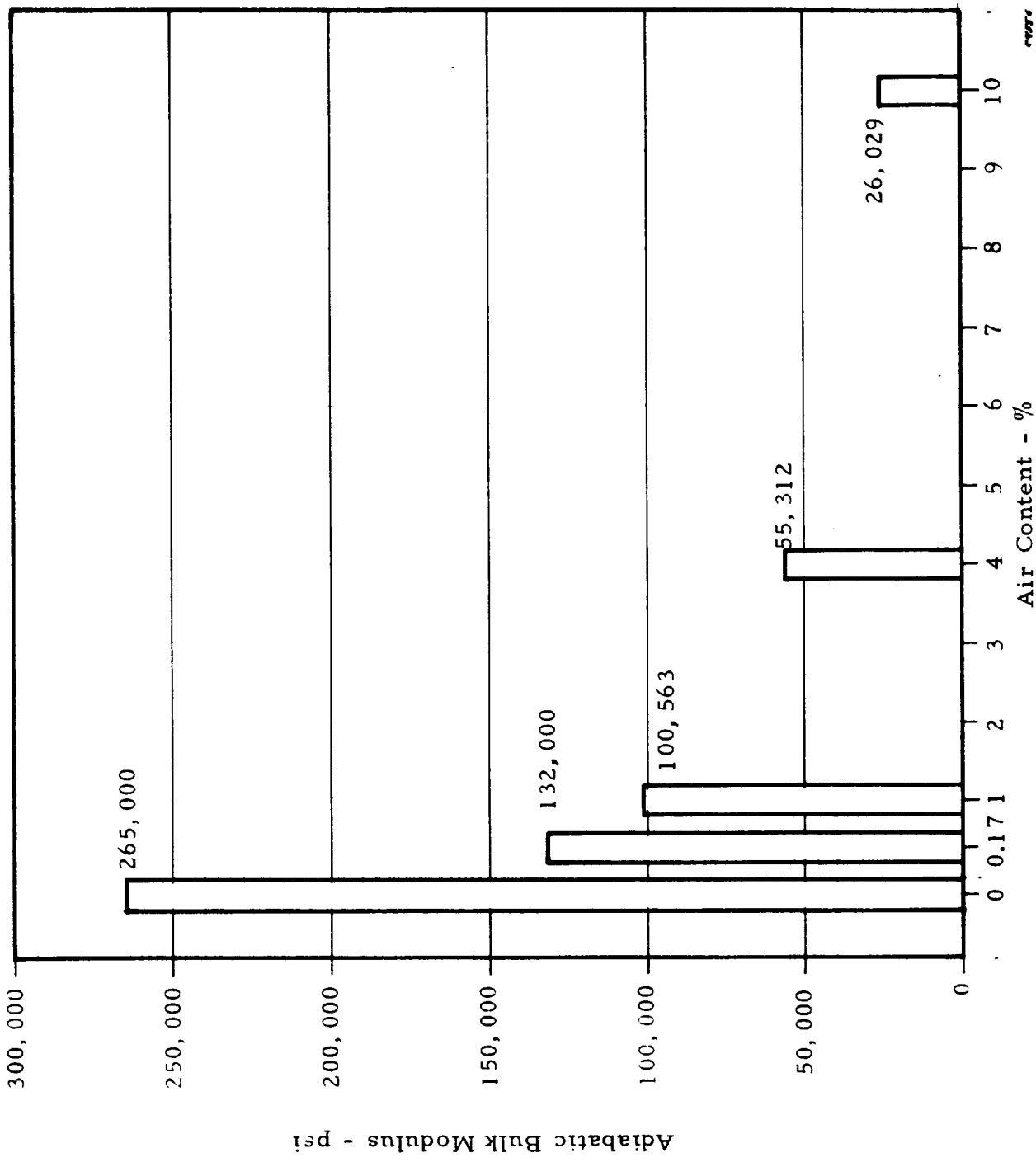

Figure II-7. Effective Bulk Modulus at 3000 psig of Hydraulic Fluid (MIL-H-5606) Containing Entrained Air Bubbles.

III. MEASUREMENT OF GAS SOLUBILITY

A. METHODS OF SOLUBILITY MEASUREMENT

Phase equilibria measurements generally involve the intimate and continued mixing of two phases until constancy of composition is attained in each phase, followed by the separation or sampling of the phases, and sample analysis. Liquid vapor equilibria at low temperatures have been measured by many workers: the Dodge and Dunbar study (Reference 1) of the oxygen-nitrogen system; Maimone's work (Reference 36) with hydrogen-nitrogen and deuterium-nitrogen; Akers' study (Reference 37) of the hydrogen-nitrogen-carbon monoxide system; the study of the helium-hydrogen system by Sonntag, Val Wylen, et al, (References 12 and 13); the Aerojet-General studies by Flaherty et al on helium and nitrogen in N_2O_4, Aerozine 50 and monomethylhydrazine (References 38 and 39), and the Stein et al (Reference 10) phase equilibria apparatus are representative of the experimental procedures which have been used to obtain liquid-vapor phase equilibria (L-V) data. (Also see Reference 5.)

B. GRAPHICAL REPRESENTATION OF PRESSURE, TEMPERATURE, AND COMPOSITION RELATIONS

For binary systems the phase rule shows that the equilibrium liquid and vapor phase compositions are invariant at fixed pressure and temperature. The data may be represented graphically by two surfaces on a three-dimensional pressure-temperature-composition diagram, each surface representing a single phase. The two surfaces merge along a critical curve, consisting of points at which the two phases become indistinguishable. It is customary to describe the equilibrium surfaces graphically by showing their projections on one or more of the three P-T-x coordinate planes. Presentations of experimental data include plots of isotherms on a P-x diagram and isobars in the T-x plane. P-T diagrams are obtained by cross-plotting data from P-x and T-x diagrams. Equilibrium constants, the ratios of vapor-phase to liquid-phase mole fractions, may be shown as a function of pressure for various isotherms.

The critical point of a pure substance has the following characteristics:

1. The liquid and vapor phases are identical
2. The temperature is the maximum at which the two phases can co-exist
3. The pressure is the maximum at which the two phases can co-exist.

In the case of binary solutions these three phenomena no longer appear at one point but are exhibited at three separate points. This can best be shown on a pressure-temperature diagram such as Figure III-1. This represents a section cut through a pressure-temperature-composition surface by a plane of constant composition. It consists of two boundary curves, - one for liquid and one for vapor of the same composition - enclosing the field in which two phases can co-exist, and which meet at the critical point C, where the two phases become identical. This point is the point of tangency of the boundary curve and an envelope curve AB that joins the critical points of the two pure components. Point C' is the maximum temperature at which a vapor of this particular composition can be condensed to a liquid, or the maximum temperature at which the two phases can co-exist in a system of this particular total composition. This point is commonly known as the "cricondentherm" (critical condensation temperature) (Reference 40) Point M represents the maximum pressure at which a system of the given composition can exist in two phases. Also, DMC is the locus of the bubble points.* The curve DMC is most easily visualized as the vapor pressure curve of the particular mixture. Similarly, EC'C is the locus of the dew points** at a series of pressures. It is interesting to note that, whereas the vapor pressure of a pure substance always increases with temperature, in the case of a binary solution it may rise to a maximum and then actually decrease as the temperature is increased in the vicinity of the critical point. This phenomenon accounts in part for some of the deviation of solutions from ideal solubility trends. Other causes for deviation are discussed in the previous section on prediction of solubilities.

---

*"Bubble point" - point of initial boiling

**"Dew point" - point of initial condensation

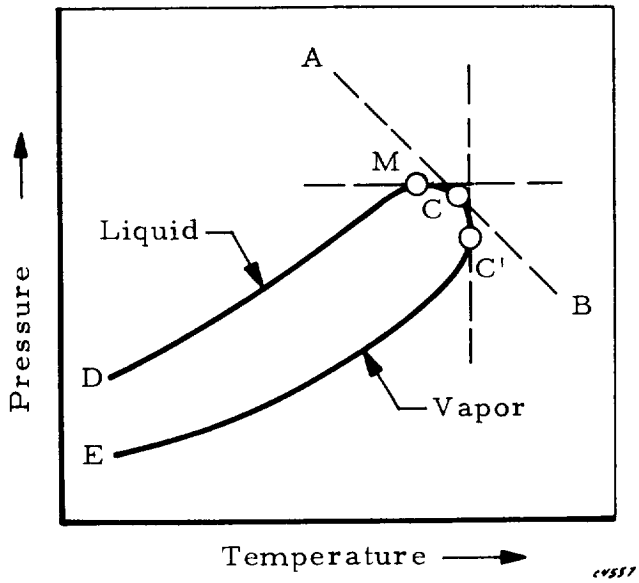

Figure III-1. Binary Pressure-Temperature at Constant Composition (Reference 40).

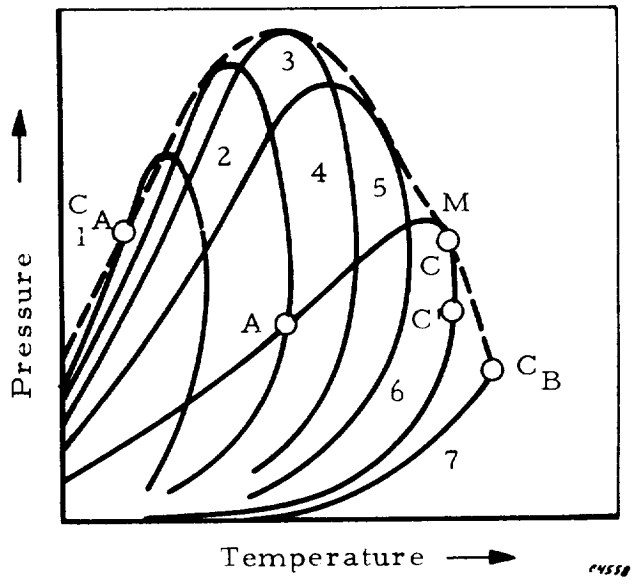

Figure III-2. Binary Pressure-Temperature Curves at Constant Composition (Reference 40).

Figure III-1 is for a single composition. To represent composition as a variable one could use a system of three coordinates and obtain a solid figure containing a P-x surface. In order to represent, at least partly, all three variables on a plane surface, we can adopt the usual expedient of taking a number of sections through this surface at constant composition and projecting the resulting curves all onto one plane as illustrated by Figure III-2. Typical systems exhibiting the behavior illustrated in this figure are CO_2-SO_2 and ethane-heptane (Reference 41). Curves 1 and 7 are the vapor-pressure curves of the two pure components, and the others are the typical curves for a mixture with a vapor and a liquid branch. The points where the vapor branch of one curve intersect the liquid branch of another represent coexisting phases in equilibrium (point A, for example). It is clear that this must be so from the fact that a liquid and vapor phase at the same pressure and temperature must be in equilibrium. Curve C_AC_B is the envelope curve joining the critical points of the two pure components, and it is the locus of the critical points of the mixtures. It is designated the "critical curve". The form of this curve shown in Figure III-2 is one of the commonest, but not the only one that has been observed. Cases have been investigated in which the critical curve exhibits a maximum and also a minimum with respect to the temperature.

Figures III-3 through III-5 show the P-x, T-x and yz curves respectively, for the type of system depicted on the P-T diagram in Figure III-2. In Figure III-3, in cross section I, the temperature is below the critical of either pure component; in II and III, it is above the critical temperature of the more volatile component but below that of the other component. Mixtures richer in component A than x_1(cross section II) or x_2 (cross section III) can no longer form two phases. In Figure III-4, cross section I, the critical pressure is below that of either component; in II it is above that of the less volatile one; in III, above the critical pressures of both components. Corresponding curves on the yx diagram at constant pressure are shown in Figure III-5.

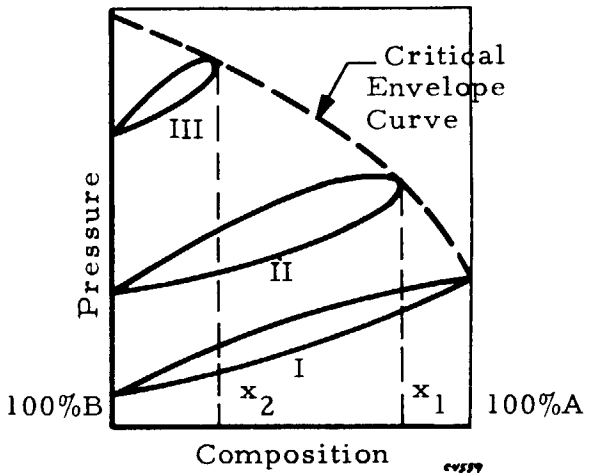

Figure III-3. Isothermal Pressure-Composition Curves of a Binary Solution in the Critical Region

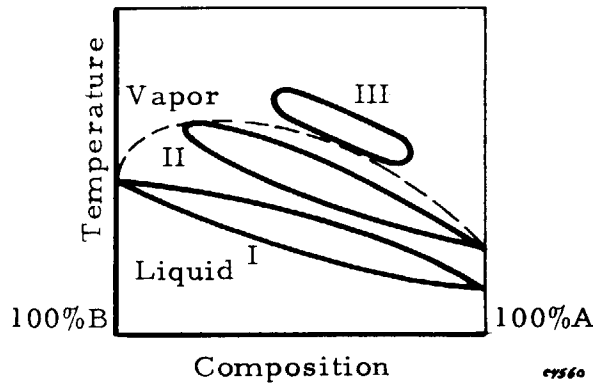

Figure III-4. Isobaric Temperature-Composition Curves of a Binary Solution in the Critical Region

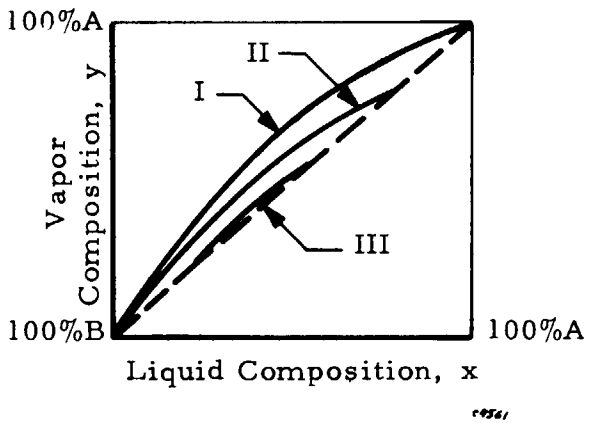

Figure III-5. Vapor-Liquid (y-x) Curves for a Binary Solution in the Critical Region

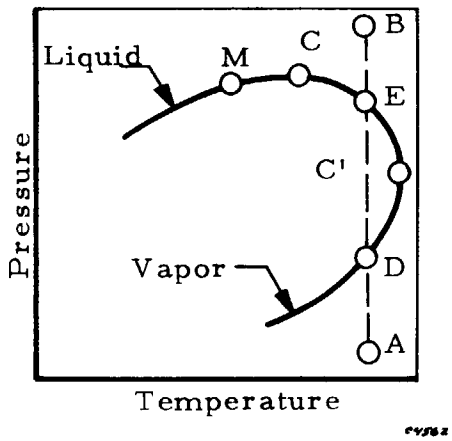

Figure III-6. Retrograde Condensation

A very interesting phenomenon takes place when a mixture whose composition lies between that of the critical point and of the cricondentherm point is isothermally compressed. In Figure III-6, which is an enlargement of the critical region in Figure III-1, line AB represents an isothermal compression at constant total composition, starting with a vapor at A. At D the dew-point line is reached; and as compression is continued, the amount of liquid at first increases, then passes through a maximum and decreases, and finally disappears altogether as the dew-point line is reached again at E. Further compression will produce no separation into two phases. This phenomenon is known as "retrograde condensation" and was first reported by J. P. Kuenen in 1892 (Reference 1 and 42).

The change in the relative amount of the two phases is more easily visualized on the P-x diagram (Figure III-7) because any vertical line through the two-phase region cuts the horizontal tie lines into segments whose lengths are proportional to the amounts of the phases. Thus, for example, HG/FH equals the ratio of the mass of liquid to the mass of vapor. At D, this ratio is zero and again at E. Between these two points it obviously passes through a maximum.

At any composition to the left of that of the critical point C, the condensation phenomena are of the ordinary type, i.e., the liquid phase first formed at the dew point continues to increase until the whole system is liquid at the bubble point. This may be seen by considering the path LN.

When the relative position of the points C and C' is as indicated in Figure III-8, we have the peculiar situation that the line of isothermal compression ADEB now reaches the liquid line at D and the phase which separates would ordinarily be regarded as a vapor phase.* As compression

*In the critical region there is no clear-cut distinction between a liquid and a vapor phase because the physical properties such as density and viscosity are very nearly equal for each phase, and in the homogeneous region above the critical point there is no difference at all. In the critical region it might be better to refer to the two phases as the "less dense" and the "more dense" phase.

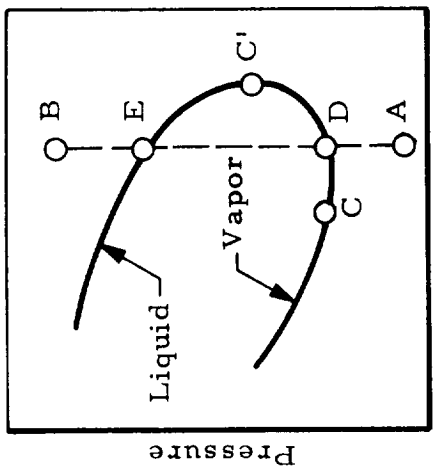

Figure III-8. Retrograde Condensation of the Second Kind

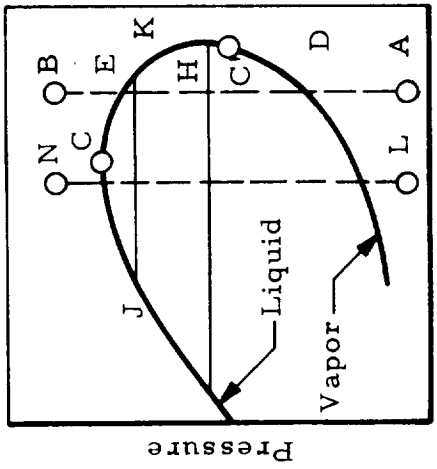

Figure III-7. Retrograde Condensation Illustrated on a Pressure-Compositional Diagram

proceeds, this would increase in amount, pass through a maximum, and then decrease to zero at E when the liquid line is again crossed. This phenomenon was predicted by Kuenen and called by him "retrograde condensation of the second kind." (This phenomenon is illustrated in the next section for the system helium-hydrogen which illustrates retrograde condensation of the first kind and also the second kind.) Similar phenomena would be predicted for an isobaric process by using either the P-T or the I-x diagrams except that in this case the composition would be one lying between those of points C and M (Figure III-1) and the type of retrograde condensation would depend on the relative position of these two points. Use of these methods of representation are shown next for a typical pressurant and propellant.

C. ILLUSTRATIVE PHASE EQUILIBRIA DATA FOR THE SYSTEM NORMAL HYDROGEN-HELIUM

Typical data plots are shown for the system normal hydrogen-helium, taken from Reference 12 to illustrate the above described graphical means of representation. The behavior of this system is seen to be typical of binary systems in which the critical temperatures of the components are relatively far apart. Similar behavior is exhibited, for example, by the systems nitrogen-hydrogen and nitrogen-helium. The closed loops in Figure III-9 represent temperatures for which the critical point occurs at a pressure below 500 psia. These loops show a region of retrograde condensation of the first kind, which is that portion of the loop lying to the right of a vertical line through the critical point. The region in which the liquid lines cross (Figure III-9 and III-10) is one of retrograde condensation of the second kind. On the T-x diagrams, this appears as a region in which individual liquid lines (isobars) have both a positive and a negative slope, Figures III-11 and III-12. This region is seen to be restricted to helium concentrations of 4 mole % or less, and to pressures below about 230 psia. Over most of the range covered in this study, the data exhibit reverse order solubility, which is defined as an increase in solubility of a constituent with increasing temperature at constant pressure.

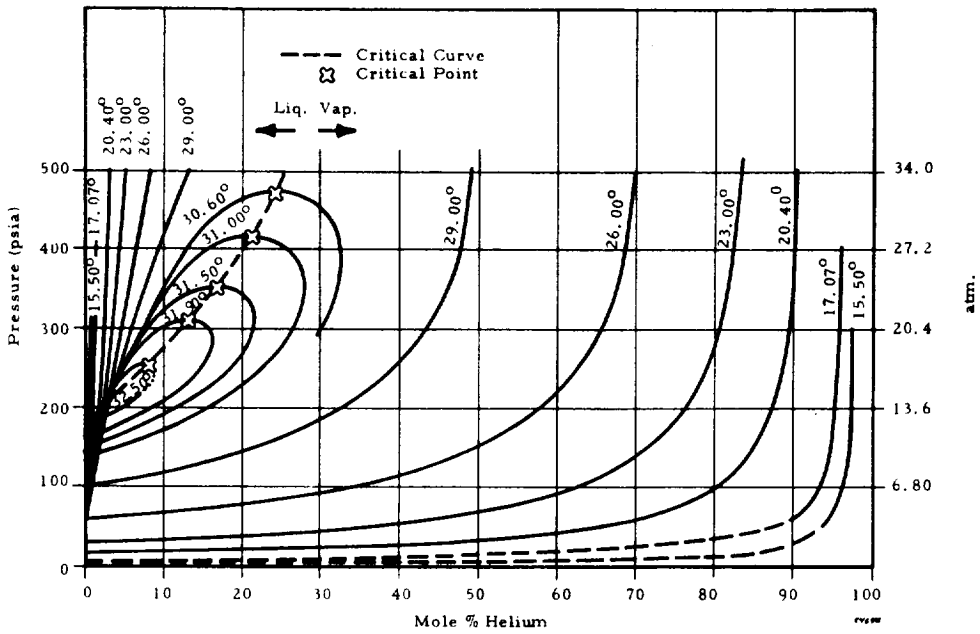

Figure III-9. Isothermal Pressure–Composition Diagram for the System Normal Hydrogen-Helium

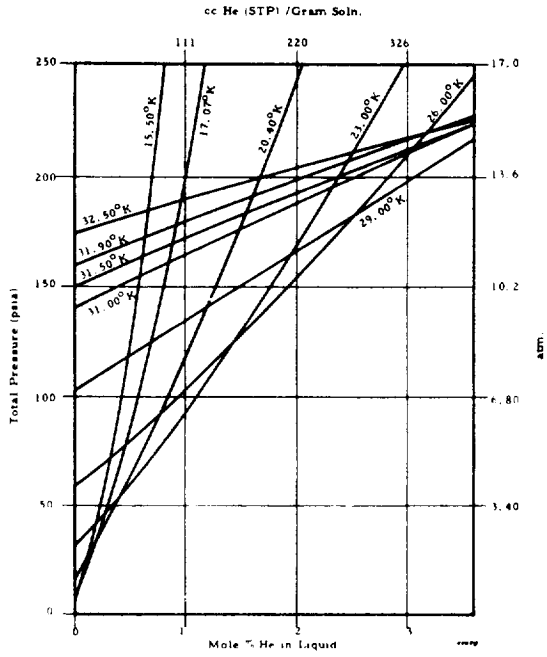

Figure III-10. Isothermal Pressure–Composition Diagram for the System Normal Hydrogen-Helium, showing Liquid Region on Expanded Scale

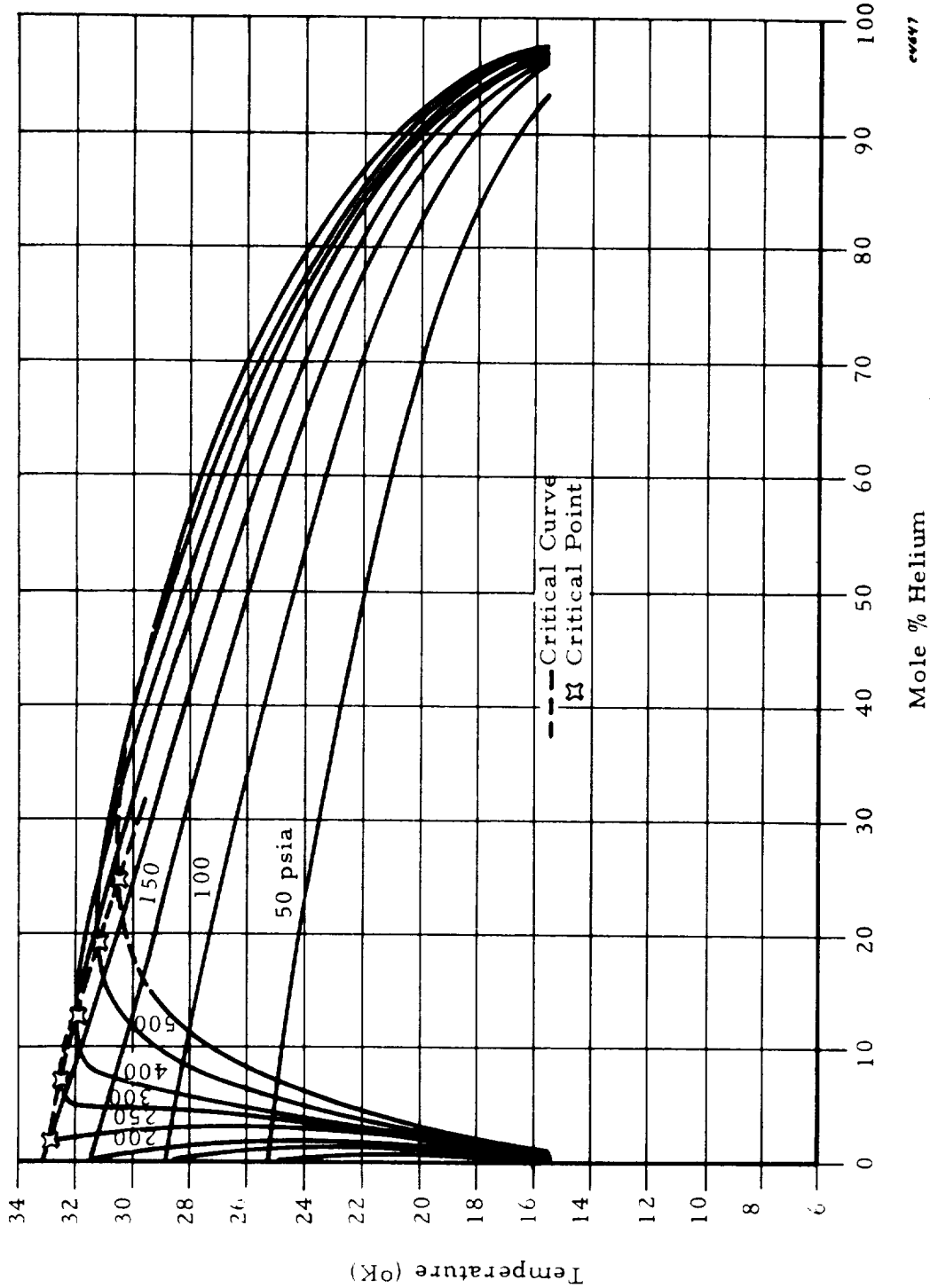

Figure III-11. Isobaric Temperature-Composition Diagram for Normal H_2-He

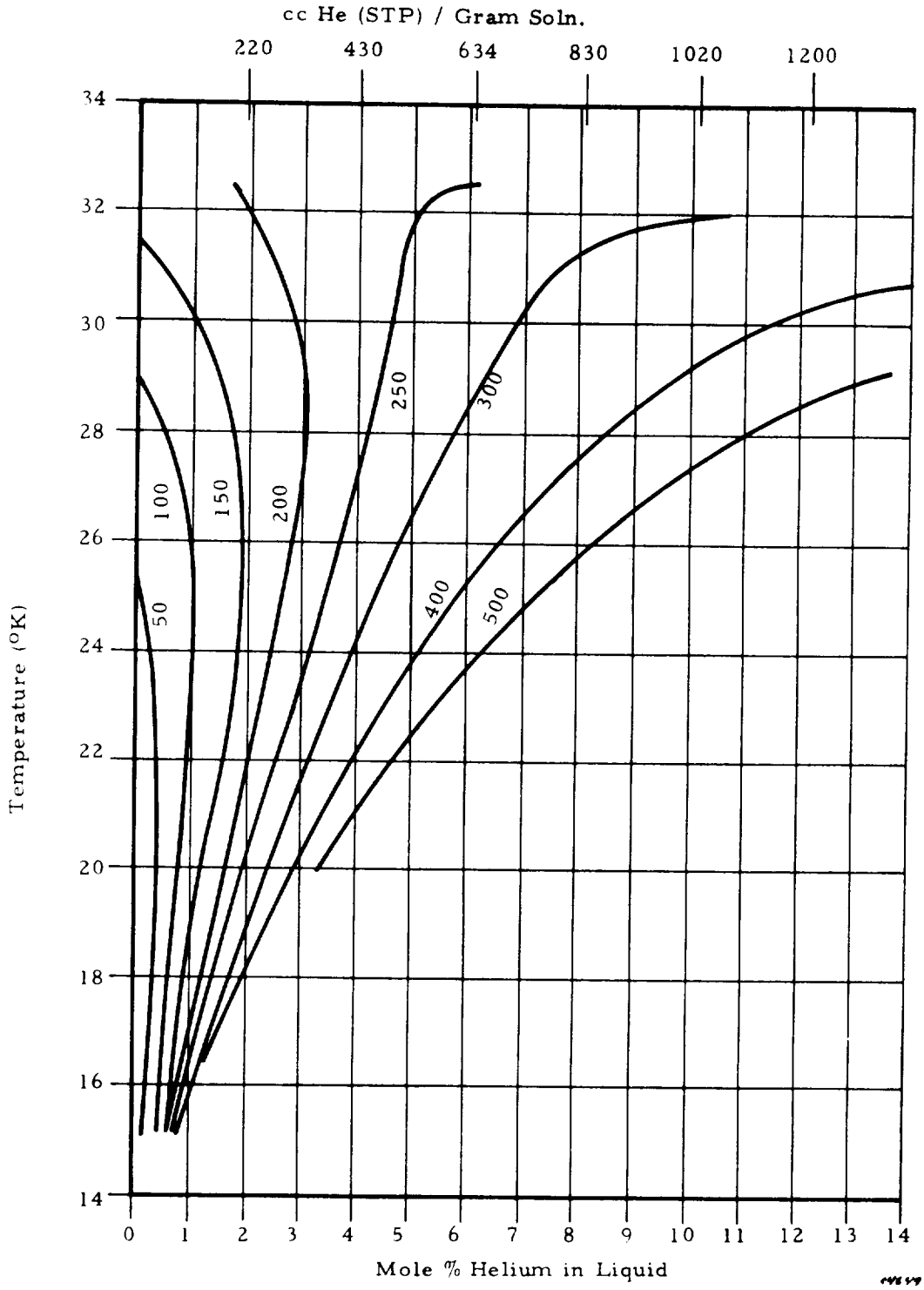

Figure III-12. Isobaric nH_2:He Temperature-Composition Diagram Showing Liquid Region on Expanded Scale

The critical curve locus indicated in Figures III-9, III-11 and III-13 has been estimated from a study of the trend of the data on P-x, T-x, and P-T plots. The loops at 31.00 and 31.50°K were almost completely closed with experimental data points, which served to define the shape of loops at nearby temperatures. The critical curve obtained from this diagram was cross plotted on T-x and P-T diagrams and found to be consistent with the data as it appears on those diagrams. On the P-T plot, this critical curve or envelope is tangent to each of the curves of constant composition, with the point of tangency representing the junction of the dew- and bubble-point curves for that composition.

The equilibrium "constants," K, the ratio s of the vapor-phase to the liquid-phase mol fractions, are shown in Figure III-14.

The very accurate partial molal properties for each component and other thermodynamic data, determined to the accuracy needed, were not available to precisely calculate theoretical phase equilibria data for this system. Further discussion on this point and a comparison of these experimental data with other test data available in the literature are in the reference from which this work is taken, Reference 12.

D. STUDIES AT McDONNELL DOUGLAS

In studies conducted at Astropower Laboratory, McDonnell Douglas Corporation, a specially developed stainless steel apparatus was used for saturation and sample selection. Gas chromatographic procedures were used for analysis. The details of the procedures are reported in Reference 46 and the numerical data are included in Section IV of this report.

The apparatus used for determination of equilibrium gas solubilities has gradually evolved after considerable investigation. The basic operations involve condensing the propellant under investigation into the evacuated bomb which is positioned inside a cryostat. The bomb and its contents are brought to the desired temperature and then pressurized to the desired level with the pressurant gas. The contents of the bomb

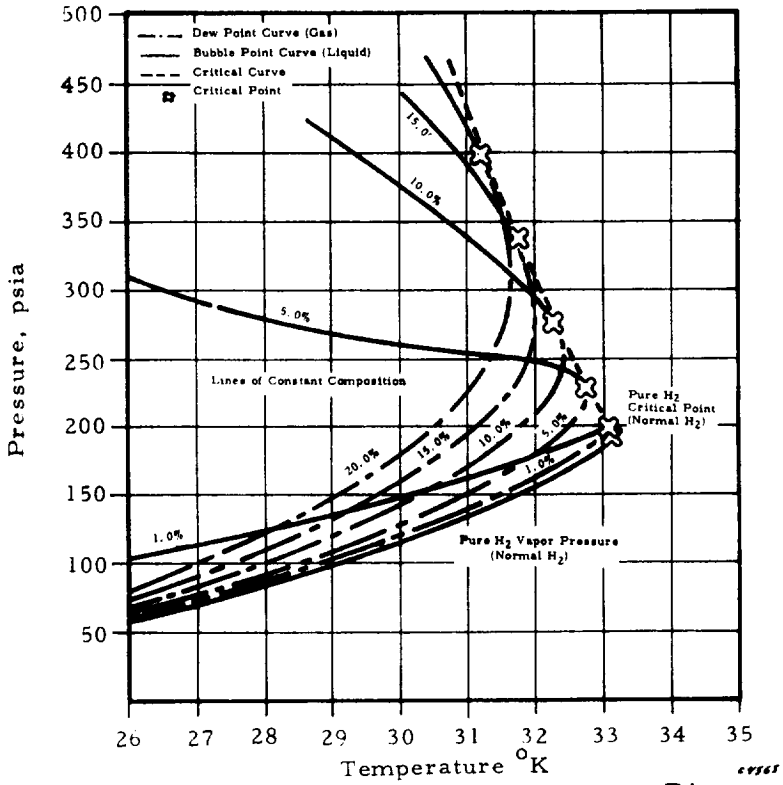

Figure III-13. Pressure-Temperature Diagram for Normal H_2-He

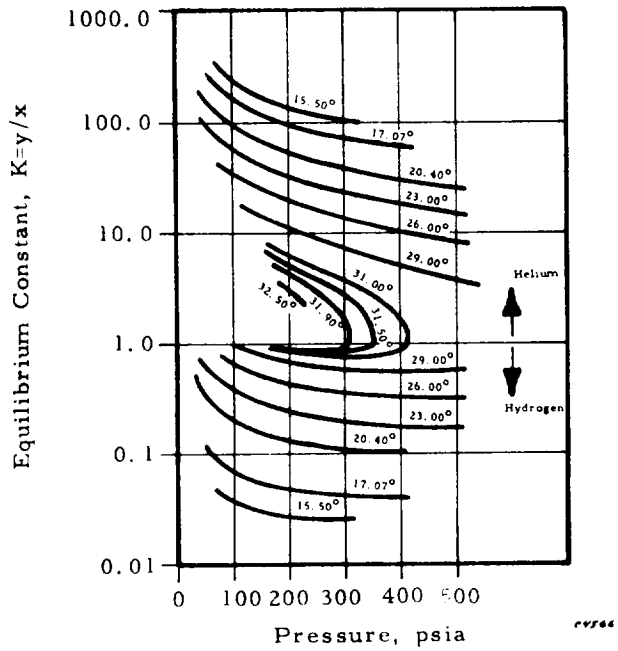

Figure III-14. Equilibrium K-Values for Normal H_2-He

are agitated by shaking the bomb mechanically. As the pressurant gas goes into solution, the pressure in the vapor phase decreases and it may be necessary to repressurize periodically to the desired level.

The pressure vessel containing the solution is constructed of stainless steel, nominally of 1-liter capacity. A Vari-drive motor, operating through a reducing gear at 4-6 rps, imparts a reciprocating motion of about one-inch amplitude to the bomb by way of the support rod which screws into the nut welded to the bomb lid. The bomb lid is equipped with three welded-in flared-tube AN nipples. One accommodates a thermocouple which is placed in a well extending into the liquid phase near the bottom of the bomb. A second thermocouple located outside the bomb senses the Dewar bath temperature and controls LN_2 or warm GN_2 addition. The cryostat is insulated with glass wool at the top and covered with polyethylene sheet to preserve a nitrogen blanket and keep out atmospheric moisture. The bomb temperature stabilizes at about $\pm$ 0.5°F because of its large thermal inertia.

After attainment of equilibrium, a liquid sample is drawn out through an eductor tube that extends into the liquid phase to the bottom of the bomb. The liquid phase sample is withdrawn by opening the bleed valve in the line, whereby the sample is forced out through the bleed valve, flashed into a vapor and collected in an evacuated cylinder. The eductor tube is designed to reduce the liquid volume in the line to a minimum; nevertheless a preliminary purging of the line is necessary to clear the eductor tube of any liquid phase not saturated with pressurant gas.

Once the representative gas sample has been collected in the sample cylinder, it is analyzed to determine the concentration of pressurant gas. The operator is obliged to resample the liquid phase after an appropriate additional time of equilibration to assure attainment of true equilibrium.

Nitrogen is used as a carrier gas when samples are being analyzed for helium, and helium is a carrier when nitrogen is being analyzed. Instrument calibrations are made using standard certified gas mixtures. Normally, a calibration sample is run after every 4th sample analysis.

Sample analysis is carried out by comparing the peak area produced by the sample with the area produced by the appropriate calibration mixture. Suitable factors are introduced if the recorder attenuation setting for a given sample size is different for the sample and calibration mixture. A constant flow rate of carrier gas, usually 35 ml/minute, is used for all analyses and calibrations.

Although the GC analysis became fairly standardized and routine, each system under examination required special consideration with respect to separation of the pressurant gas peak and considerable column experimentation was required.

Some of the propellants produce oxygen by reaction with the constituents of the column materials. This is not a problem if helium is the constituent of analytical interest, as the oxygen peak is readily separated from helium. However, if nitrogen is being analyzed, the oxygen cannot readily be separated and it causes interference because of its higher thermal conductivity. In some cases, it proved expeditious to use oxygen as a carrier gas for nitrogen analysis when oxygen was formed in the GC column. Because of the fairly small difference in thermal conductivity between oxygen and nitrogen, this procedure is feasible only if the nitrogen content of the sample is fairly high, viz., about 5% or more by volume.

IV. PRESSURANT SOLUBILITIES IN PROPELLANTS

A. INTRODUCTION

Data for various pressurant, oxidizer, and fuel systems are presented in graphic and tabular form in the following subsections. See the Table of Contents of this volume for a listing of the specific gas and propellant systems for which data have been compiled.

The data in this Design Guide do not include all the available solubility information of the systems listed. Material that is superseded by more recent or accurate data has not been included unless the older material presented information of specific value that was not adequately covered otherwise. In nearly all cases the reader can be led to further information on a specific system by consulting the references given here. The authors have endeavored to cover both the open and classified literature up to July 1968.

For ease of reference, the material is organized into the following groups: pressurant gases, propellant oxidizers, and propellant fuels, in the generally accepted sense of these terms. The order of propellants in each group is alphabetical. For each group a table of pertinent physical properties of the compounds involved is included in the preliminary discussion.

The data in most systems are presented in both isothermal and isobaric composition diagrams for easy reference and interpolation in areas of interest. Tables of experimental data are included where they may be of further use (i.e. in preparing accurate expanded plots in specific pressure regions). It should be noted that in all cases the pressures given are total system pressures (not component partial pressures) unless otherwise stated. On most of the isothermal pressure-composition diagrams (e.g. Figure IV-23) the curves have been extended to zero concentration of pressurant gas, and the x-axis intercept is the vapor pressure of the pure propellant at the temperature of the isotherm.

Nomographic presentation of gas solubility data is rarely used in practice, but it can be of great value where frequent references to a system

are needed which involve tedious and inaccurate interpolation. As an example of this technique, the Astropower Laboratory data for the fluorine-helium system has been reduced to the pressure-temperature-composition nomograph shown in Figure IV-1. The ease of making interpolations involving all three variables, as illustrated in the key, is apparent. The reader is directed to the book by Levens (Reference 43) for the mechanics of constructing such diagrams for particular cases.

B. PRESSURANT GASES

Properties of ten selected pressurant gases are given in Table IV-1. However, of these ten, helium and nitrogen are the only widely used pressurant gases for propellant systems, although hydrogen, neon and argon see occasional service.

TABLE IV-1

PROPERTIES OF SELECTED PRESSURANT GASES (Reference 90)

Pressurant Gas	γ Cp/Cv (60°F)	Molecular Weight	Boiling Point at 1 Atm (°R)	Critical Properties		Gas Specific Heat Cp-BTU/lb°R Nominal Temp/ Low Press.
				Temperature (°R)	Pressure (psia)	
Air	1.4	29	142	239	547	0.24
Ammonia	1.28	17	432	730	1640	0.523
Argon	1.67	39.9	15	271	706	0.125
Carbon dioxide	1.28	44	351	548	1073	0.18
Helium	1.66	4	8	10	33	1.25
Hydrogen	1.4	2	37	60	188	3.39
Methane	1.26	16	201	343	674	0.55
Neon	1.64	20.2	50	80	394	0.25
Nitrogen	1.4	28	140	227	493	0.25
Propane	1.13	44.1	415	666	617	0.25

Since the binary system liquid nitrogen-helium has received extensive study, its equilibrium composition data are also included in this section.

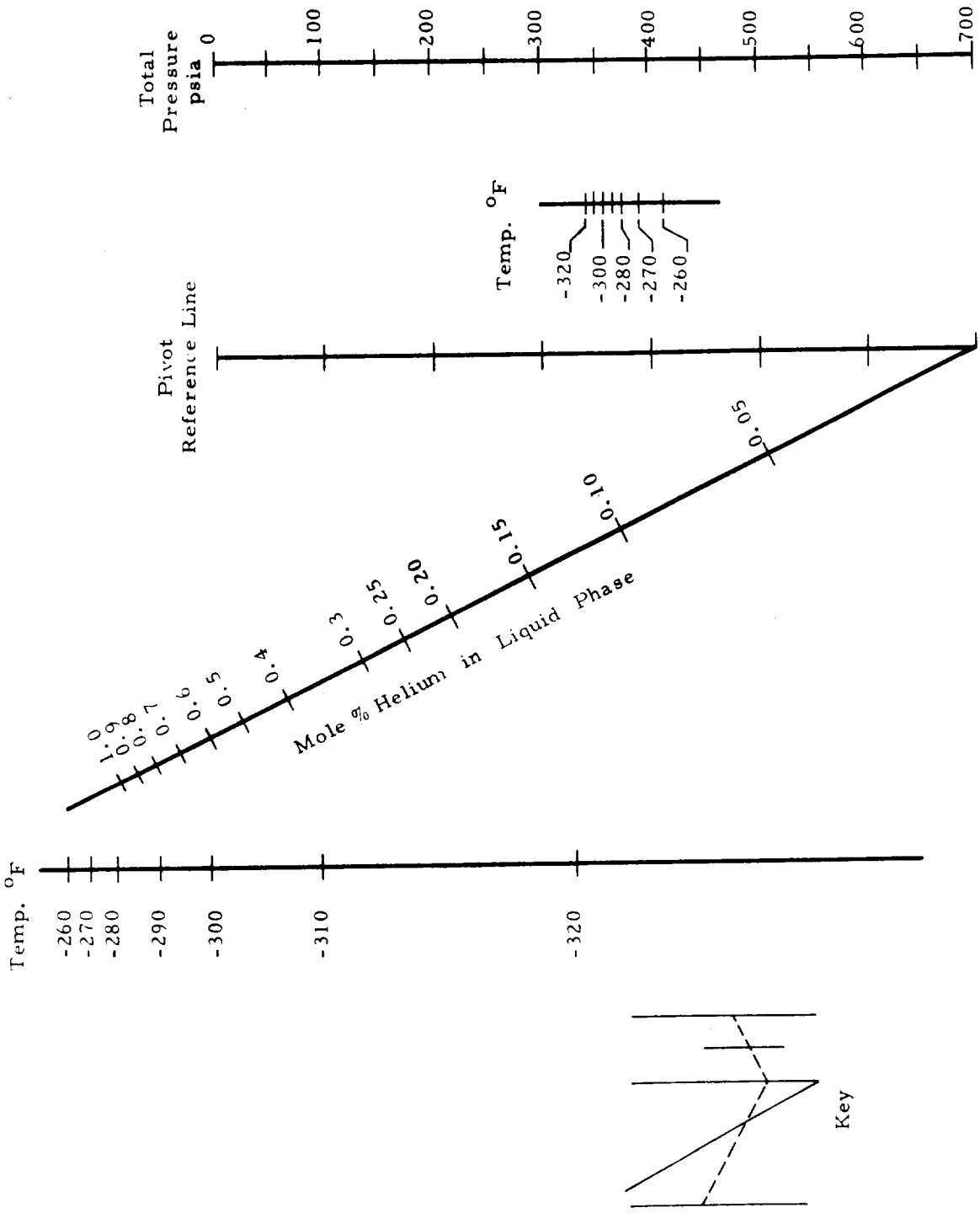

Figure IV-1. Nomograph - Helium Solubility in Liquid Fluroine

TABLE IV-2

PHYSICAL PROPERTIES OF PROPELLANT OXIDIZERS

Oxidizer	Mol. Formula	Mol. Wt.	M. P. °R	B. P. °R	Tc °R	Pc psia	Liquid Range °R	Ref.
Chlorine Pentafluoride	ClF_5	130.45	306.3	468.1	749.1	769	432.8	47
Chlorine Trifluoride	ClF_3	92.45	352.6	512.9	805	838	452	91
Dioxygen Difluoride	O_2F_2	70.00	197	399.4 dec.	–	–	200 est.	49
70% FLOX[a]	–	36.20 (ave.)	NA	244 est.	NA	NA	160 est.	50
Fluorine	F_2	38.00	96.4	153.1	259.9	808	163.5	47
MON-10[b]	–	85.8 (ave.)	–	–	NA	NA	–	–
Nitrogen Tetroxide	N_2O_4	92.02	447.9	529.8	777	1470	329	91
Nitrogen Trifluoride	NF_3	71.01	116.7	260.8	421.3	657	304.6	47
Nitryl Fluoride	NO_2F	65.01	192	361.3	629.1	–	437.1	55
Oxygen	O_2	32.00	97.8	162.3	277.8	730.6	180.0	91
Oxygen Difluoride	OF_2	54.00	89	231	388	719	299	63
Perchloryl Fluoride	ClO_3F	102.45	228.9	407.5	663	779	434	91
Tetrafluorohydrazine	N_2F_4	104.02	197.7	358.7	559.2	625	361.5	47

(a) Seventy percent by weight of fluorine in oxygen.

(b) Ten percent by weight of nitric oxide in nitrogen tetroxide.

Solubility data for helium in liquid nitrogen are given in Figure IV-2. These data are taken from Reference 44. There is good agreement between this work and the older work of Kharakhorin (Reference 45). Kharakhorin's data are plotted in Figures IV-3 and IV-4 for pressures to 200 atm.

C. SOLUBILITY DATA FOR PRESSURANT GASES IN PROPELLANT OXIDIZERS

Pertinent physical properties for the oxidizers considered here are listed in Table IV-2. The tabulated solubility data and/or the data plots for the oxidizer-pressurant systems which are available are presented in the following sections.

1. Chlorine Pentafluoride-Helium

See Section 2.

2. Chlorine Pentafluoride-Nitrogen

Solubilities of helium and nitrogen in liquid chlorine pentafluoride were measured by Astropower Laboratory for this Design Guide under Contract NAS7-548. The solubility data for these two systems are tabulated in Table IV-3; experimental details may be found in Reference 46.

TABLE IV-3

SOLUBILITY OF HELIUM AND NITROGEN IN LIQUID CHLORINE PENTAFLUORIDE

Test Temperature °F	Vapor Pressure of Propellant psia[a]	Mole Percent Concentration			
		Helium		Nitrogen	
		300 psia	700 psia	300 psia	700 psia
-100	0.59	0.120	0.300	3.53	8.17
-50	3.24	0.196	0.485	3.27	7.43
0	12.1	0.308	0.715	3.35	7.66
+50	34.8	0.412	0.990	2.96	7.61

(a) Reference 47.

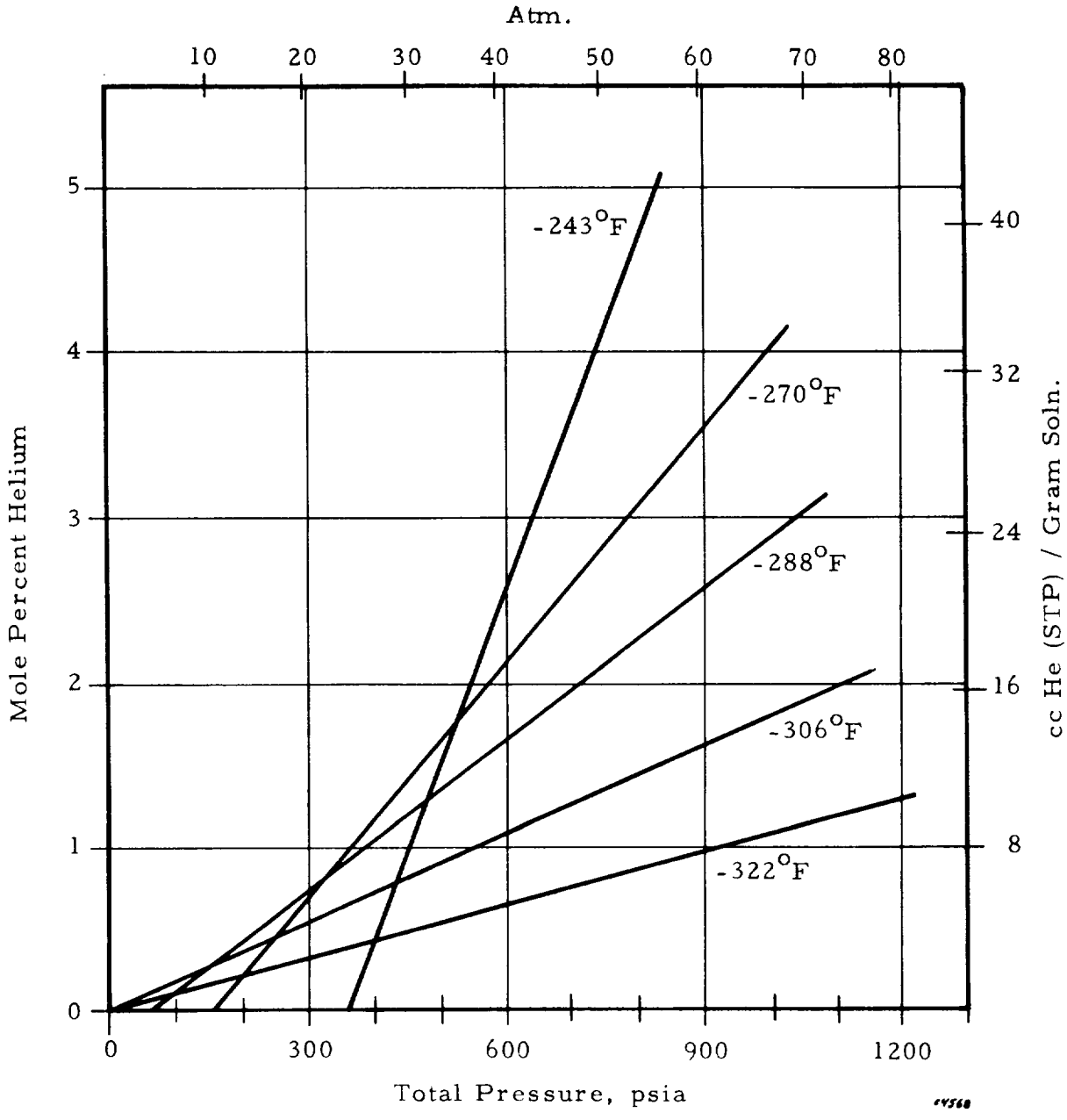

Figure IV-2. Isothermal Pressure – Composition Diagram For the System Liquid Nitrogen-Helium

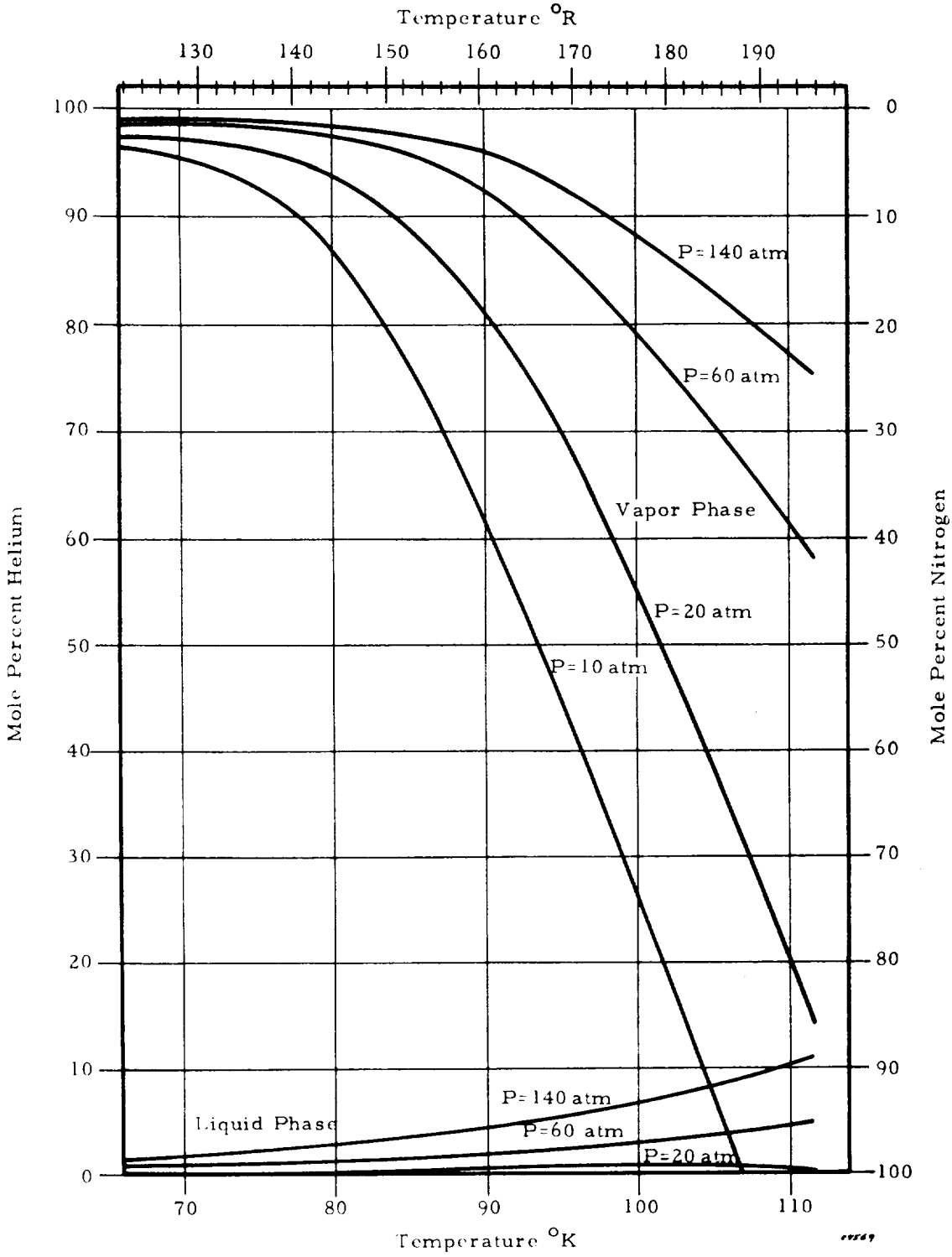

Figure IV-3. Isobaric Equilibrium Concentration for the Binary System Nitrogen-Helium

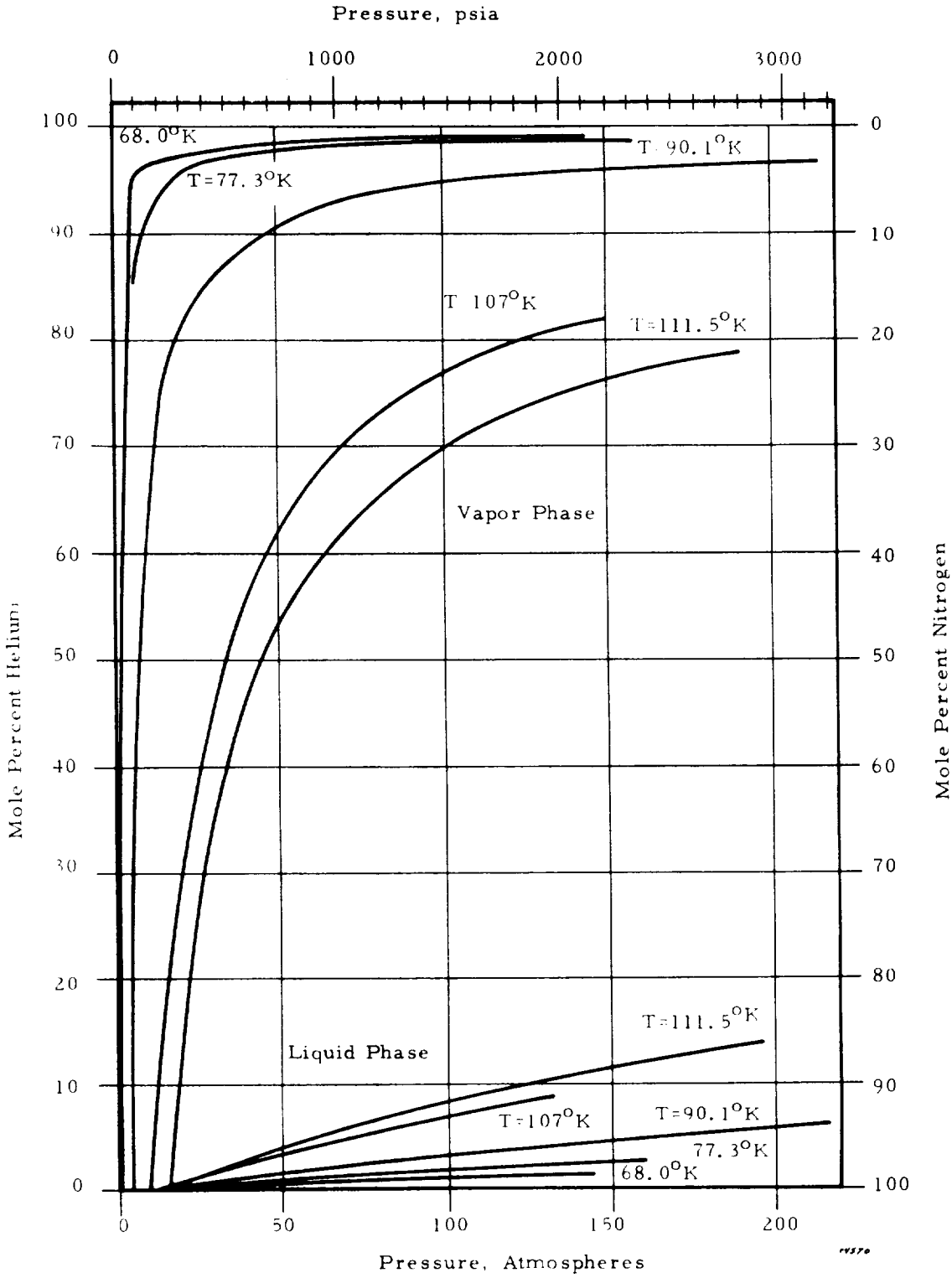

Figure IV-4. Isothermal Equilibrium Concentration Diagram for the Binary System Nitrogen-Helium

The results reported in the table are obtained from duplicate analyses for two successive samples. Agreement of these values within experimental error was accepted as indication that solution equilibrium had been attained.

These data are presented as isothermal pressure-composition and isobaric temperature-composition plots in Figures IV-5, IV-6, IV-7 and IV-8. Isobars at 150 and 500 psia have been constructed by interpolation for each system.

3. Chlorine Trifluoride-Helium

See Section 4.

4. Chlorine Trifluoride-Nitrogen

Solubilities of helium and nitrogen in liquid chlorine trifluoride were measured by Astropower Laboratory for this Design Guide, under Contract NAS7-548. The solubility data for these two systems are given in Table IV-4; experimental details may be found in Reference 46.

TABLE IV-4

SOLUBILITY OF HELIUM AND NITROGEN IN LIQUID CHLORINE TRIFLUORIDE

Test Temperature °F	Vapor Pressure of Propellant psia[a]	Mole Percent Concentration			
		Helium		Nitrogen	
		300 psia	700 psia	300 psia	700 psia
-100	0.20	0.025	0.079	0.770	1.91
-50	1.8	0.061	0.160	0.915	1.85
0	4.4	0.101	0.255	0.896	2.07
+50	13.9	0.154	0.340	1.07	2.42

(a) Reference 48.

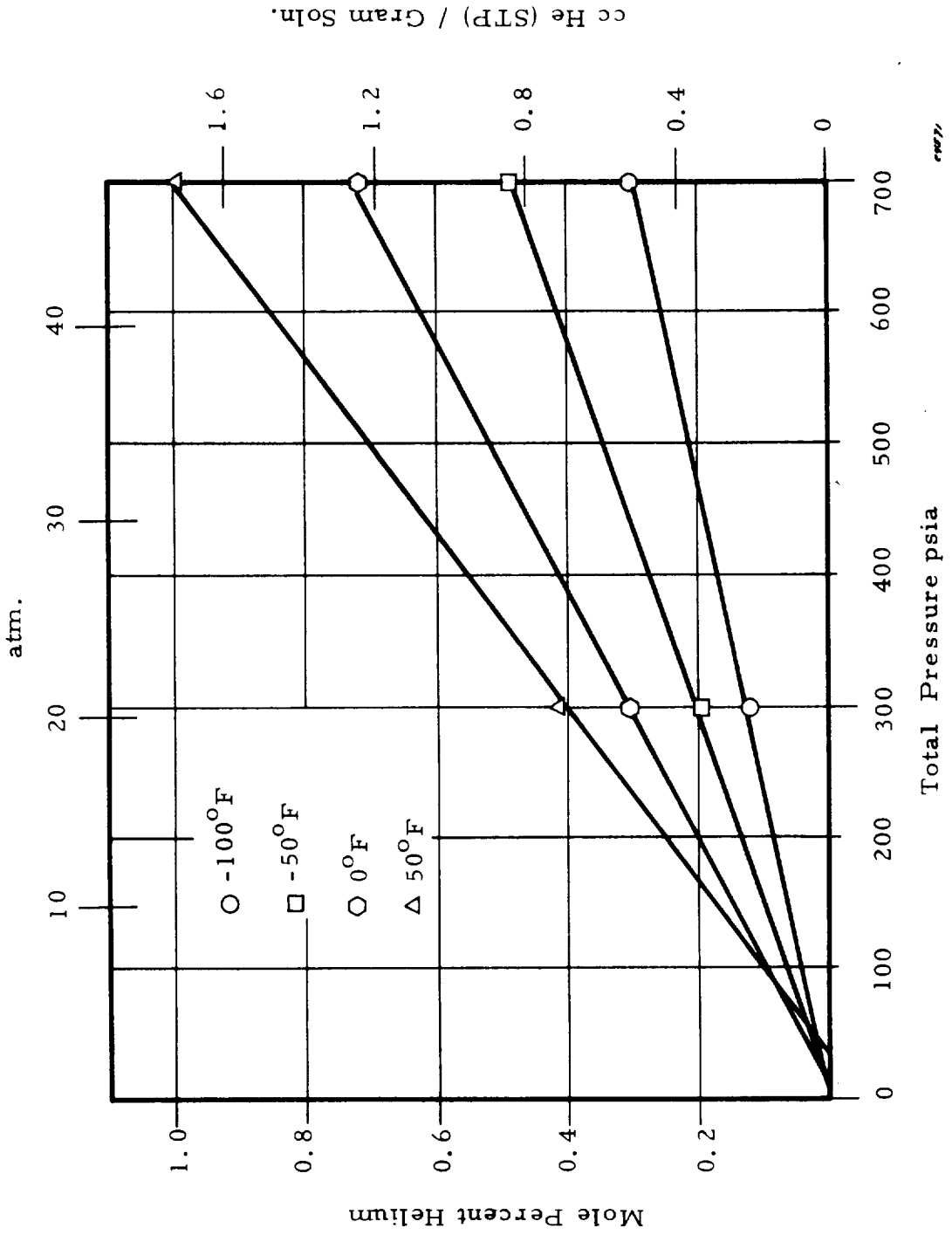

Figure IV - 5. Isothermal Pressure-Composition Diagram For The System Liquid Chlorine Pentafluoride-Helium.

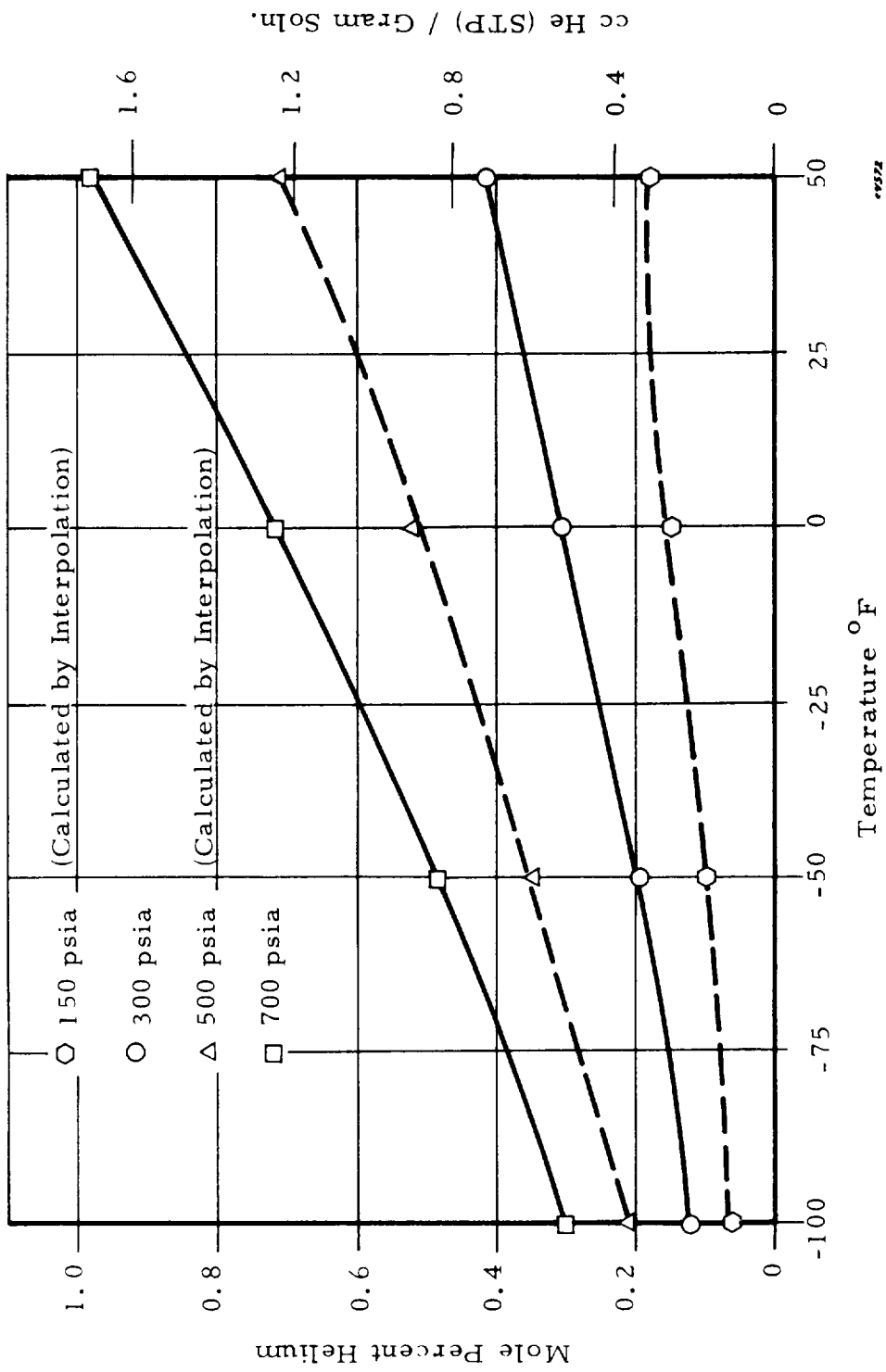

Figure IV-6. Isobaric Temperature-Composition Diagram For The System Liquid Chlorine Pentafluoride-Helium.

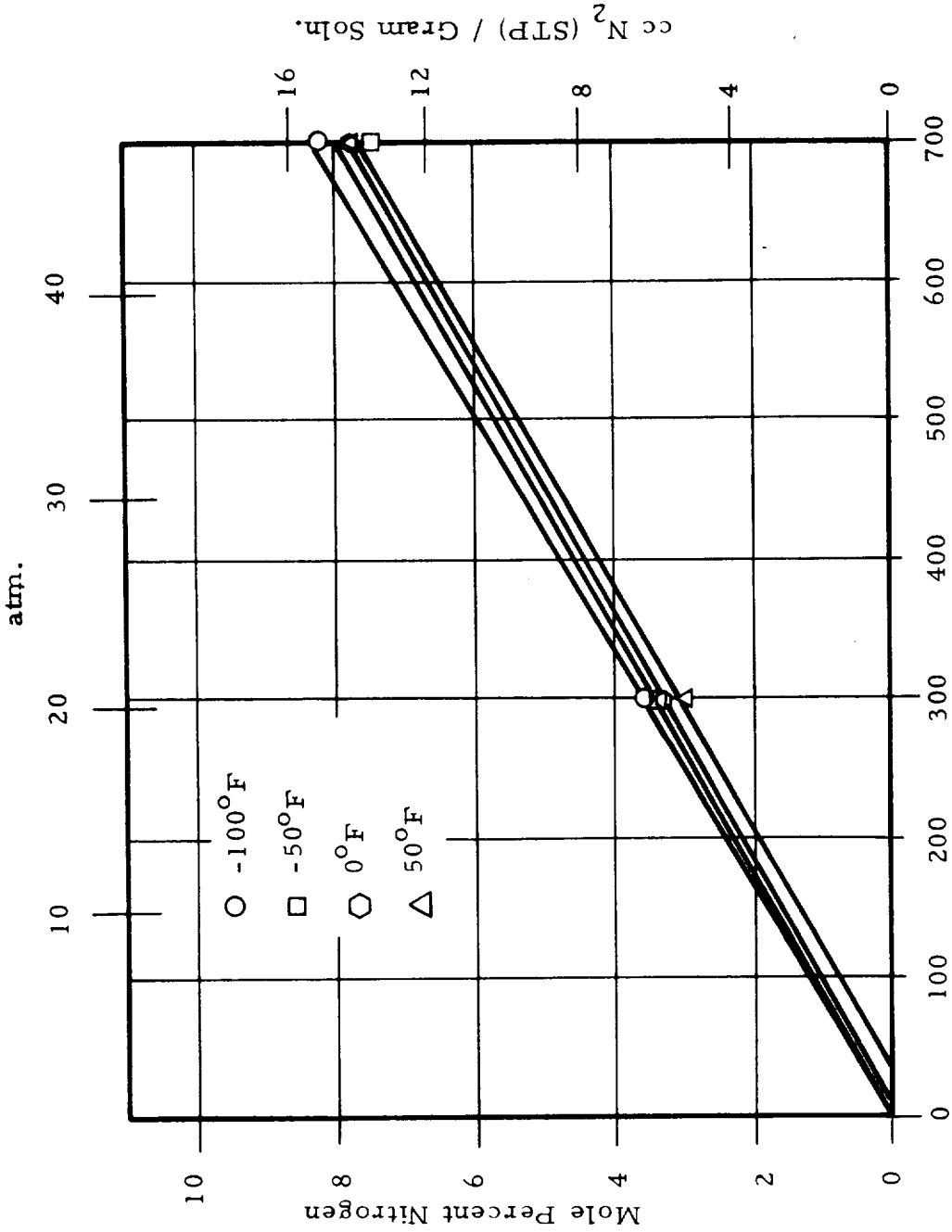

Figure IV-7. Isothermal Pressure-Composition Diagram For The System Liquid Chlorine Pentafluoride-Nitrogen.

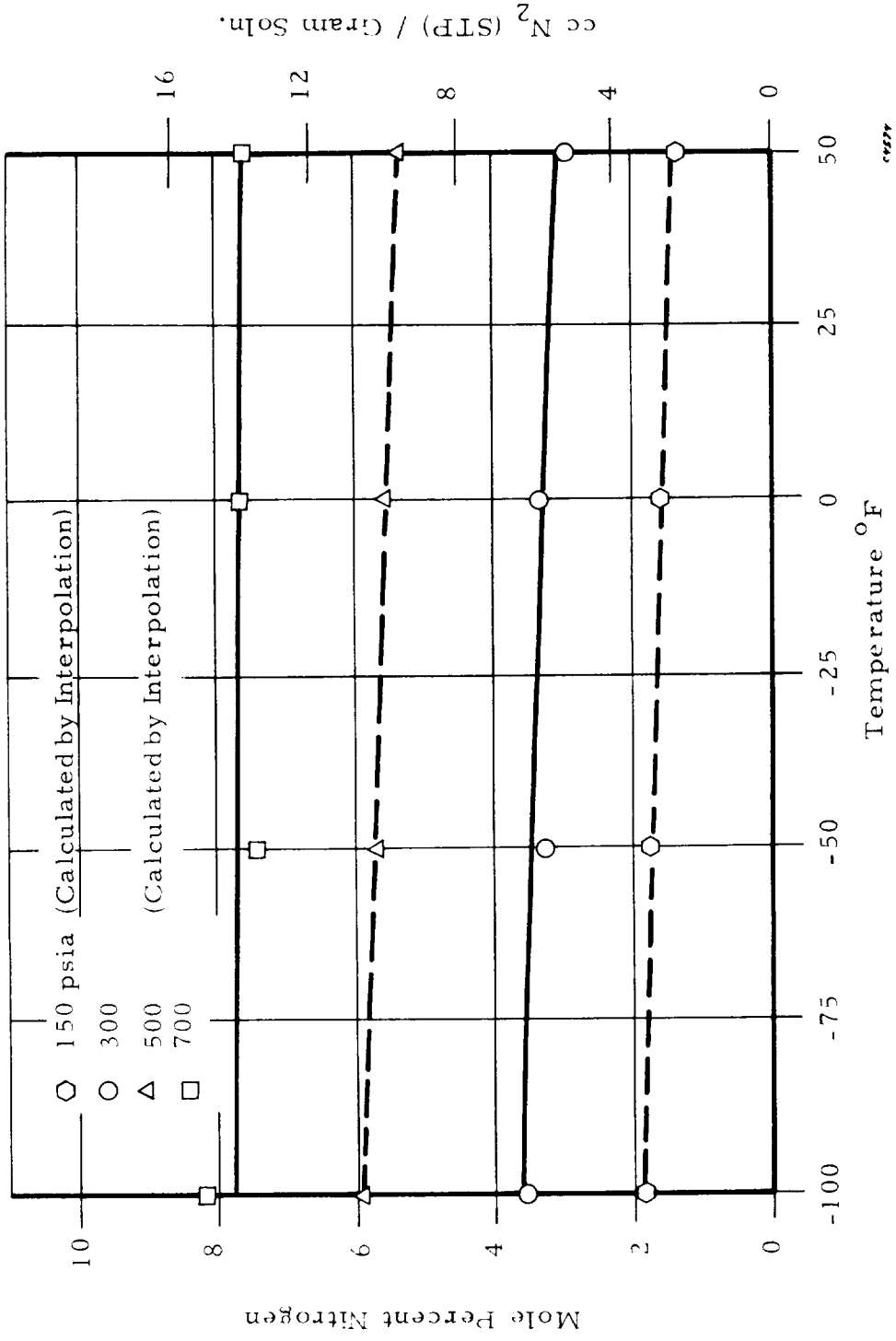

Figure IV-8. Isobaric Temperature-Composition Diagram For The System Liquid Chlorine Pentafluoride-Nitrogen.

The results reported in the table are obtained from duplicate analyses for two successive samples; agreement of these values within experimental error was accepted as indication that solution equilibrium had been attained.

These data are presented as isothermal pressure-composition and isobaric temperature-composition plots in Figures IV-9, IV-10, IV-11, and IV-12. Isobars at 150 and 500 psia have been constructed for each system by interpolation. It is noteworthy that the solubility of nitrogen is quite low and shows an inverse temperature relationship; i.e. the solubility increases with temperature.

5. Dioxygen Difluoride-Helium

The solubility of helium in liquid dioxygen difluoride was measured by Astropower Laboratory for this Design Guide under Contract NAS7-548. The solubility data for this system is tabulated in Table IV-5; experimental details may be found in Reference 46. The results reported in the table are obtained from duplicate analyses for two successive samples; agreement of these values within experimental error was accepted as indication that solution equilibrium had been attained.

TABLE IV-5

SOLUBILITY OF HELIUM IN LIQUID DIOXYGEN DIFLUORIDE

Test Temperature °F	Vapor Pressure of Propellant torr[a]	Mole Percent Concentration Helium	
		300 psia	700 psia
-200.0°	4.5	0.018	0.041
-150.0°	50	0.060	0.130

(a) Reference 49.

These data are presented in an isothermal pressure-composition plot in Figure IV-13.

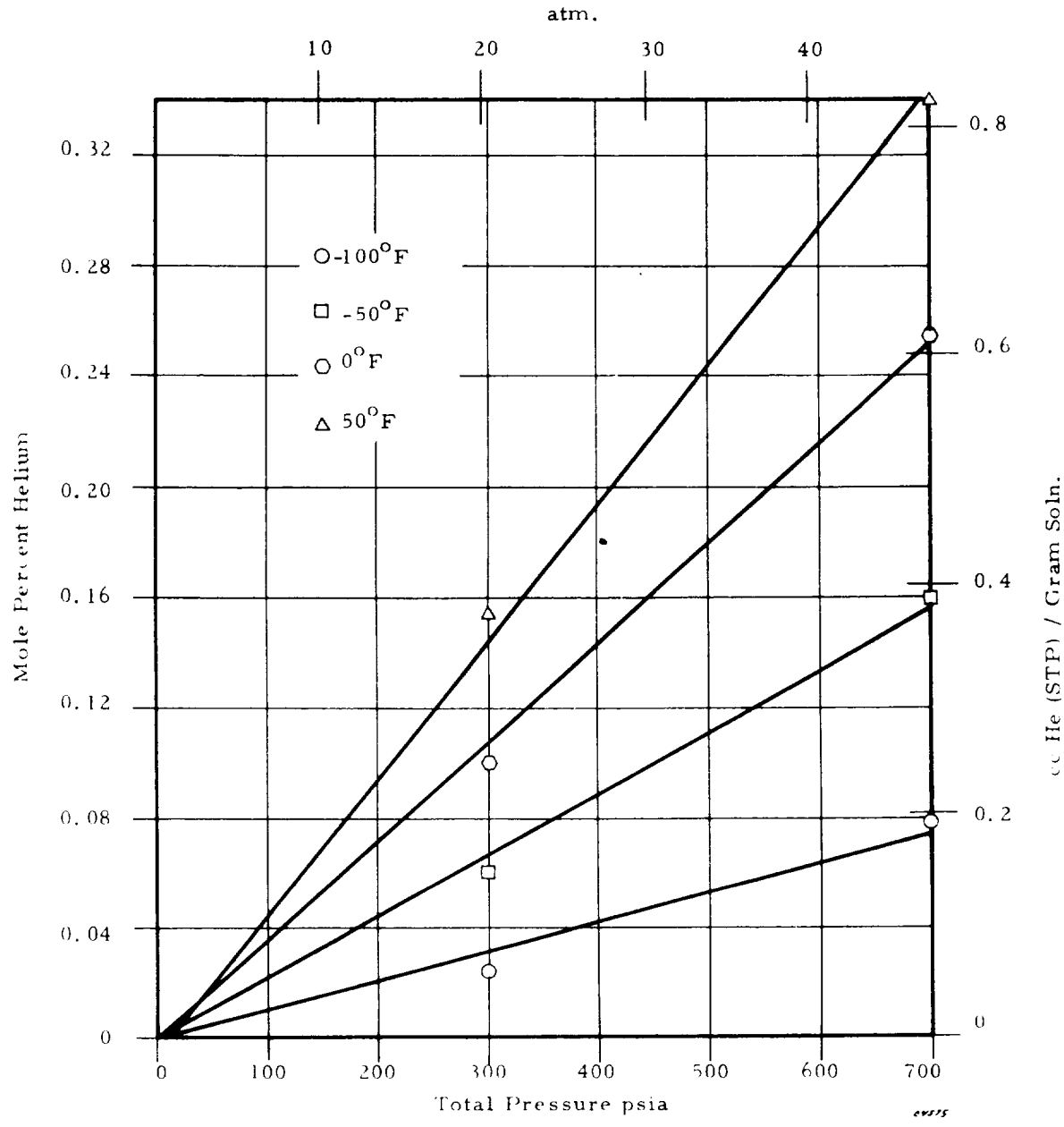

Figure IV-9. Isothermal Pressure-Composition Diagram for the Systme Liquid Chlorine Trifluoride-Helium

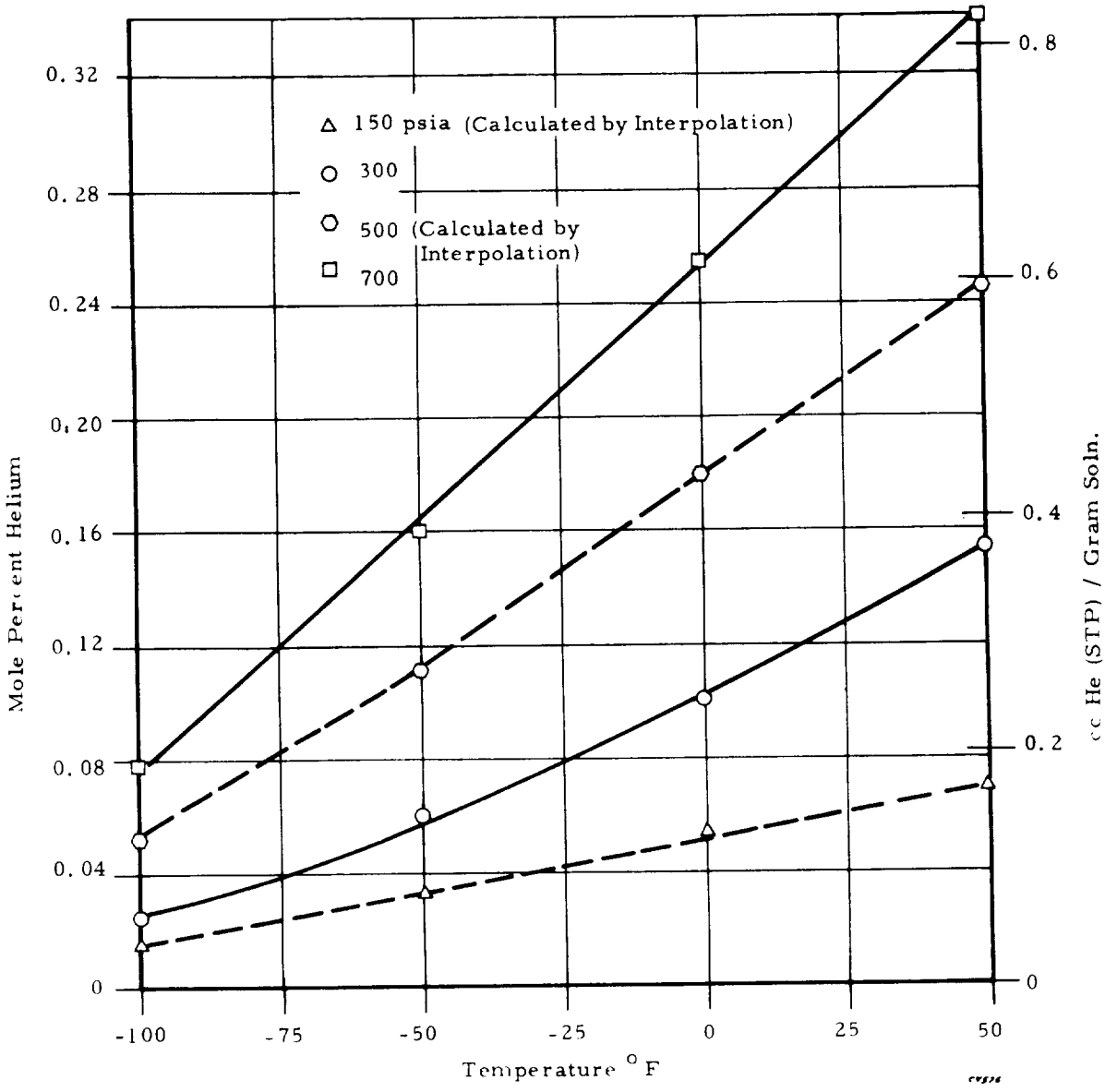

Figure IV-10. Isobaric Temperature-Composition Diagram for the System Liquid Chlorine Trifluoride-Helium

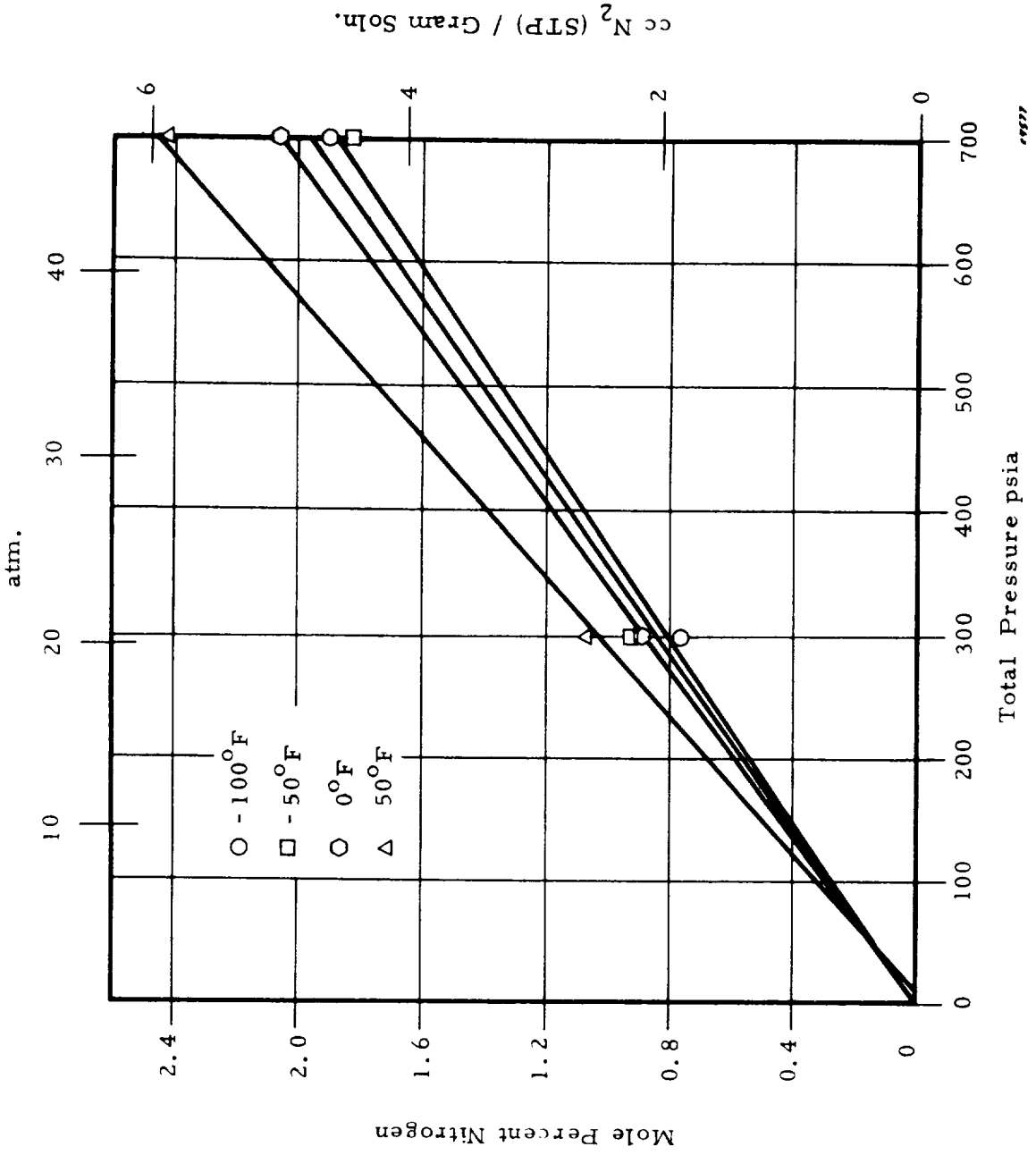

Figure IV-11. Isothermal Pressure-Composition Diagram for the System Liquid Chlorine Trifluoride-Nitrogen

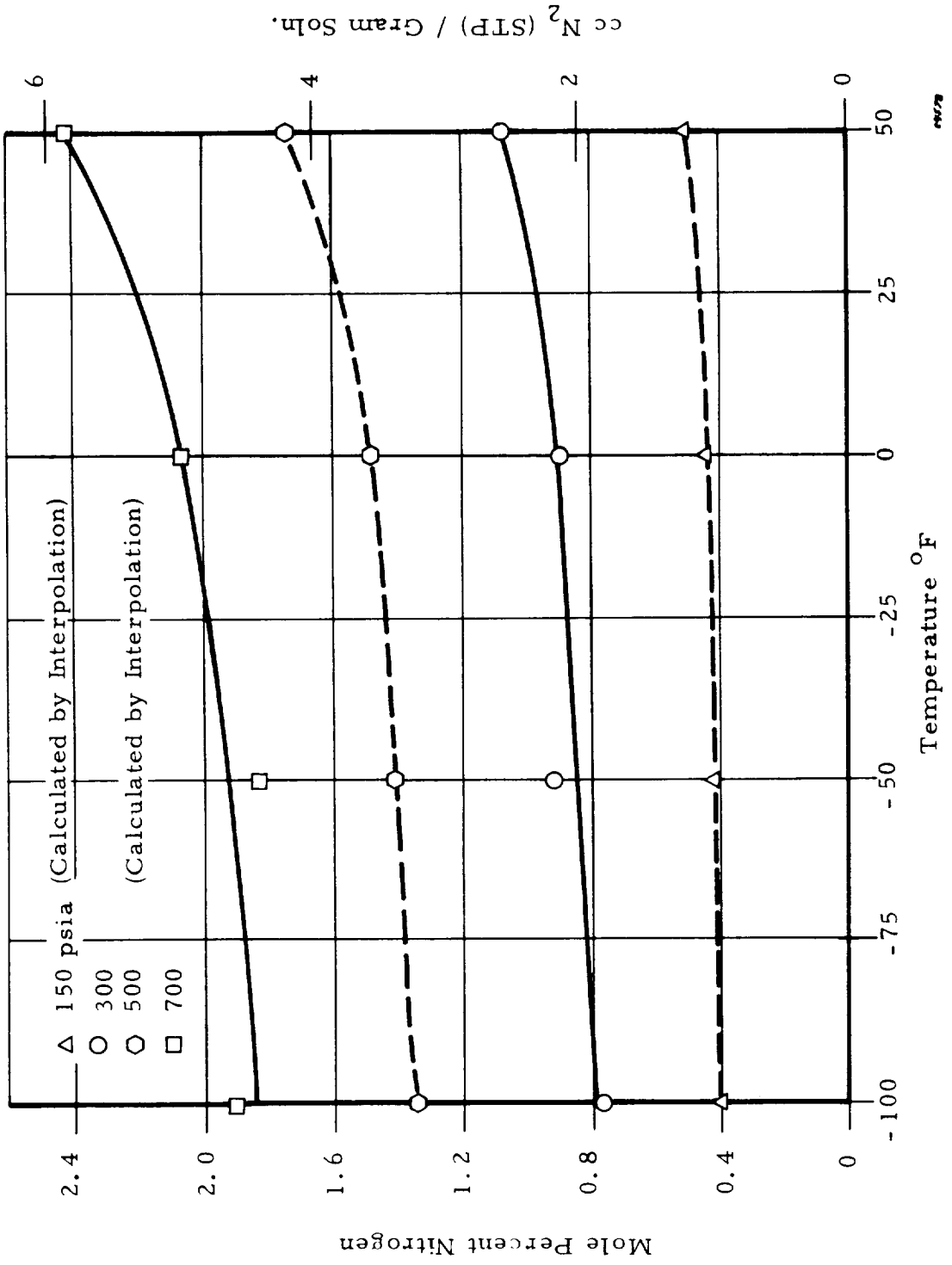

Figure IV-12. Isobaric Temperature-Composition Diagram For The System Liquid Chlorine Trifluoride-Nitrogen

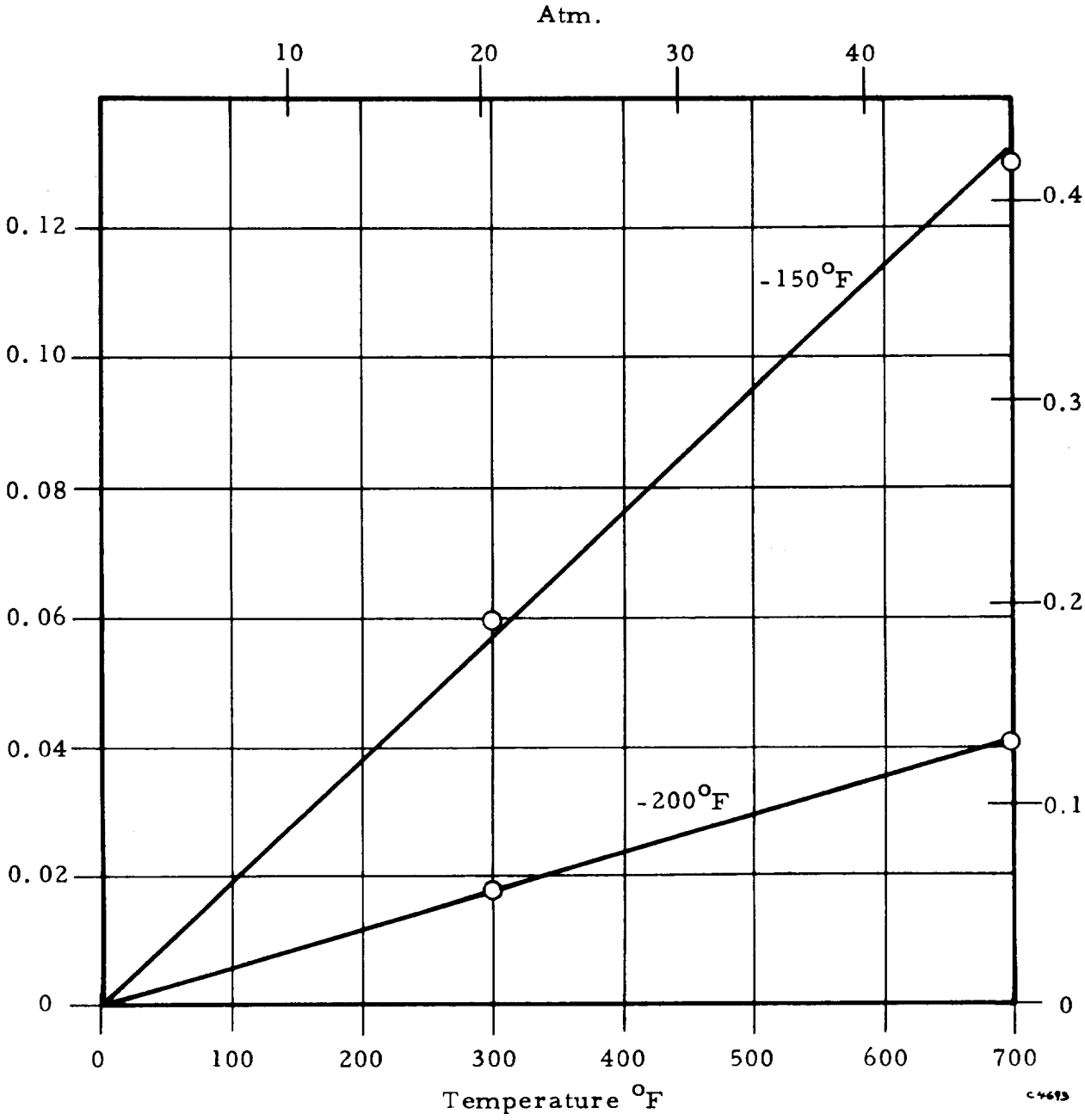

Figure IV-13. Isothermal Pressure – Composition Diagram For the System Liquid Dioxygen Difluoride-Helium

6. 70% FLOX-Helium

The solubility of helium in liquid 70% FLOX (70% by weight of fluorine in oxygen) was measured by Astropower Laboratory for this Design Guide, under Contract NAS7-548. The solubility data for this system is tabulated in Table IV-6; experimental details may be found in Reference 46. The results reported in the table are from duplicate analyses for two successive samples; agreement of these values within experimental error was accepted as indication that solution equilibrium had been attained.

TABLE IV-6

SOLUBILITY OF HELIUM IN LIQUID 70-FLOX

Test Temperature °F	Vapor Pressure of Propellant psia(a)	Mole Percent Concentration Helium	
		300 psia	700 psia
-320	5	0.094	0.230
-300	20	0.217	0.579
-280	48	0.314	0.797
-260	120	0.354	1.15

(a) Reference 50.

These data are presented as isothermal pressure-composition and isobaric temperature-composition plots in Figures IV-14 and IV-15. Isobars at 150 and 500 psia have been constructed for this system by interpolation.

7. Fluorine-Helium

The solubility of helium in liquid fluorine was measured by Astropower Laboratory for this Design Guide, under Contract NAS7-548. The solubility data for this system is tabulated in Table IV-7; experimental details may be found in Reference 46. The results reported in the table are

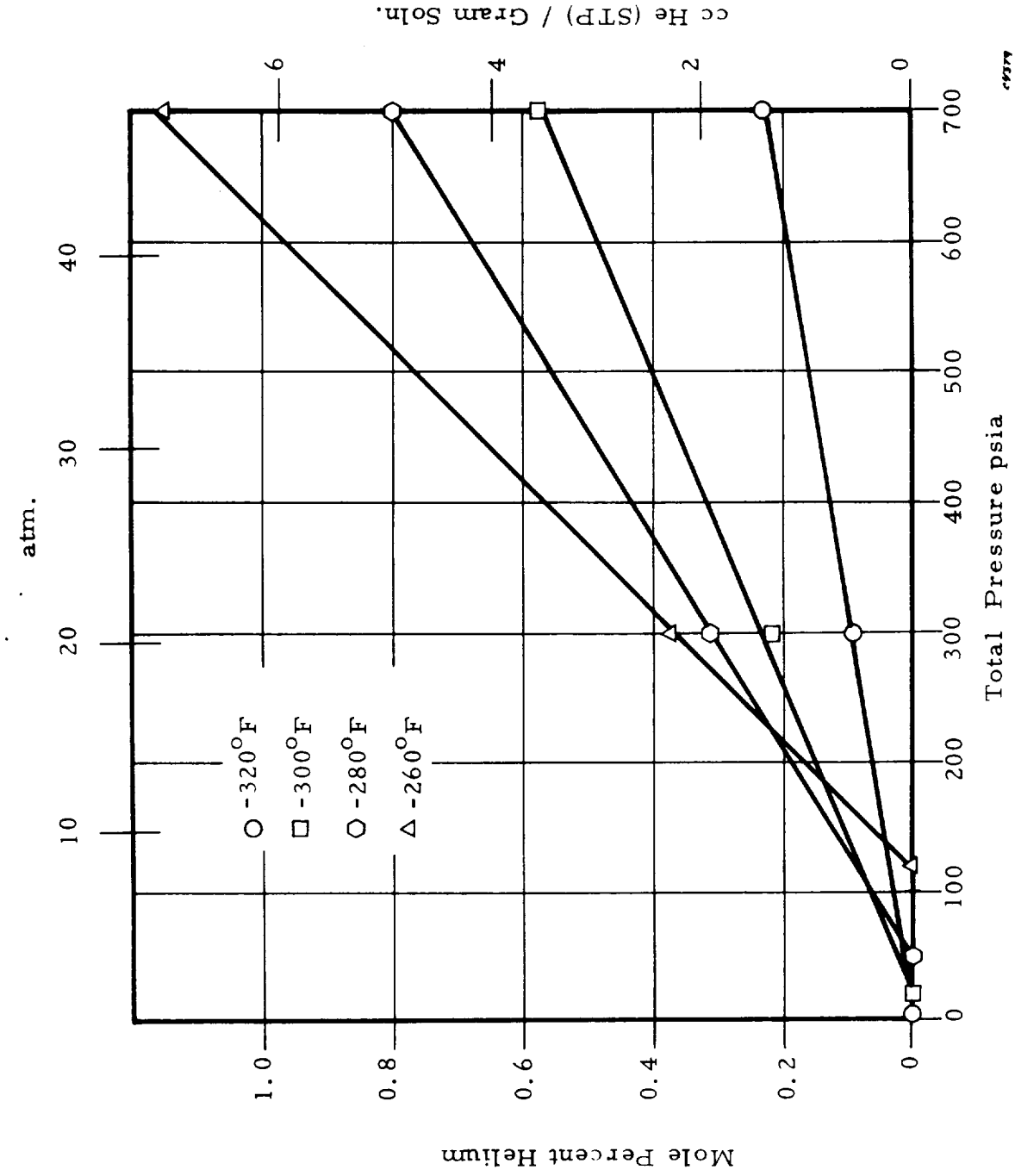

Figure IV-14. Isothermal Pressure-Composition Diagram For The System Liquid 70% FLOX-Helium

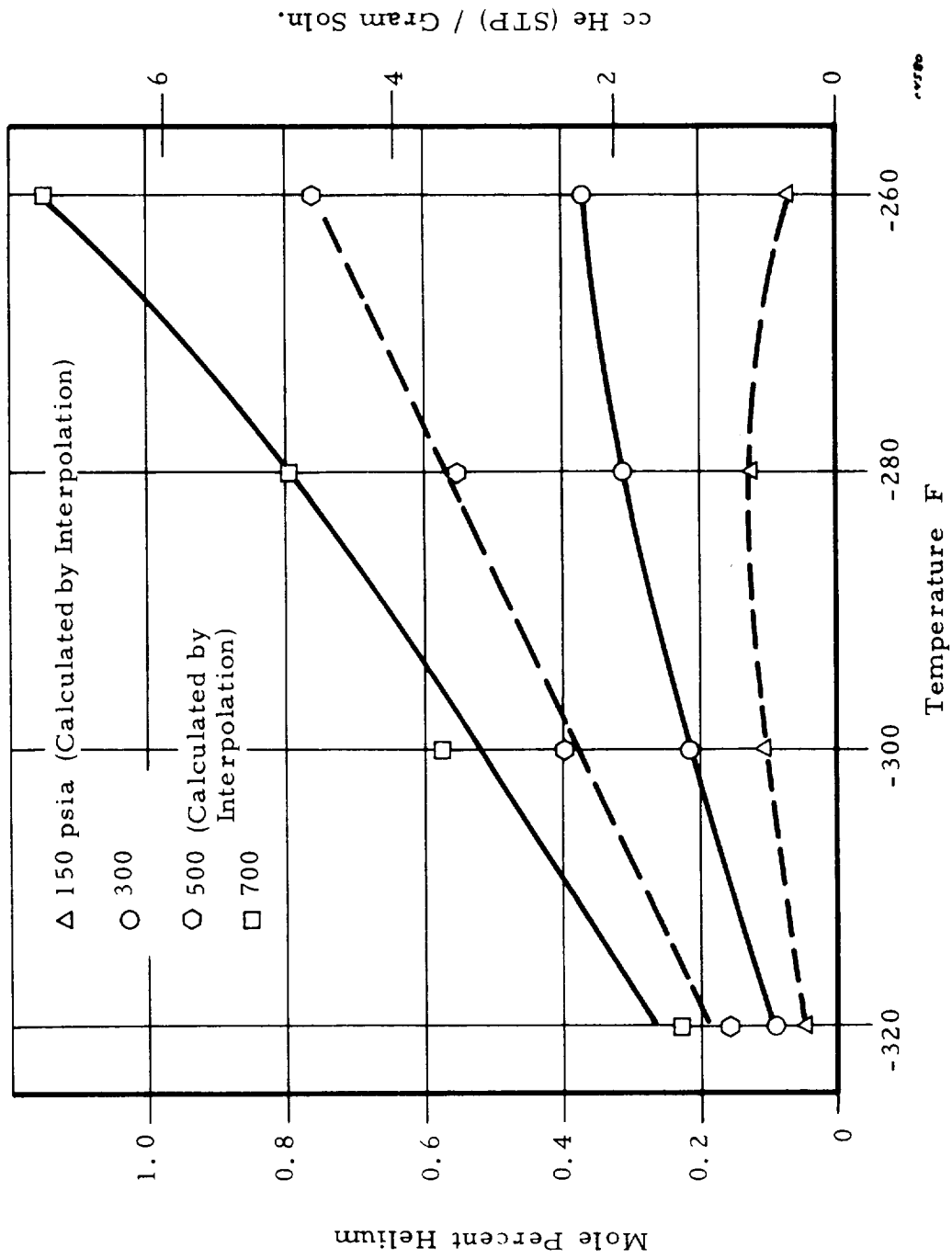

Figure IV-15. Isobaric Temperature-Composition Diagram For The System Liquid 70% FLOX-Helium

from duplicate analyses for two successive samples; agreement of these values within experimental error was accepted as indication that solution equilibrium had been attained.

TABLE IV-7

SOLUBILITY OF HELIUM IN LIQUID FLUORINE

Test Temperature °F	Vapor Pressure of Propellant psia[a]	Mole Percent Concentration Helium	
		300 psia	700 psia
-320	6	0.101	0.242
-300	22	0.231	0.577
-280	52	0.344	0.895
-260	140	0.339	1.14

(a) Reference 47.

These data are presented as isothermal pressure-composition and isobaric temperature-composition plots in Figures IV-16 and IV-17. Isobars at 150 and 500 psia have been constructed for this system by interpolation.

8. MON-10-Helium

Figure IV-18 presents a selected summary of solubility data for helium in MON-10 (mixed oxides of nitrogen containing 9.23 wt. % nitric oxide). The data cover a temperature range of 50° to 120°F and pressures of 300 to 720 psia (22 to 49 atm). These data were obtained from Reference 51.

9. Nitrogen Tetroxide-Argon

See Section 12.

10. Nitrogen Tetroxide-Helium

See Section 12.

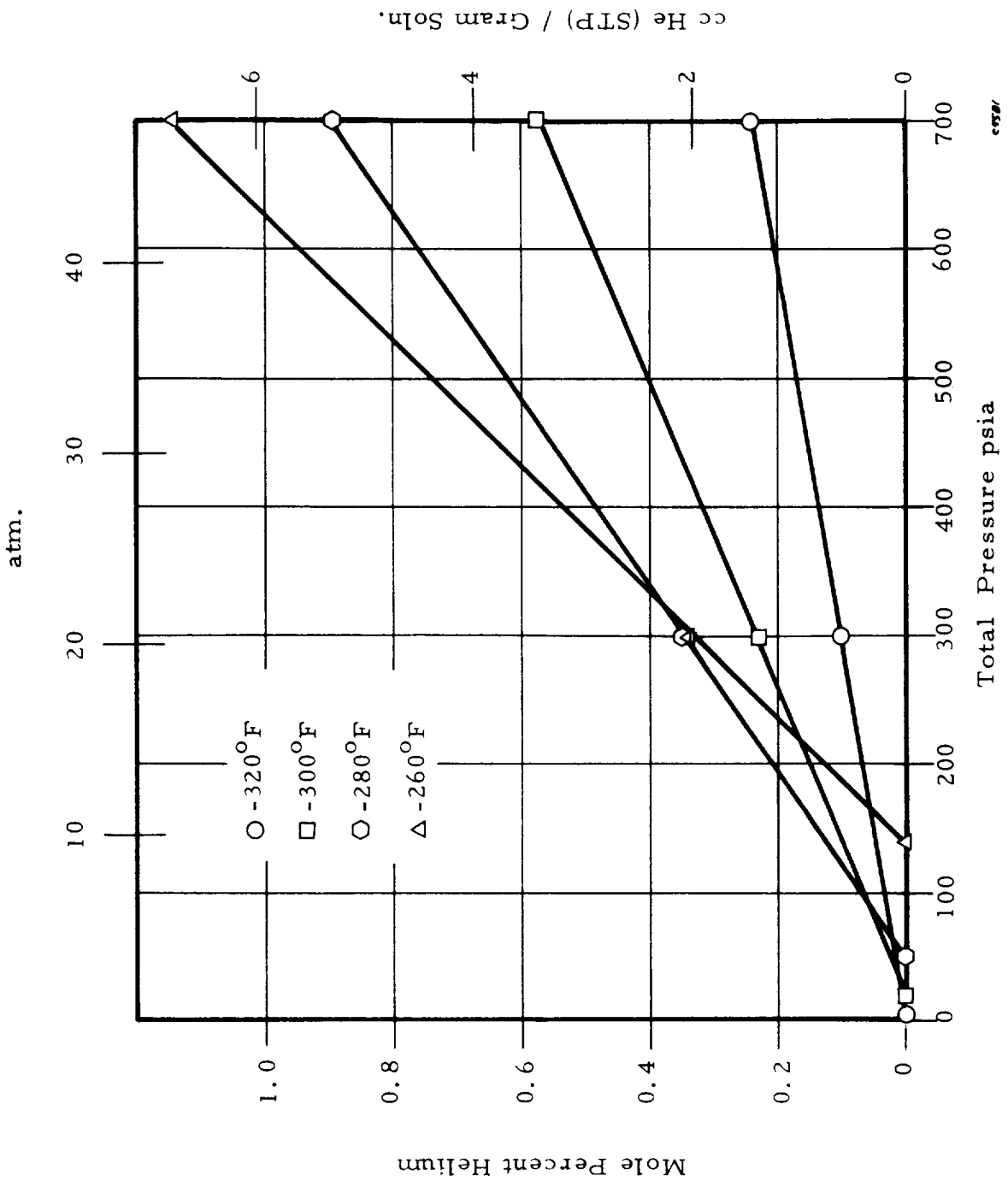

Figure IV-16. Isothermal Pressure-Composition Diagram For The System Liquid Fluorine-Helium.

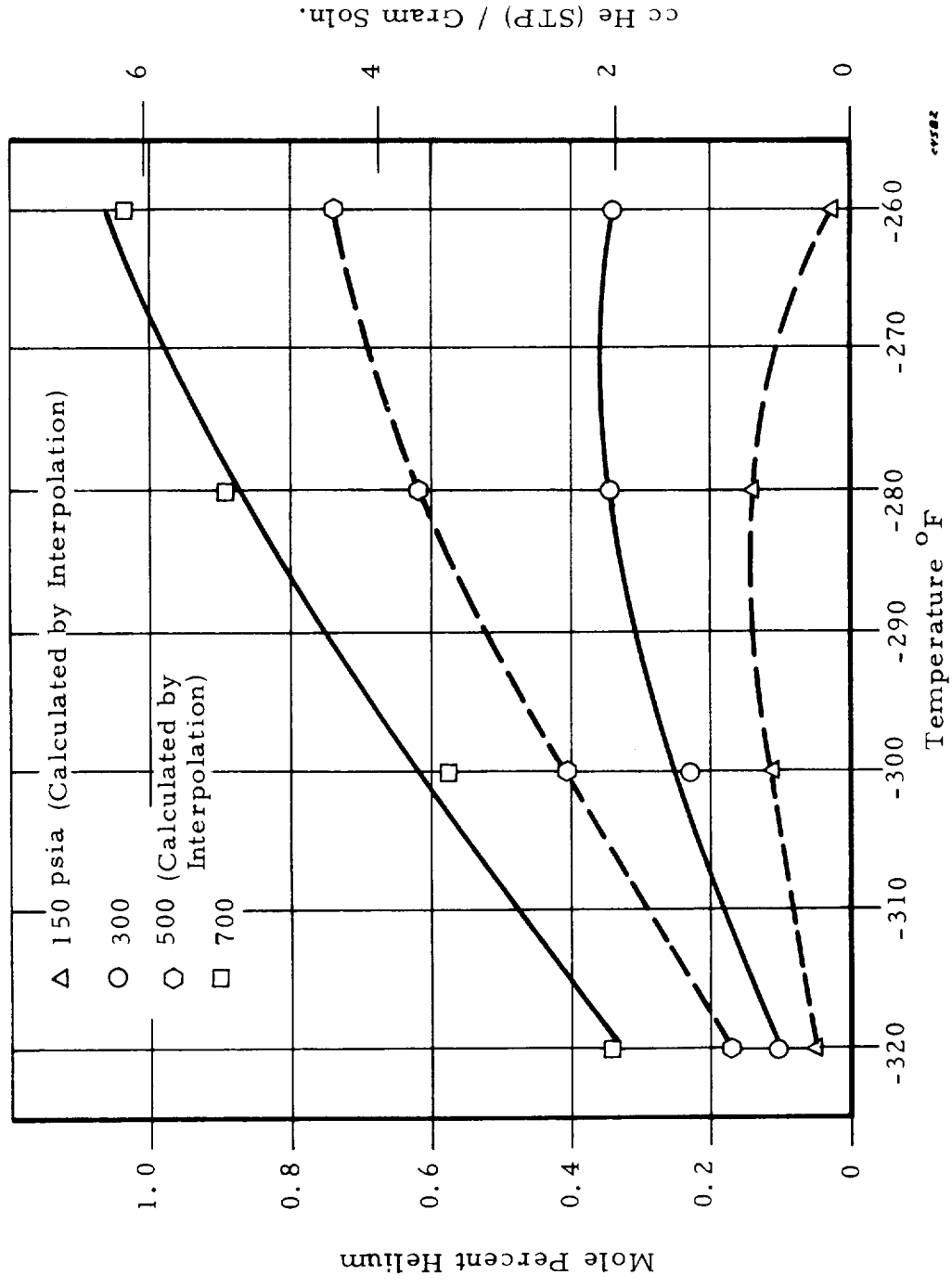

Figure IV-17. Isobaric Temperature-Composition Diagram For The System Liquid Fluorine-Helium.

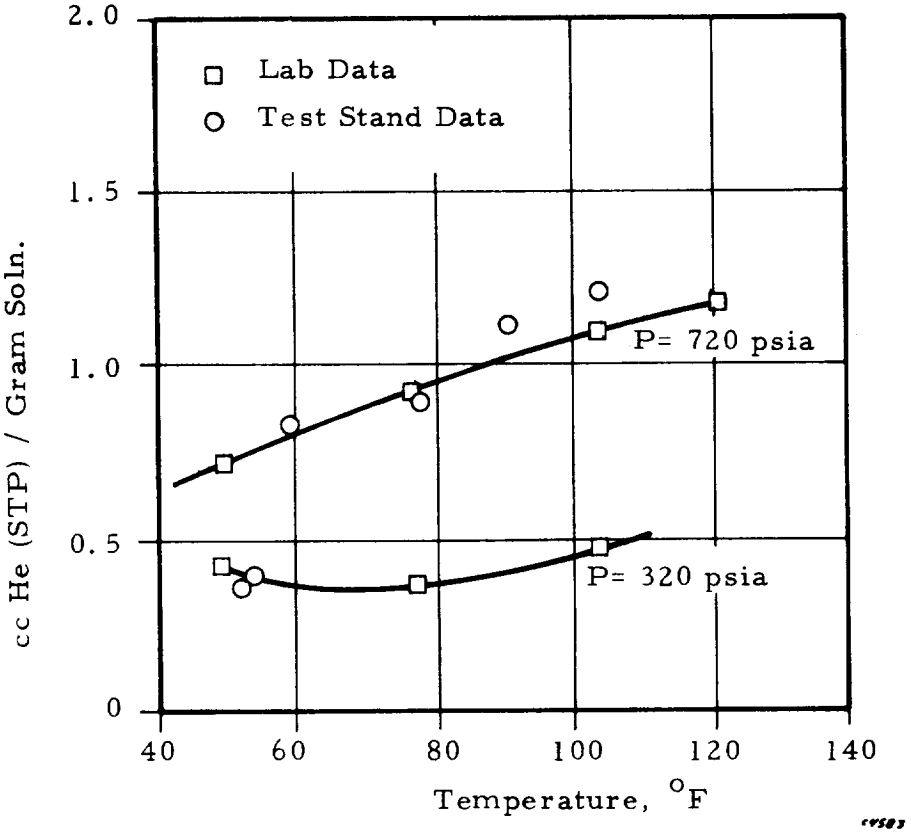

Figure IV-18. Isobaric Temperature - Composition Diagram for the System Liquid Mon 10-Helium

11. Nitrogen Tetroxide-Oxygen

See Section 12.

12. Nitrogen Tetroxide-Nitrogen

The solubilities of argon, helium, oxygen and nitrogen in nitrogen tetroxide in the low pressure region of 0.5 to 2 atm have been reported by Chang and Gokcen (Reference 52). Their data are summarized in Table IV-8.

Data for the solubility of helium and nitrogen in liquid nitrogen tetroxide at slightly higher pressures have been determined by Bell Aerosystems Co. (Reference 53), and are given in Table IV-9.

Solubilities of helium and nitrogen in this oxidizer have also been determined at 300 and 700 psia by Aerojet-General Corporation (References 38 and 39), and these data are given in the isobaric temperature-composition plots of Figures IV-19 and IV-20.

13. Nitrogen Trifluoride-Helium

See Section 14.

14. Nitrogen Trifluoride-Nitrogen

The solubilities of helium and nitrogen in liquid nitrogen trifluoride were measured by Astropower Laboratory for this Design Guide, under Contract NAS 7-548. The solubility data for these two systems are tabulated in Table IV-10; experimental details may be found in Reference 46. The results are from duplicate analyses for two successive samples; agreement of these values within experimental error was accepted as indication that solution equilibrium had been attained.

These data are presented as isothermal pressure-composition and isobaric temperature-composition plots in Figures IV-21, IV-22, IV-23, and IV-24. Additional isobars at 150 and 500 psia have been constructed for each system by interpolation.

TABLE IV-8

SOLUBILITIES OF He, N_2, O_2, AND Ar IN LIQUID N_2O_4[a]

T, °K	He			N_2			O_2			Ar		
	P	10^4X	10^4K	P	10^4X	10^4K	P	10^4X	10^4K	P	10^4X	10^4K
262.02	0.5261	0.289	0.55	0.5916	3.28	5.54	0.6041	5.34	8.84	0.7110	6.18	8.69
	1.0149	0.599	0.59	0.6186	3.44	5.56	1.2017	10.58	8.80	1.2670	11.16	8.81
	1.2393	0.694	0.56	1.2964	7.38	5.69	1.3091	11.47	8.76	1.5162	13.28	8.76
	1.8346	1.12	0.61	1.3192	7.51	5.69	1.6119	14.23	8.83	1.8037	15.85	8.79
	1.9125	1.05	0.55	1.9440	10.91	5.61	1.9876	17.40	8.75	1.9080	16.83	8.82
				1.9500	11.08	5.68						
273.15	0.4951	0.361	0.73	0.3504	2.09	5.96	0.2643	2.43	9.19	0.3582	3.24	9.05
	0.6624	0.453	0.68	0.3811	2.32	6.09	0.6275	5.78	9.21	0.5702	5.15	9.03
	0.9566	0.698	0.73	0.4716	2.83	6.00	1.1241	10.30	9.16	0.6879	6.29	9.14
	1.2315	0.852	0.69	0.6830	4.06	5.94	1.7950	16.37	9.12	0.9366	8.50	9.08
	1.4186	0.950	0.67	0.8972	5.39	6.01				1.8425	16.76	9.10
	1.8770	1.30	0.69	0.9389	5.63	6.00						
				1.4283	8.60	6.02						
				1.5043	8.95	5.95						
				1.7951	10.77	6.00						
288.10	0.9773	0.870	0.89									
	1.3153	1.13	0.86									
298.15	0.3917	0.401	1.02	0.3801	2.47	6.50	0.3728	3.76	10.09	0.3801	3.77	9.92
	0.3963	0.404	1.02	0.5909	3.85	6.52	0.4989	5.16	10.34	0.4158	4.08	9.81
	0.7836	0.830	1.06	0.7222	4.82	6.67	0.5745	5.97	10.39	0.4897	4.80	9.80
	1.0192	1.00	0.98	0.7393	4.88	6.60	0.9963	10.08	10.12	0.6340	6.22	9.81
	1.1195	1.11	0.99	0.8457	5.54	6.55	1.0809	10.70	9.90	0.8037	7.94	9.88
	1.1455	1.23	1.07	1.1125	7.41	6.66				0.9912	9.72	9.81
				1.3032	8.59	6.59				1.1053	10.89	9.85
303.16	0.5759	0.615	1.07	0.5604	3.81	6.80	0.4441	4.73	10.65	0.4470	4.42	9.89
	0.8867	0.909	1.03	0.8380	5.74	6.85	0.9189	9.47	10.31	0.5912	5.85	9.90

[a]P, atm; X, mole fraction; K = X/P.

TABLE IV-9

SOLUBILITY OF HELIUM AND NITROGEN
IN LIQUID NITROGEN TETROXIDE

Pressurizing Gas	Total Gas Pressure (psia)	Temperature (°F)	Solubility (wt%)
Helium	54.3	73	0.04 ± 0.01
	63	60	0.02 ± 0.004
	55.4	32	0.02 ± 0.01
Nitrogen	63.7	70	0.20 ± 0.01
	64.2	32	0.14 ± 0.01

TABLE IV-10

SOLUBILITY OF HELIUM AND NITROGEN
IN LIQUID NITROGEN TRIFLUORIDE

Test Temperature °F	Vapor Pressure of Propellant psia(a)	Mole Percent Concentration			
		Helium		Nitrogen	
		300 psia	700 psia	300 psia	700 psia
-320	<1	0.020	0.041	—	—
-250	3.0	0.099	0.324	—	—
-220	6.5	—	—	43.8	—
-200	14.7	0.341	0.824	26.5	72.2
-175	34	—	—	18.5	52.8
-150	70	0.500	1.56	13.5	38.3

(a) Reference 54.

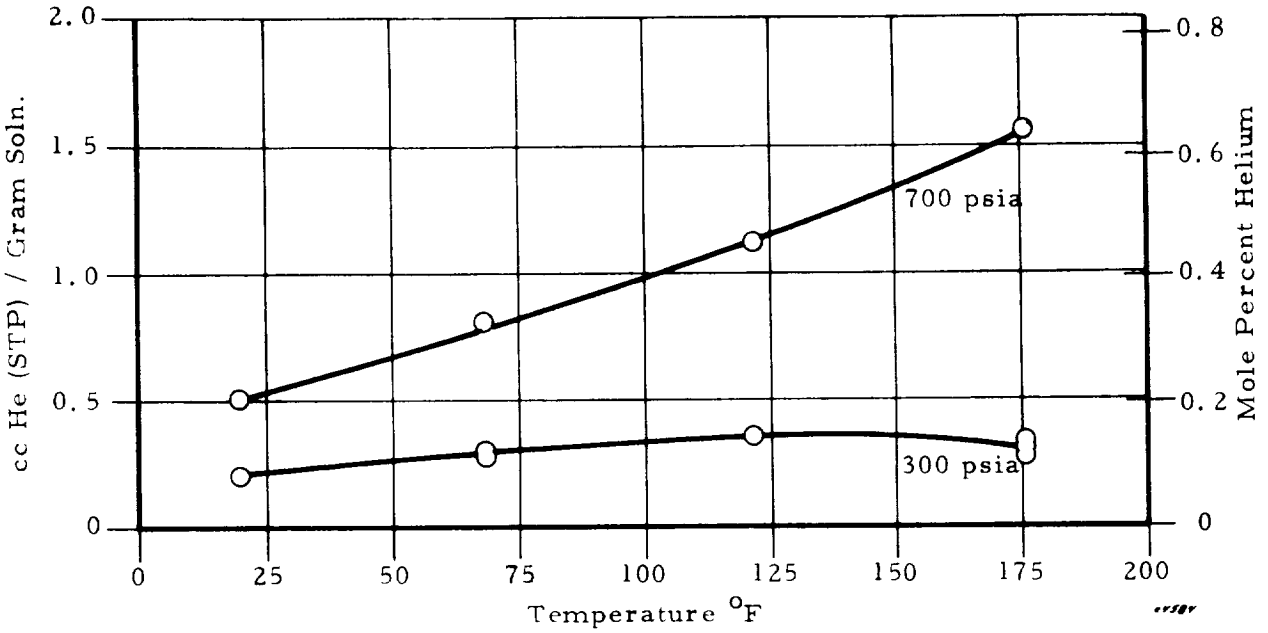

Figure IV-19. Isobaric Temperature-Composition Diagram for the System Liquid Nitrogen Tetroxide-Helium

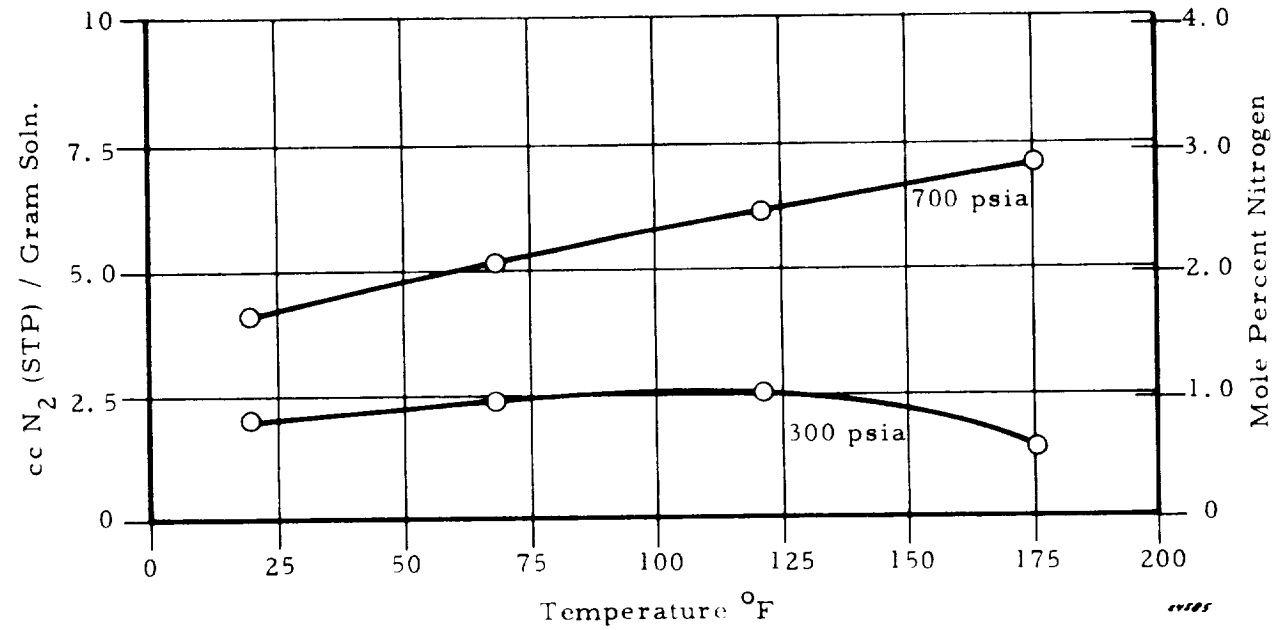

Figure IV-20. Isobaric Temperature-Composition Diagram for the System Liquid Nitrogen Tetroxide-Nitrogen

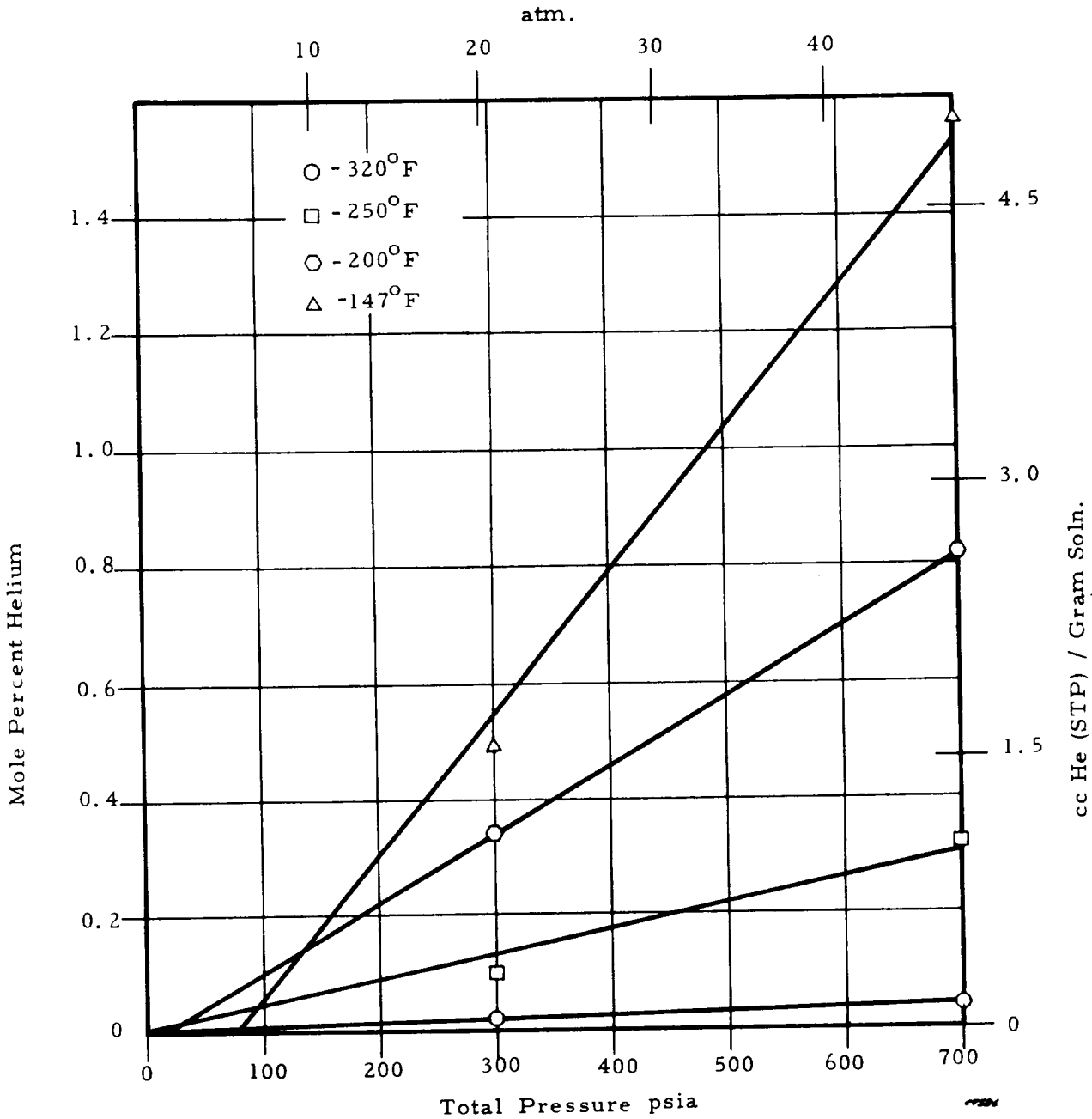

Figure IV-21. Isothermal Pressure-Composition Diagram for the System Liquid Nitrogen Trifluoride-Helium

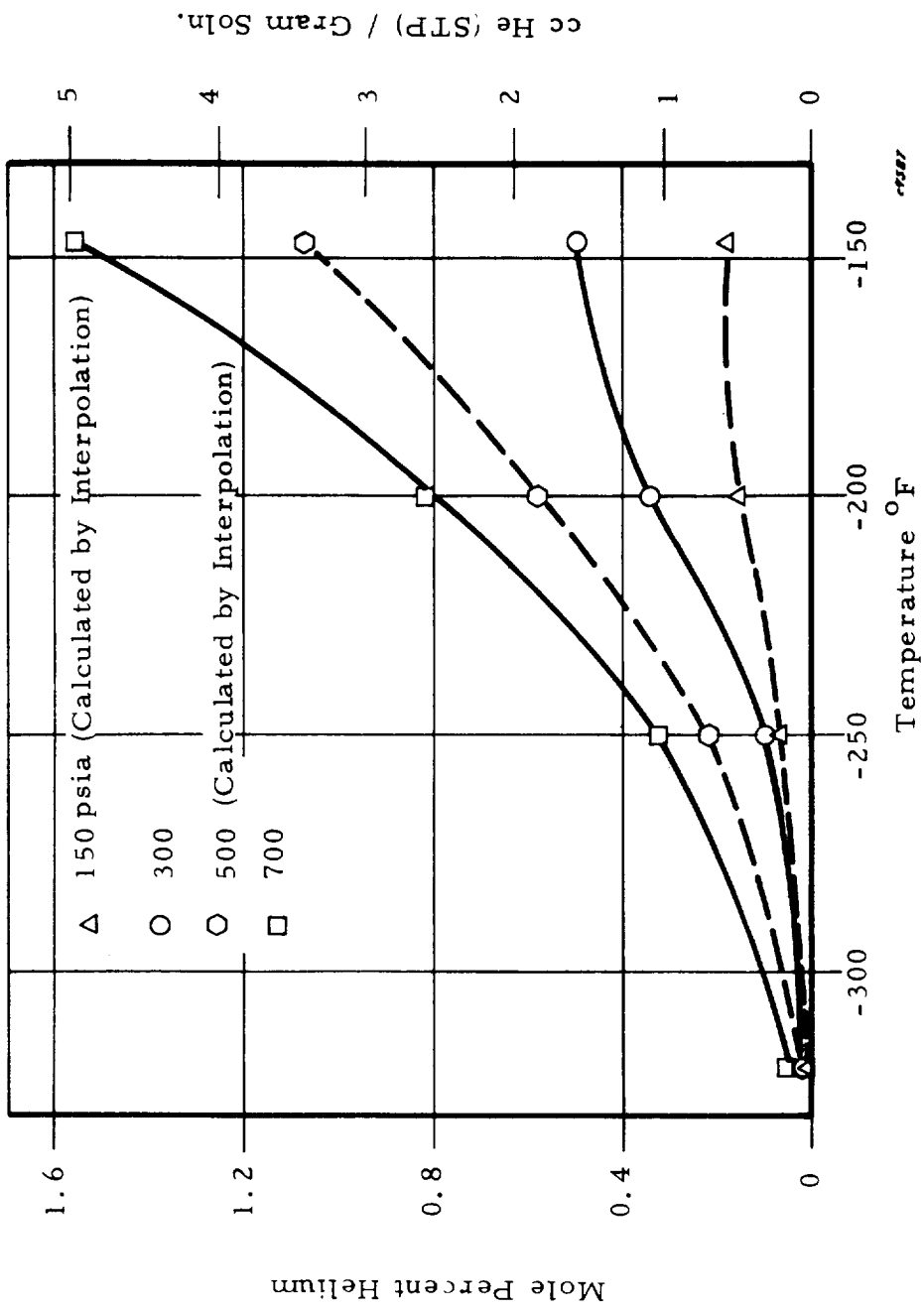

Figure IV-22. Isobaric Temperature-Composition Diagram For The System Liquid Nitrogen Trifluoride-Helium.

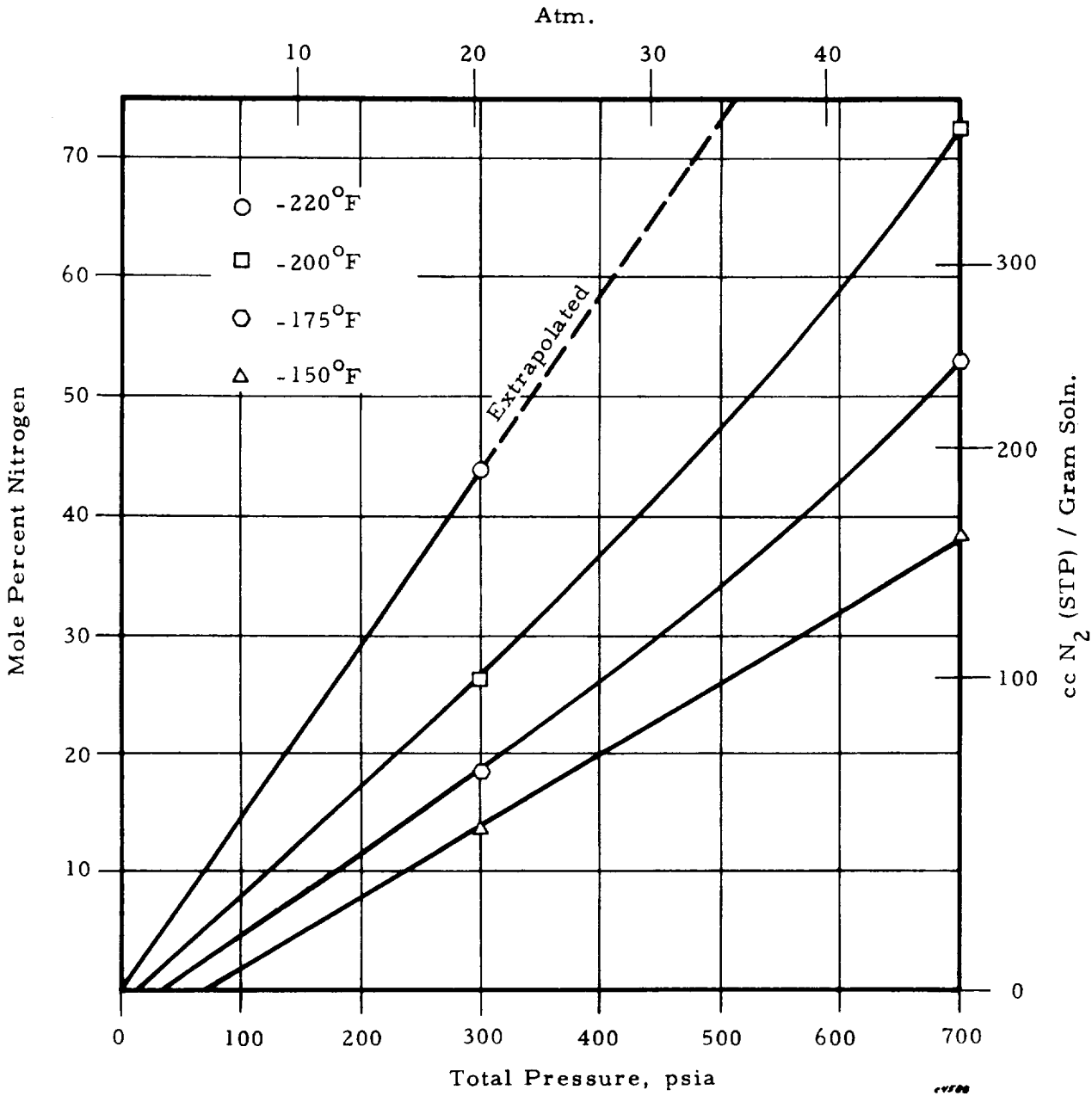

Figure IV-23. Isothermal Pressure-Composition Diagram for the System Liquid Nitrogen Trifluoride-Nitrogen

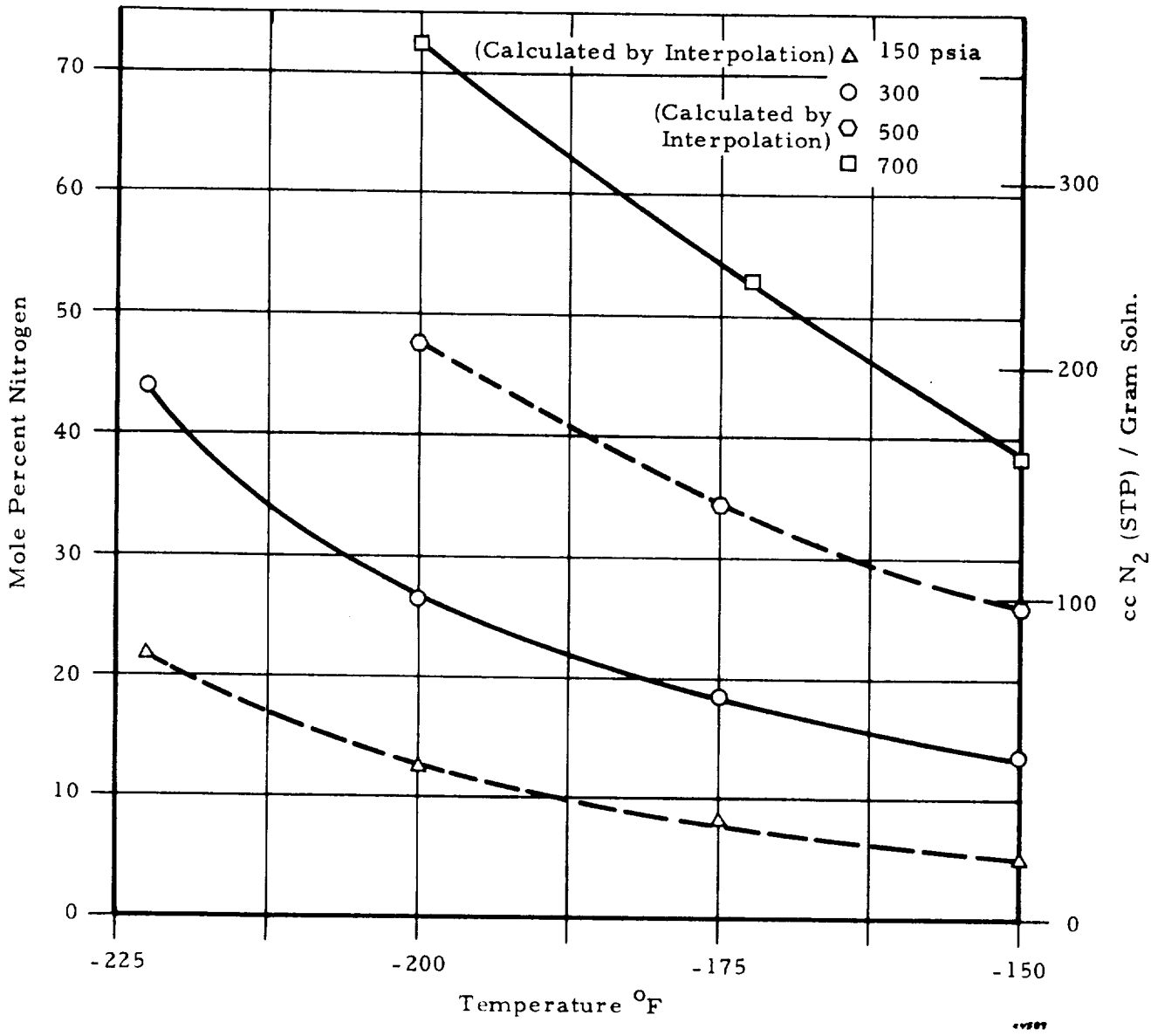

Figure IV-24. Isobaric Temperature-Composition Diagram for the System Liquid Nitrogen Trifluoride-Nitrogen

Because of the very high solubility of nitrogen in nitrogen trifluoride, Henry's Law is not obeyed and the corresponding isothermal plots in Figure IV-23 are shown as curves. Due to experimental difficulties, no data was obtained for this system above 300 psia at -220°F; consequently the -220°F isotherm is plotted as a straight line and can be considered as only approximate.

15. Nitryl Fluoride-Helium

See Section 16.

16. Nitryl Fluoride-Nitrogen

The solubilities of both helium and nitrogen in liquid nitryl fluoride were measured by Astropower Laboratory for this Design Guide, under Contract NAS7-548. The solubility data for these two systems are tabulated in Table IV-11; experimental details may be found in Reference 46. The results reported in the table are obtained from duplicate analyses for two successive samples; agreement of these values within experimental error was accepted as indication that solution equilibrium had been attained.

TABLE IV-11

SOLUBILITY OF HELIUM AND NITROGEN IN LIQUID NITRYL FLUORIDE

Test Temperature °F	Vapor Pressure of Propellant psia[a]	Mole Percent Concentration			
		Helium		Nitrogen	
		300 psia	700 psia	300 psia	700 psia
-150	3	0.054	0.127	2.89	6.62
-100	14	0.108	0.248	1.98	4.82
-50	60	0.176	0.433	1.89	4.29[b]
0	118	0.195	0.666	1.37	4.24

(a) Reference 55.

(b) 680 psia.

These data are presented as isothermal pressure-composition and isobaric temperature-composition plots in Figures IV-25, IV-26, IV-27, and IV-28. Additional isobars at 150 and 500 psia have been constructed for each system by interpolation.

17. Oxygen-Helium

Figures IV-29 through IV-32 are taken from Reference 56. Figure IV-29 is an isothermal pressure-liquid phase composition diagram for this system at total pressures up to 200 atmospheres in the temperature range of 70° to 150°K. The region of this plot from 0 to 70 atmosphere total pressure is shown expanded in Figure IV-30. The corresponding data for the vapor phase is given in terms of oxygen concentration in Figure IV-31. A plot of equilibrium K factors (concentration ratios) for the major component in each phase is included in Figure IV-32.

The solubility of helium in liquid oxygen was also measured by Astropower Laboratory for this Design Guide, under Contract NAS 7-548. The solubility data for this system are tabulated in Table IV-12; experimental details may be found in Reference 46.

TABLE IV-12

SOLUBILITY OF HELIUM IN LIQUID OXYGEN

Test Temperature °F	Vapor Pressure of Propellant psia(a)	Mole Percent Concentration Helium	
		300 psia	700 psia
-320.0 ± 0.1	2.5	0.086	0.194
-280.5 ± 0.5	37	0.261	0.658
-259.8 ± 1.8	80	0.427	1.09
-238.6 ± 1.4	160	0.311	1.35

(a) Reference 57.

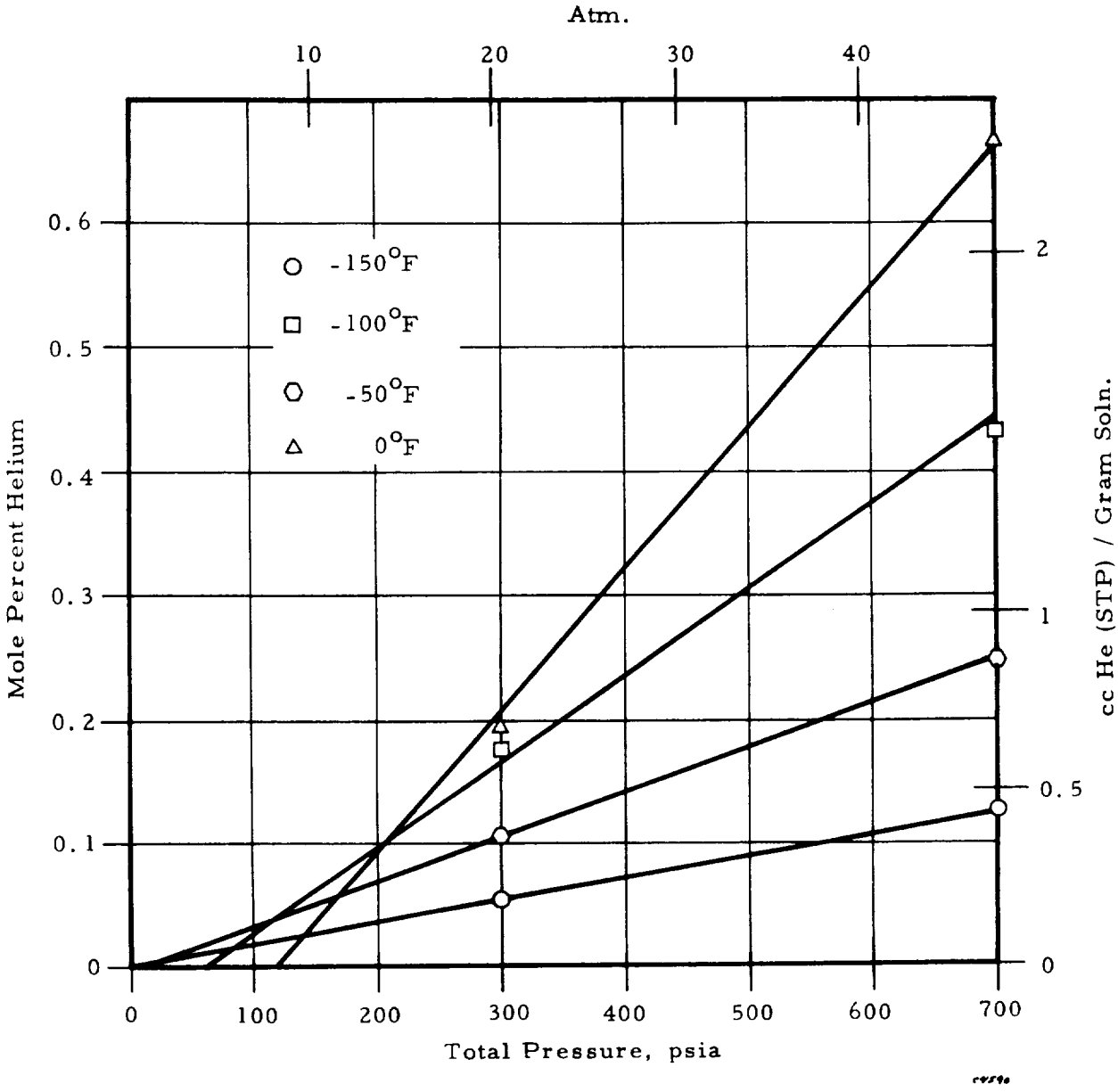

Figure IV-25. Isothermal Pressure-Composition Diagram for the System Liquid Nitryl Fluoride-Helium

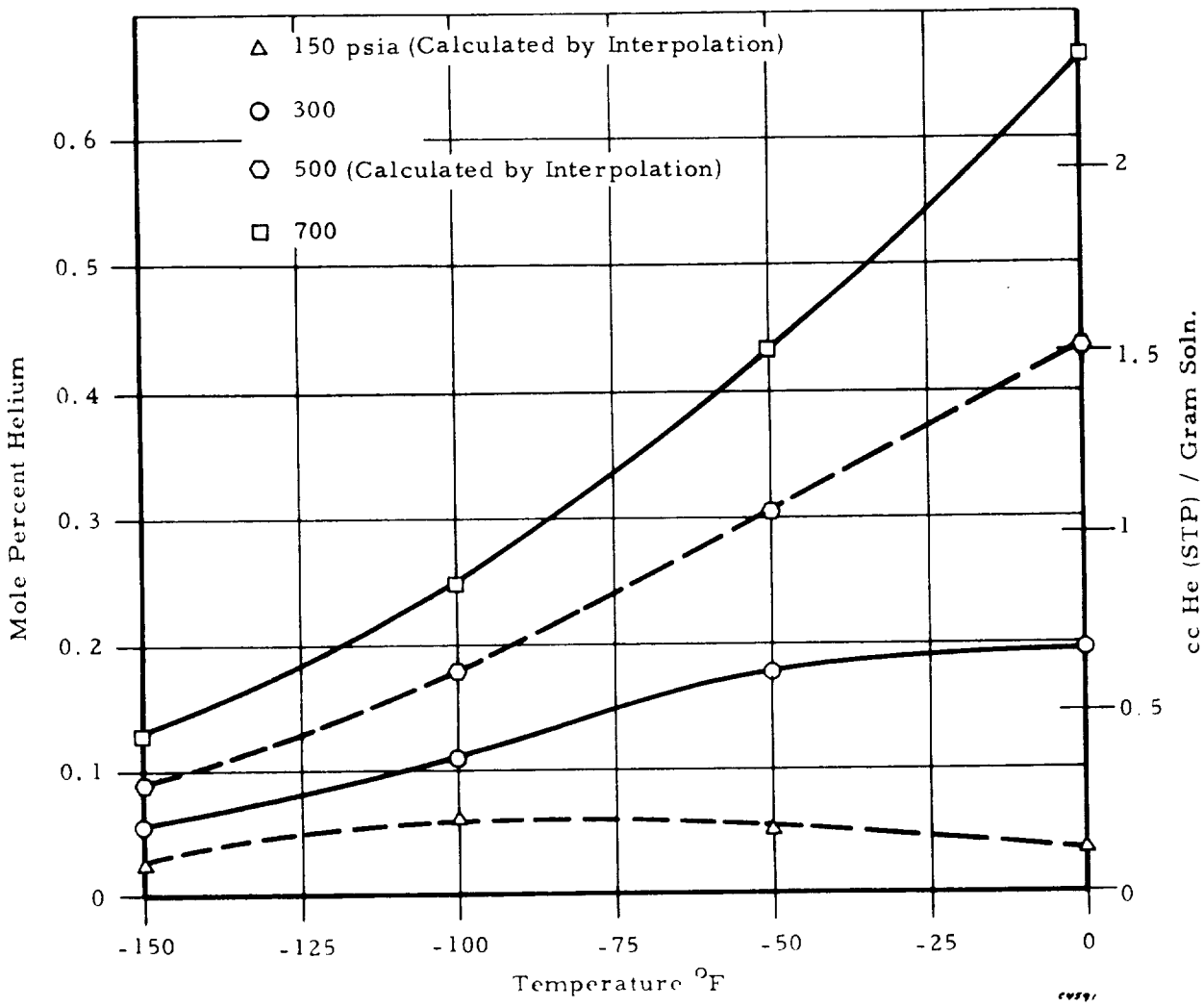

Figure IV-26. Isobaric Temperature-Composition Diagram for the System Liquid Nitryl Fluoride-Helium

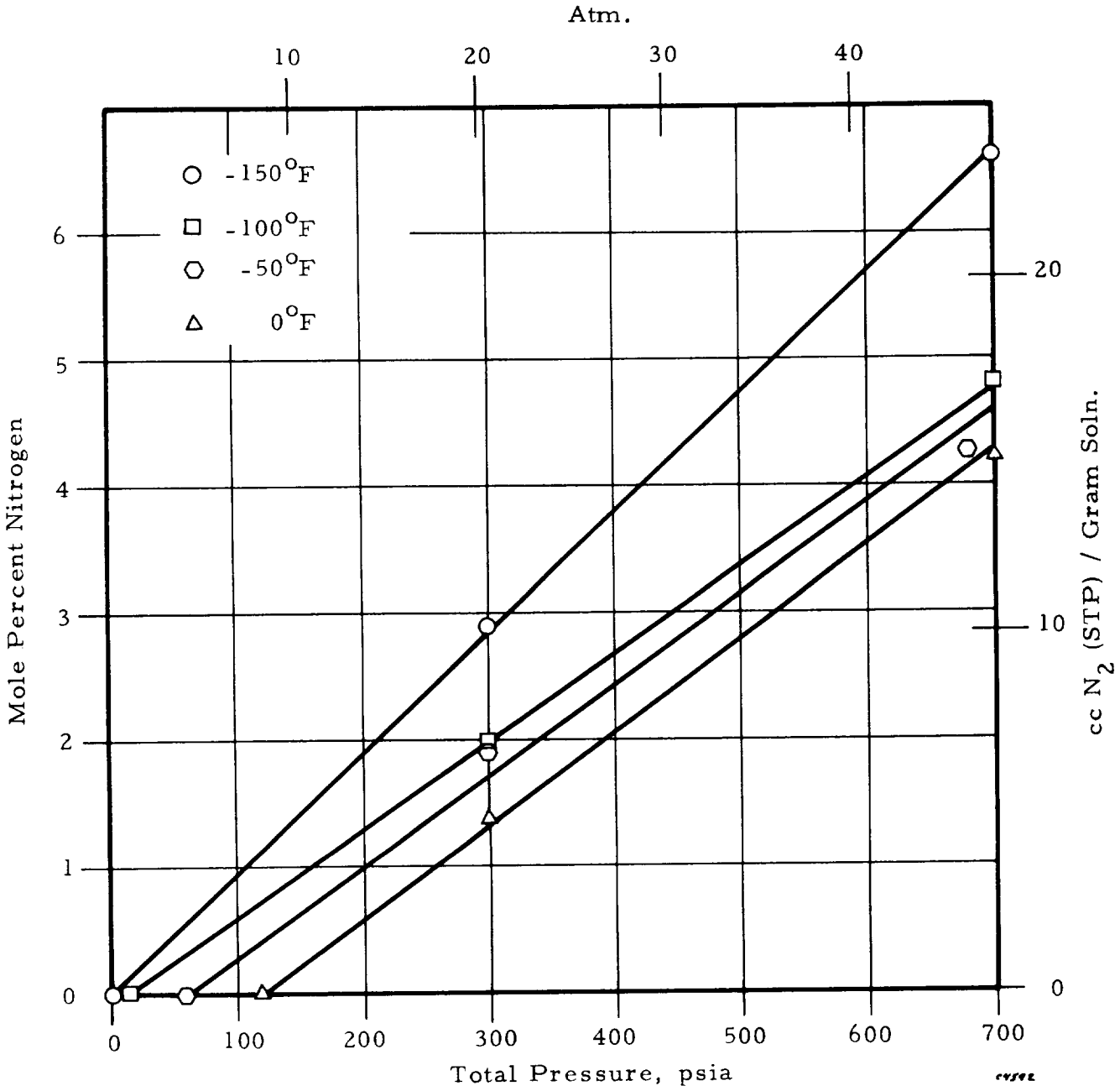

Figure IV-27. Isothermal Pressure – Composition Diagram for the System Liquid Nitryl Fluoride-Nitrogen

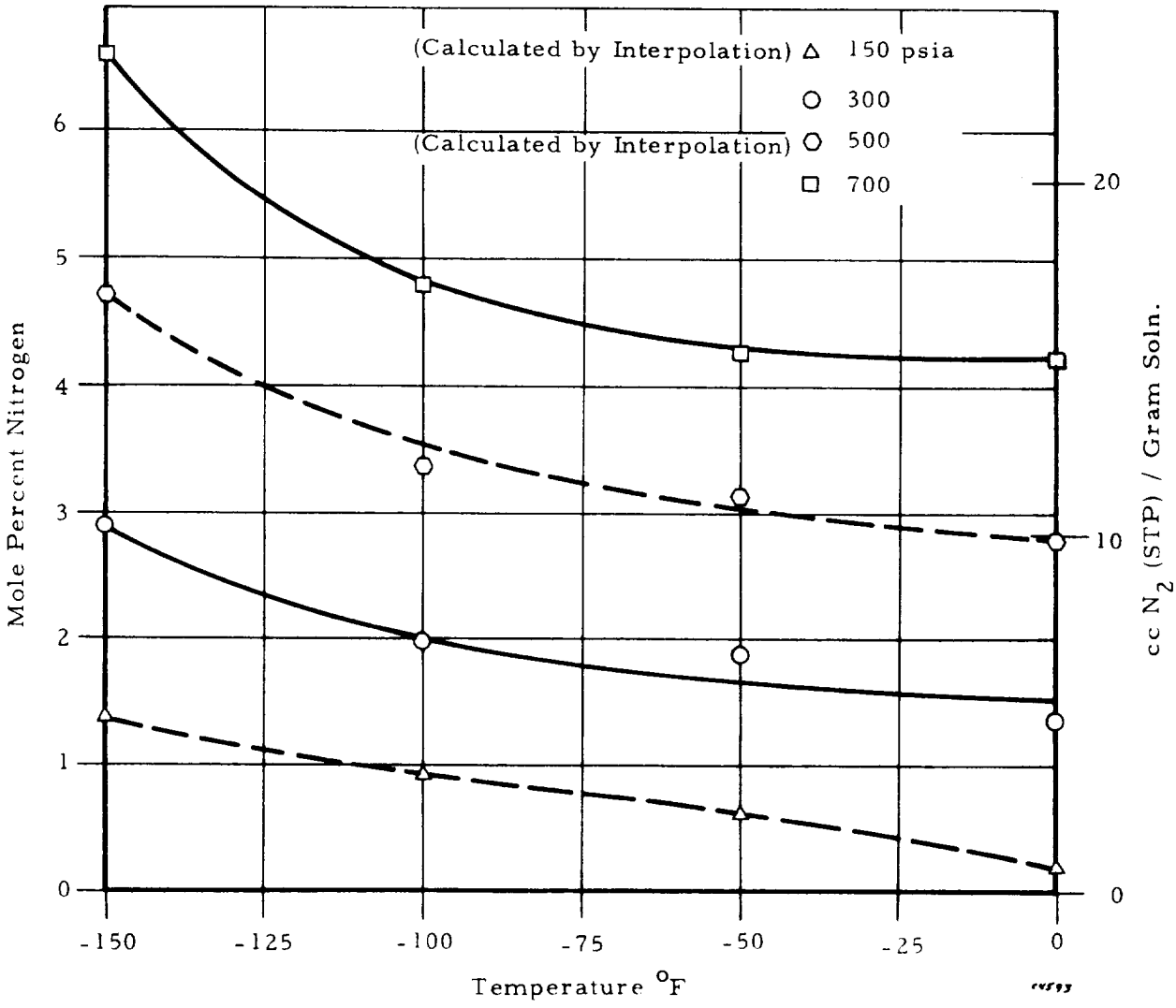

Figure IV-28. Isobaric Temperature-Composition Diagram for the System Liquid Nitryl Fluoride-Nitrogen

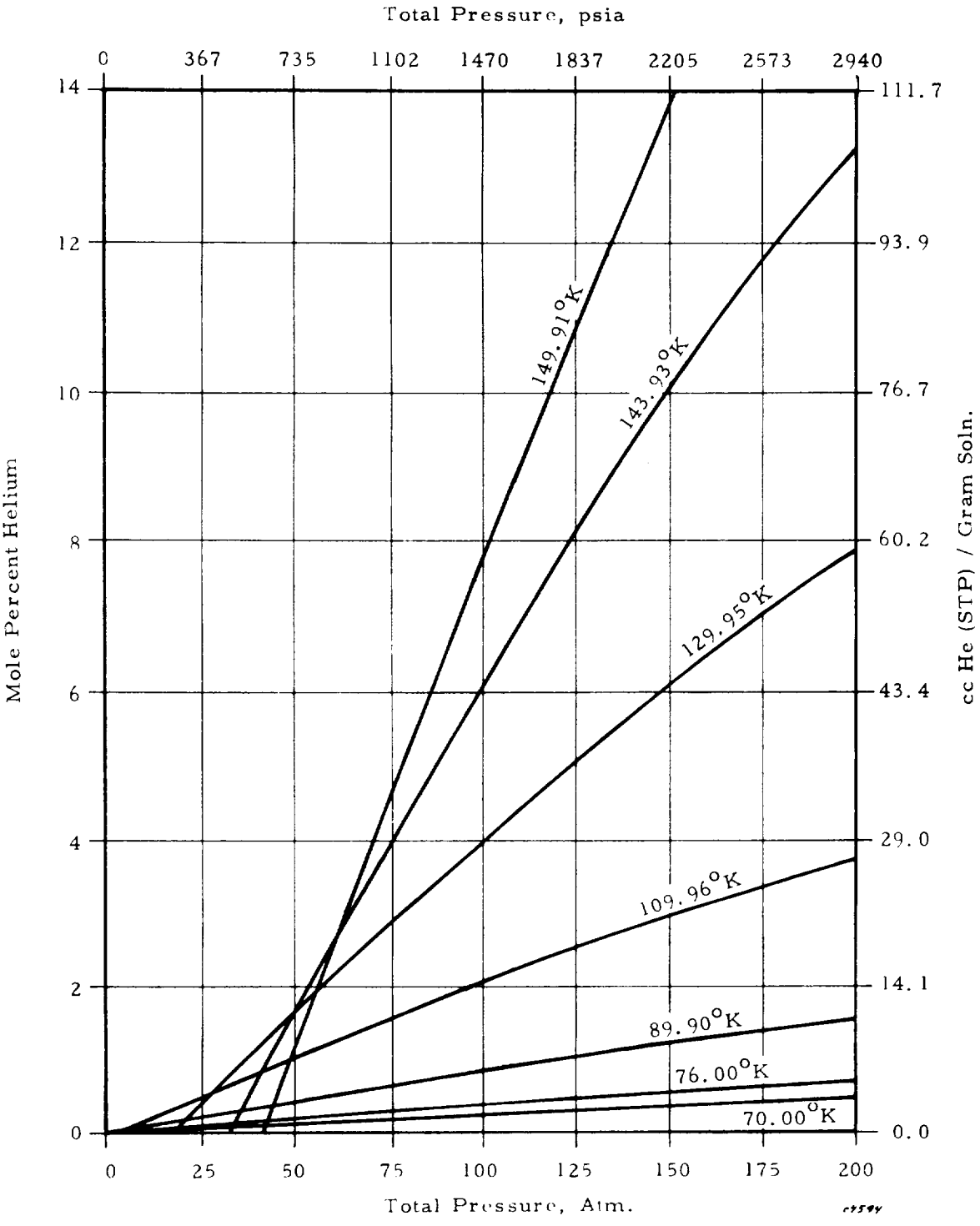

Figure IV-29. Isothermal Pressure-Composition Diagram for Oxygen-Helium in the Liquid Region

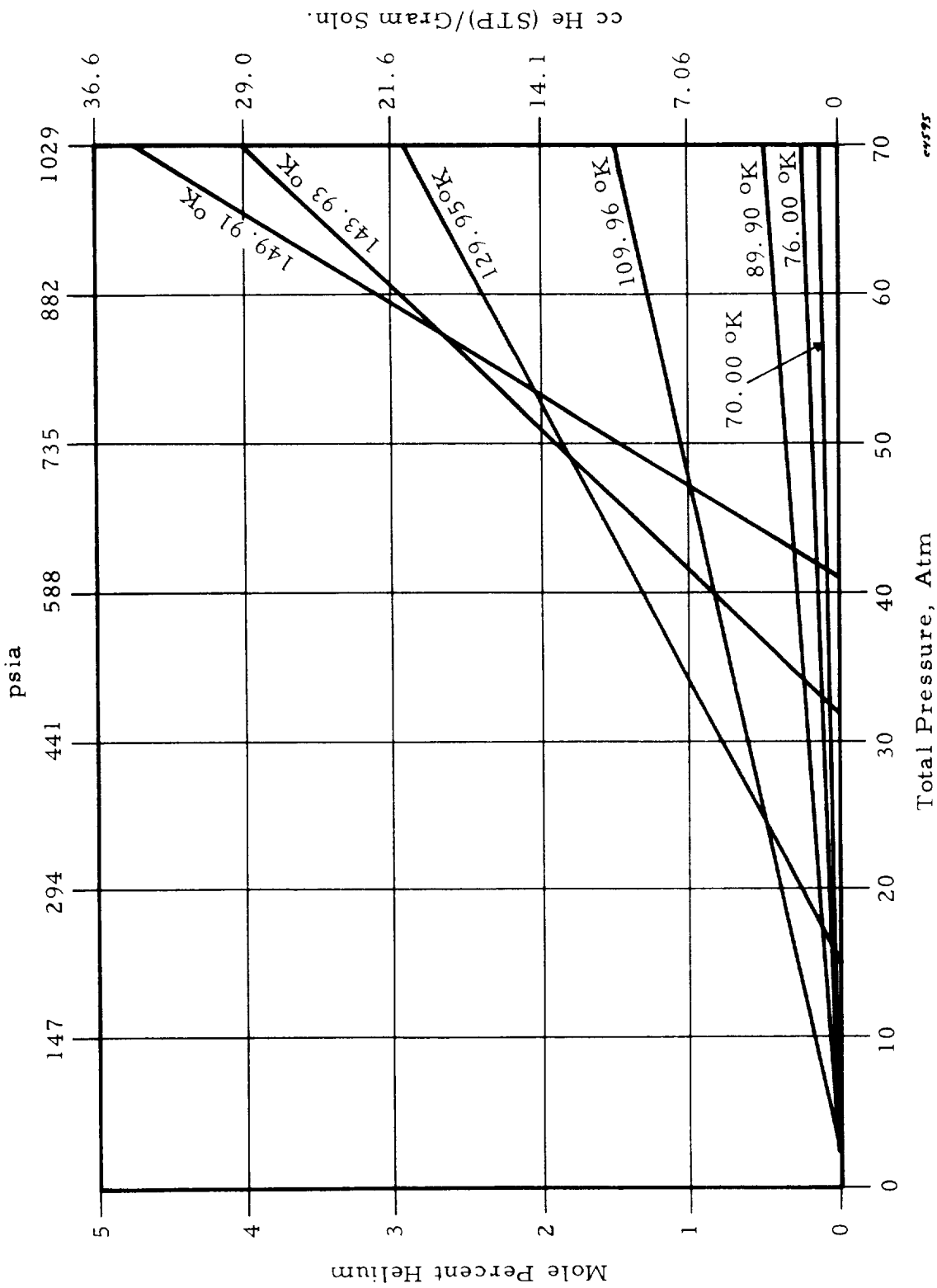

Figure IV-30. Isothermal Pressure - Composition Diagram for Oxygen-Helium System, Showing Expanded Liquid Region

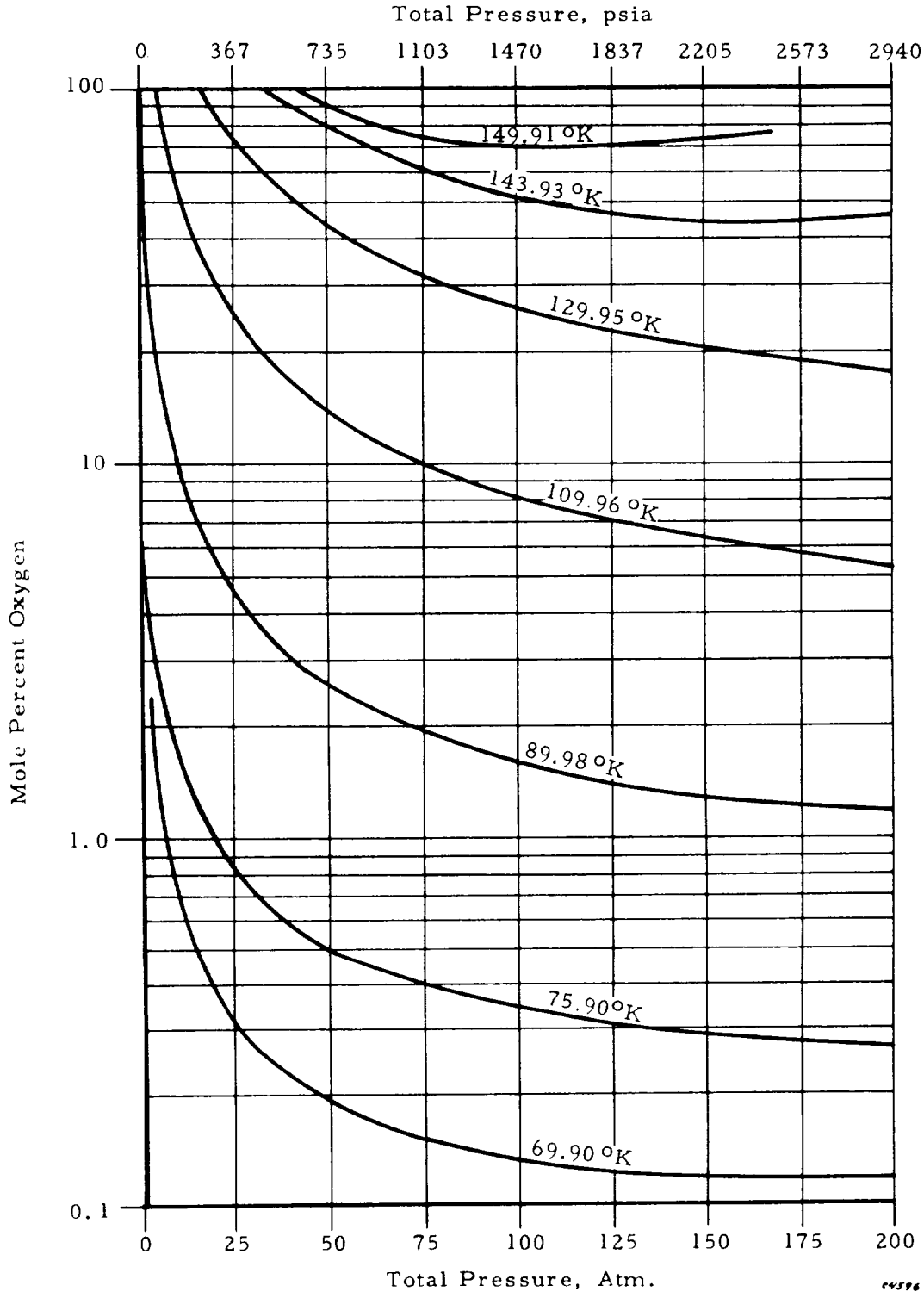

Figure IV-31. Isothermal Pressure-Composition Diagram for Oxygen-Helium System in the Vapor Region

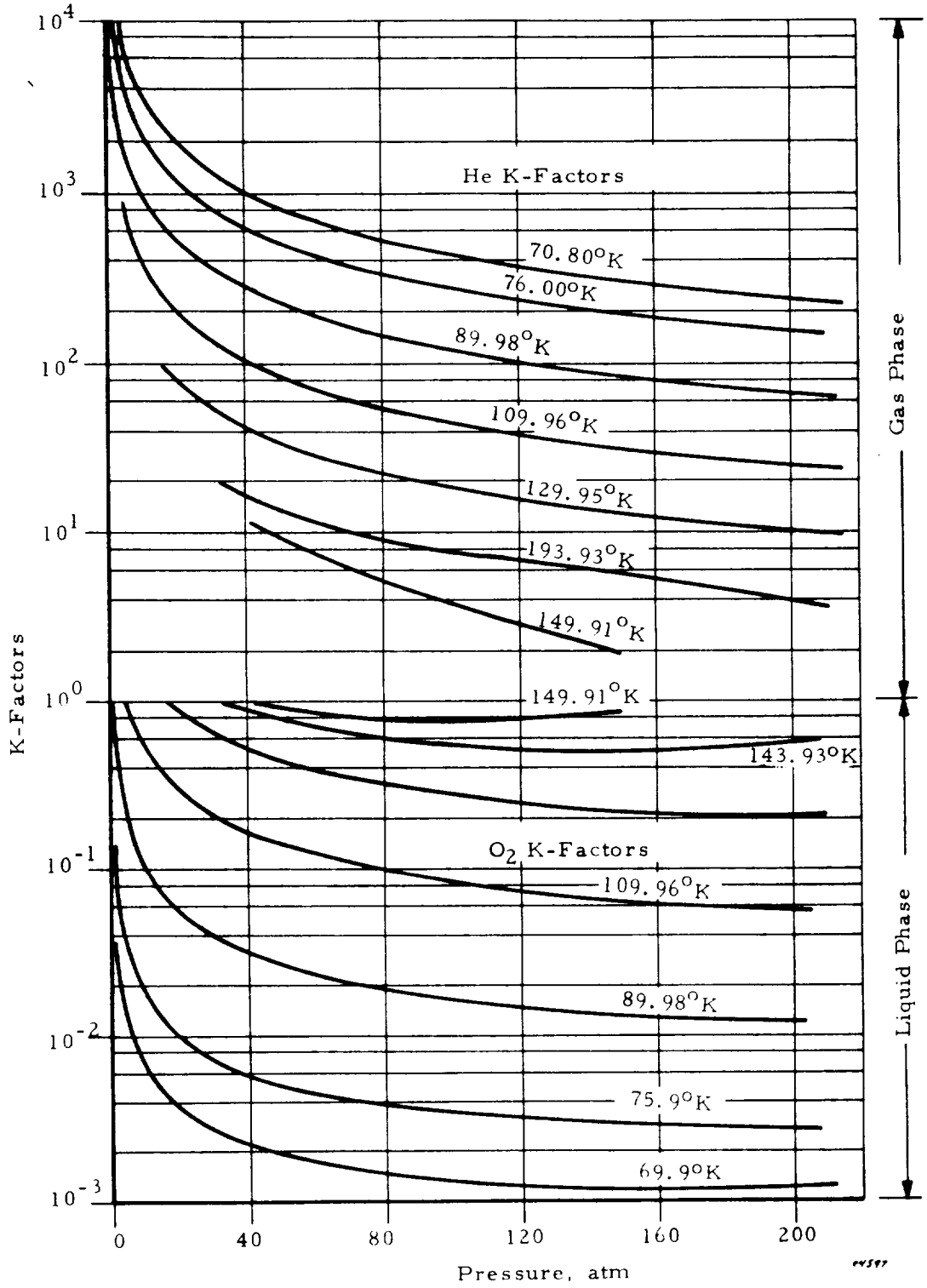

Figure IV-32. Equilibrium K - Factors for Oxygen-Helium System

The results reported in the table are obtained from duplicate analyses for two successive samples; agreement of these values within experimental error was accepted as indication that solution equilibrium had been attained. These data are presented as isothermal pressure-composition and isobaric temperature-composition plots in Figures IV-33 and IV-34. Additional isobars at 200 and 500 psia have been constructed for each system by interpolation.

18. Oxygen-Nitrogen

Although the term "solubility," as used in the present context, does not apply to this binary system, equilibrium concentration data are presented here for their practical value.

The following graphs represent data on the equilibrium of nitrogen in liquid oxygen taken from Reference 58 (the basic sources are also listed below). Figures IV-35 and IV-36 are isothermal pressure-concentration diagrams for nitrogen-oxygen mixtures. Figure IV-35 is based on values obtained by Reference 59 for isotherms of 65°K, 70°K, and 77.5°K in the pressure range of 1 psia to 15 psia (0.1 - 1.02 atm). The equilibrium concentrations in Figure IV-36 for the 90.5°K, 99.94°K, 110.05°K, 119.92°K, and 125°K isotherms were taken from Reference 1 and the values for the 85°K isotherm is from Reference 60. The pressure range for this data is 15 psia to 470 psia (1 to 32 atm). Figure IV-37 is an isobaric temperature-concentration diagram for nitrogen-oxygen mixtures for three pressures, 15, 20 and 30 psia and is obtained from the data of References 60, 61 and 62.

19. Oxygen Difluoride-Helium

See Section 20.

20. Oxygen Difluoride-Nitrogen

The solubilities of helium and nitrogen in liquid oxygen difluoride were measured by Astropower Laboratory for this Design Guide, under Contract NAS 7-548. The solubility data for these two systems are tabulated in Table IV-13; experimental details may be found in Reference 46.

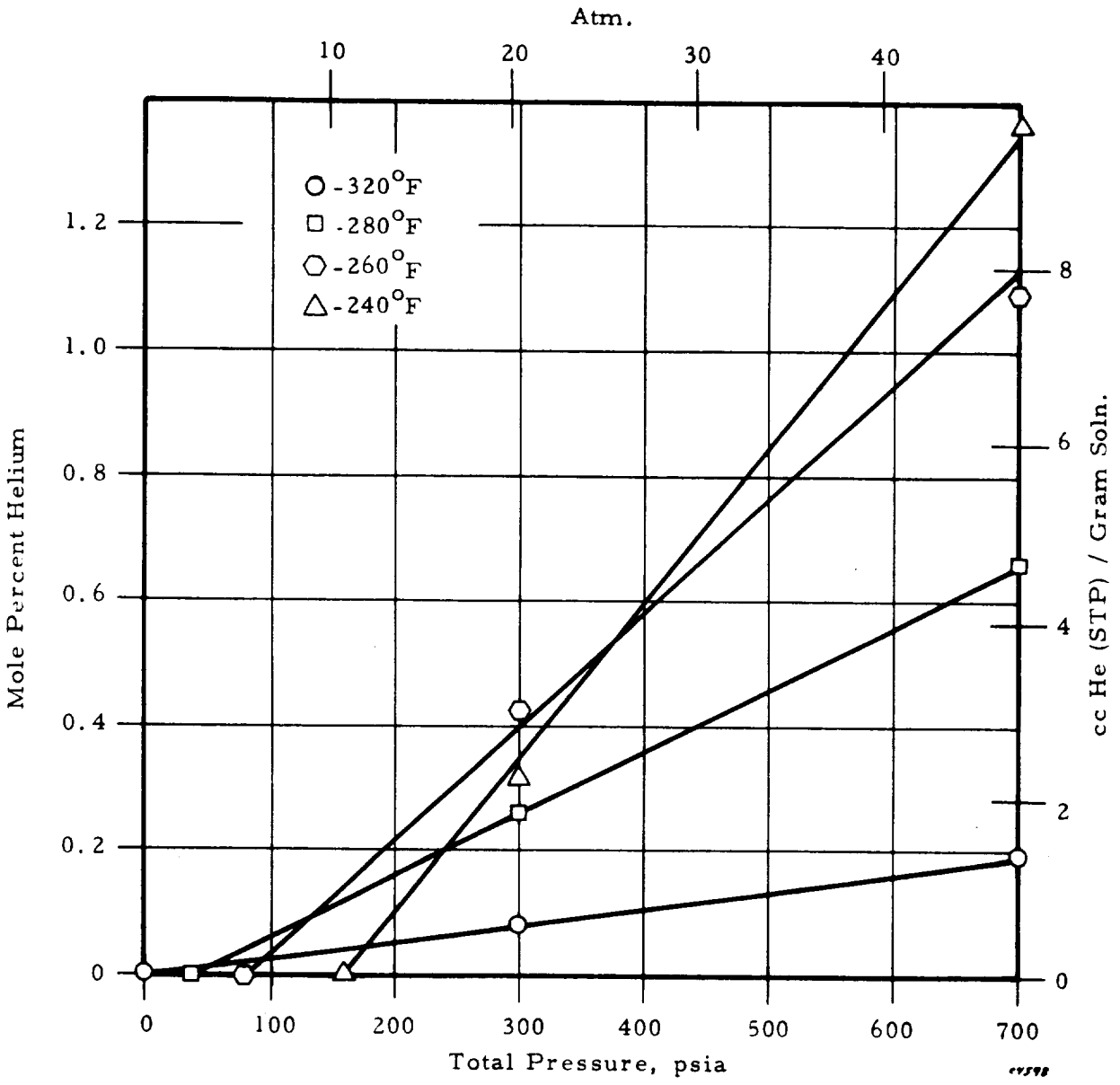

Figure IV-33. Isothermal Pressure-Composition Diagram for the System Liquid Oxygen-Helium

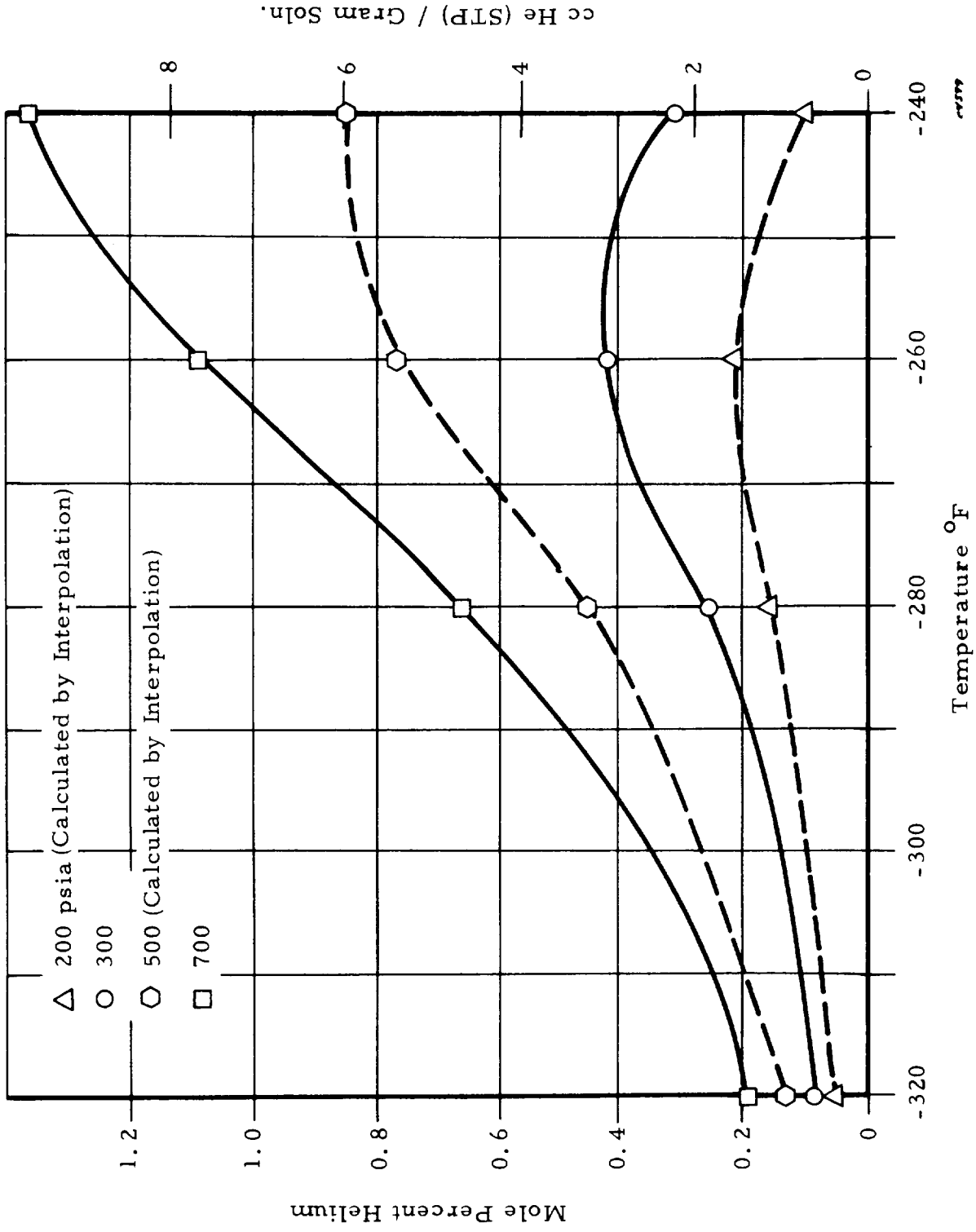

Figure IV-34. Isobaric Temperature – Composition Diagram for the System Liquid Oxygen-Helium

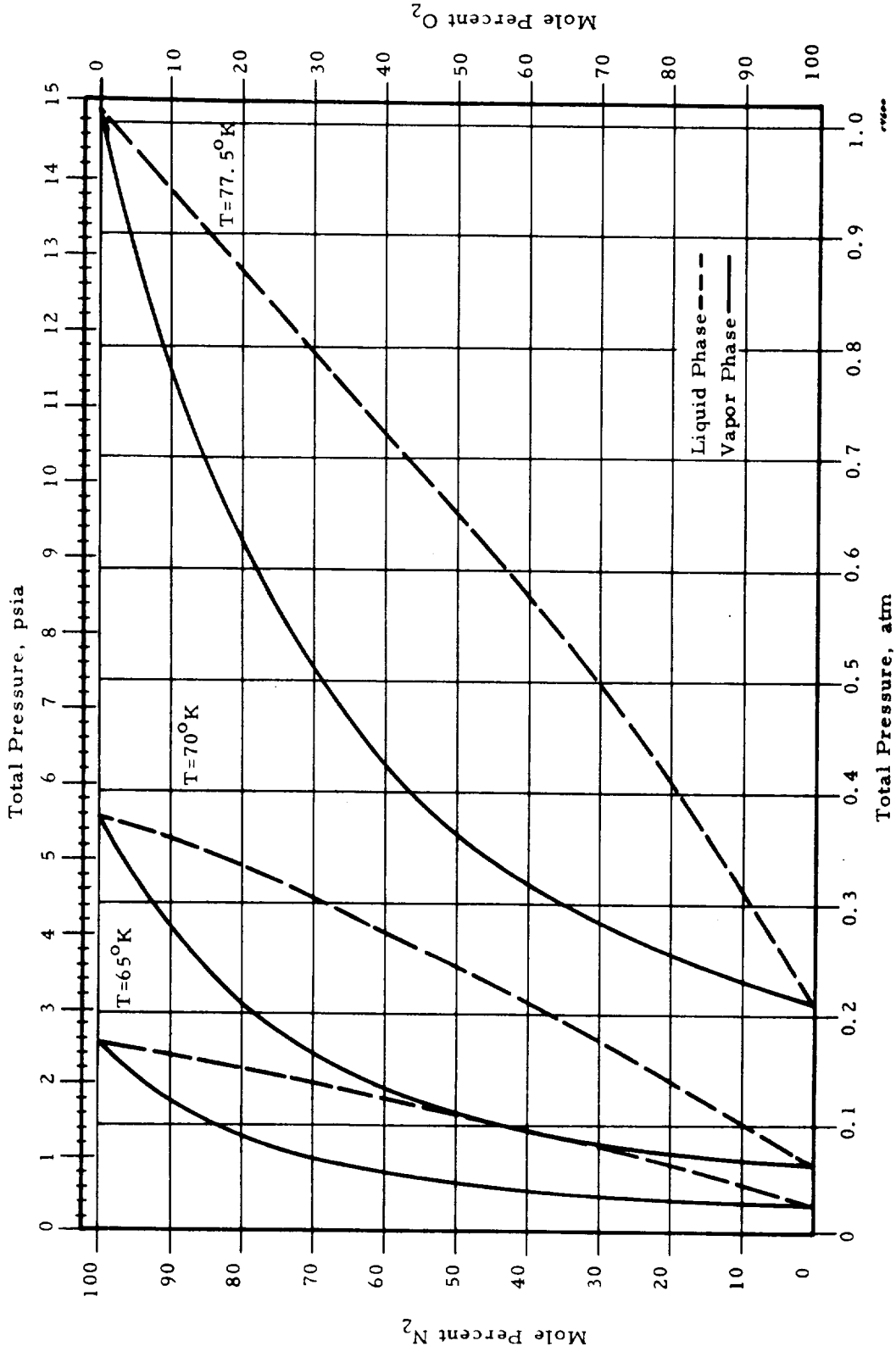

Figure IV-35. Isothermal Equilibrium Concentration of Nitrogen-Oxygen Mixtures

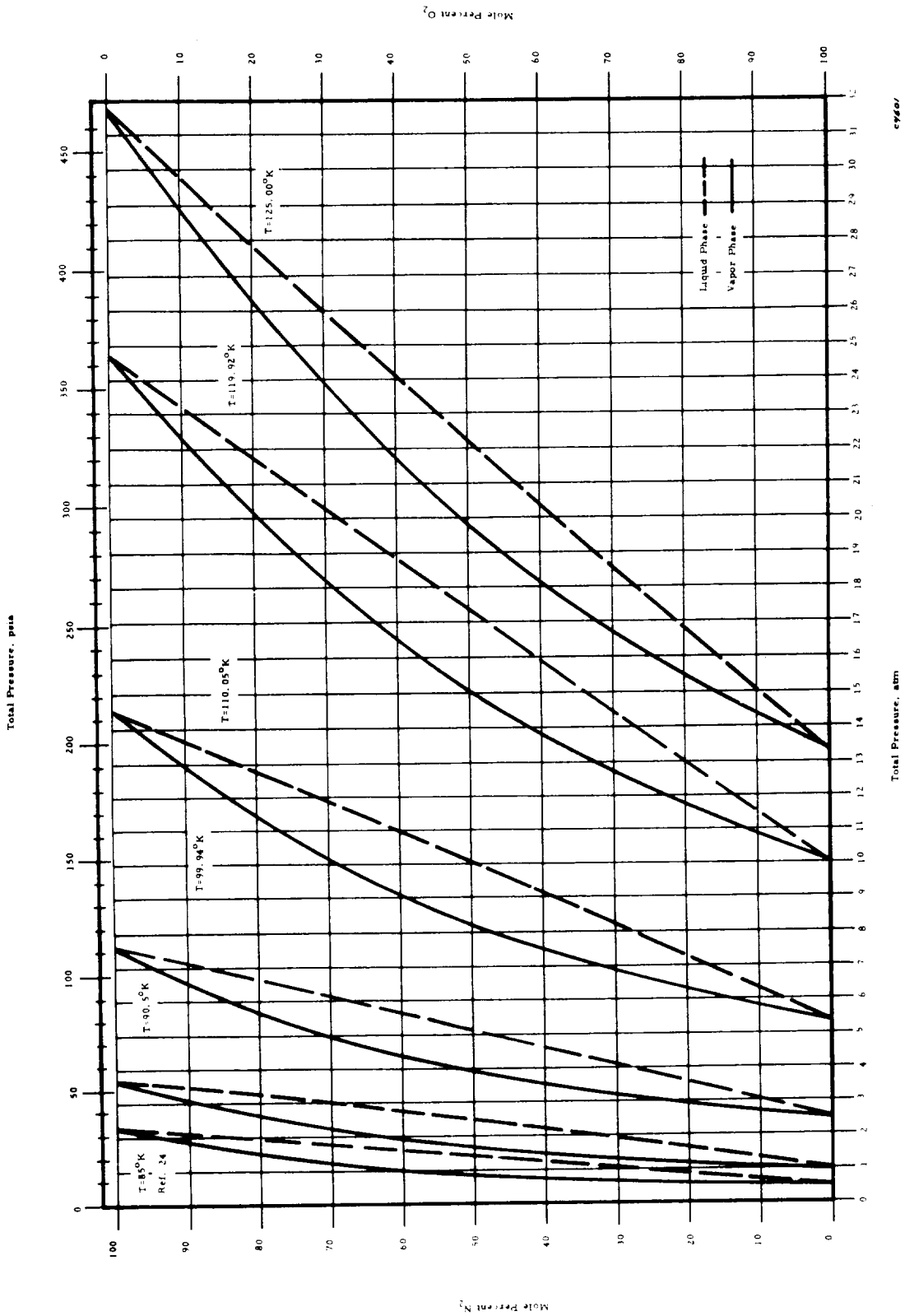

Figure IV-36. Isothermal Equilibrium Concentrations of Nitrogen-Oxygen Mixtures

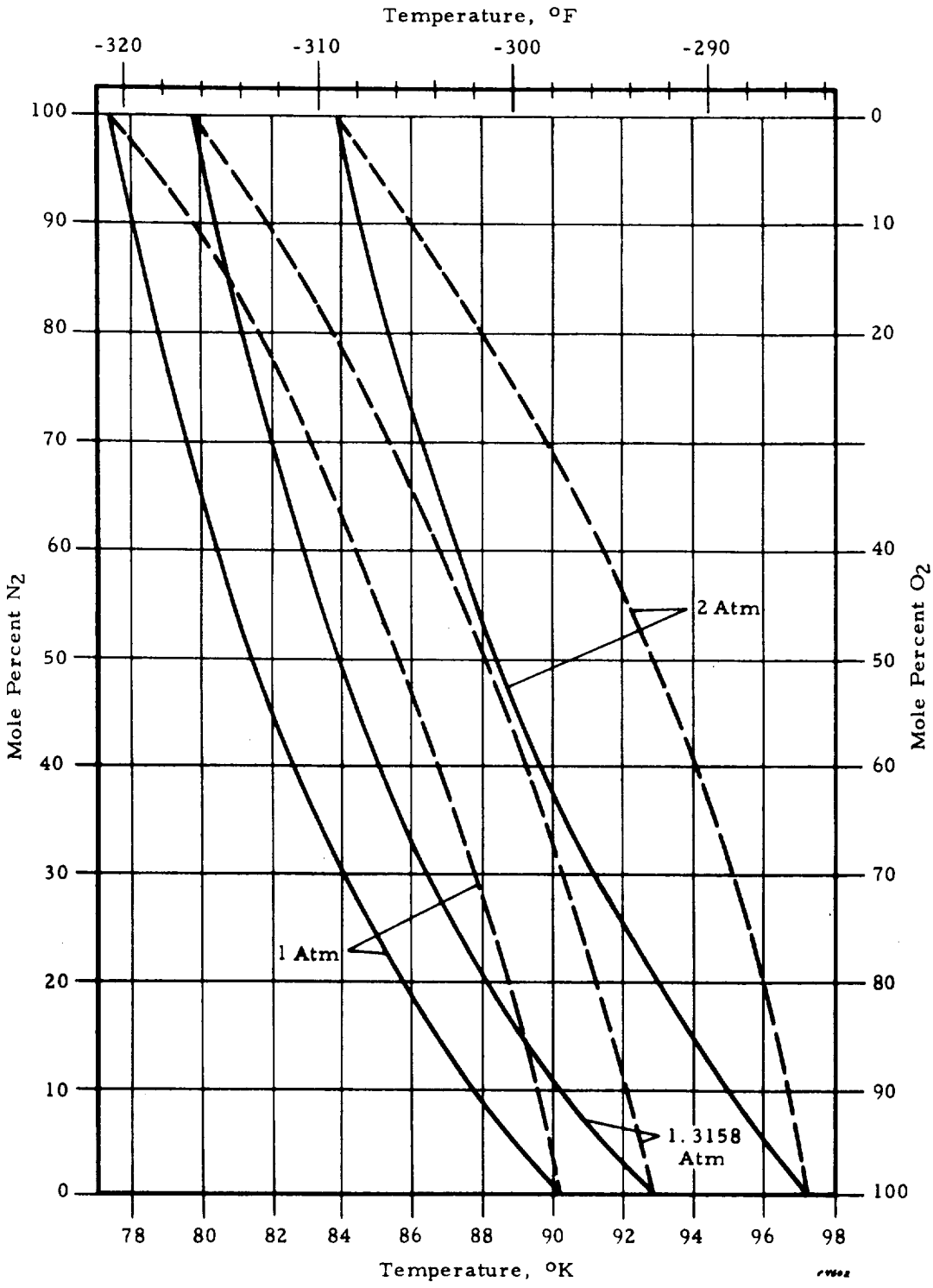

Figure IV-37. Isobaric Equilibrium Concentrations of Nitrogen-Oxygen Mixtures

TABLE IV-13

SOLUBILITY OF HELIUM AND NITROGEN
IN LIQUID OXYGEN DIFLUORIDE

Test Temperature °F	Vapor Pressure of Propellant psia[a]	Mole Percent Concentration			
		Helium		Nitrogen	
		300 psia	700 psia	300 psia	700 psia
-320	<1	0.024	0.030	—	—
-270	1.5	0.098	0.203	—	—
-220	29	0.252	0.588	—	—
-200	45	—	—	23.1	61.5[b]
-170	115	0.344	1.08	14.1	49.9
-150	205	—	—	6.12	35.8

(a) Reference 63.

(b) 600 psia.

The results reported in the table are obtained from duplicate analyses for two successive samples; agreement of these values within experimental error was accepted as indication that solution equilibrium had been attained.

These data are presented as isothermal pressure-composition and isobaric temperature-composition plots in Figures IV-38, IV-39, IV-40, and IV-41. Additional isobars at 150 and 500 psia have been constructed for these systems by interpolation.

In the system oxygen difluoride-nitrogen the useful operating range is limited by the condensation of nitrogen (-226°F at 700 psia) and the vapor pressure of the solvent (300 psia at -130°F). A further experimental limitation was imposed by the very high solubility of nitrogen at the lower temperatures. Consequently only the temperature range of -150° to -200°F was investigated between 300 and 700 psia. The non-linear plots in Figure IV-40 indicate considerable deviation from Henry's Law at these high pressurant gas concentrations.

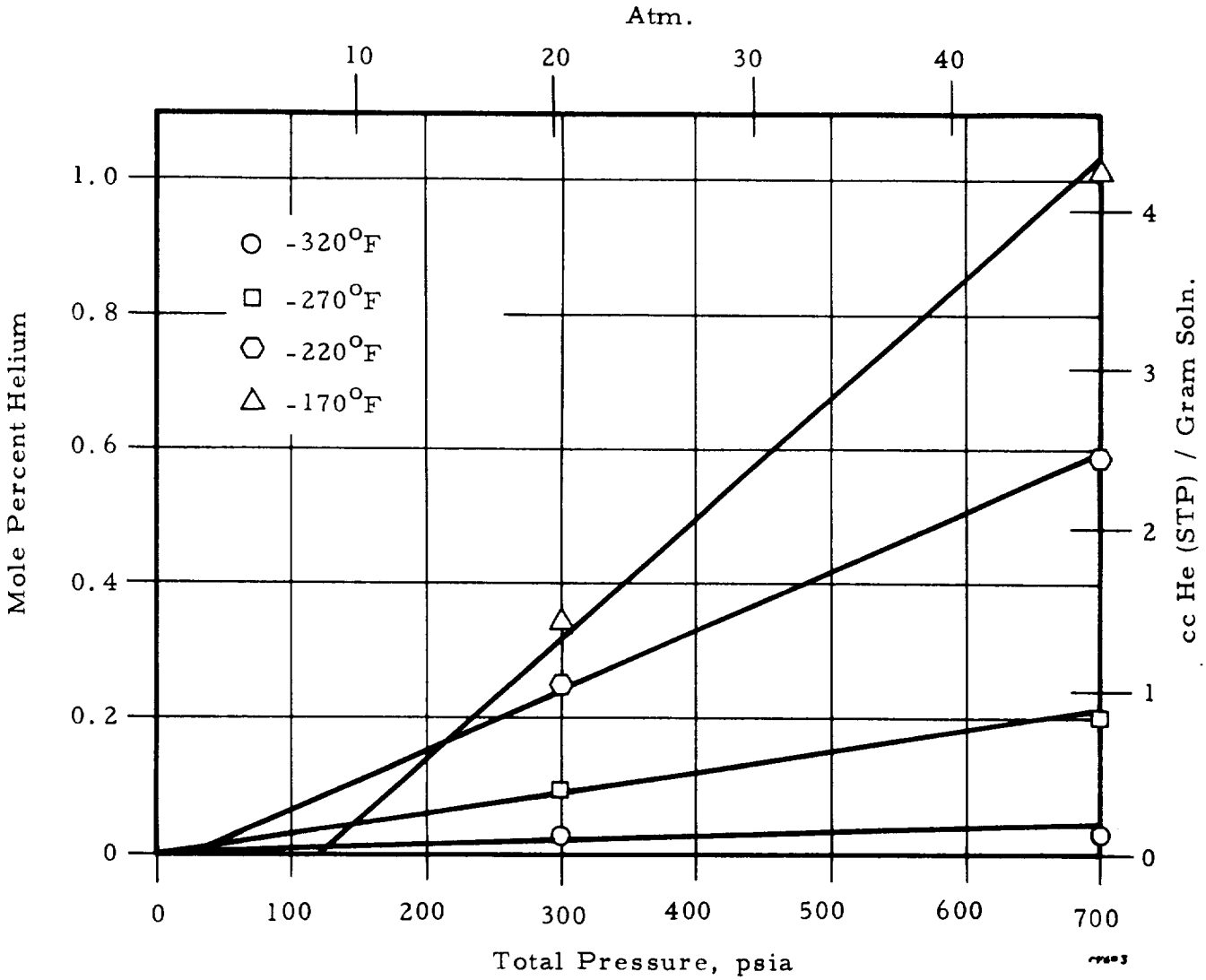

Figure IV-38. Isothermal Pressure – Composition Diagram for the System Liquid Oxygen Difluoride-Helium

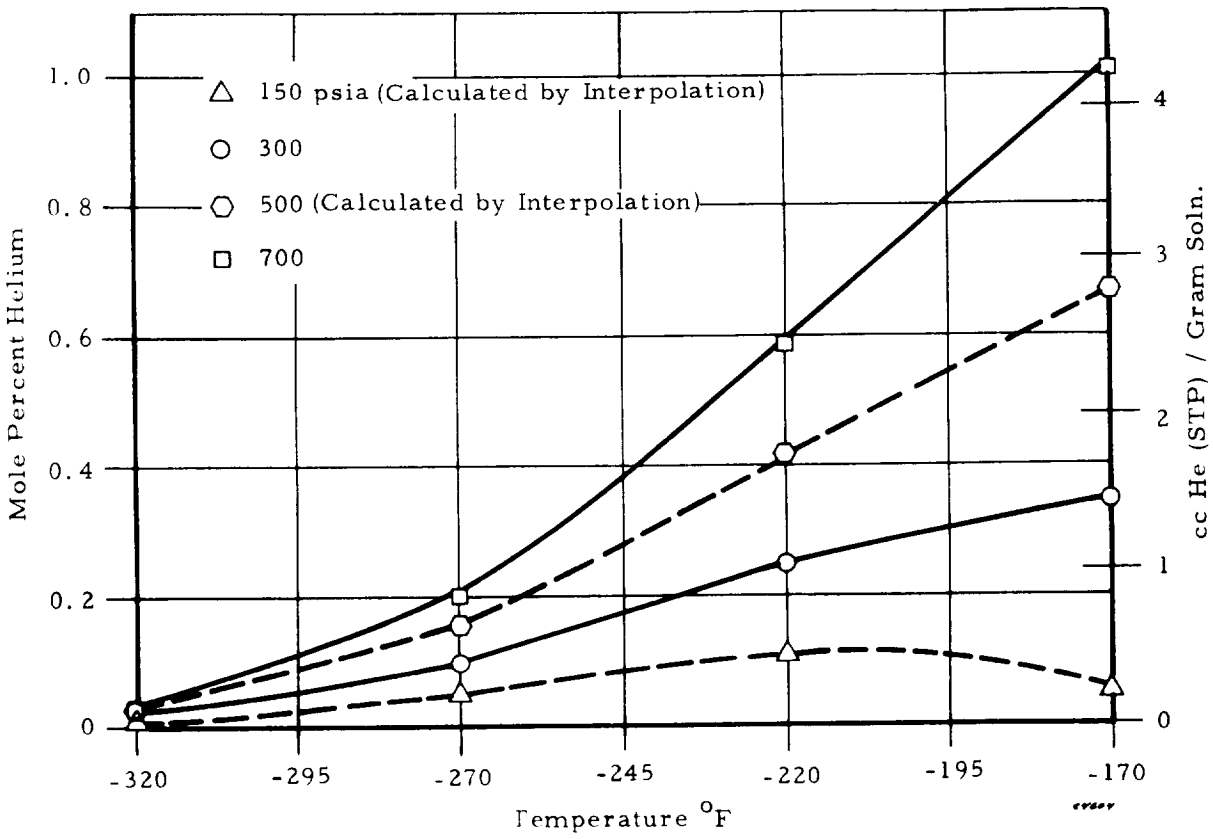

Figure IV-39. Isobaric Temperature-Composition Diagram for the System Liquid Oxygen Difluoride-Helium

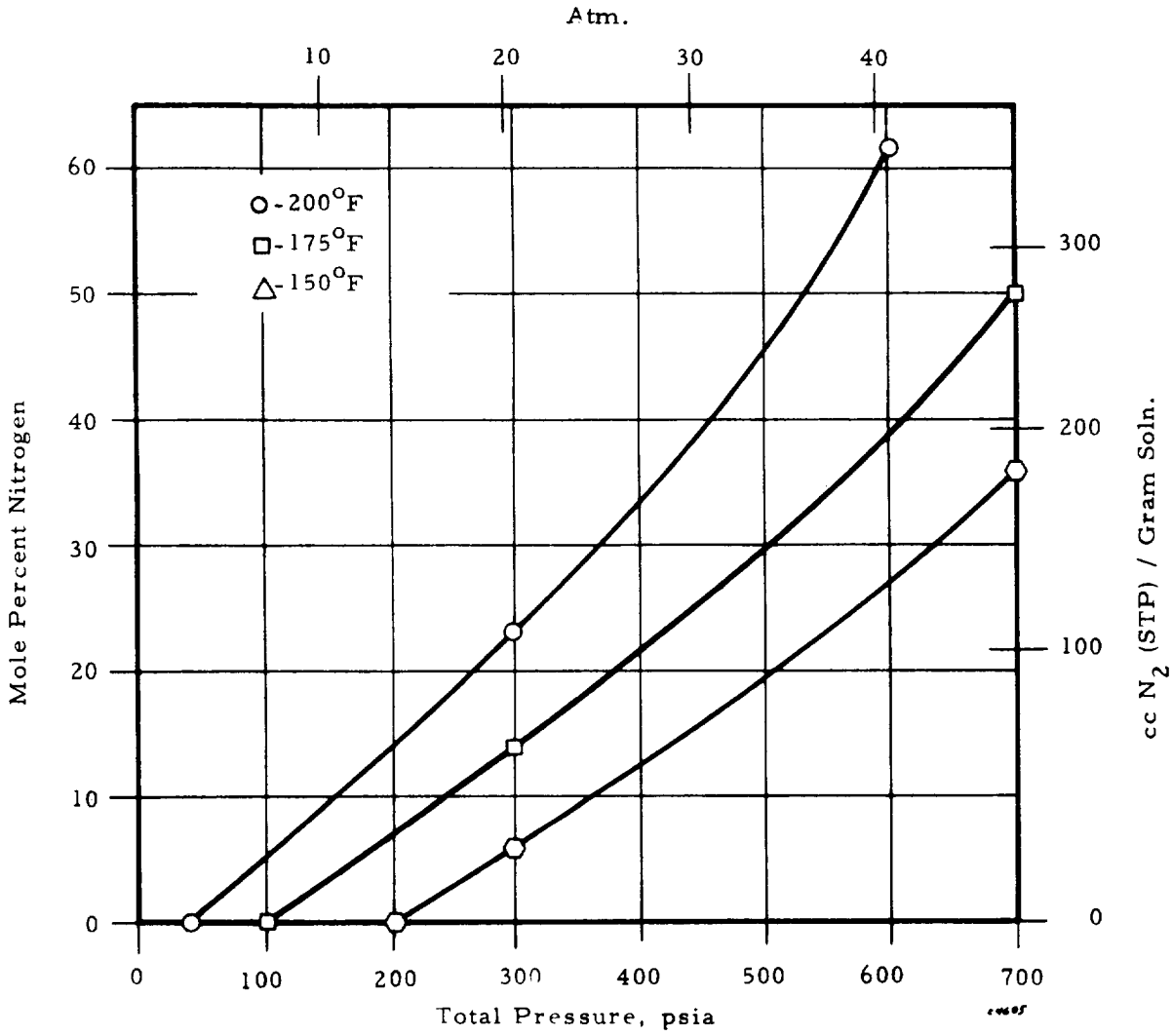

Figure IV-40. Isothermal Pressure-Composition Diagram for the System Liquid Oxygen Difluoride-Nitrogen

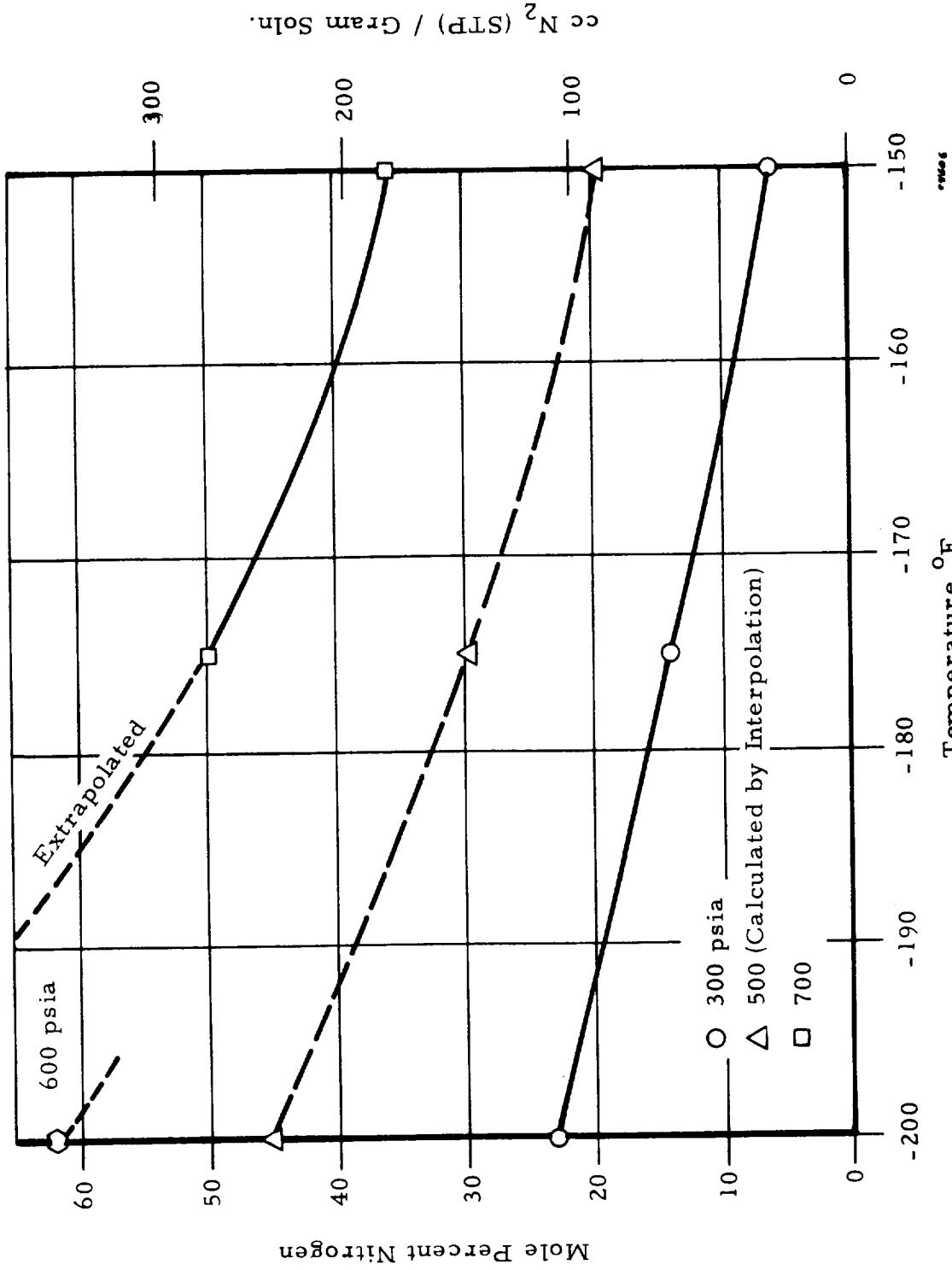

Figure IV-41. Isobaric Temperature – Composition Diagram for the System Liquid Oxygen Difluoride-Nitrogen

21. Perchloryl Fluoride-Helium

See Section 22.

22. Perchloryl Fluoride-Nitrogen

The solubilities of helium and nitrogen in liquid perchloryl fluoride were measured by Astropower Laboratory for this Design Guide, under Contract NAS7-548. The solubility data for these two systems are tabulated in Table IV-14; experimental details may be found in Reference 46. The results reported in the table are obtained from duplicate analyses for two successive samples; agreement of these values within experimental error was accepted as indication that solution equilibrium had been attained.

TABLE IV-14

SOLUBILITY OF HELIUM AND NITROGEN IN LIQUID PERCHLORYL FLUORIDE

Test Temperature °F	Vapor Pressure of Propellant psia[a]	Mole Percent Concentration			
		Helium		Nitrogen	
		300 psia	700 psia	300 psia	700 psia
-150	0.5	0.090	0.284	5.75	12.9
-100	3.5	0.223	0.518	4.96	11.3
-50	16.7	0.298	0.761	4.49	10.7
0	44	0.438	1.21	3.89	9.53

(a) Reference 47.

These data are presented as isothermal pressure-composition and isobaric temperature-composition plots in Figures IV-42, IV-43, IV-44, and IV-45. Additional isobars at 150 and 500 psia have been constructed for each system by interpolation.

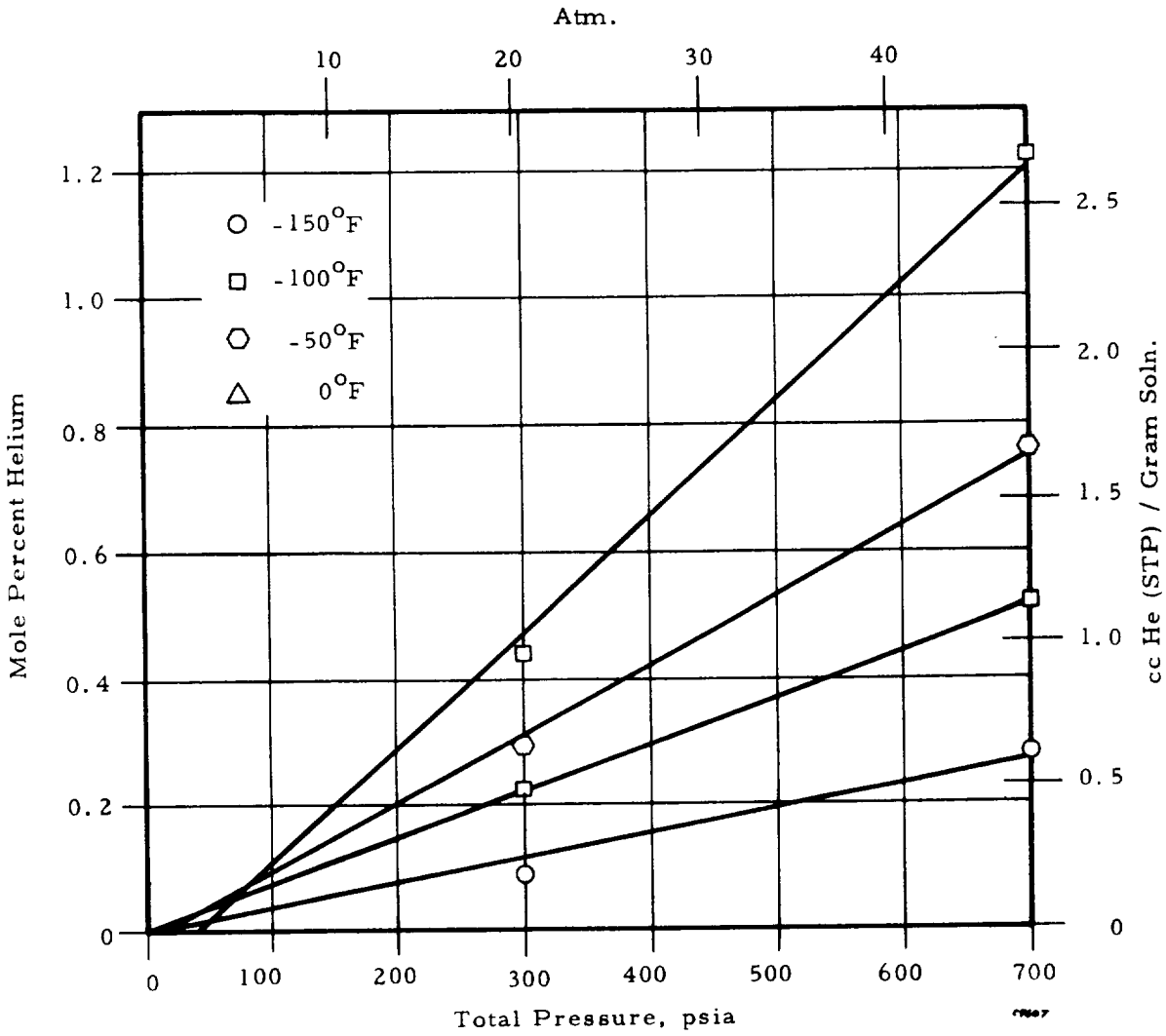

Figure IV-42. Isothermal Pressure-Composition Diagram for the System Liquid Perchloryl Fluoride-Helium

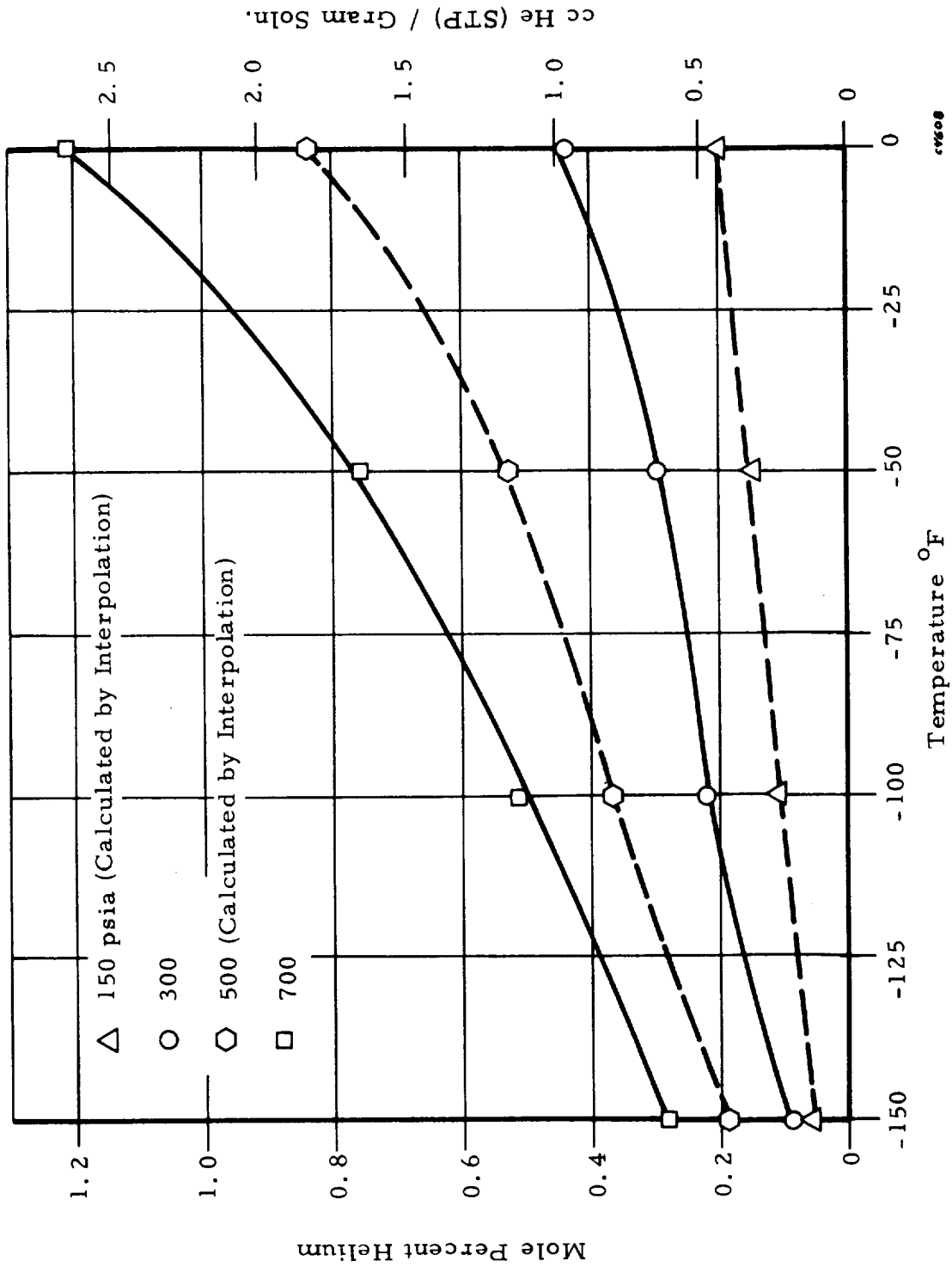

Figure IV-43. Isobaric Temperature – Composition Diagram for the System Liquid Perchloryl Fluoride-Helium

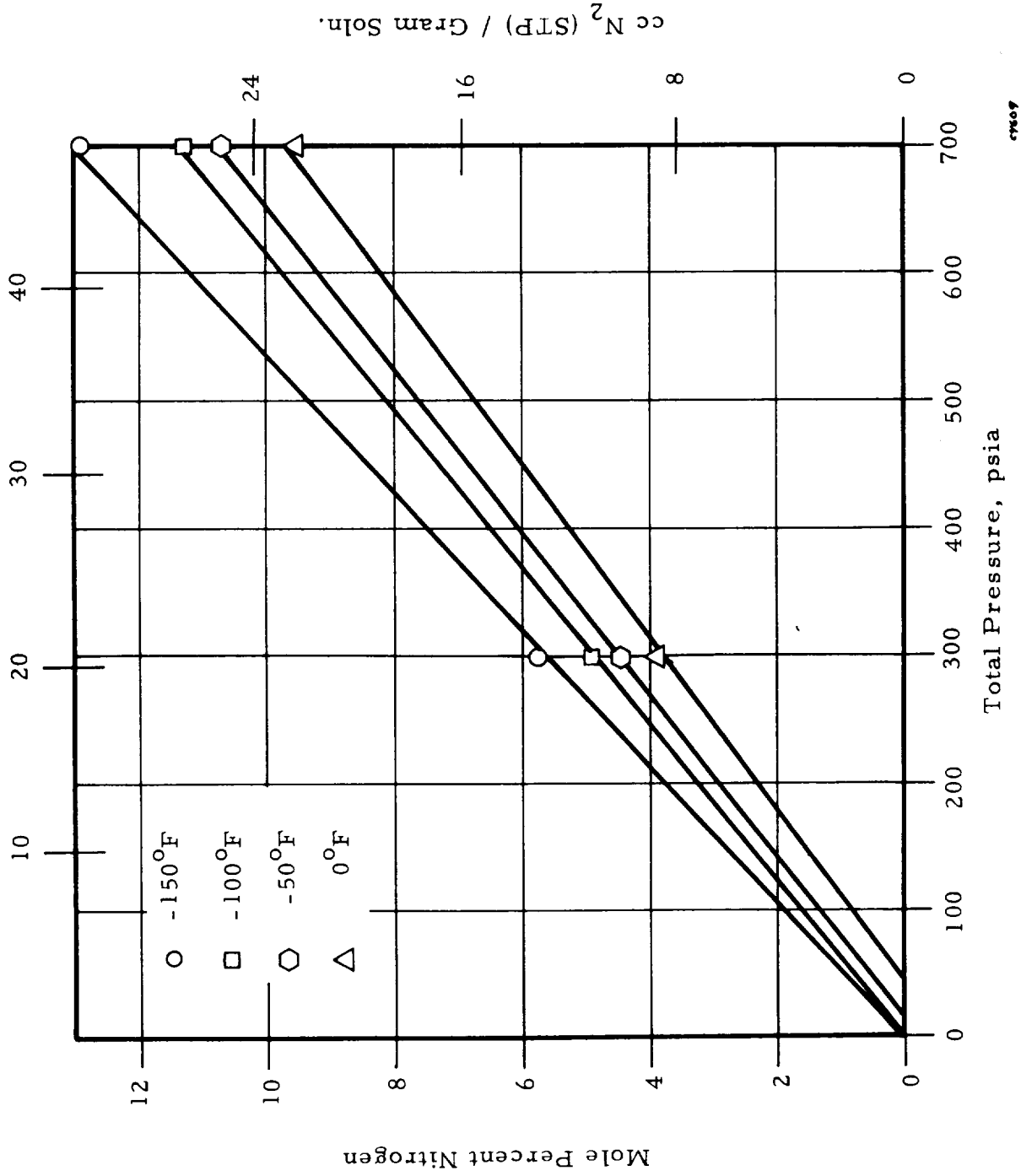

Figure IV-44. Isothermal Pressure – Composition Diagram for the System Liquid Perchloryl Fluoride-Nitrogen

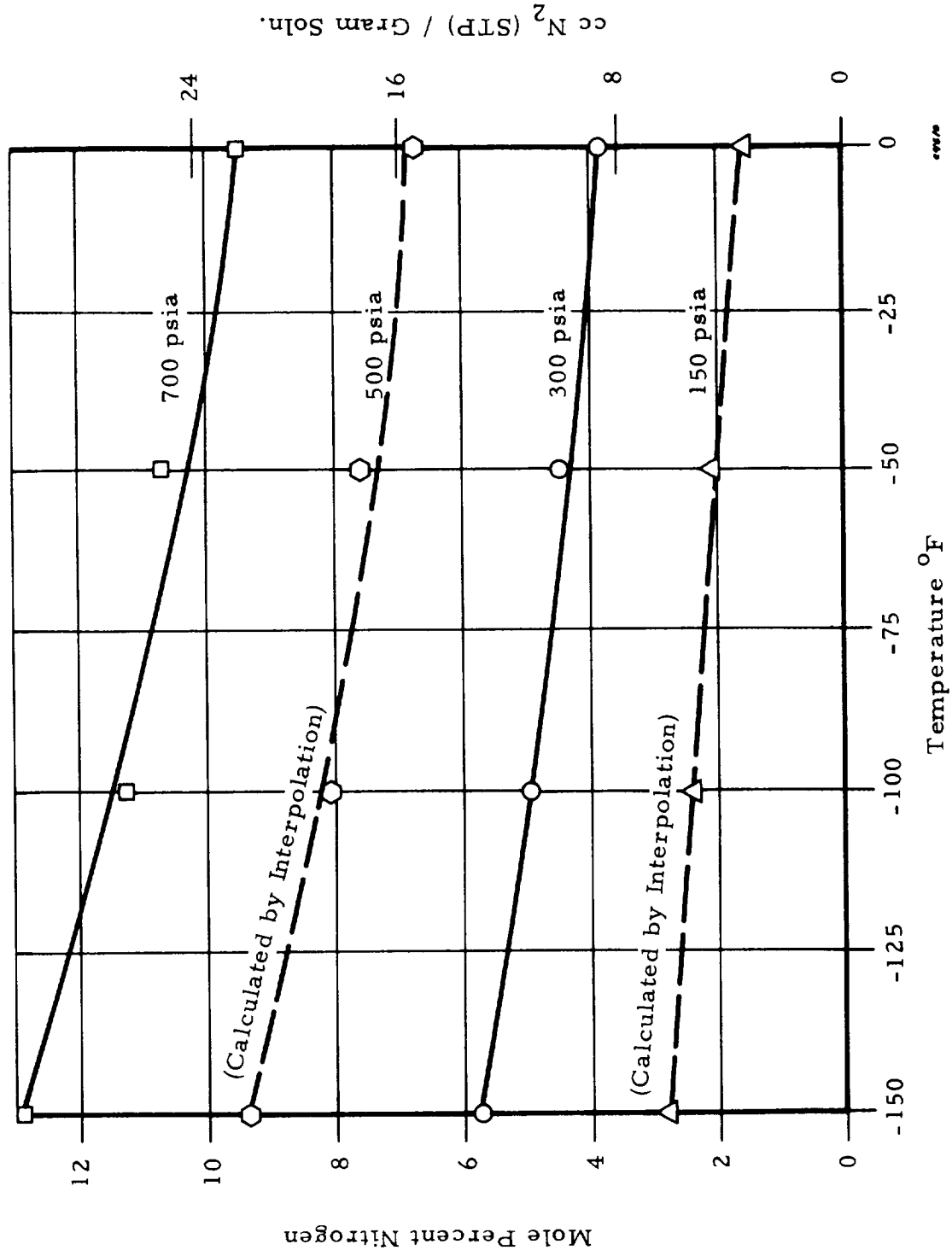

Figure IV-45. Isobaric Temperature – Composition Diagram for the System Liquid Perchloryl Fluoride-Nitrogen

23. Tetrafluorohydrazine-Helium

See Section 24.

24. Tetrafluorohydrazine-Nitrogen

The solubilities of helium and nitrogen in liquid tetrafluorohydrazine were measured by Astropower Laboratory for this Design Guide, under Contract NAS7-548. The solubility data for these two systems are tabulated in Table IV-15; experimental details may be found in Reference 46. The results reported in the table are obtained from duplicate analyses for two successive samples; agreement of these values within experimental error was accepted as indication that solution equilibrium had been attained.

TABLE IV-15

SOLUBILITY OF HELIUM AND NITROGEN IN LIQUID TETRAFLUOROHYDRAZINE

Test Temperature °F	Vapor Pressure of Propellant psia[a]	Mole Percent Concentration			
		Helium		Nitrogen	
		300 psia	700 psia	300 psia	700 psia
-200	0.7	0.165	0.405	18.6	42.3
-150	4.0	0.303	0.746	11.2	24.8
-100	14.7	0.479	1.24	8.93	20.9
-50	38	0.652	1.73	6.24	16.6

(a) Reference 64.

These data are presented as isothermal pressure-composition and isobaric temperature-composition plots in Figures IV-46, IV-47, IV-48, and IV-49. Additional isobars at 150 and 500 psia have been constructed for each system by interpolation.

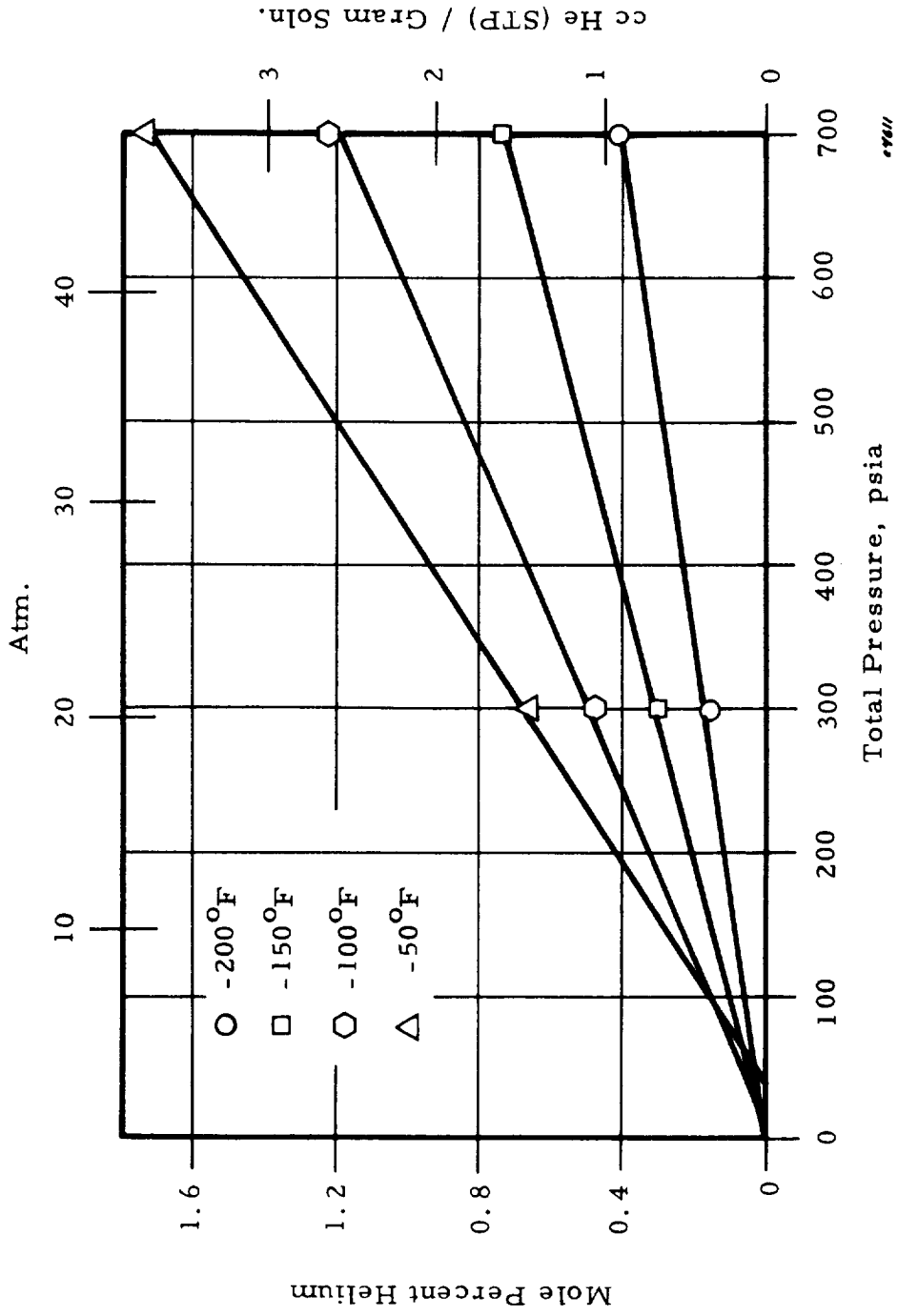

Figure IV-46. Isothermal Pressure – Composition Diagram for the System Liquid Tetrafluorohydrazine-Helium

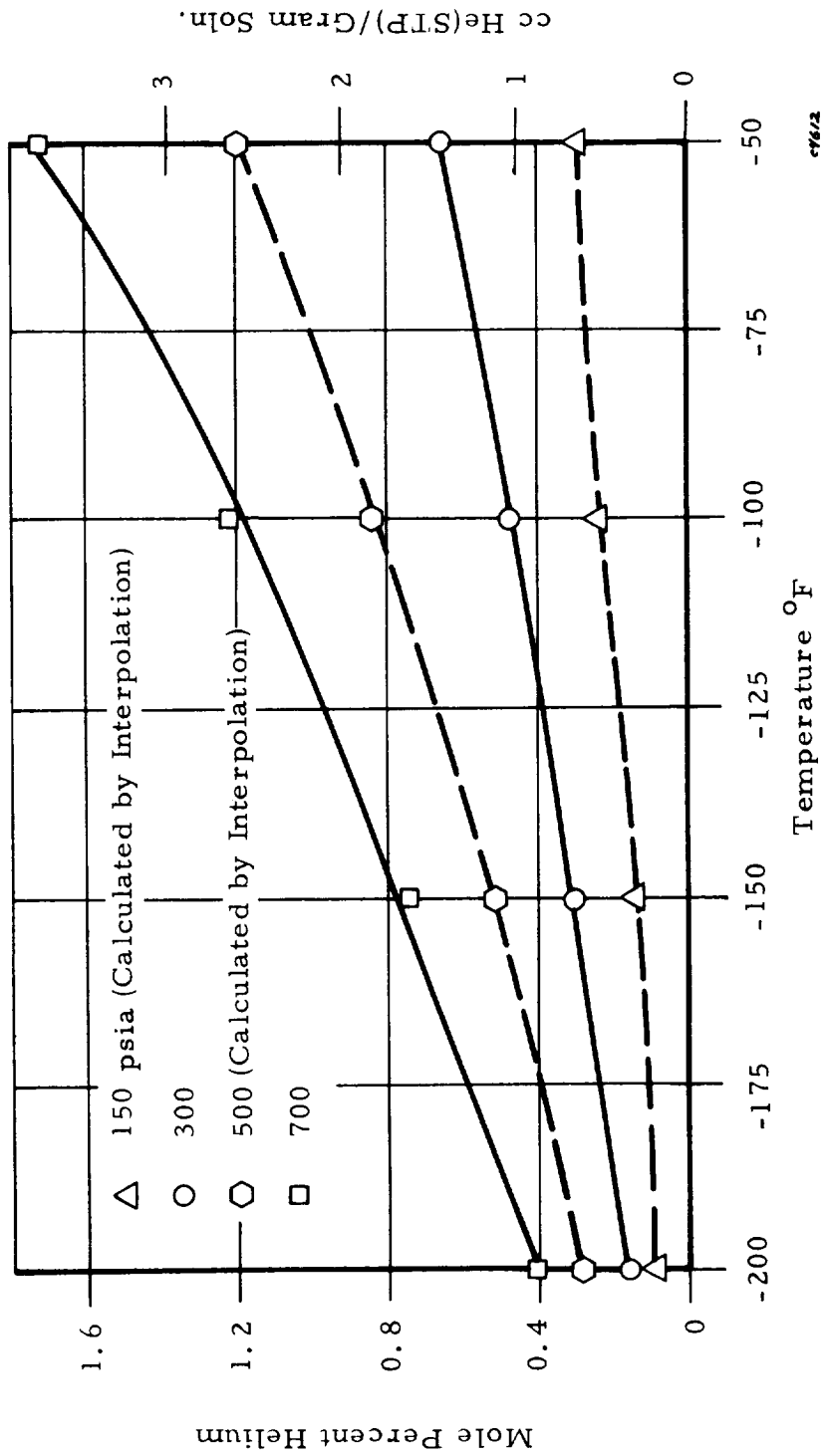

Figure IV-47. Isobaric Temperature – Composition Diagram for the System Liquid Tetrafluorohydrazine-Helium

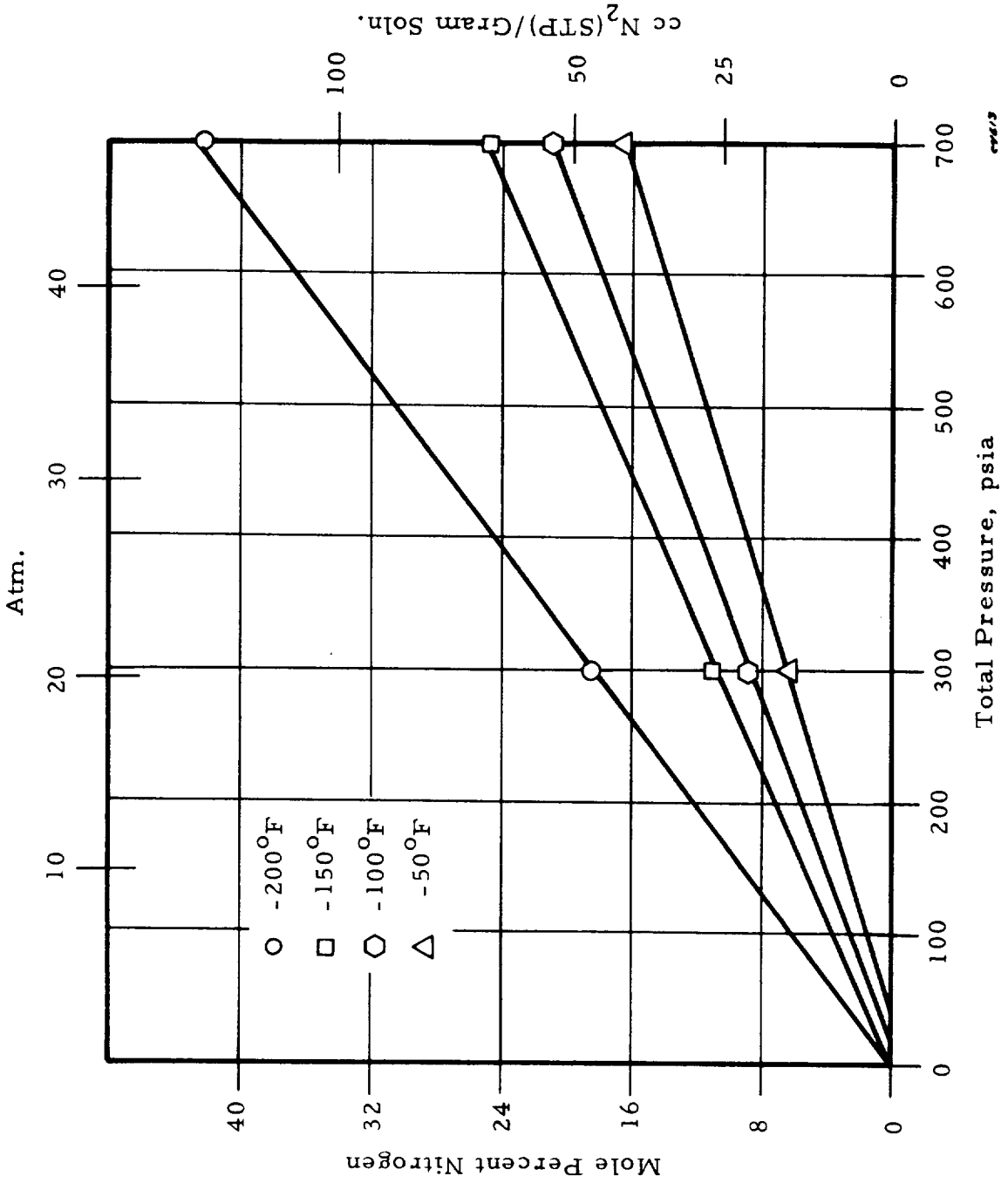

Figure IV-48. Isothermal Pressure – Composition Diagram for the System Liquid Tetrafluorohydrazine-Nitrogen

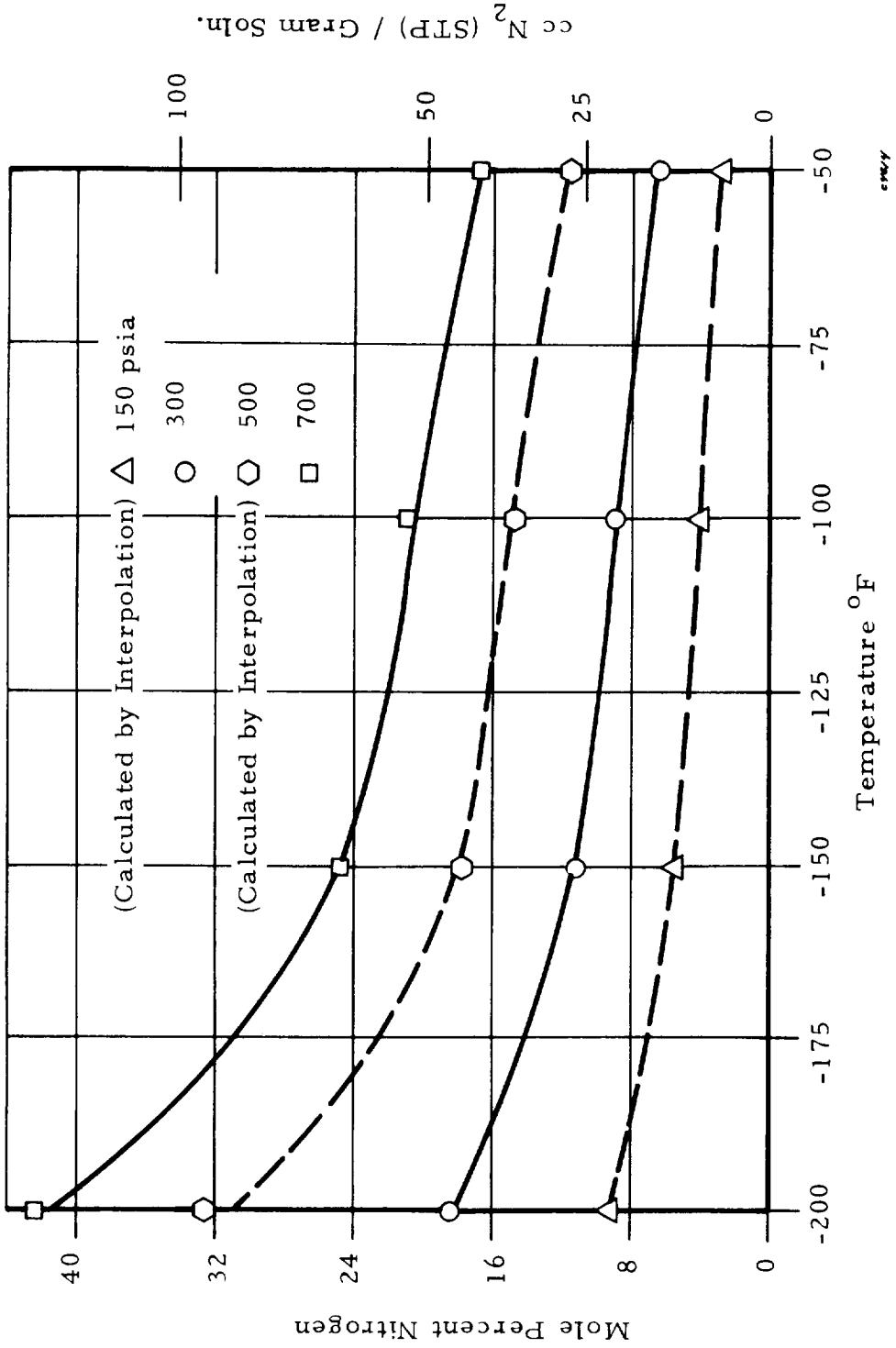

Figure IV-49. Isobaric Temperature-Composition Diagram For The System Liquid Tetrafluorohydrazine-Nitrogen.

D. SOLUBILITY DATA FOR PRESSURANT GASES IN PROPELLANT FUELS

Pertinent physical properties for the fuels considered here are listed in Table IV-16. The tabulated solubility data and/or solubility data plots for the fuel-pressurant systems that are available are presented in the following sections.

1. Aerozine 50-Ammonia

See Section 3.

2. Aerozine 50-Helium

See Section 3.

3. Aerozine 50-Nitrogen

The solubility of helium, nitrogen, and ammonia in Aerozine-50 fuel blend (50 wt% N_2H_4 - 50 wt% UDMH) is shown in Table IV-17. These data are from Reference 65. Figures IV-50 and IV-51 show data for helium and nitrogen solubility at higher pressures, which were reported by Aerojet-General Corporation (References 38 and 39).

4. Ammonia-Helium

See Section 5.

5. Ammonia-Nitrogen

The solubilities of both helium and nitrogen in liquid ammonia were measured by Astropower Laboratory for this Design Guide, under Contract NAS7-548. The solubility data for these two systems are tabulated in Tavle IV-18; experimental details may be found in Reference 46. The results reported in the table are obtained from duplicate analyses for two successive samples; agreement of these values within experimental error was accepted as indication that solution equilibrium had been attained.

These data are presented as isothermal pressure-composition and isobaric temperature-composition plots in Figures IV-52, IV-53, IV-54,

TABLE IV-16

PHYSICAL PROPERTIES OF PROPELLANT FUELS

Fuel	Formula	Mol. Wt.	M. P. °R	B. P. °R	Tc °R	Pc psia	Liquid Range °R	Ref.
Aerozine 50	(a)	45 (ave)	478-481	618	1094 (calc)	1696 (calc)	614	47
Ammonia	NH_3	17.03	351.9	431.6	729.8	1636	377.9	47
Diborane	B_2H_6	27.69	193.7	325.1	521.8	581	328	66
Ethane	C_2H_6	30.07	161.8	332.2	549.8	708.3	388.0	90
Ethylene	C_2H_4	28.05	186.8	304.7	509.7	750	322.9	91
Hydrazine	N_2H_4	32.04	494.4	696.0	1176	2132	682	47
Hydrogen (Normal)	H_2	2.016	25.2	36.7	59.9	190.8	34.7	47
Methane	CH_4	16.04	163.1	201.1	343.3	673.1	180.2	90
Monomethylhydrazine	$(CH_3)N_2H_3$	46.08	397.2	652.2	1054	1195	647	47
Monomethylhydrazine Monohydrate	$(CH_3)N_2H_3 \cdot H_2O$	64.10	—	—	—	—	—	
Pentaborane	B_5H_9	63.17	407.6	596.8	—	—	—	47
Propane	C_3H_8	44.10	153.8	415.9	665.9	617.4	512.1	89
Trimethylborane	$B(CH_3)_3$	55.92	201.0	455.7	690 (est)	—	488 (est)	86
UDMH (unsym.-dimethylhydrazine	$(CH_3)_2N_2H_2$	60.08	388.7	606	942	786	553	47

(a) 50 wt. % hydrazine in UDMH.

TABLE IV-17

SOLUBILITY OF AMMONIA, HELIUM AND NITROGEN IN AEROZINE 50

Pressurant Gas	Temperature °F	Pressure psia	Concentration Mole Percent
Ammonia	70.5	44.4	0.095 ± .004
Ammonia	57.5	38.0	0.098 ± .004
Helium	71.5	63.6	0.0011 ± .003
Helium	33.0	60.7	0.0007
Nitrogen	70.0	86.0	0.0030
Nitrogen	32.0	79.4	0.0030

TABLE IV-18

SOLUBILITY OF HELIUM AND NITROGEN IN LIQUID AMMONIA

Test Temperature °F	Vapor Pressure of Propellant psia(a)	Mole Percent Concentration			
		Helium		Nitrogen	
		300 psia	700 psia	300 psia	700 psia
-100	1.3	—	—	0.030	0.070
-50	7.5	0.009	0.021	0.067	0.136
0	30	0.015	0.044	0.100	0.225
25	54	0.027	0.063	—	—
50	89	0.031	0.087	0.130	0.345

(a) Reference 57.

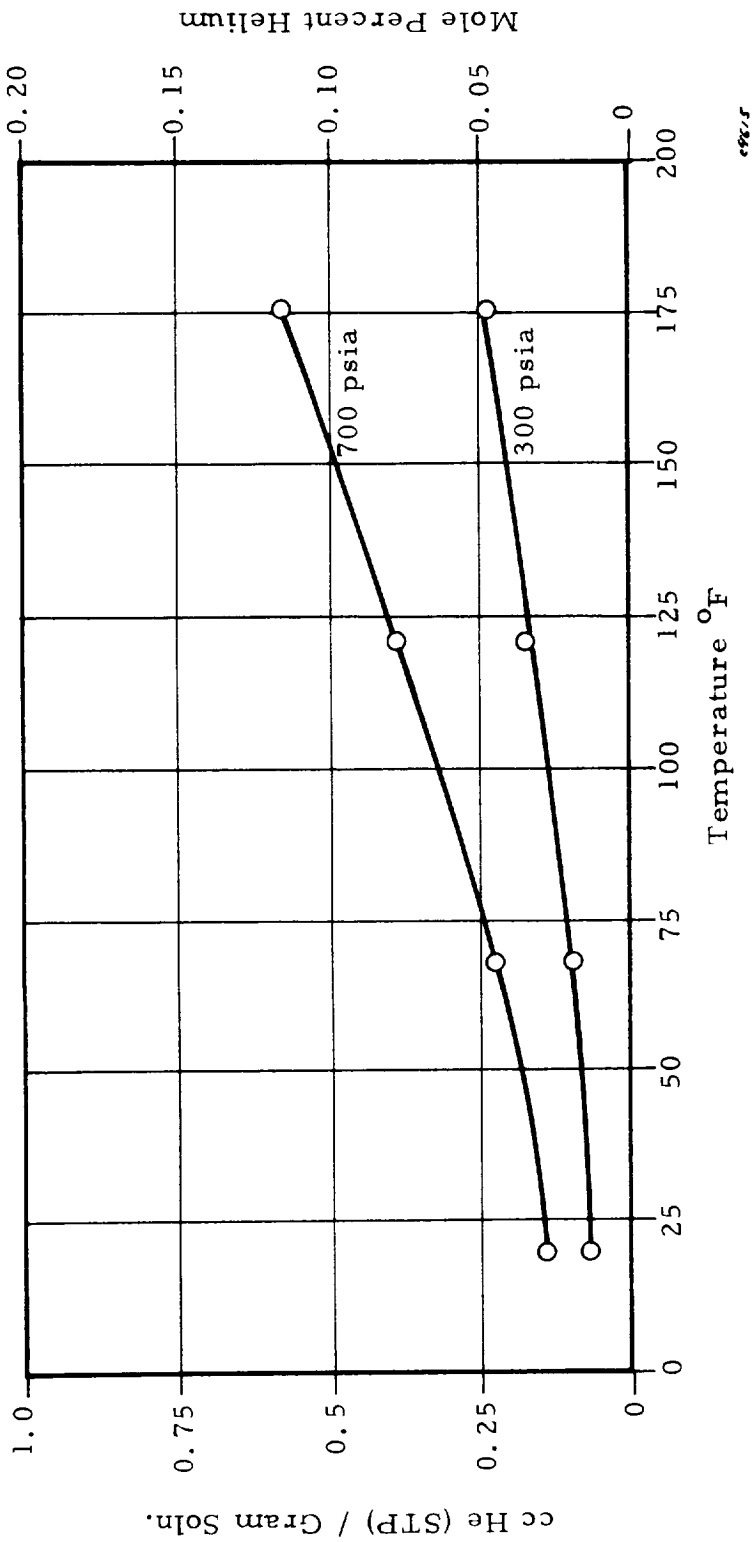

Figure IV-50. Isobaric Temperature – Composition Diagram For the System Liquid Aerozine 50-Helium

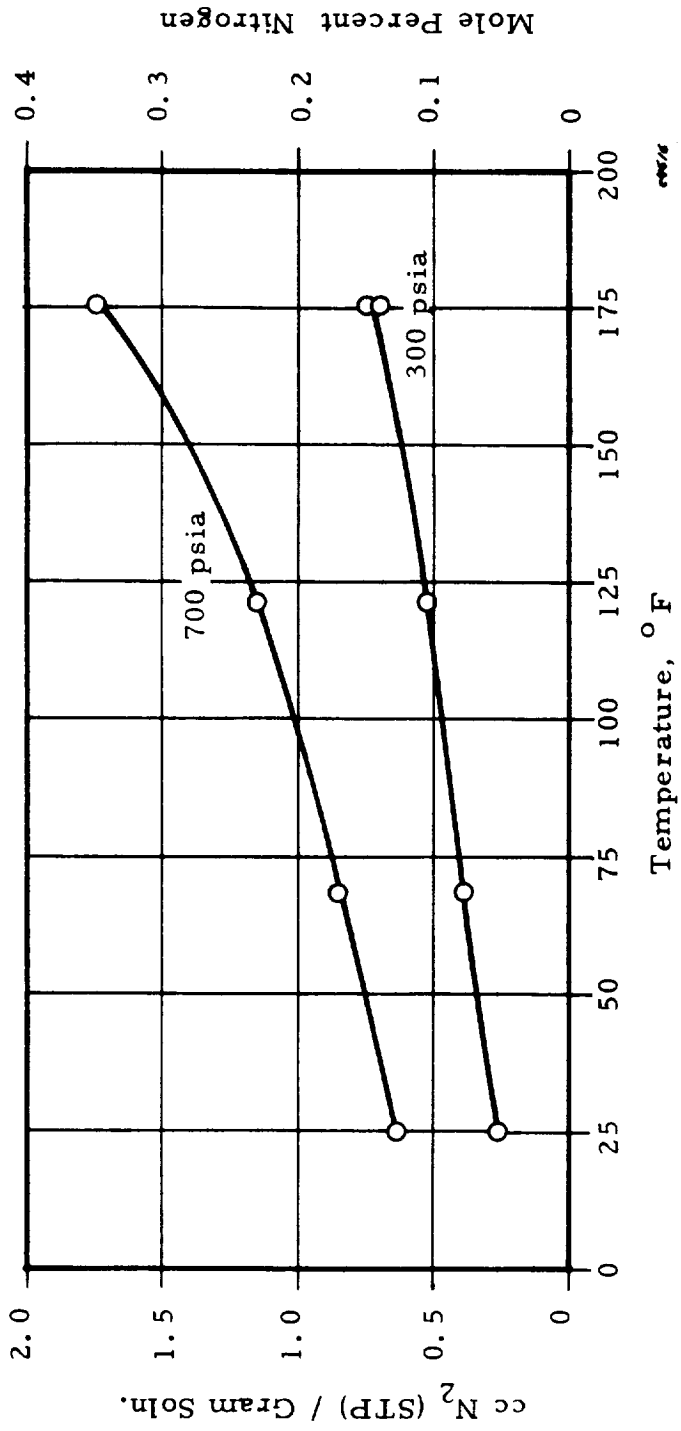

Figure IV-51. Isobaric Temperature-Composition Diagram for the System Liquid Aerozine 50-Nitrogen.

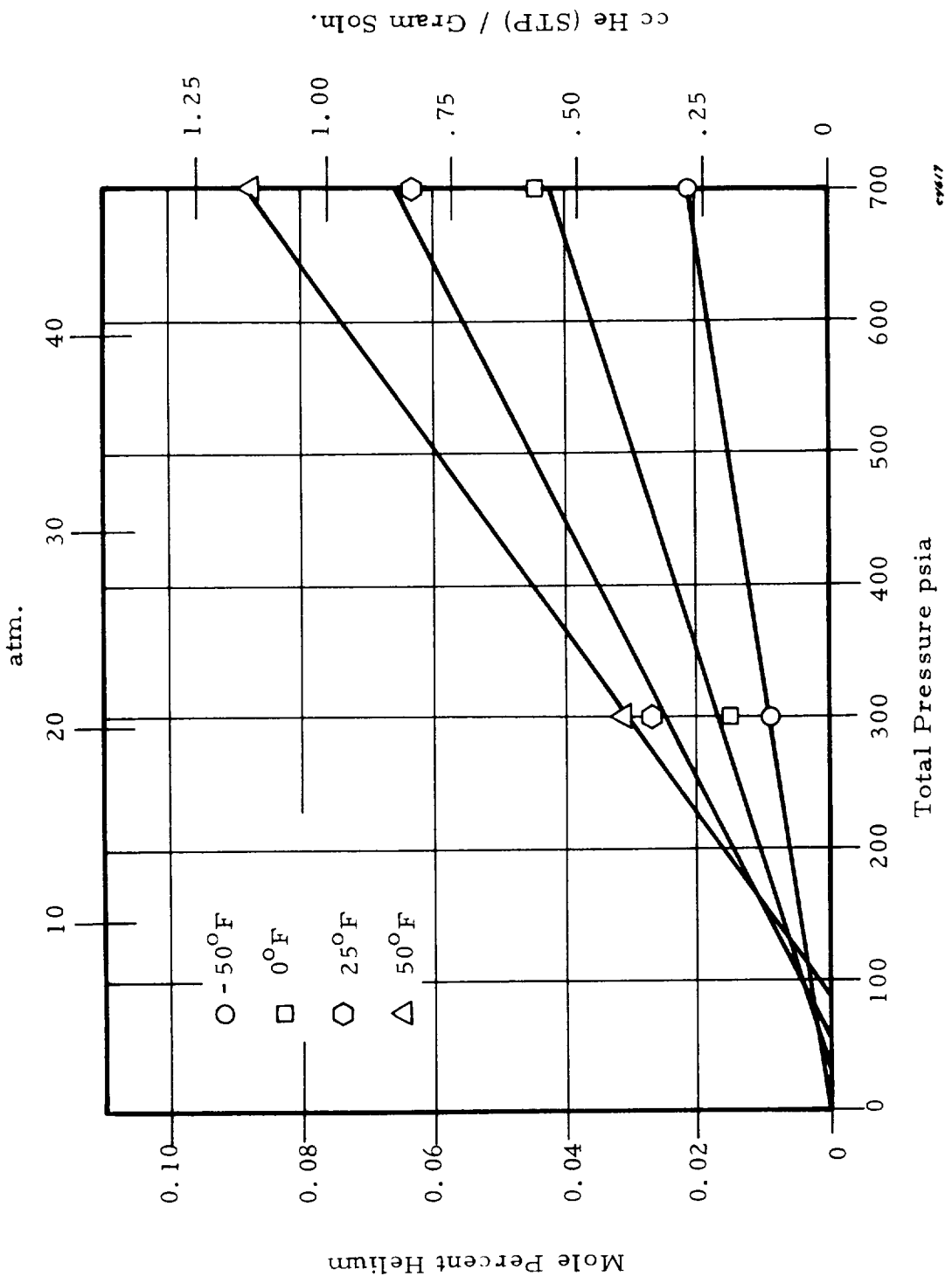

Figure IV-52. Isothermal Pressure-Composition Diagram For The System Liquid Ammonia-Helium

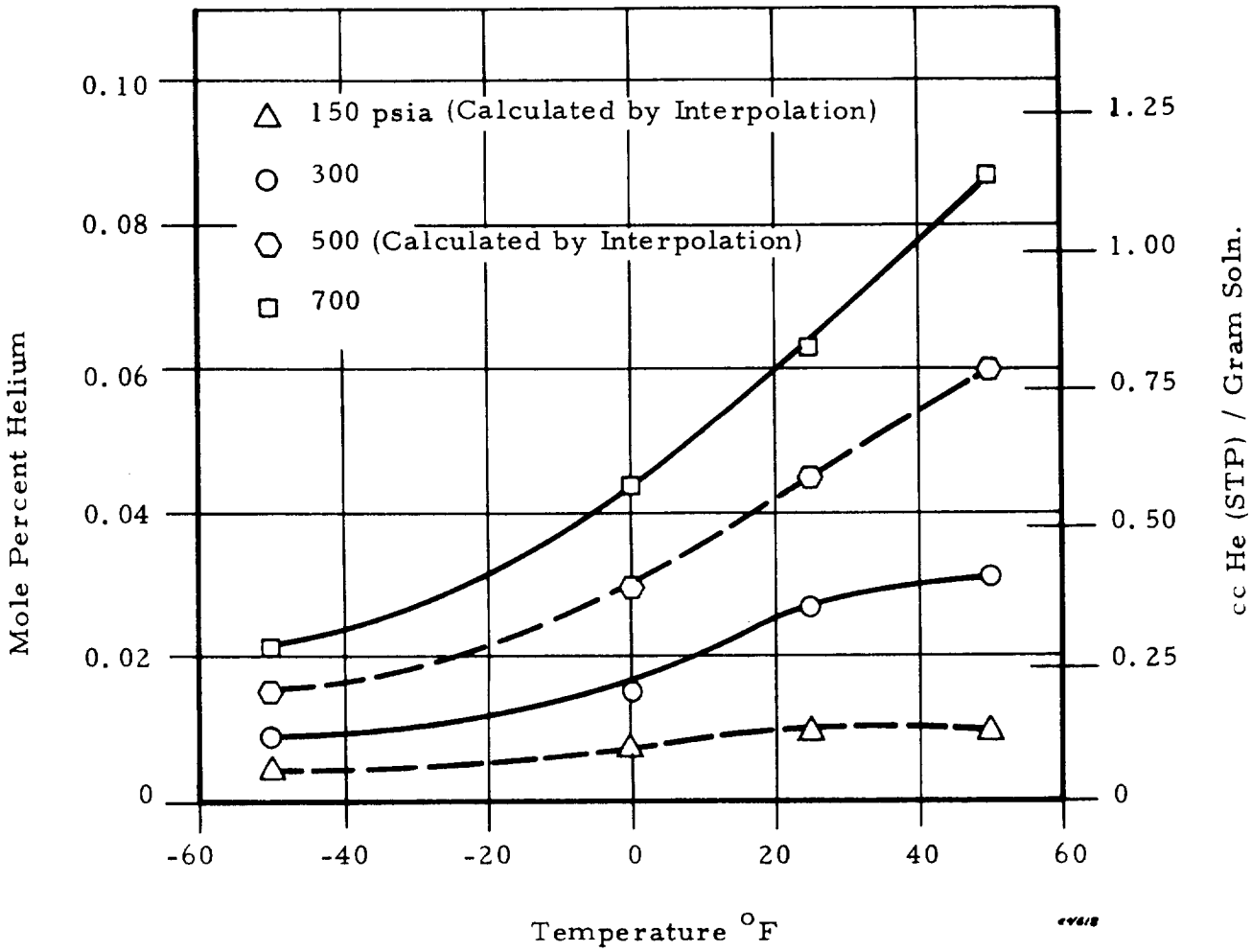

Figure IV-53. Isobaric Temperature-Composition Diagram For The System Liquid Ammonia-Helium

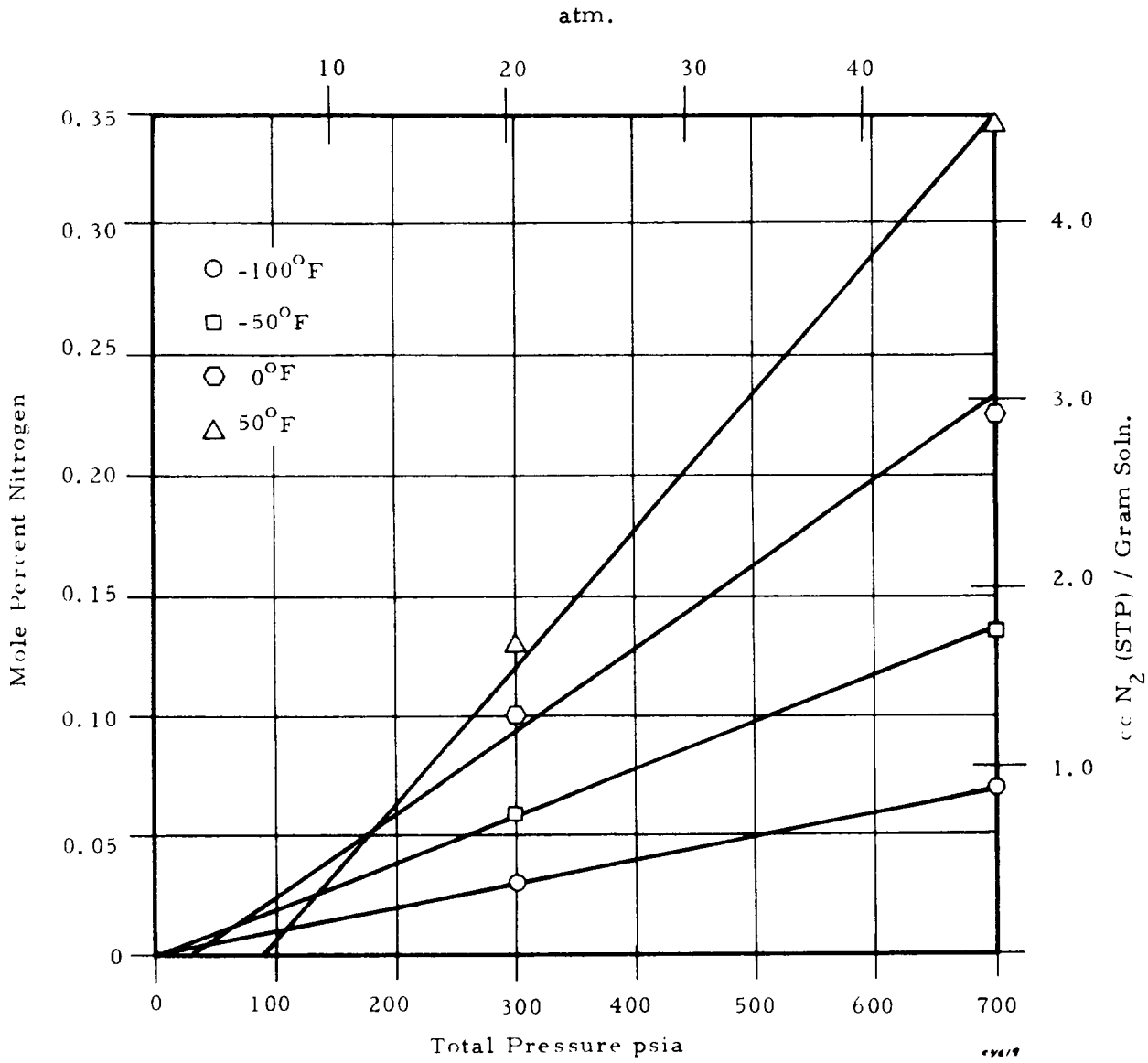

Figure IV-54. Isothermal Pressure-Composition Diagram for the System Liquid Ammonia-Nitrogen

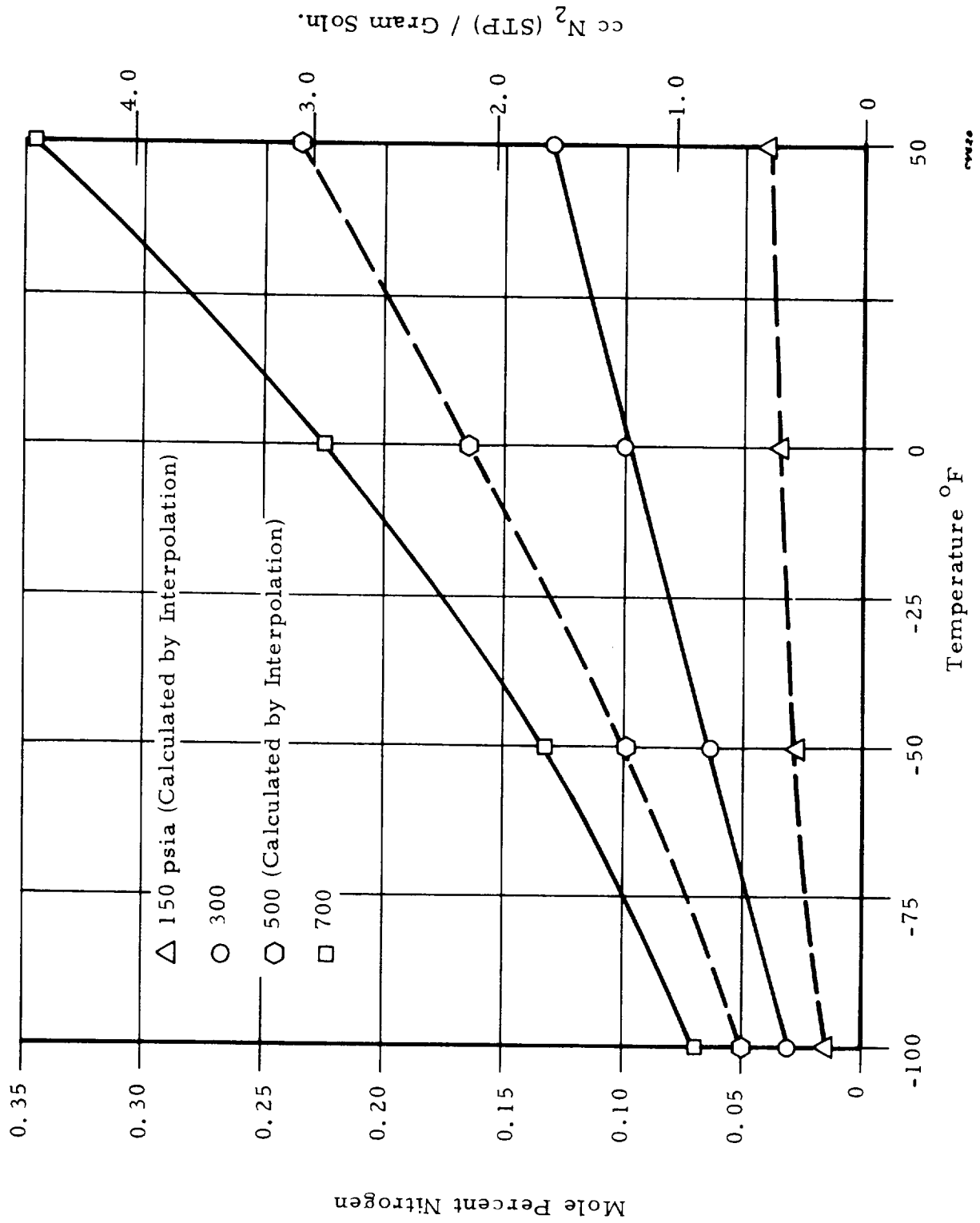

Figure IV-55. Isobaric Temperature-Composition Diagram For The System Liquid Ammonia-Nitrogen

and IV-55. Additional isobars at 150 and 500 psia have been constructed for each system by interpolation.

6. Diborane-Helium

See Section 7.

7. Diborane-Nitrogen

The solubilities of both helium and nitrogen in liquid diborane were measured by Astropower Laboratory for this Design Guide, under Contract NAS7-548. The solubility data for these two systems are tabulated in Table IV-19; experimental details may be found in Reference 46. The results reported in the table are obtained from duplicate analyses for two successive samples; agreement of these values within experimental error was accepted as indication that solution equilibrium had been attained.

TABLE IV-19

SOLUBILITY OF HELIUM AND NITROGEN IN LIQUID DIBORANE

Test Temperature °F	Vapor Pressure of Propellant psia[a]	Mole Percent Concentration			
		Helium		Nitrogen	
		300 psia	700 psia	300 psia	700 psia
-200	1	0.084	0.173	11.5	28.9
-150	9	0.183	0.468	7.78	19.6
-100	43	0.348	0.929	5.97	16.6
-50	110	0.448	1.47	4.05	13.9

(a) Reference 66.

These data are presented as isothermal pressure-composition and isobaric temperature-composition plots in Figures IV-56, IV-57, IV-58, and IV-59. Additional isobars at 150 and 500 psia have been constructed for

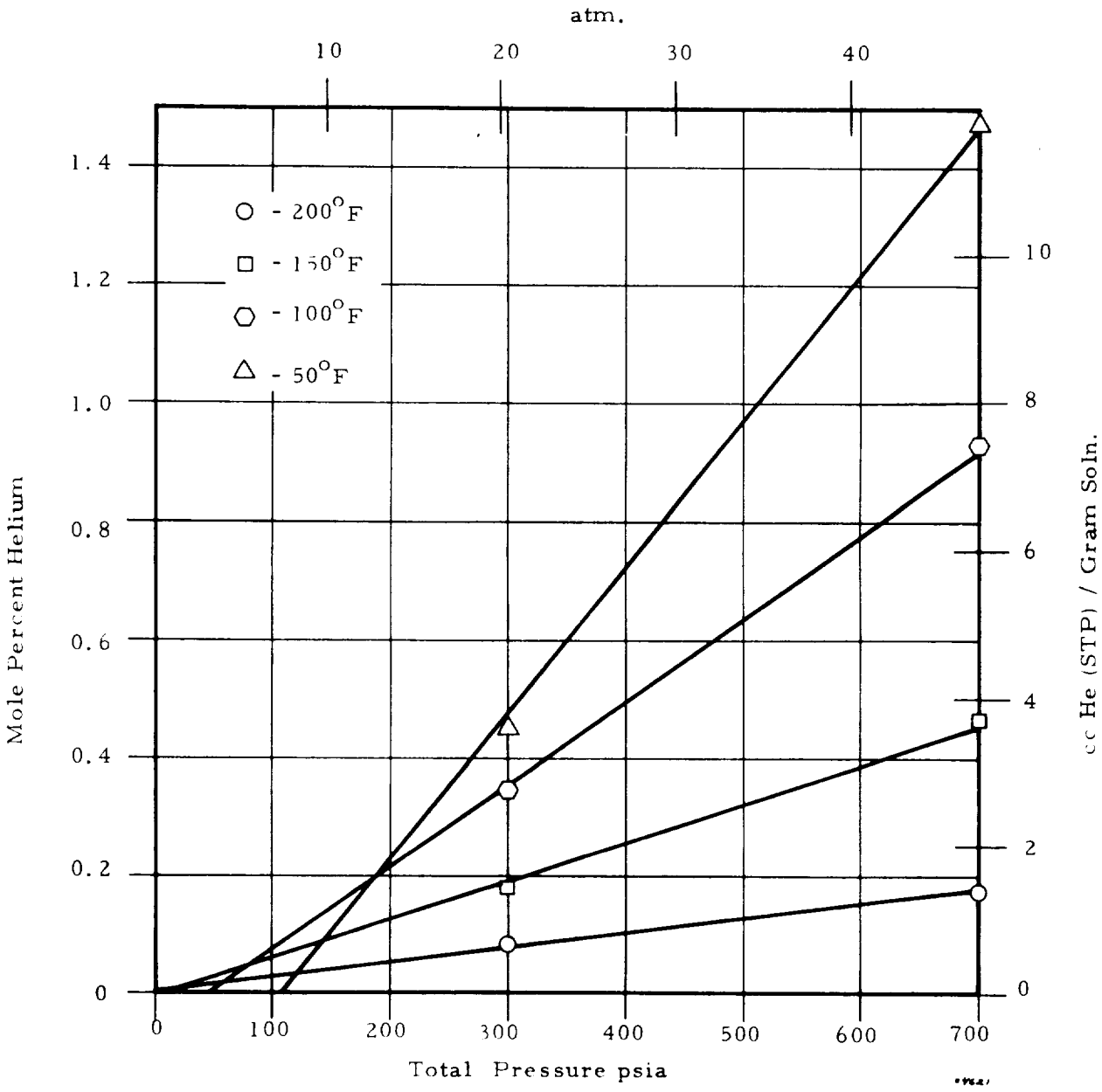

Figure IV-56. Isothermal Pressure-Composition Diagram for the System Liquid Diborane-Helium

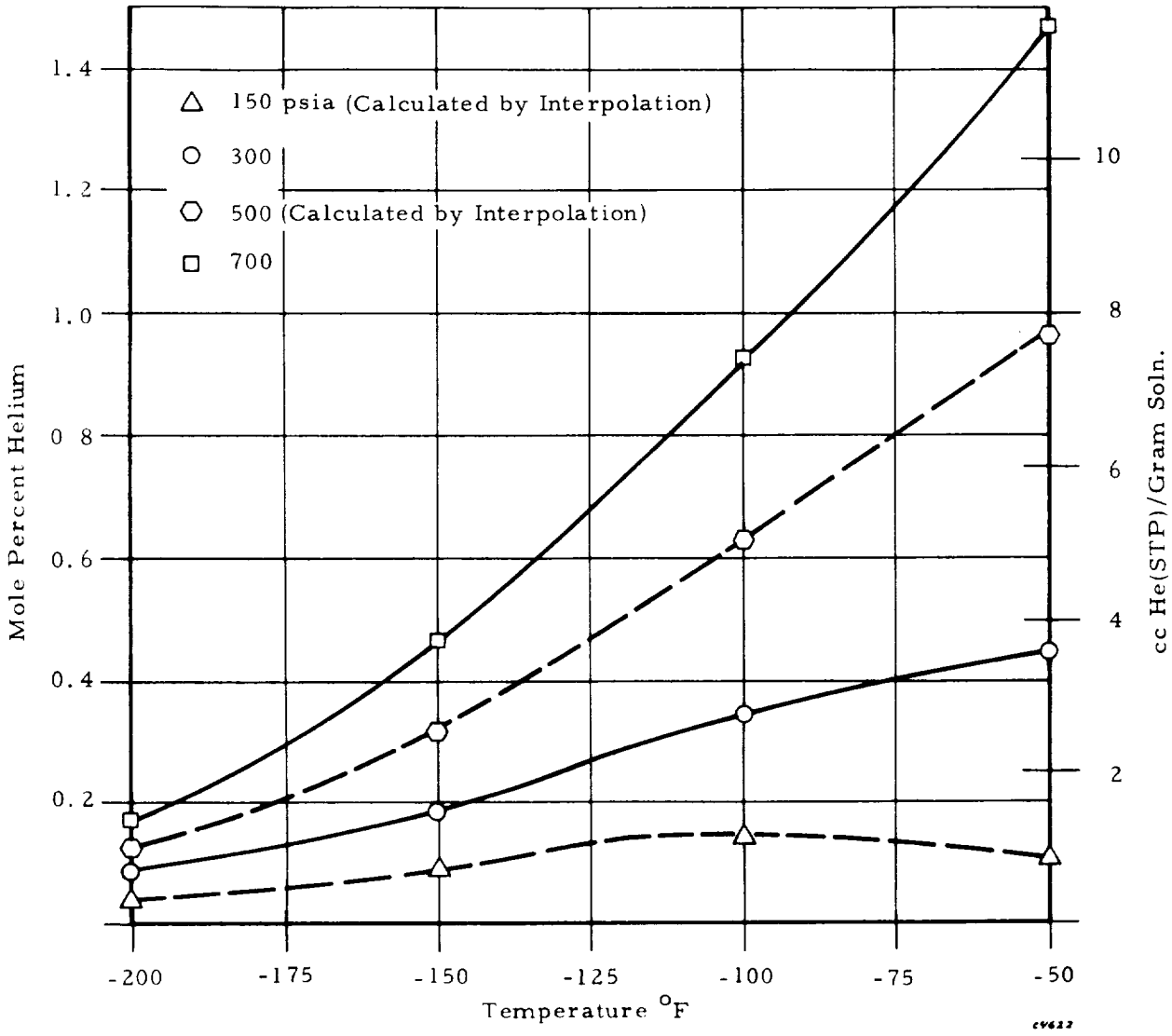

Figure IV-57. Isobaric Temperature-Composition Diagram for the System Liquid Diborane-Helium

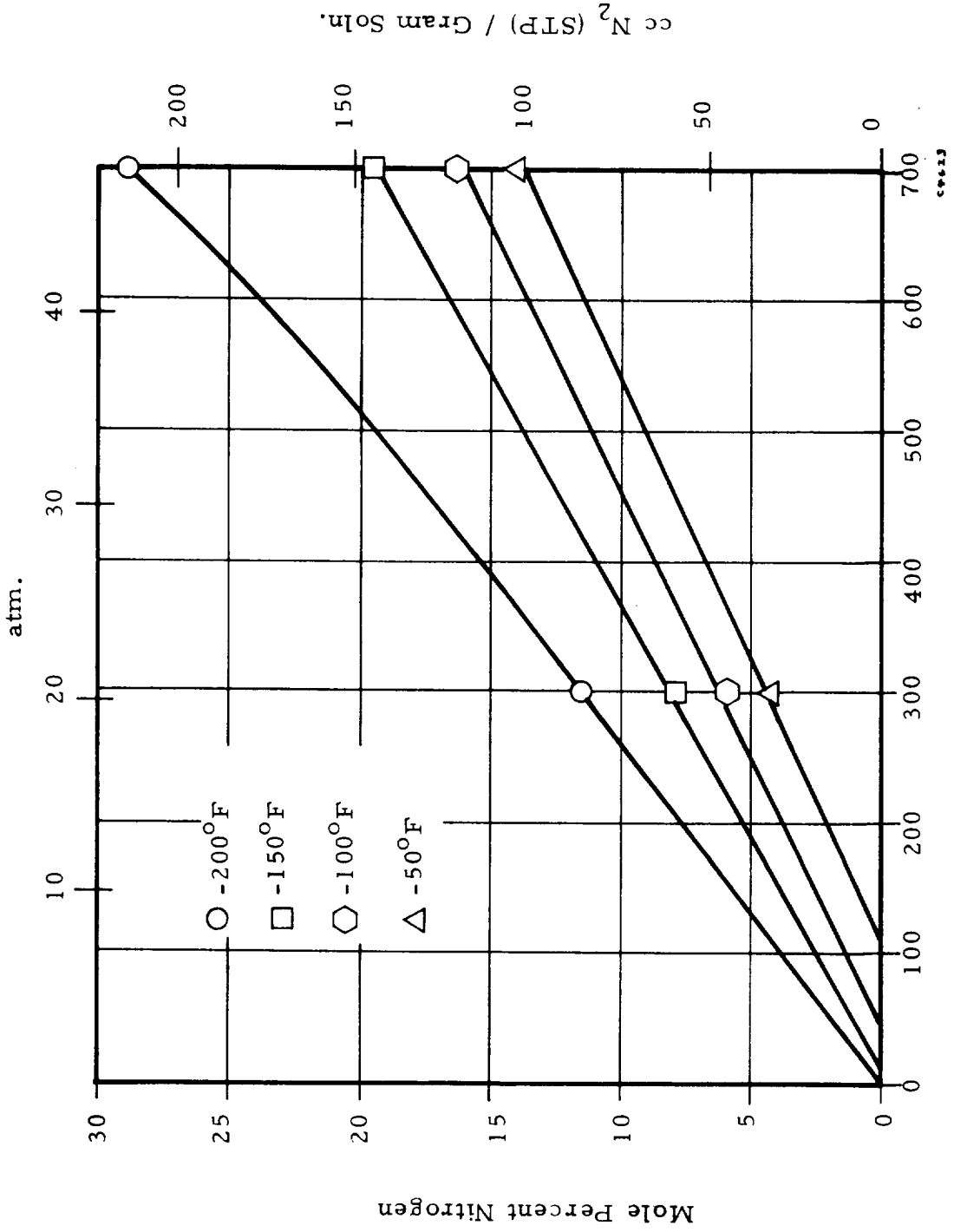

Figure IV-58. Isothermal Pressure-Composition Diagram For The System Liquid Diborane-Nitrogen.

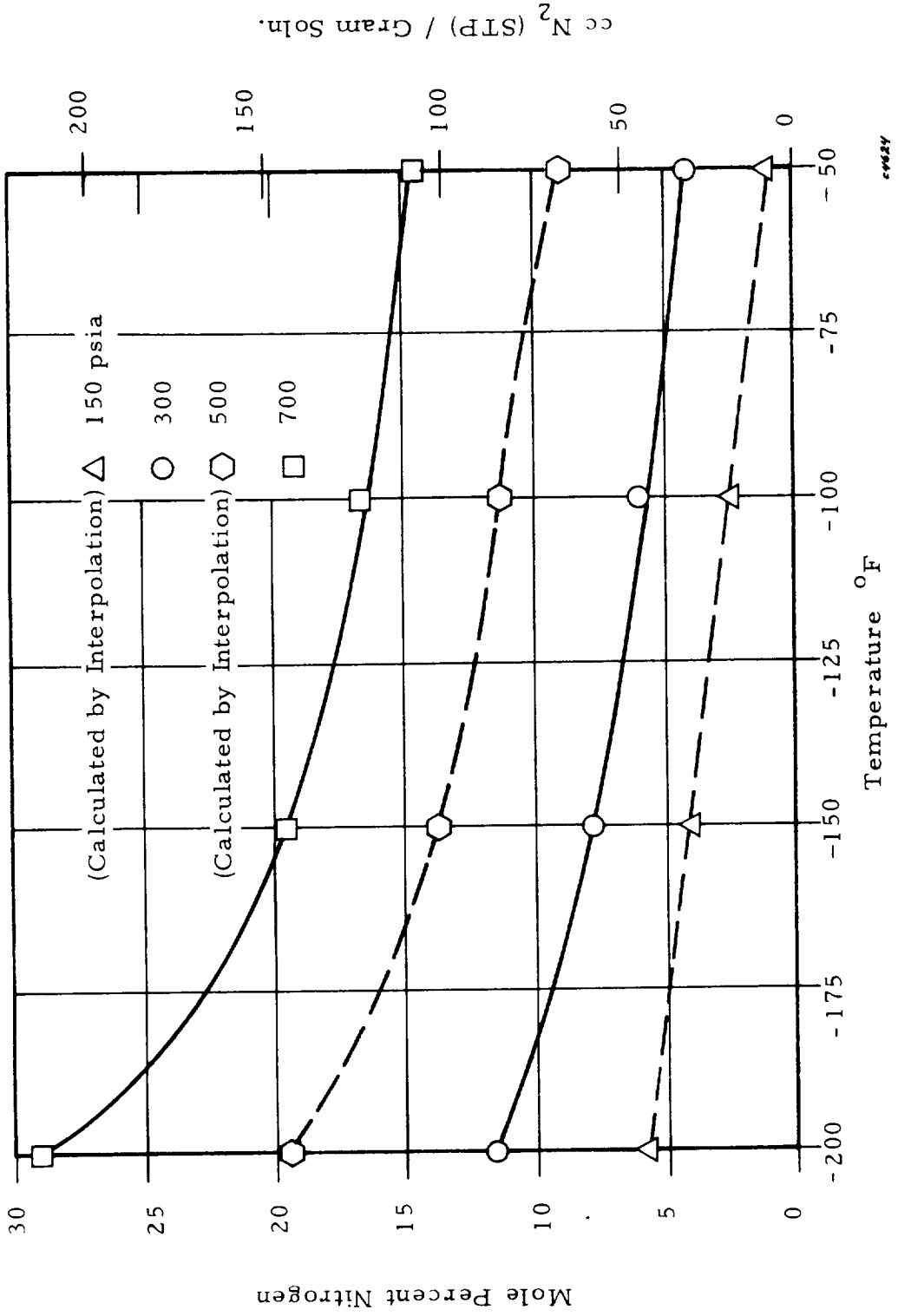

Figure IV-59. Isobaric Temperature-Composition Diagram For The System Liquid Diborane-Nitrogen

each system by interpolation. It is noted that the solubility of nitrogen in diborane appears to deviate from Henry's Law at the higher concentrations of pressurant, and the -200°F plot in Figure IV-58 is curved.

8. Diborane-Hydrogen

The solubility of hydrogen in diborane has been reported (Reference 67) in the temperature range of -260° to -130°F and the pressure range of 100 to 600 psia. Data derived from this paper is presented in isothermal and isoboric plots in Figures IV-60 and IV-61.

9. Ethane-Helium

See Section 10.

10. Ethane-Nitrogen

The solubilities of both helium and nitrogen in liquid ethane were measured by Astropower Laboratory for this Design Guide, under Contract NAS7-548. The solubility data for these two systems are tabulated in Table IV-20; experimental details may be found in Reference 46. The results reported in the table are obtained from duplicate analyses for two successive samples; agreement of these values within experimental error was accepted as indication that solution equilibrium had been attained.

TABLE IV-20

SOLUBILITY OF HELIUM AND NITROGEN IN LIQUID ETHANE

Test Temperature °F	Vapor Pressure of Propellant psia[a]	Mole Percent Concentration			
		Helium		Nitrogen	
		300 psia	700 psia	300 psia	700 psia
-200	0.9	0.07	0.18	10.6	27.1
-150	7.1	0.15	0.33	7.40	17.7
-100	31	0.27	0.64	5.61	14.3
-50	91	0.38	1.09	4.71	12.3

(a) Reference 68.

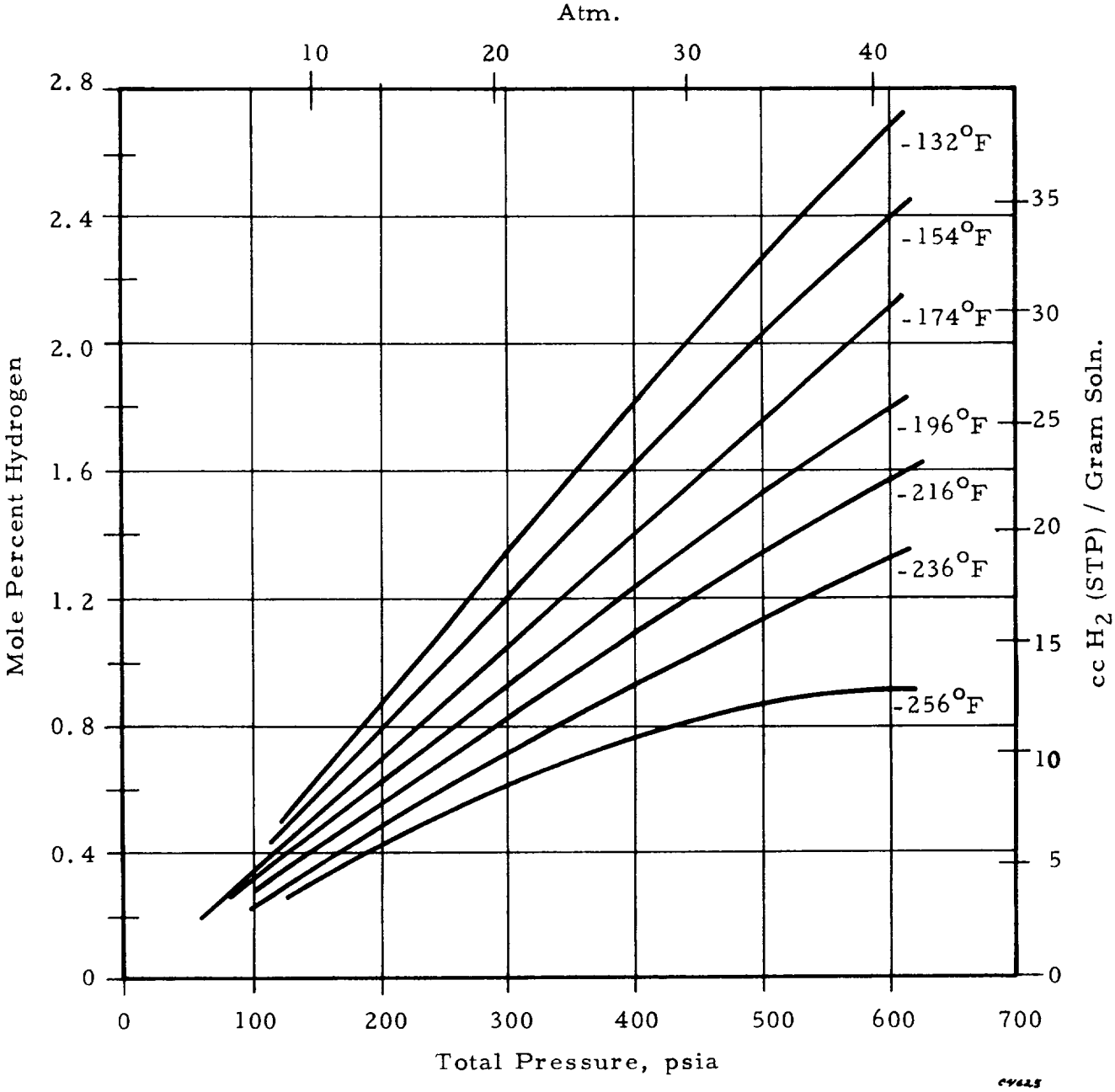

Figure IV-60. Isothermal Pressure – Composition Diagram For the System Liquid Diborane- Hydrogen

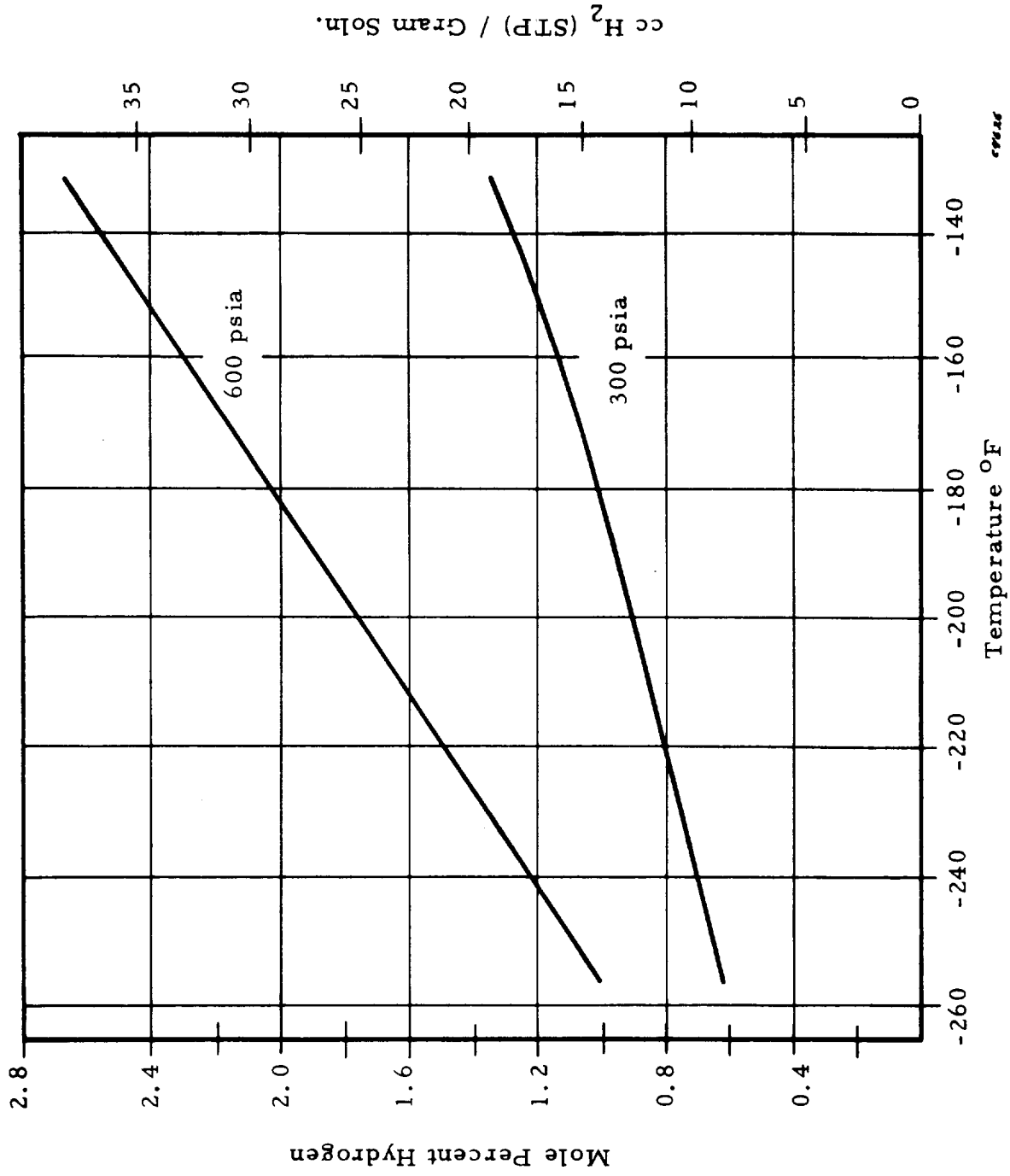

Figure IV-61. Isobaric Temperature-Composition Diagram for the System Liquid Diborane-Hydrogen.

These data are presented as isothermal pressure-composition and isobaric temperature-composition plots in Figures IV-62, IV-63, IV-64, and IV-65. Additional isobars at 150 and 500 psia have been constructed for each system by interpolation.

11. Ethane-Hydrogen

This system has been studied by Katz et. al. (Reference 69). Their results are given in Figure IV-66 as an isothermal plot of liquid phase composition versus pressure over the temperature range of -275° to +50°F and pressure range of 300 to 8000 psia. Table IV-21 summarizes all their experimental data in terms of equilibrium constants K^* for both components, between the two phases. This data has been used to construct isothermal and isobaric solubility diagrams showing the expanded liquid phase region below 2000 psia (Figures IV-67 and IV-68). The isothermal curves of Figure IV-67 have been extrapolated to zero hydrogen concentration using ethane vapor pressure data from Reference 92.

12. Ethylene-Helium

See Section 13.

13. Ethylene-Nitrogen

The solubilities of both helium and nitrogen in liquid ethylene were measured by Astropower Laboratory for this Design Guide, under Contract NAS7-548. The solubility data for these two systems are tabulated in Table IV-22; experimental details may be found in Reference 46. The results reported in the table are obtained from duplicate analyses for two successive samples; agreement of these values within experimental error was accepted as indication that solution equilibrium had been attained.

These data are presented as isothermal pressure-composition and isobaric temperature-composition plots in Figures IV-69, IV-70, IV-71,

---

*K_A = Mole % A in vapor/Mole % A in liquid.

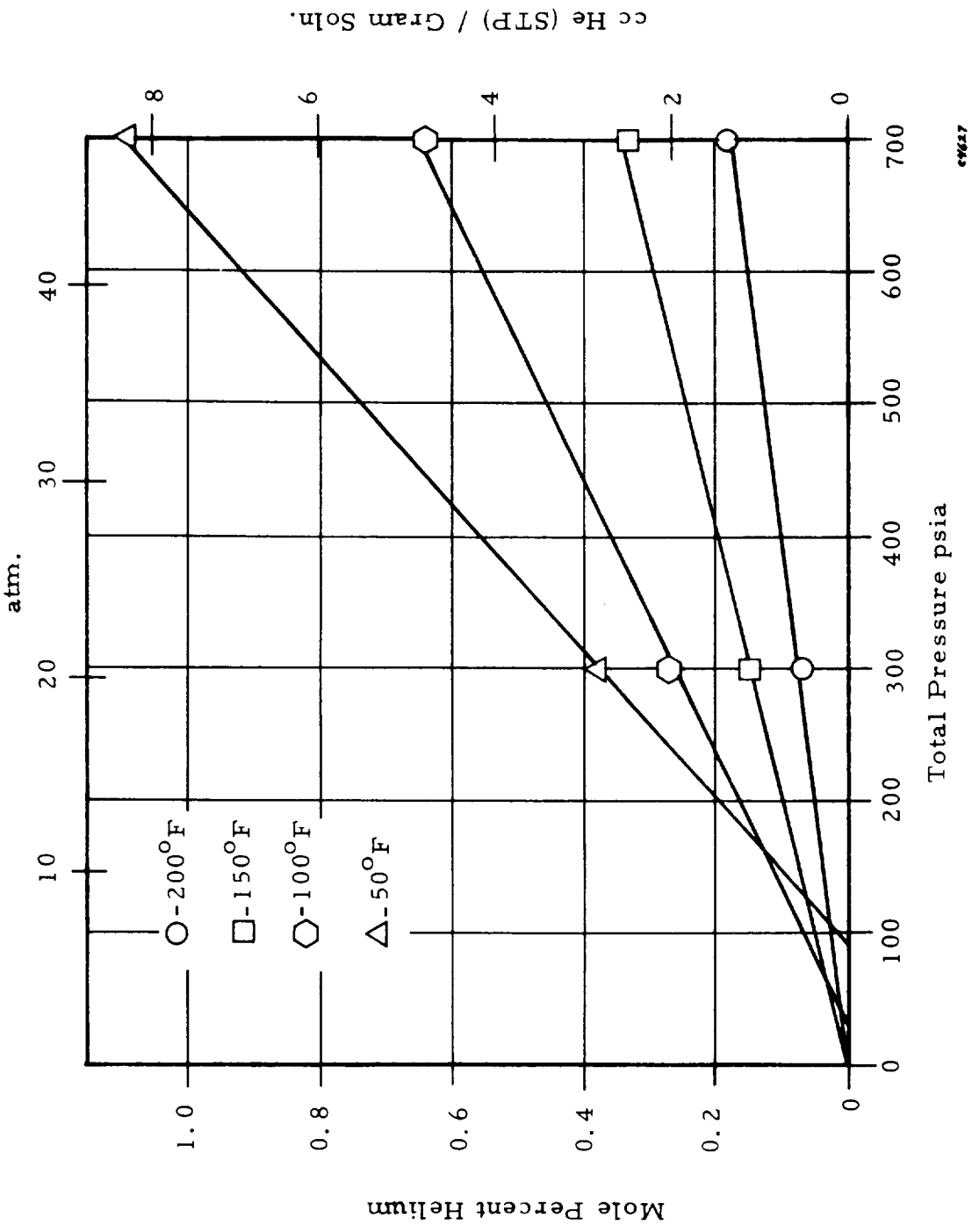

Figure IV-62. Isothermal Pressure-Composition Diagram For The System Liquid Ethane-Helium.

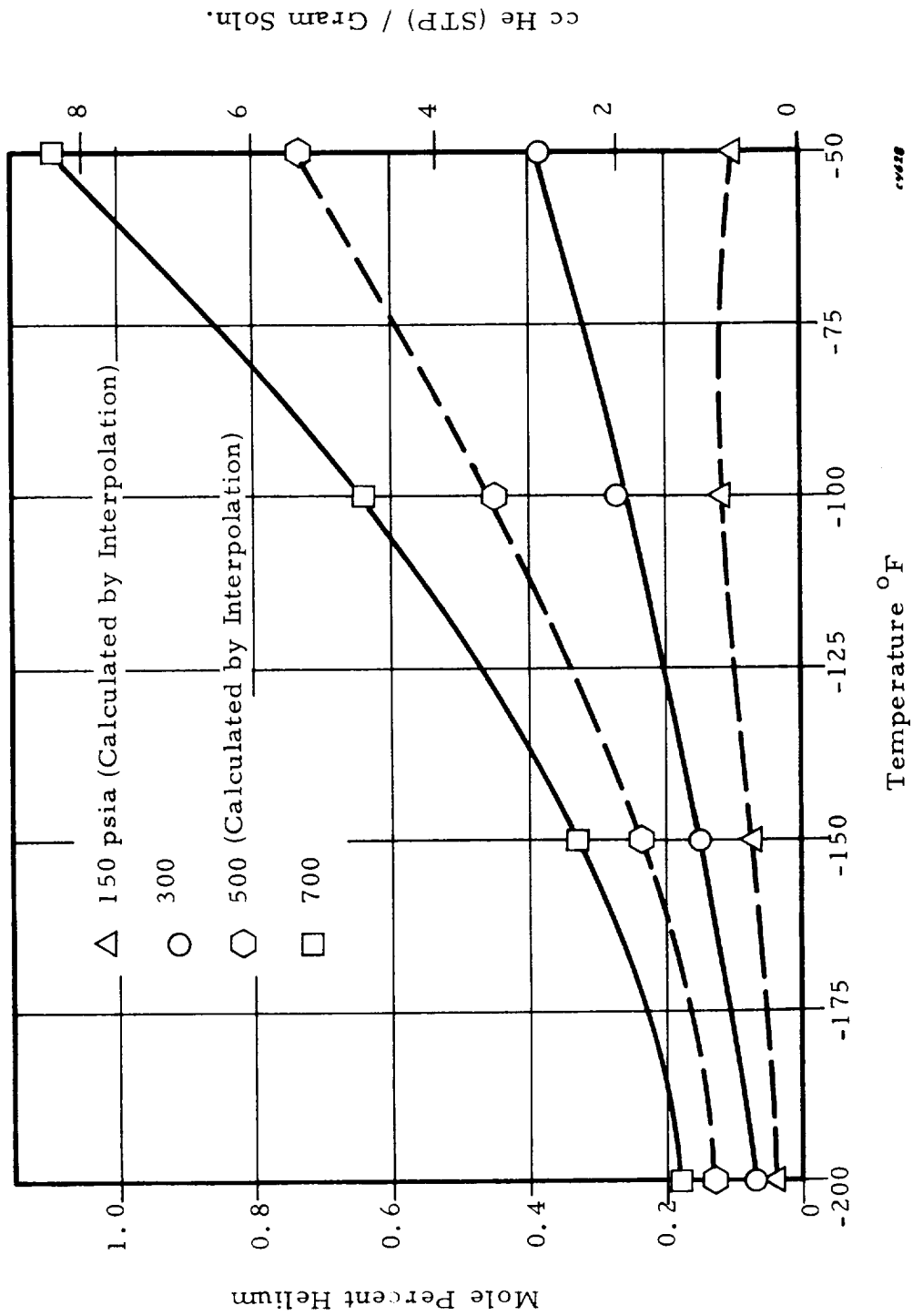

Figure IV-63. Isobaric Temperature-Composition Diagram For The System Liquid Ethane-Helium.

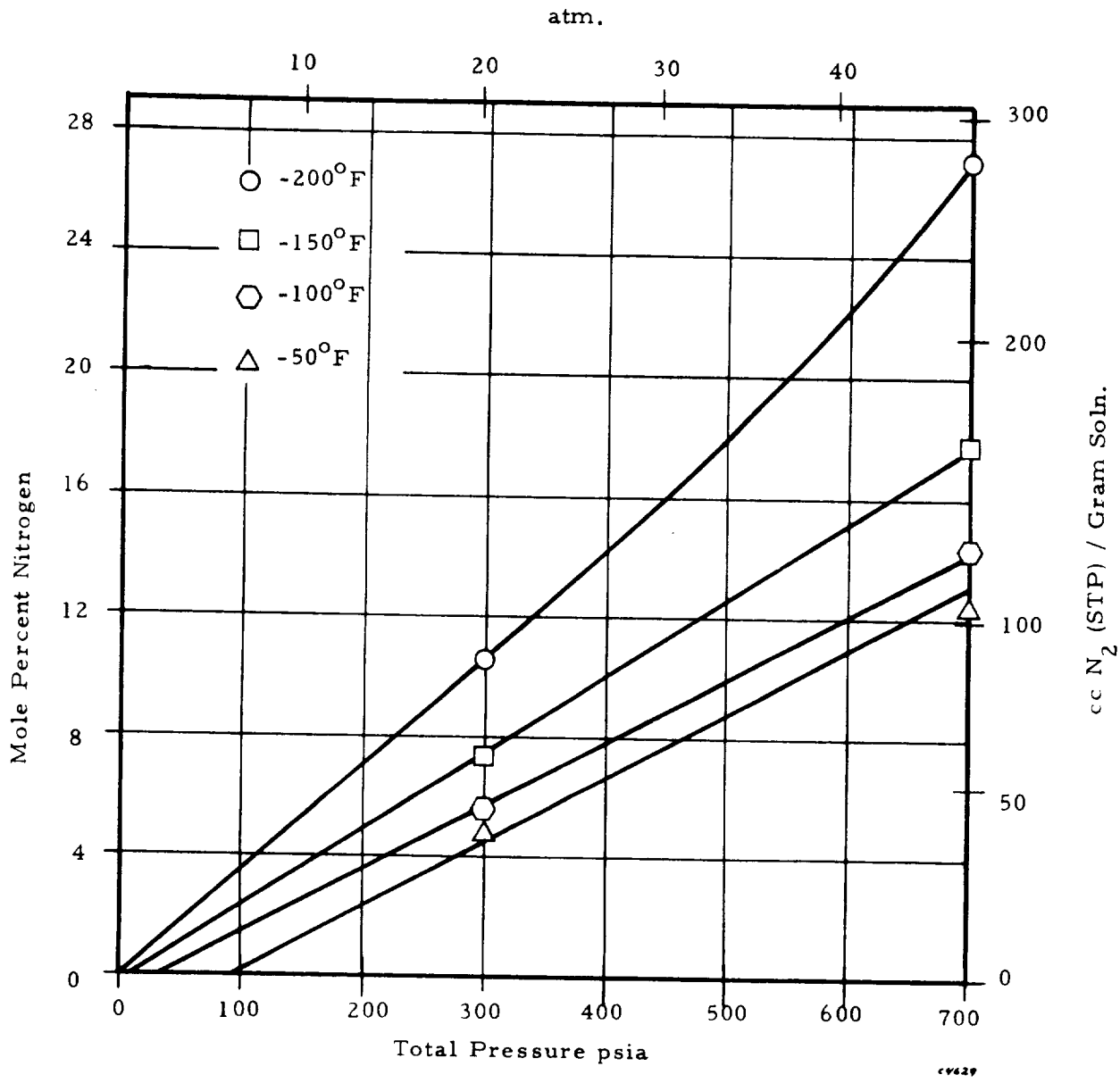

Figure IV-64. Isothermal Pressure-Composition Diagram for the System Liquid Ethane-Nitrogen

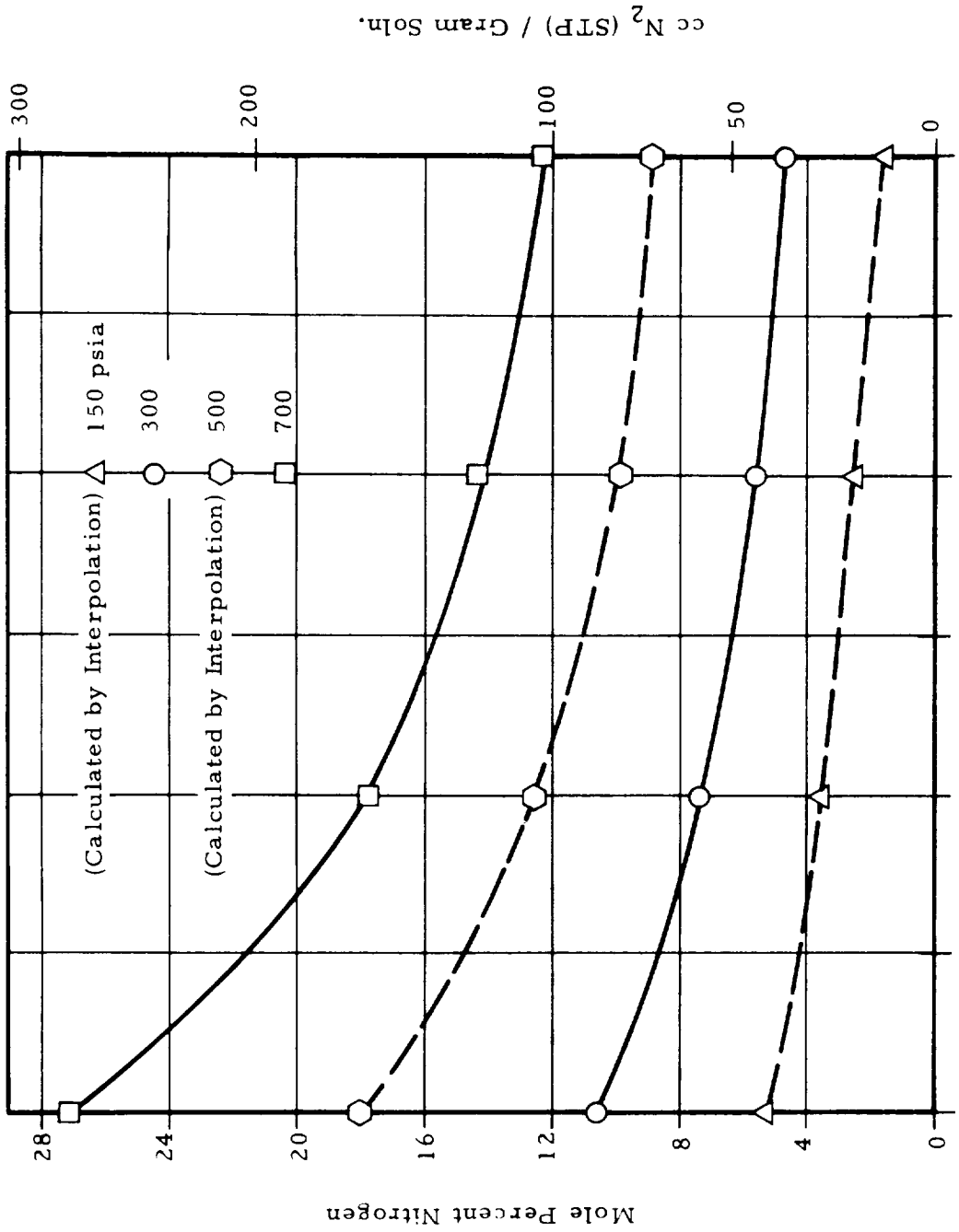

Figure IV-65. Isobaric Temperature-Composition Diagram for the System Liquid Ethane-Nitrogen

TABLE IV-21

LIQUID-VAPOR EQUILIBRIUM CONSTANTS FOR THE SYSTEM ETHANE-HYDROGEN

Temperature °F	Total Pressure, psia					
	250	500	1000	2000	4000	8000
+50 KH_2		12.1	6.45	3.21	2.135 (2500)	
KC_2H_6		0.922	0.657	0.567	0.632 (2500)	
0 KH_2	48.8	24.4	12.2	6.12	2.82	1.853 (6000)
KC_2H_6	0.896	0.534	0.347	0.264	0.296	0.616 (6000)
-50 KH_2	75.4	36.8	18.1	9.05	4.49	2.17
KC_2H_6	0.424	0.246	0.148	0.113	0.116	0.219
-100 KH_2	101.2	49.0	24.3	12.4	6.35	3.38
KC_2H_6	0.150	0.0850	0.0545	0.0432	0.0463	0.0750
-150 KH_2	124.4	62.2	31.3	16.3	8.75	4.86
KC_2H_6	0.0362	0.0206	0.0143	0.0127	0.0157	0.0277
-200 KH_2	160	83.0	43.2	23.6	13.1	7.45
KC_2H_6	0.00462	0.00314	0.00266	0.00272	0.00432	0.00934
-250 KH_2	238	129	70.8	40.0	22.7	13.5
-275 KH_2	320	179	100	57.4	33.3	19.8

Values in parentheses show pressure for indicated K.

TABLE IV-22

SOLUBILITY OF HELIUM AND NITROGEN IN LIQUID ETHYLENE

Test Temperature °F	Vapor Pressure of Propellant psia[a]	Mole Percent Concentration			
		Helium		Nitrogen	
		300 psia	700 psia	300 psia	700 psia
-200	2.5	0.056	0.136	9.07	24.6
-150	16	0.143	0.323	6.52	16.4
-100	62	0.220	0.578	4.67	13.3
-50	176	0.230	1.01	2.61	11.1

(a) Reference 70.

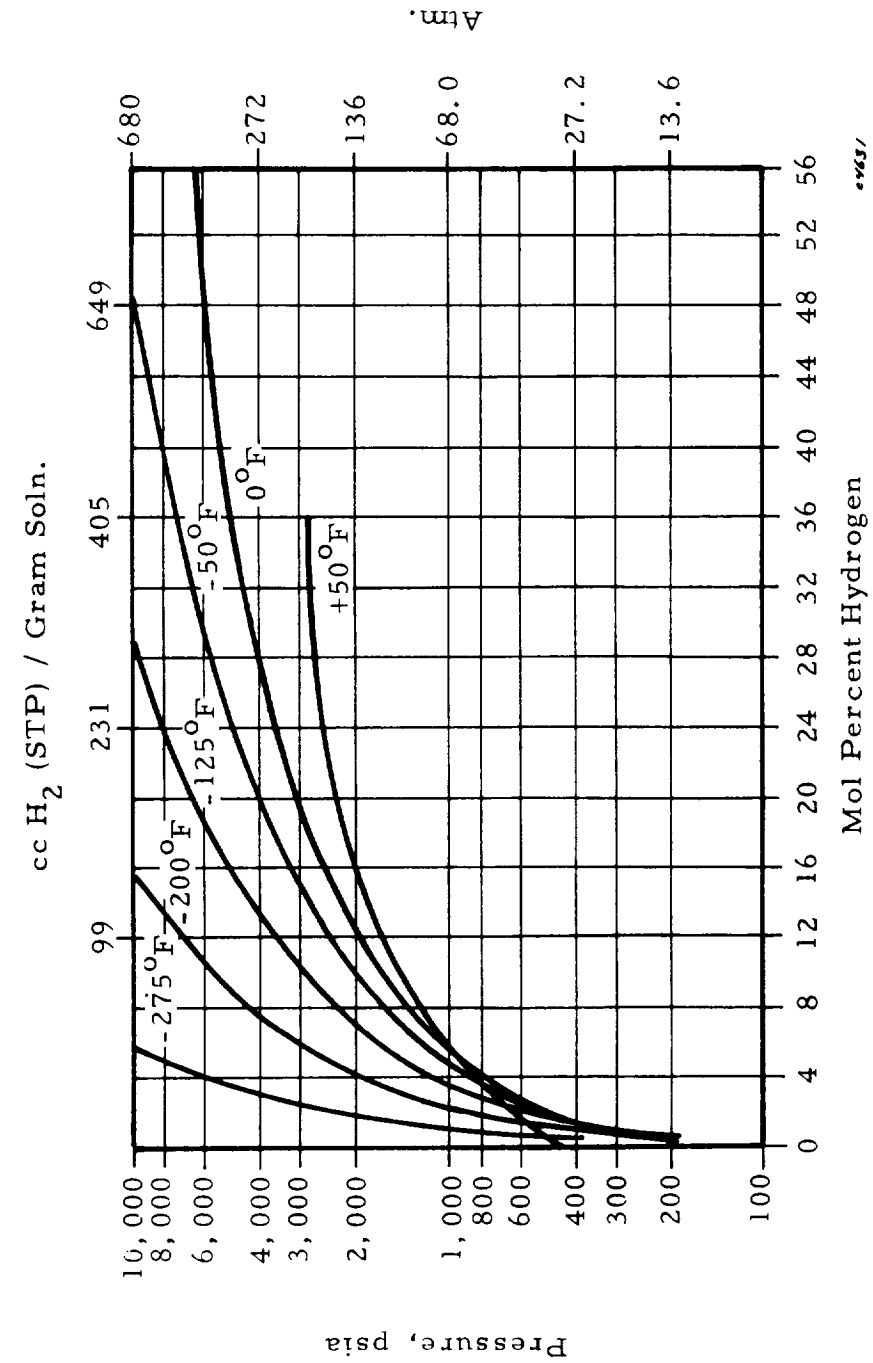

Figure IV-66. Isothermal Pressure – Composition Diagram For the System Liquid Ethane-Hydrogen

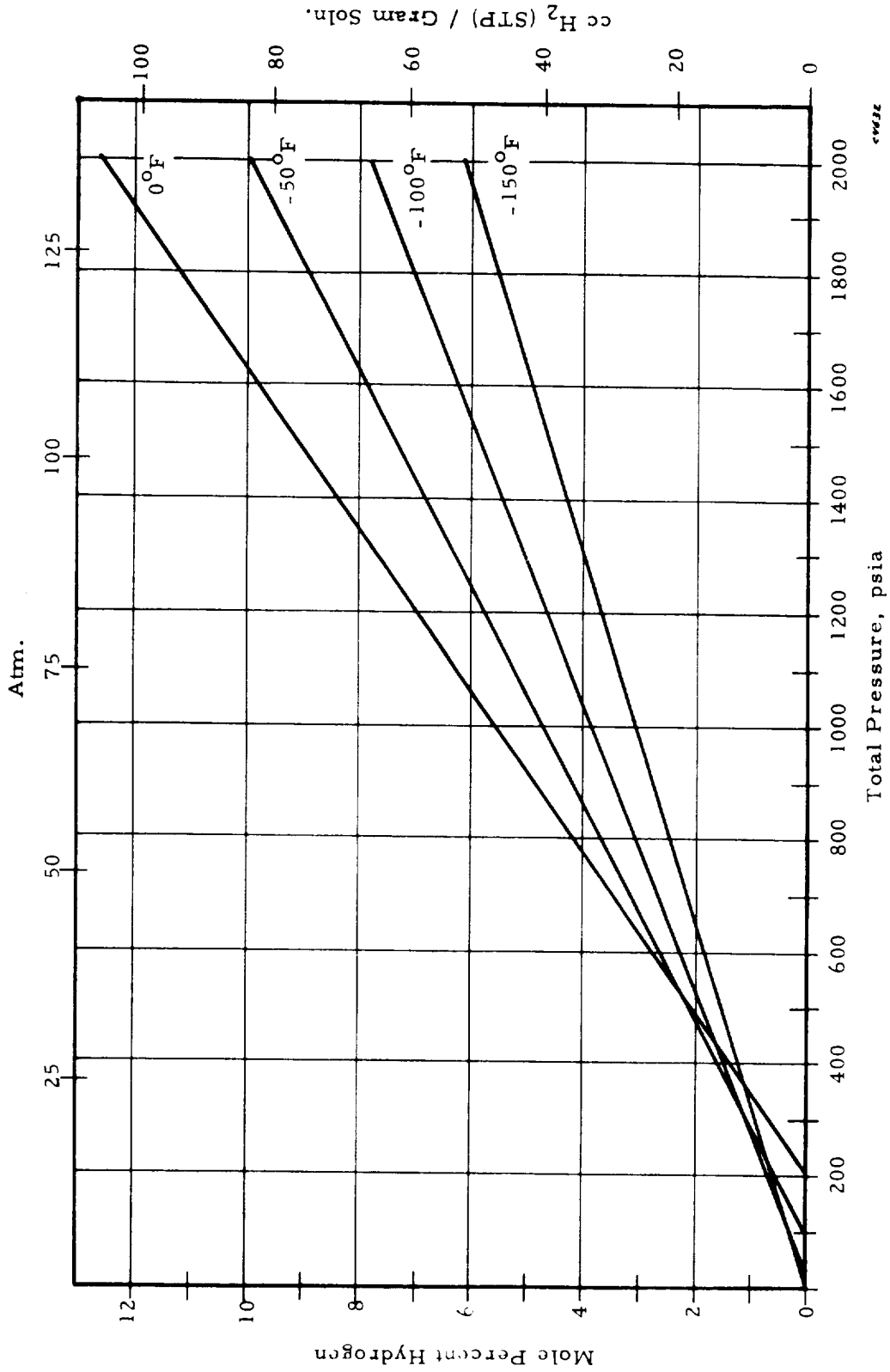

Figure IV-67. Isothermal Pressure-Composition Diagram for the System Liquid Ethane-Hydrogen

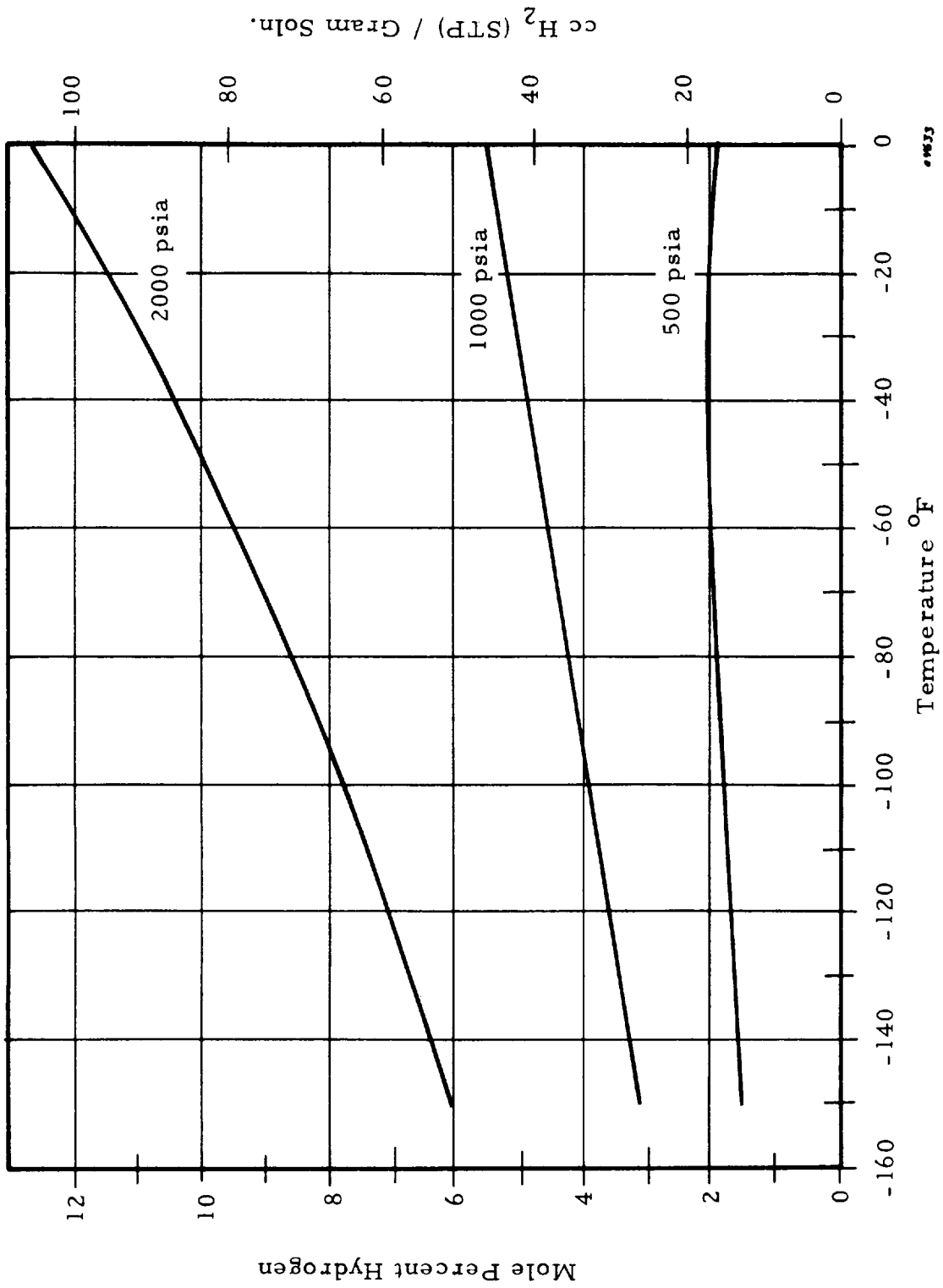

Figure IV-68. Isobaric Temperature – Composition Diagram For the System Liquid Ethane-Hydrogen

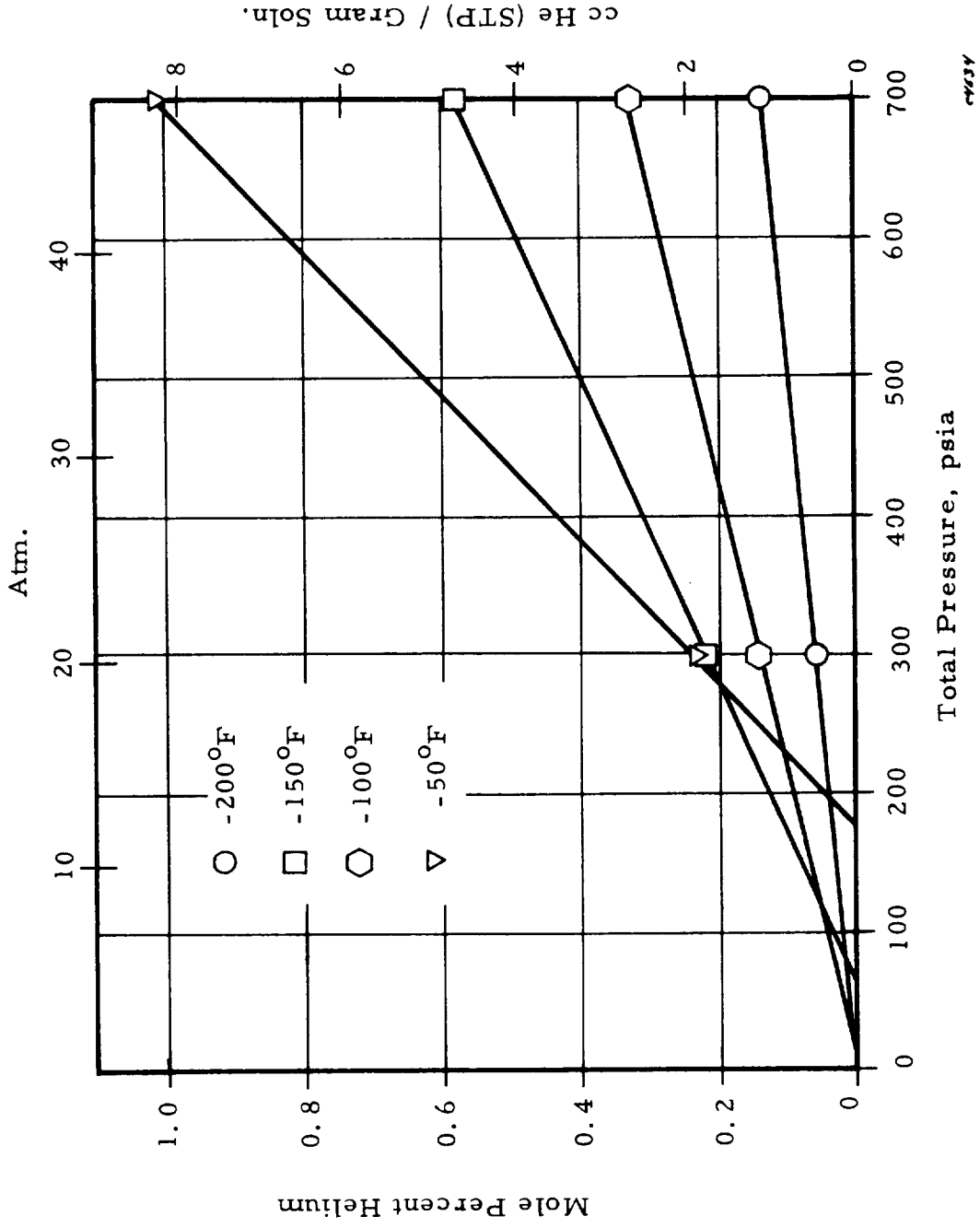

Figure IV-69. Isothermal Pressure – Composition Diagram for the System Liquid Ethylene-Helium

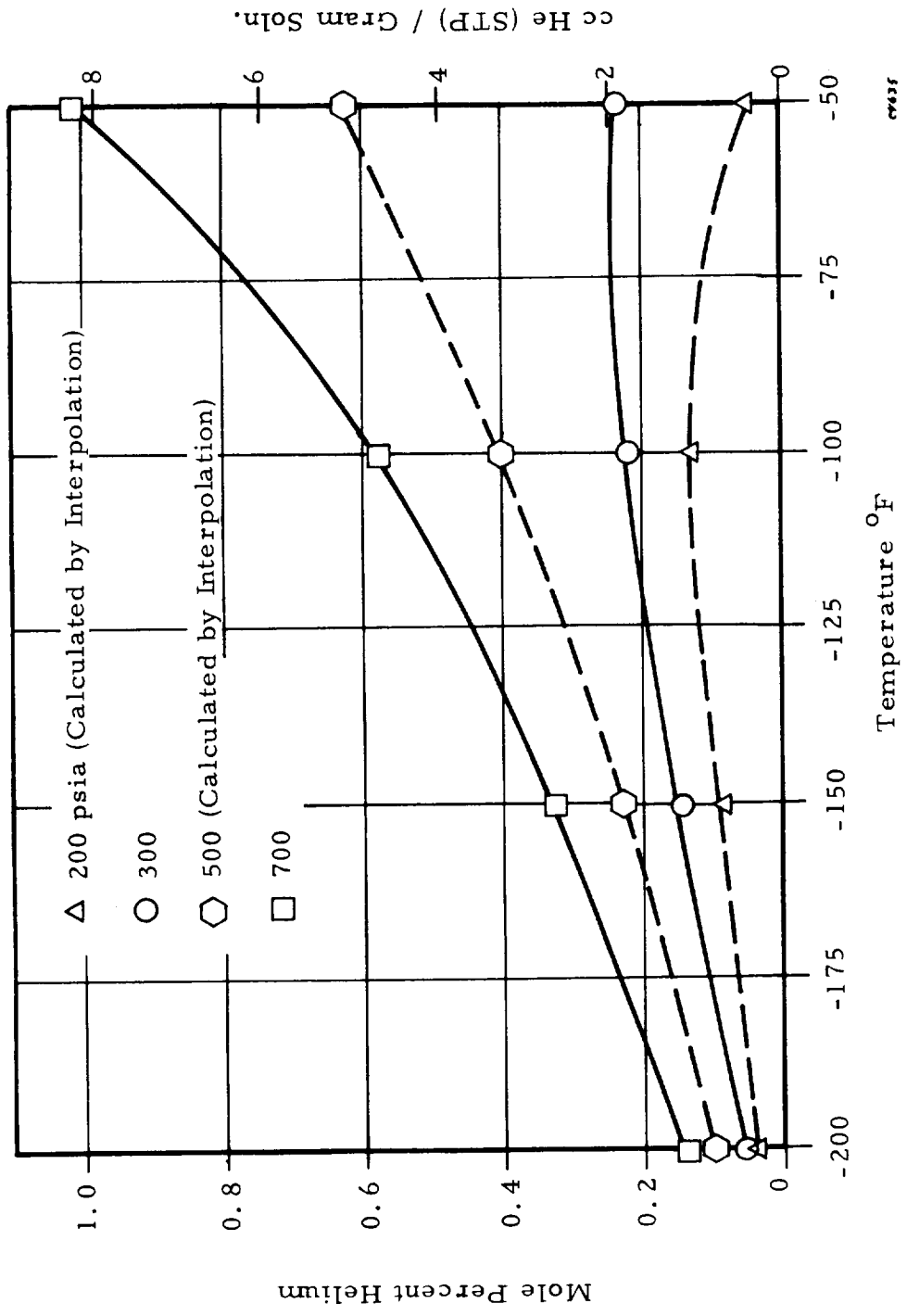

Figure IV-70. Isobaric Temperature – Composition Diagram for the System Liquid Ethylene-Helium

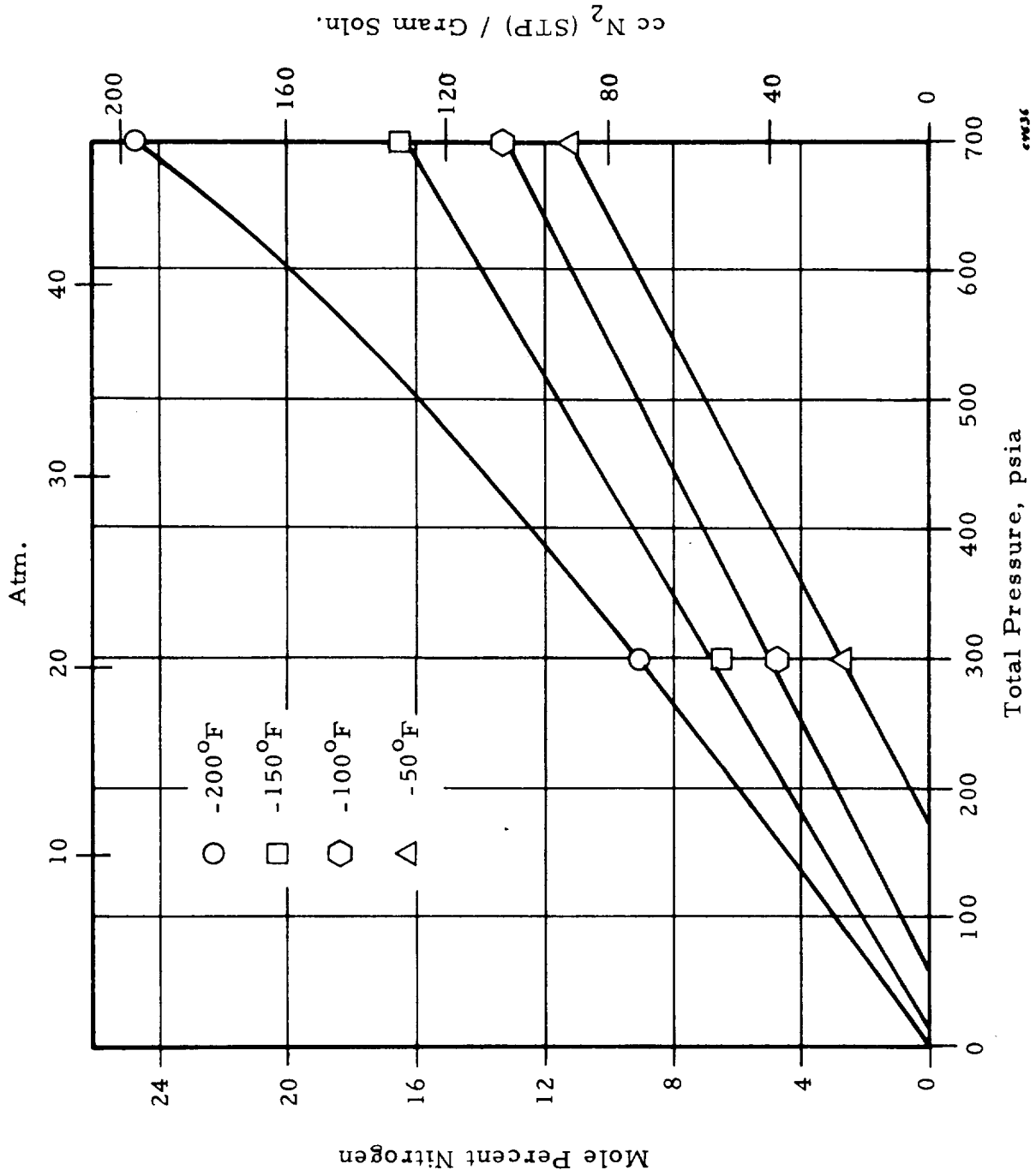

Figure IV-71. Isothermal Pressure – Composition Diagram for the System Liquid Ethylene-Nitrogen

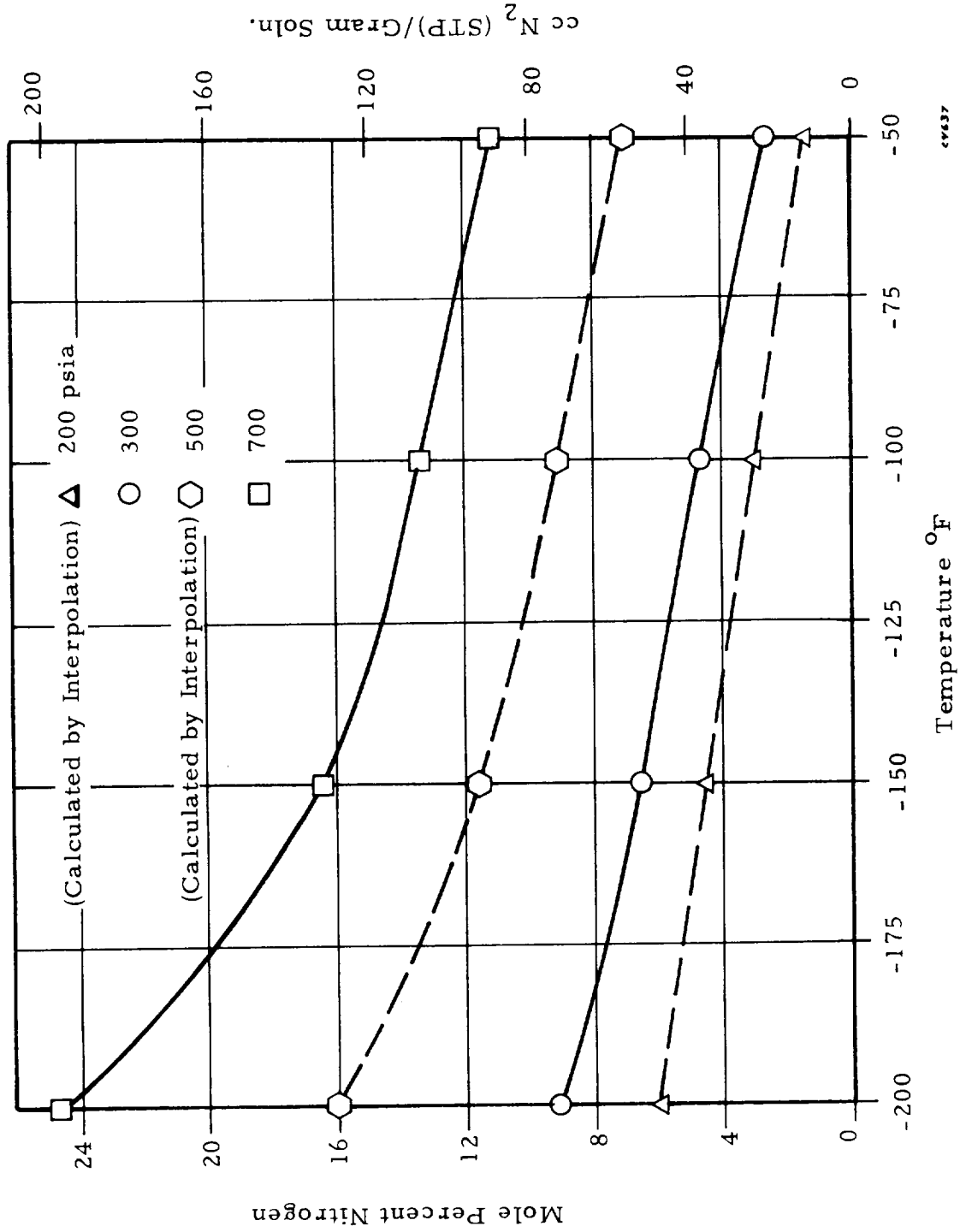

Figure IV-72. Isobaric Temperature – Composition Diagram for the System Liquid Ethylene-Nitrogen

and IV-72. Additional isobars at 200 and 500 psia have been constructed for each system by interpolation.

14. Ethylene-Hydrogen

This system has been studied by Katz et. al. (Reference 69). Their data are given in Figure IV-73 as an isothermal plot of liquid phase composition versus pressure over the range of -250° to 0°F and 200 to 8000 psia. Table IV-23 summarizes all their data in terms of equilibrium constants K* for both components, between the two phases. This data has been used to construct isothermal and isobaric solubility diagrams showing the expanded liquid phase region below 2000 psia (Figures IV-74 and IV-75). The isothermal curves of Figure IV-74 have been extrapolated to zero hydrogen concentration using ethylene vapor pressure data from Reference 92.

15. Hydrazine-Argon

See Section 17.

16. Hydrazine-Helium

See Section 17.

17. Hydrazine-Nitrogen

Solubility data for these three systems have been reported (Reference 71) in the low pressure region of 15 to 30 psia, and are summarized in Table IV-24.

The systems hydrazine-helium and hydrazine-nitrogen have also been studied at pressures up to 700 psia (References 38 and 39). Isobaric solubility plots are shown in Figures IV-76 and IV-77. This same data has been used to plot the isothermal pressure-composition diagram given in Figures IV-78 and IV-79; note that all these isotherms extend essentially from the origin because of the low vapor pressure of hydrazine at the temperatures involved.

---

*K_A = mole % of A in vapor/mole % of A in liquid.

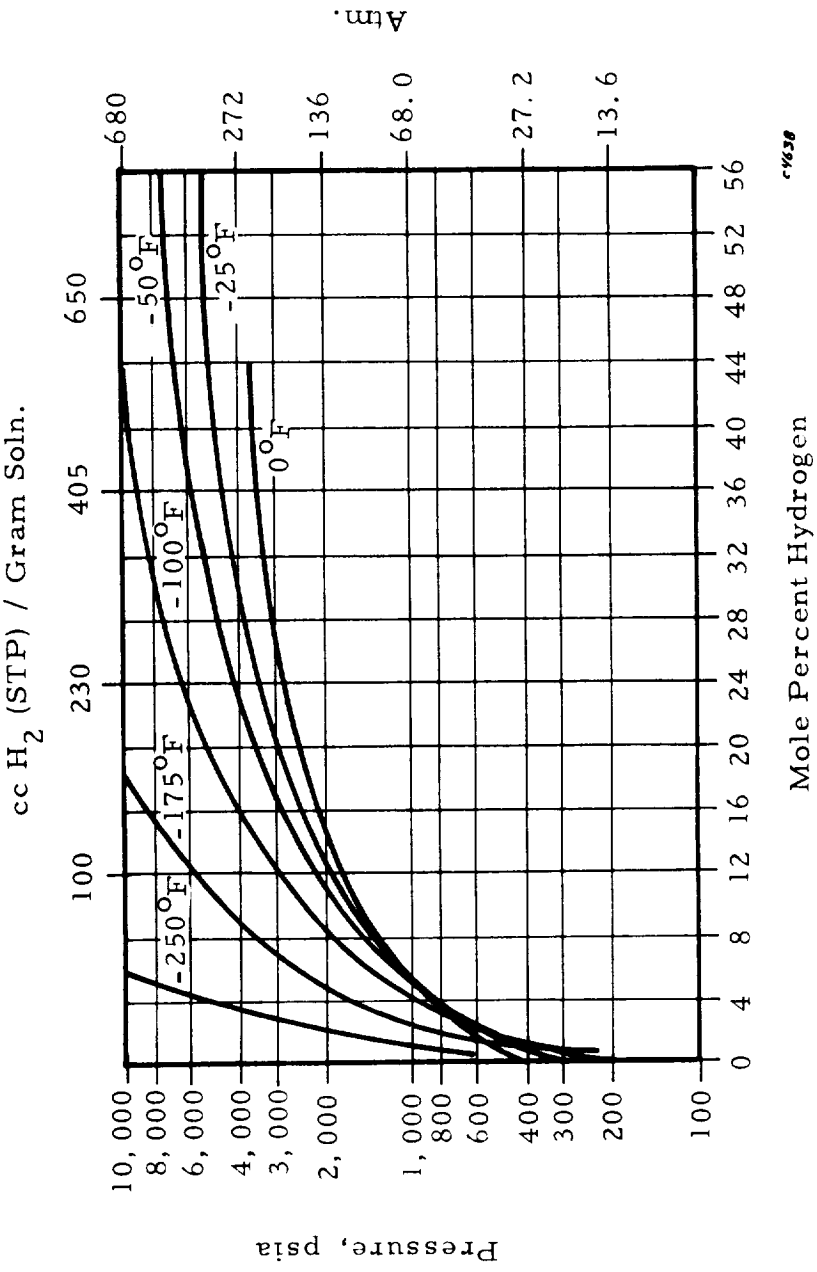

Figure IV-73. Isothermal Pressure – Composition Diagram For the System Liquid Ethylene-Hydrogen

TABLE IV-23

LIQUID-VAPOR EQUILIBRIUM CONSTANTS FOR THE SYSTEM ETHYLENE-HYDROGEN

Temperature °F	Pressure, psia					
	250	500	1000	2000	4000	8000
0 KH_2		17.1	8.10	3.94	2.15 (3000)	1.42 (3500)
KC_2H_4		0.863	0.600	0.496	0.581 (3000)	0.764 (3500)
-25 KH_2		23.1	11.25	5.50	2.43	1.53 (5000)
KC_2H_4		0.660	0.431	0.338	0.408	0.652(5000)
-50 KH_2	56.0	28.2	14.4	7.35	3.51	1.50 (7000)
KC_2H_4	0.764	0.452	0.284	0.214	0.236	0.543 (7000)
-100 KH_2	84.2	41.3	21.2	10.8	5.75	2.91
KC_2H_4	0.320	0.189	0.121	0.0924	0.0883	0.148
-150 KH_2	123.6	62.0	31.8	16.5	8.82	4.95
KC_2H_4	0.0780	0.0500	0.0346	0.0293	0.0305	0.0456
-175 KH_2	147	75.1	38.6	20.2	10.9	6.25
KC_2H_4	0.0408	0.0268	0.0201	0.0179	0.0212	0.0328
-200 KH_2	188	96.4	50.3	26.6	14.60	8.75
-250 KH_2	308	159	82.7	44.8	28.5	18.7

Values in parentheses show pressure for indicated K.

TABLE IV-24

SOLUBILITIES OF ARGON, HELIUM AND NITROGEN IN LIQUID HYDRAZINE

Temp °F	Argon		Helium		Nitrogen	
	P(a) psia	Mole % x10^3	P(a) psia	Mole % x10^3	P(a) psia	Mole % x10^3
41.00	16.77	1.04	18.12	0.51	16.82	0.56
	31.19	2.20	32.21	1.08	30.61	1.21
68.02	13.45	1.03	16.76	0.52	15.41	0.69
	26.42	2.13	30.04	1.10	16.33	0.71
					28.97	1.45
					30.29	1.51
95.05	15.52	1.44	16.01	0.57	15.93	0.84
	29.57	2.85	19.27	0.68	31.01	1.80
			29.29	1.17		
			33.89	1.44		

(a) Partial pressure of the pressurant gas.

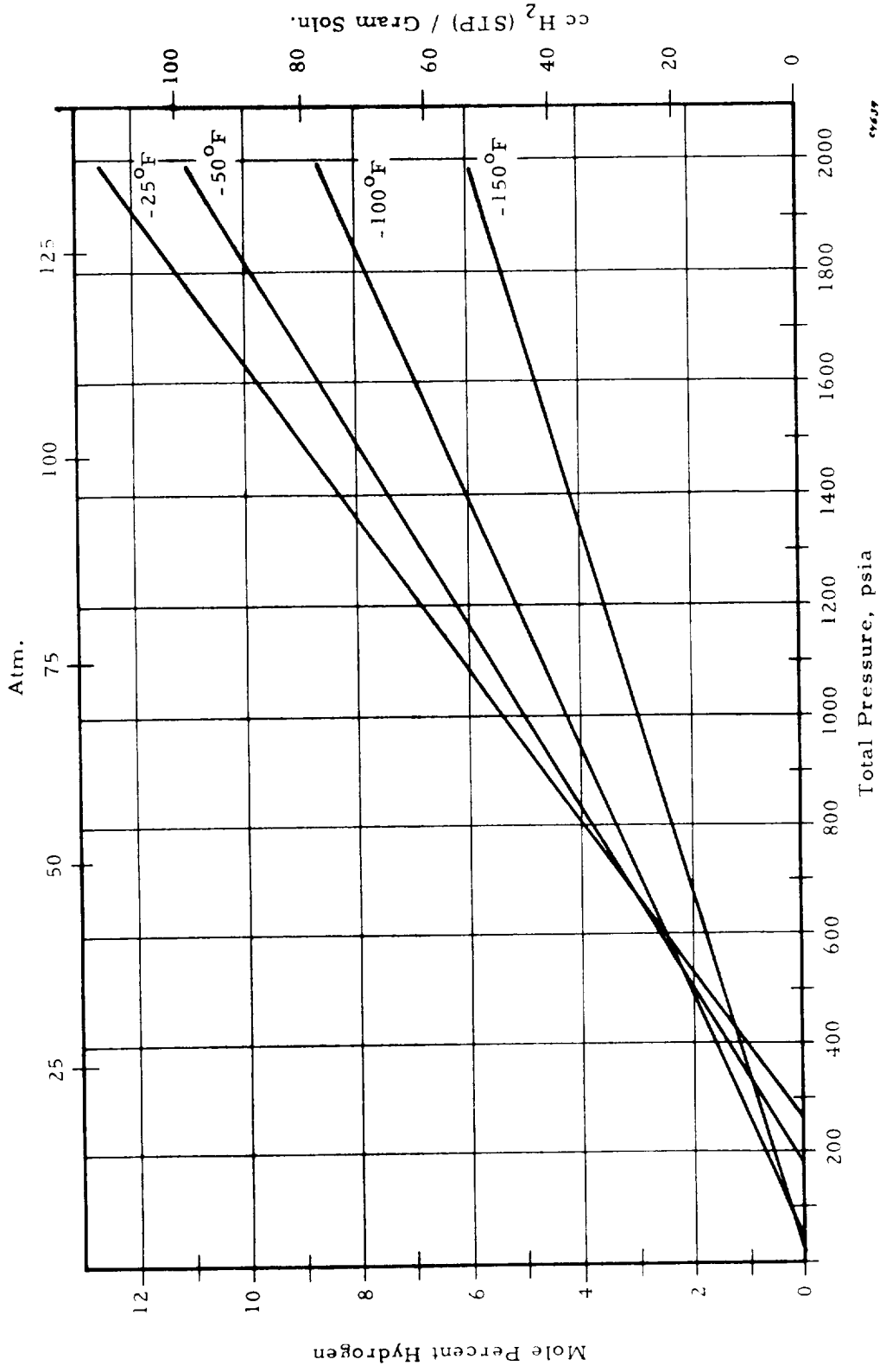

Figure IV-74. Isothermal Pressure—Composition Diagram for the System Liquid Ethylene-Hydrogen

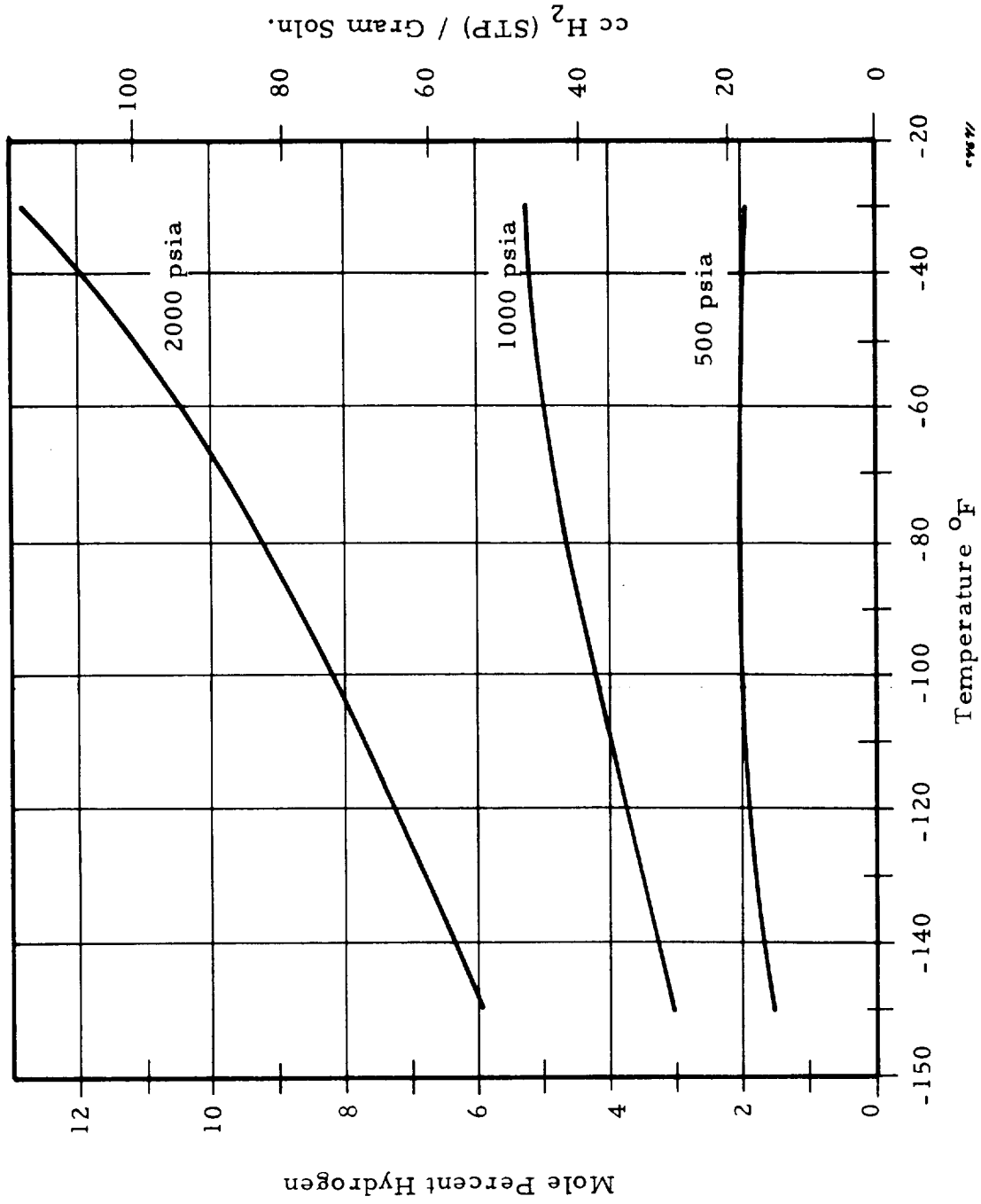

Figure IV-75. Isobaric Temperature – Composition Diagram For the System Liquid Ethylene-Hydrogen

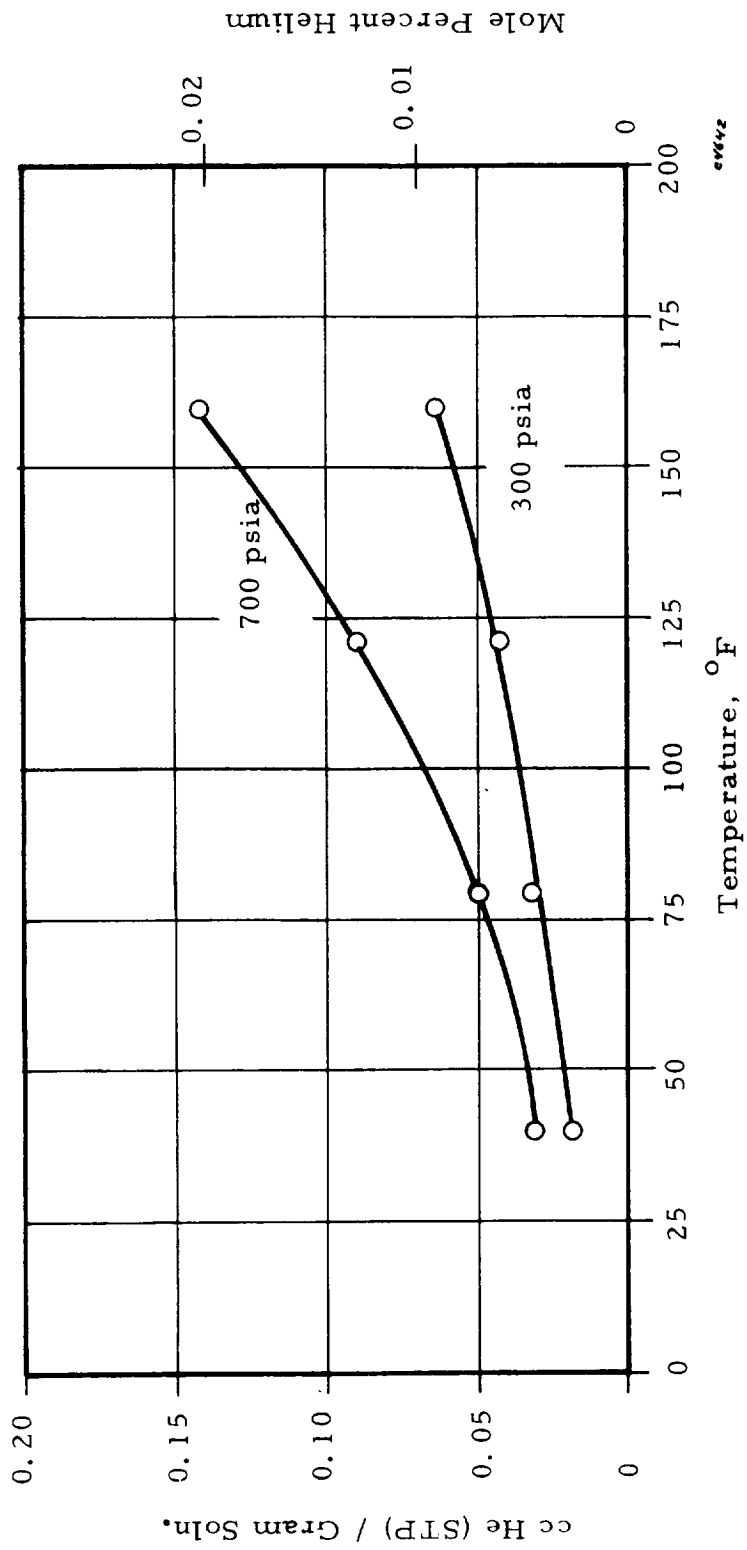

Figure IV-76. Isobaric Temperature-Composition Diagram for the System Liquid Hydrazine-Helium.

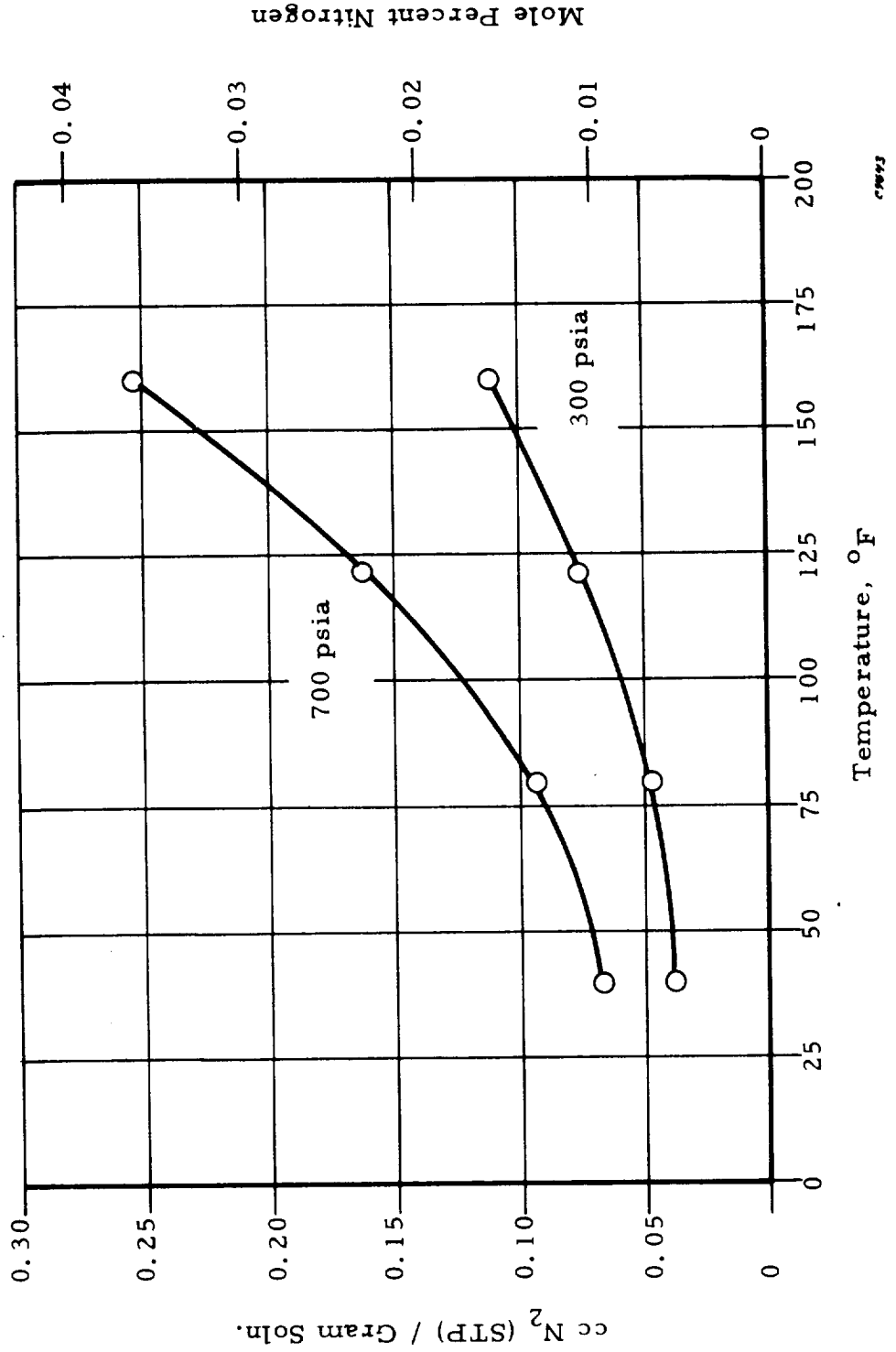

Figure IV-77. Isobaric Temperature - Composition Diagram for the System Liquid Hydrazine-Nitrogen

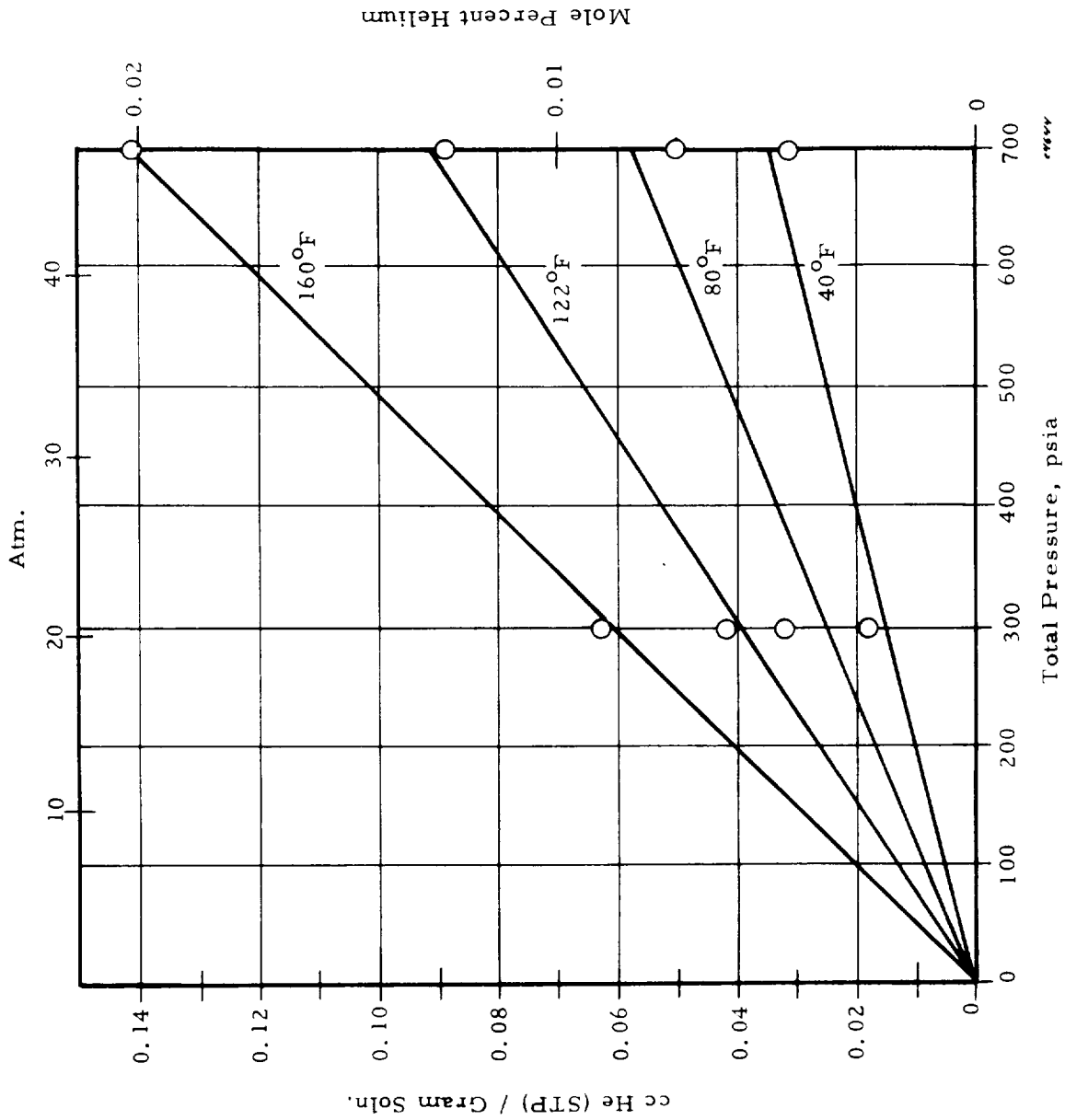

Figure IV-78. Isothermal Pressure-Composition Diagram for the System Liquid Hydrazine-Helium

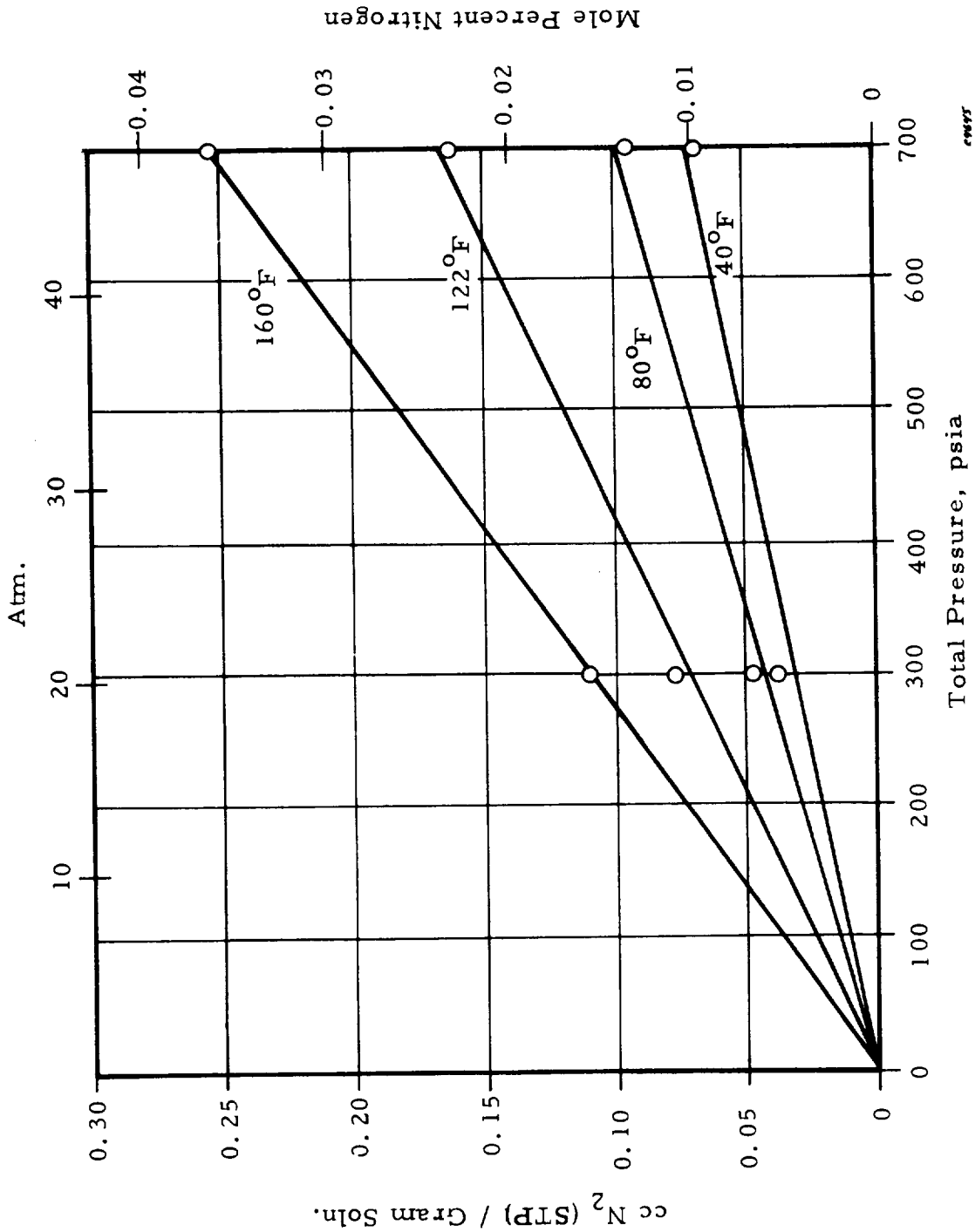

Figure IV-79. Isothermal Pressure – Composition Diagram For the System Liquid Hydrazine-Nitrogen

18. Hydrogen (Normal)-Helium

See Section 19.

19. Hydrogen (Equilibrium)-Helium

Hydrogen exists in two modifications, ortho and para, which have measurably different physical properties. In the liquid state these forms give rise to two mixtures of practical significance; "normal" hydrogen has a 75% ortho-25% para composition representing the room temperature gas equilibrium mixture, and "equilibrium" hydrogen has the composition 0.21% ortho-99.79% para which is stable at 20.40°K. The solubility of helium in both mixtures has been studied extensively by Sonntag et. al., (References 12 and 72) and the data used here is taken from them. These authors also discuss critically the prior work on these systems.

For the purpose of this Design Guide, the liquid phase compositions of both normal and equilibrium hydrogen-helium systems were found to be almost identical within experimental error, and solubility data for the more extensively investigated normal system may be taken as representative of both. However, measurable differences were found between the vapor phase compositions of the two systems at higher temperatures, and hence the equilibrium hydrogen data is included in the regions where these differences exist.

Table IV-25 presents the experimental data, presumably smoothed, for both phases of the normal hydrogen system. Figures IV-80 and IV-81 give complete isothermal and isobaric plots of these data; expanded diagrams of the data in the liquid regions are shown in Figures IV-82 and IV-83.

In the equilibrium hydrogen system, minor increases in the helium vapor phase concentrations over those for normal hydrogen were measured above 20.40°K, and are attributable to the slightly higher solvent vapor pressures. The three graphs, IV-84 through IV-86, show comparative isothermal plots for the two systems in the range of 20.40° to 31.00°K. It

TABLE IV-25

SOLUBILITY OF HELIUM IN NORMAL HYDROGEN

Temperature (°K)	Pressure (psia)	Mole % He	
		Liquid	Vapor
15.50	49.5	–	93.78
	75.0	0.29	95.51
	100.0	0.46	96.31
	125.0	0.51	96.77
	150.0	0.55	97.02
	175.0	0.64	97.14
	200.0	0.71	97.29
	250.0	0.82	97.41
	300.0	0.87	97.48
17.07	56.5	0.36	89.67
	75.0	0.43	91.86
	100.0	0.57	93.30
	125.0	0.72	94.12
	150.5	0.80	94.64
	175.0	0.89	95.03
	200.0	1.00	95.15
	250.0	1.14	95.56
	300.0	1.31	95.82
	400.0	1.51	95.90
20.40	35.0	0.34	53.60
	50.0	0.41	65.45
	75.0	0.61	75.40
	100.0	0.84	80.30
	125.0	1.05	83.20
	150.0	1.30	84.80
	175.0	1.54	86.03
	200.0	1.67	87.13
	250.0	2.05	88.41
	300.0	2.36	88.98
	400.0	2.96	90.08
	500.0	3.39	90.35
23.00	50.0	0.38	37.00
	75.0	0.75	53.44
	100.0	1.15	62.90
	125.0	1.36	67.87
	150.0	1.72	71.75
	175.0	2.15	74.35
	200.0	2.39	76.30
	250.0	2.91	78.78
	300.0	3.55	80.55
	400.0	4.58	82.34
	500.0	5.46	83.30
26.00	81.0	0.67	22.60
	100.0	0.97	33.50
	125.0	1.43	43.37
	150.0	1.92	49.77
	200.0	2.86	56.90
	250.0	3.64	62.67
	300.0	4.76	65.65
	400.0	6.64	68.58
	500.0	8.48	70.02
29.00	127.0	0.91	14.03
	151.0	1.50	21.92
	175.0	2.20	27.75
	200.0	3.07	32.93
	250.0	4.59	39.54
	300.0	6.21	43.70
	400.0	9.63	47.95
	500.0	13.35	49.20
30.60	300.0	7.29	30.32
	400.0	13.24	32.60
	450.0	17.95	30.36
31.00	176.5	1.49	11.28
	199.0	2.51	15.59
	250.0	4.78	22.58
	300.0	7.49	26.57
	325.0	8.73	27.55
	350.0	11.03	27.85
	375.0	12.93	27.59
	400.0	15.64	25.78
	413.0	20.87	21.85
31.50	177.0	1.27	7.67
	200.0	2.30	11.94
	225.0	3.61	15.64
	250.0	4.83	18.35
	275.0	6.26	20.30
	300.0	8.18	21.37
	325.0	10.47	21.49
	351.0	16.59	17.58
31.90	174.5	0.81	4.00
	200.0	2.07	8.31
	220.0	3.17	11.75
	238.5	4.29	13.86
	250.5	4.99	14.82
	261.5	–	15.62
	275.5	6.87	16.19
	289.5	8.71	16.35
	300.0	10.10	15.88
	308.5	12.02	–
32.50	188.5	0.89	3.12
	200.0	1.68	4.80
	220.0	3.10	7.45
	242.0	5.09	–
	250.0	5.99	–
	258.0	6.75	–

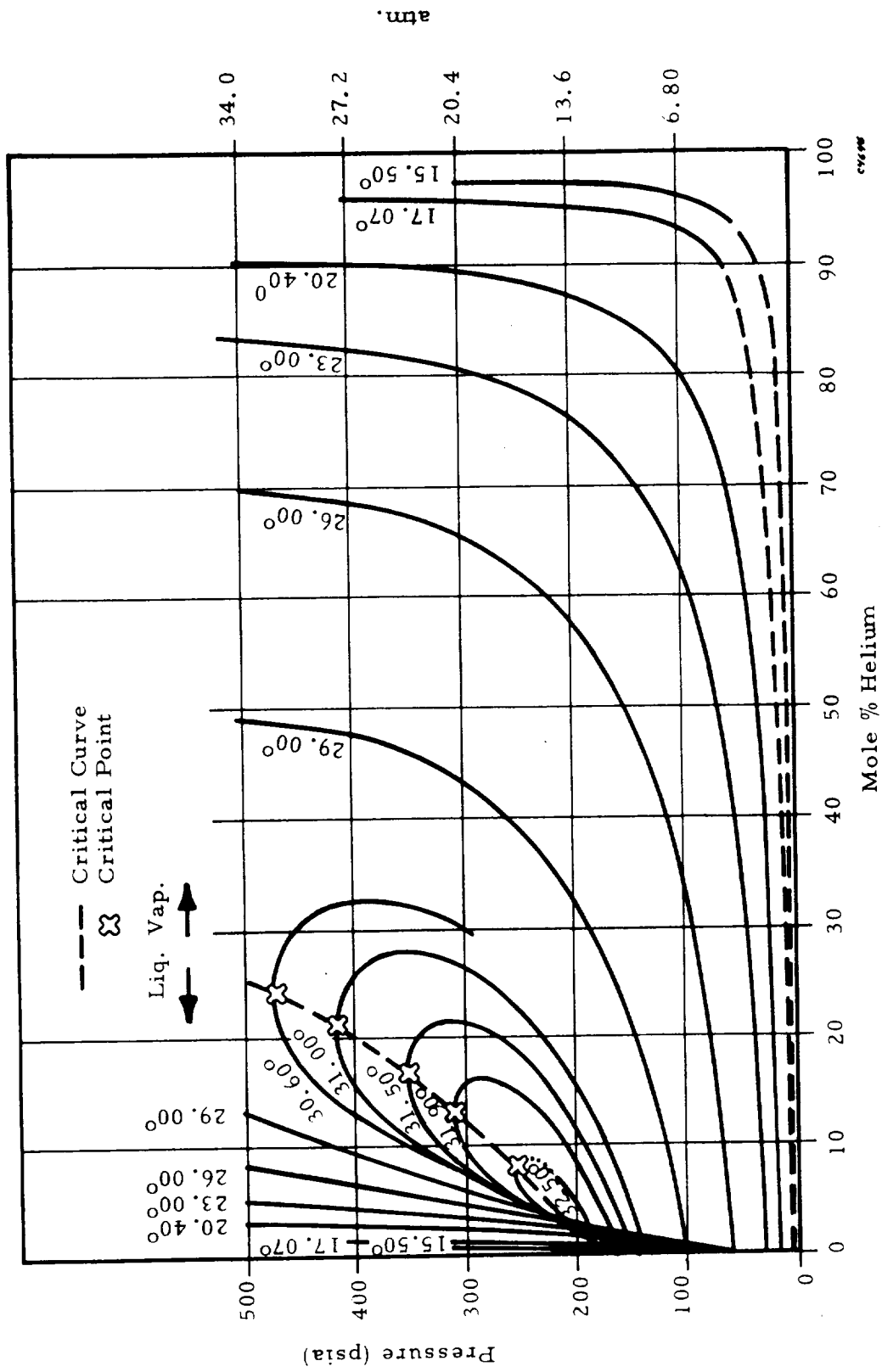

Figure IV-80. Isothermal Pressure-Composition Diagram for the System Normal Hydrogen-Helium

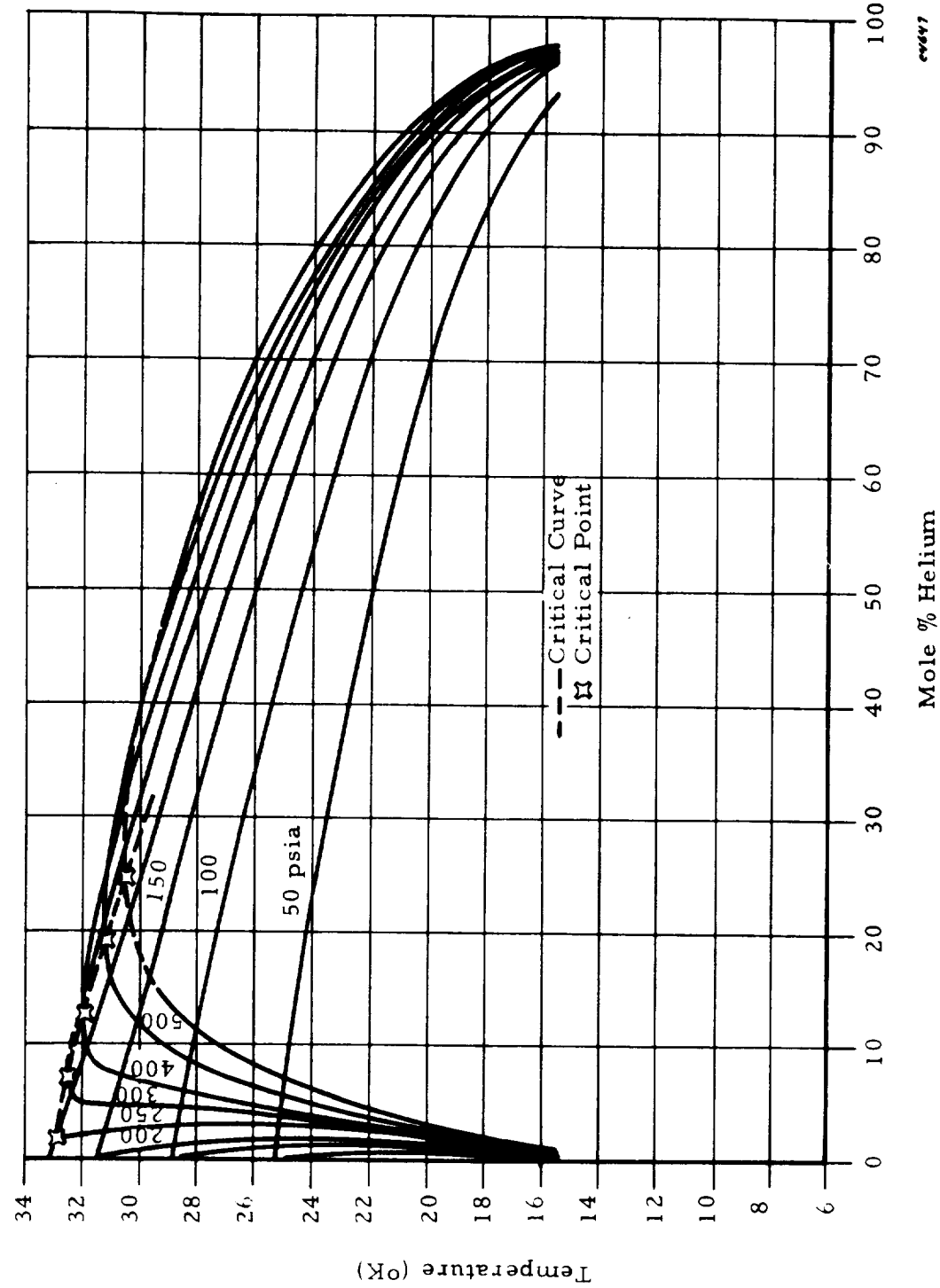

Figure IV-81. Isobaric Temperature-Composition Diagram for the System Normal Hydrogen-Helium

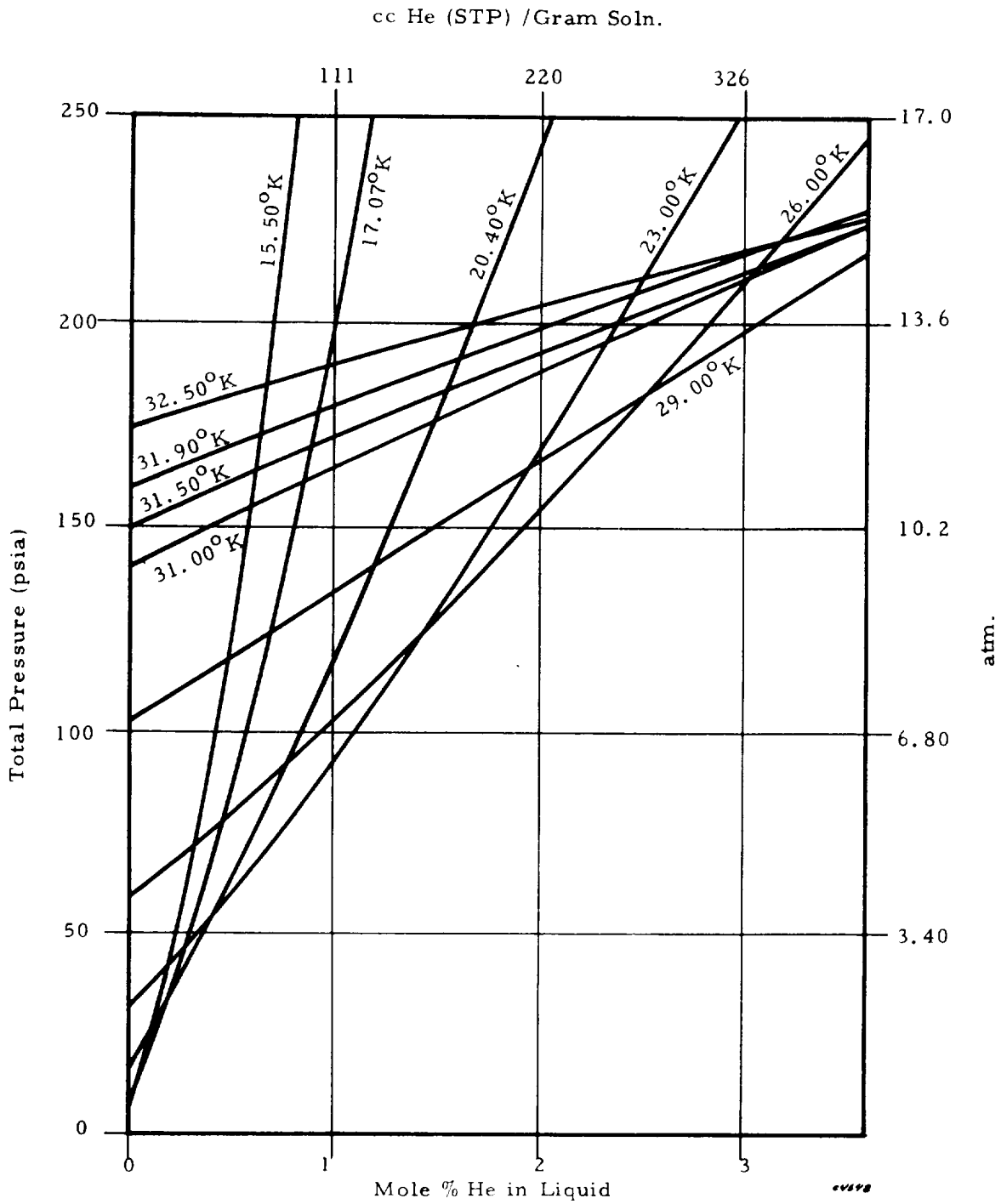

Figure IV-82. Isothermal Pressure-Composition Diagram for the System Normal Hydrogen-Helium, showing Liquid Region on Expanded Scale

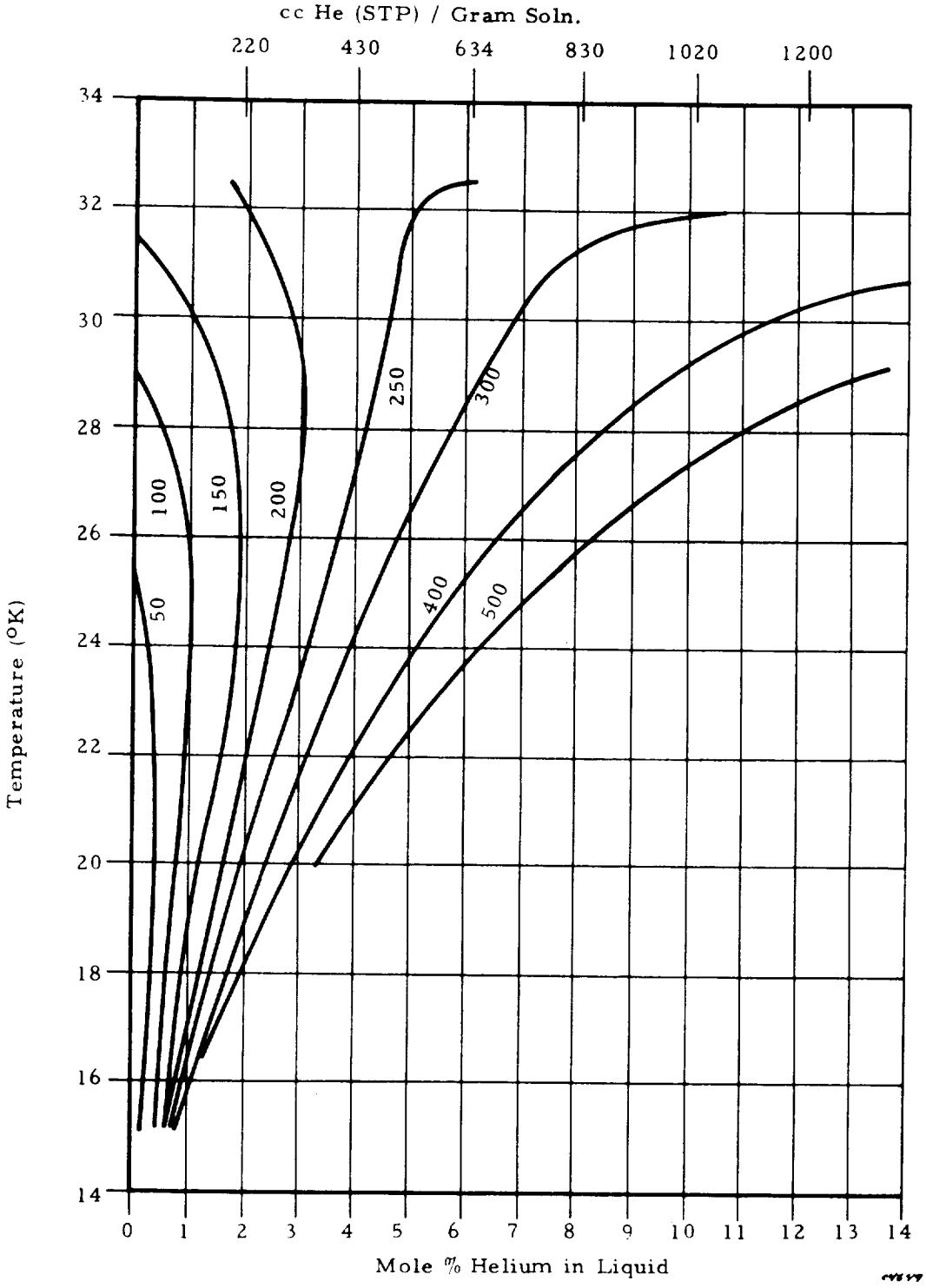

Figure IV-83. Isobaric Temperature-Composition Diagram for the System Normal Hydrogen-Helium Showing Liquid Region on Expanded Scale

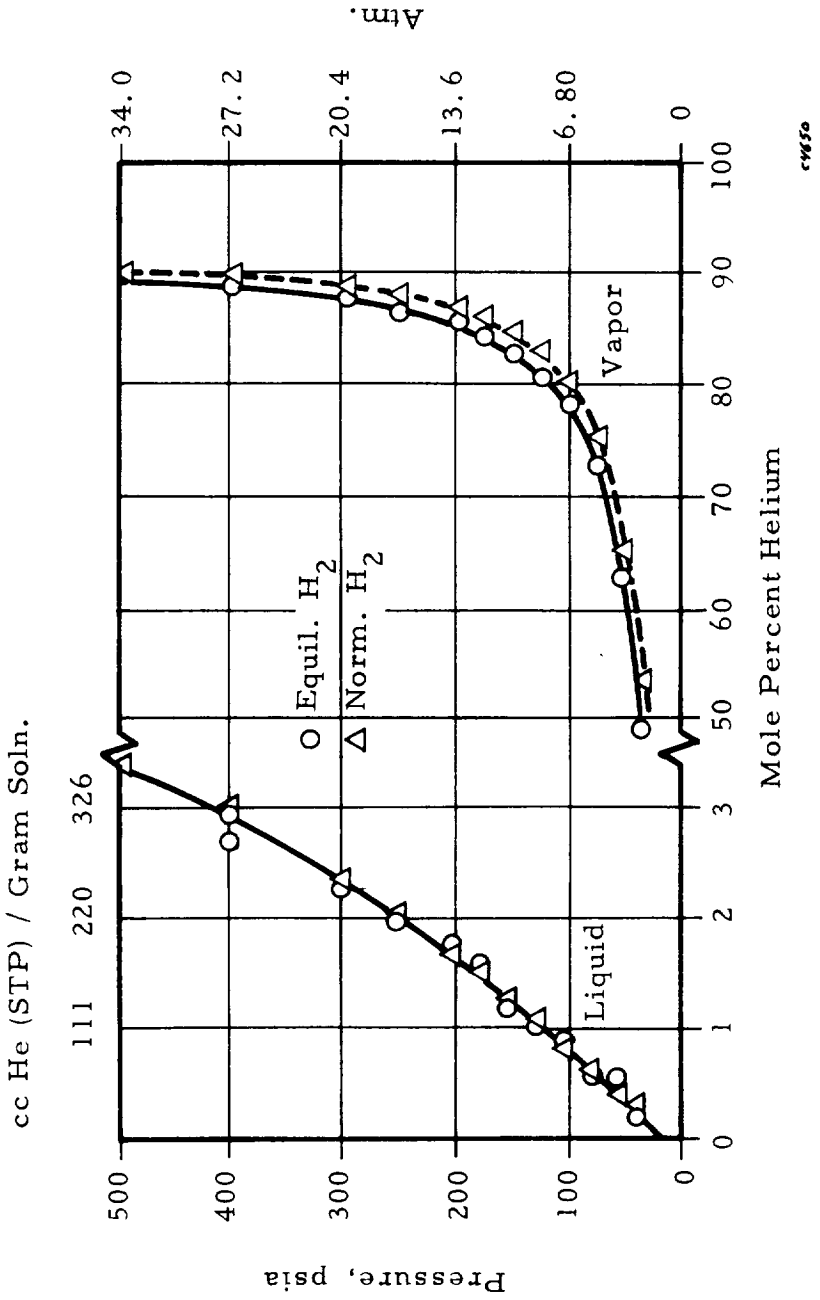

Figure IV-84. Comparison of Normal and Equilibrium Hydrogen Data at 20.40°K

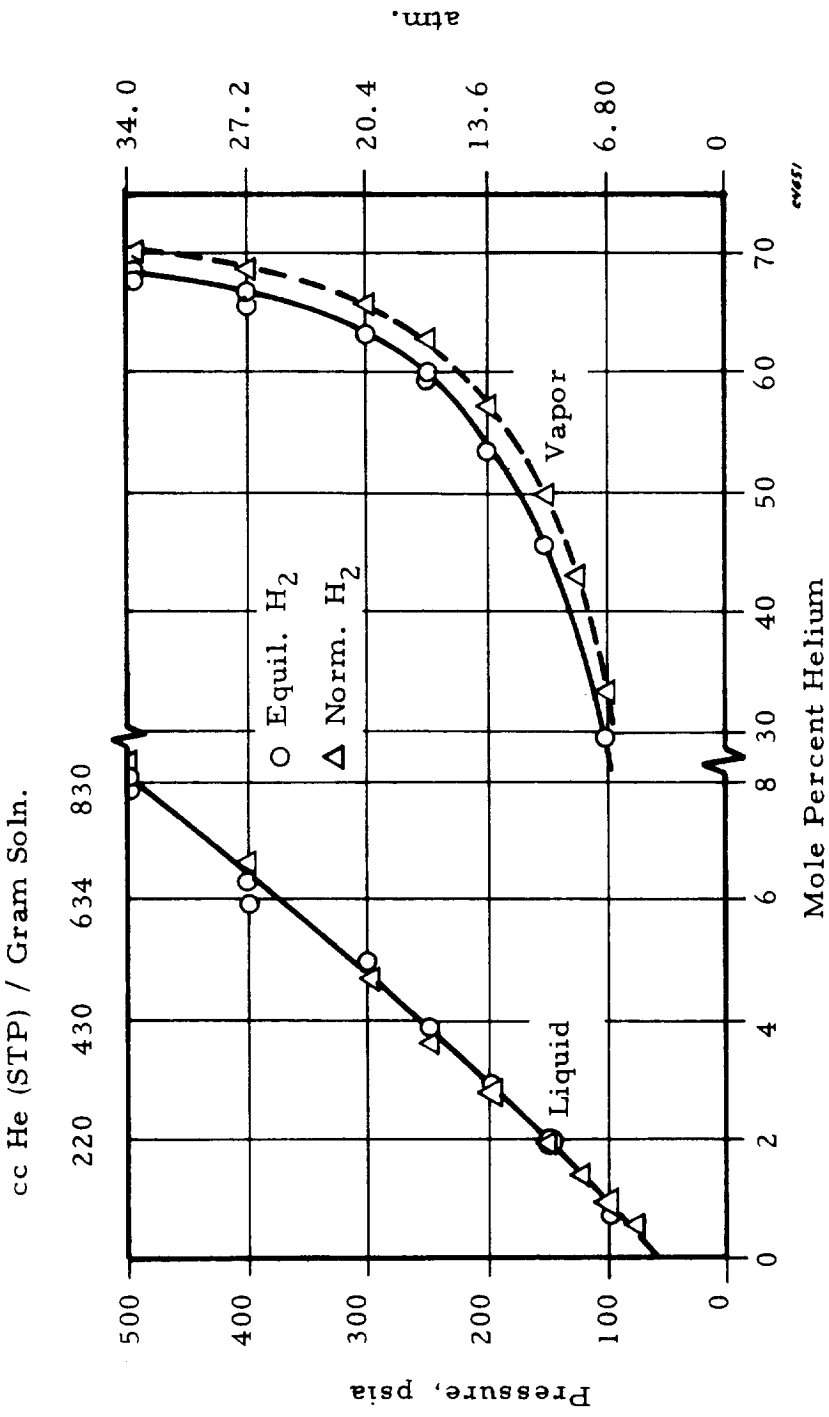

Figure IV-85. Comparison of Normal and Equilibrium Hydrogen Data at 26.00°K.

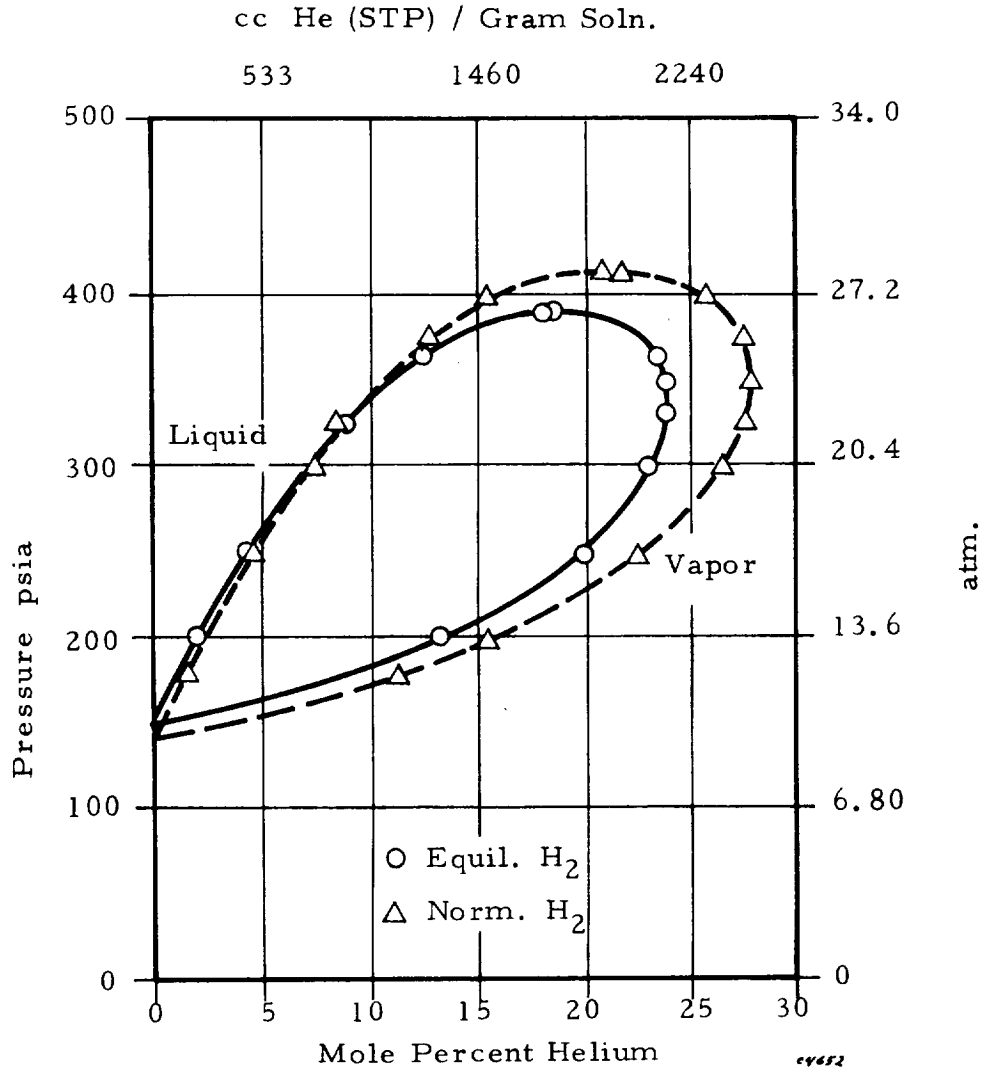

Figure IV-86. Comparison of Normal and Equilibrium Hydrogen Data at 31.00°K.

may be noted that the authors felt that slight measured differences in liquid phase helium concentration at 31.00° were above experimental error (note Figure IV-86). They also indicated that ortho ⇄ para conversion during the experimental work would have been negligible and should not have perturbed the results.

20. Methane-Helium

The system methane-helium has been extensively studied by Heck and Hiza (Reference 73), from the methane triple point to near the critical temperature of methane. Their complete experimental data is presented in Table IV-26.

Because the above compilation is so comprehensive, only selected data of present interest, in the range of -290 to -180°F and 0 to 700 psia, are given here in graphical form. These isothermal and isobaric composition plots are shown in Figures IV-87 and IV-88.

21. Methane-Hydrogen

The data of Katz et. al. (References 75 and 76) have been used for this binary system. Complete two-phase isothermal and isobaric composition diagrams are presented in Figures IV-89 and IV-90. Similar plots showing their data for the liquid region on an expanded scale have also been constructed (Figures IV-91 and IV-92).

22. Methane-Nitrogen

Isobaric equilibrium concentrations of the methane-nitrogen system over the pressure range of 15 to 700 psia and between -320 and -120°F are plotted in Figure IV-93. This graph, taken from Reference 58, employs data from References 77 and 81, and has been used to construct the isothermal pressure-composition diagram for the liquid phase in the region of 0-600 psia, which is shown in Figure IV-94.

23. Monomethylhydrazine-Argon

See Section 25.

TABLE IV-26

EXPERIMENTAL LIQUID-VAPOR EQUILIBRIUM DATA FOR THE SYSTEM HELIUM-METHANE

T, °K	P_0[a] atm.	P_1[b] atm.	Mole % He in Liquid	Mole % CH_4 in Gas	T, °K	P_0, atm.	P_1, atm.	Mole % He in Liquid	Mole % CH_4 in Gas
94.97	0.1954	4.75	0.012	4.20	109.90	0.8630	20.15	0.151	4.63
±0.02		10.05	0.034	1.90	±0.02		35.20	0.262	2.79
		20.00	0.069	1.00			41.00	0.304	2.44
		39.75	0.136	0.595			70.30	0.488	1.49
		60.00	----	0.434			89.80	0.604	1.22
		69.00	0.226	----			101.5	----	1.08
		84.60	0.274	0.363			102.0	0.679	----
		90.30	0.285	----			131.4	0.833	0.948
		117.4	0.363	0.253			162.6	0.978	0.822
		142.6	0.419	0.231			190.5	1.11	----
		161.9	0.472	0.196			199.1	----	0.721
		180.4	----	0.210					
		192.0	0.524	----					
124.85	2.639	11.20	0.125	25.9	154.80	12.685	17.40	----	78.8
±0.03		20.20	0.216	14.3	±0.04		37.20	1.03	----
		40.20	0.499	7.90			43.10	1.30	36.8
		63.60	0.799	5.17			62.30	1.89	----
		85.50	1.04	3.95			78.60	----	21.5
		112.2	1.31	3.07			79.50	2.35	----
		142.5	1.60	2.58			108.5	3.19	----
		171.7	1.84	2.22			108.9	----	16.2
		201.3	2.09	2.01			143.0	4.13	12.9
139.83	6.286	22.80	0.447	29.8			171.6	4.80	10.8
±0.03		39.20	0.789	18.8			201.2	5.37	10.0
		62.40	----	12.4					
		81.80	1.63	9.45					
		112.0	2.14	7.42					
		142.4	2.62	----					
		172.0	3.04	5.23					
		199.0	3.41	4.73					
169.81	22.864	32.50	0.640	78.3	184.83	37.887	44.50	----	93.07
±0.05		55.30	2.06	53.1	±0.05		66.60	3.52	78.8
		58.00	2.17	----			87.50	----	66.9
		66.90	2.61	----			88.00	5.58	----
		82.00	3.52	39.9			111.9	7.73	56.4
		107.2	4.69	33.1			152.4	11.1	48.1
		114.6	4.99	----			178.0	12.6	43.8
		141.9	6.12	26.2			202.6	13.7	40.8
		168.6	7.16	23.0					
		195.9	8.06	----					

(a) P_0 = Vapor pressure of methane, calculated from the expressions of Kirk (Reference 74).

(b) P_1 = Total system pressure.

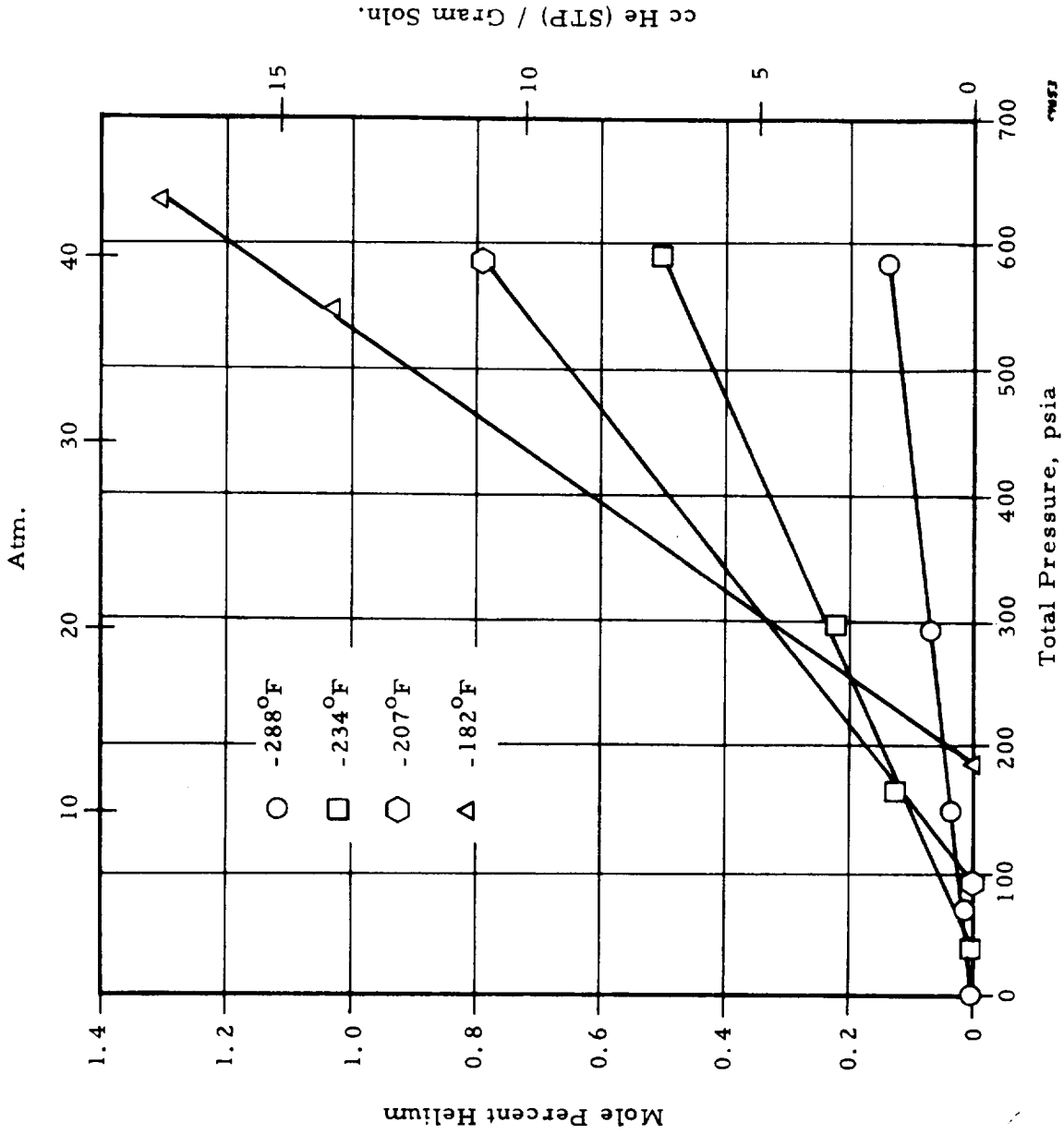

Figure IV-87. Isothermal Pressure-Composition Diagram for the System Liquid Methane-Helium

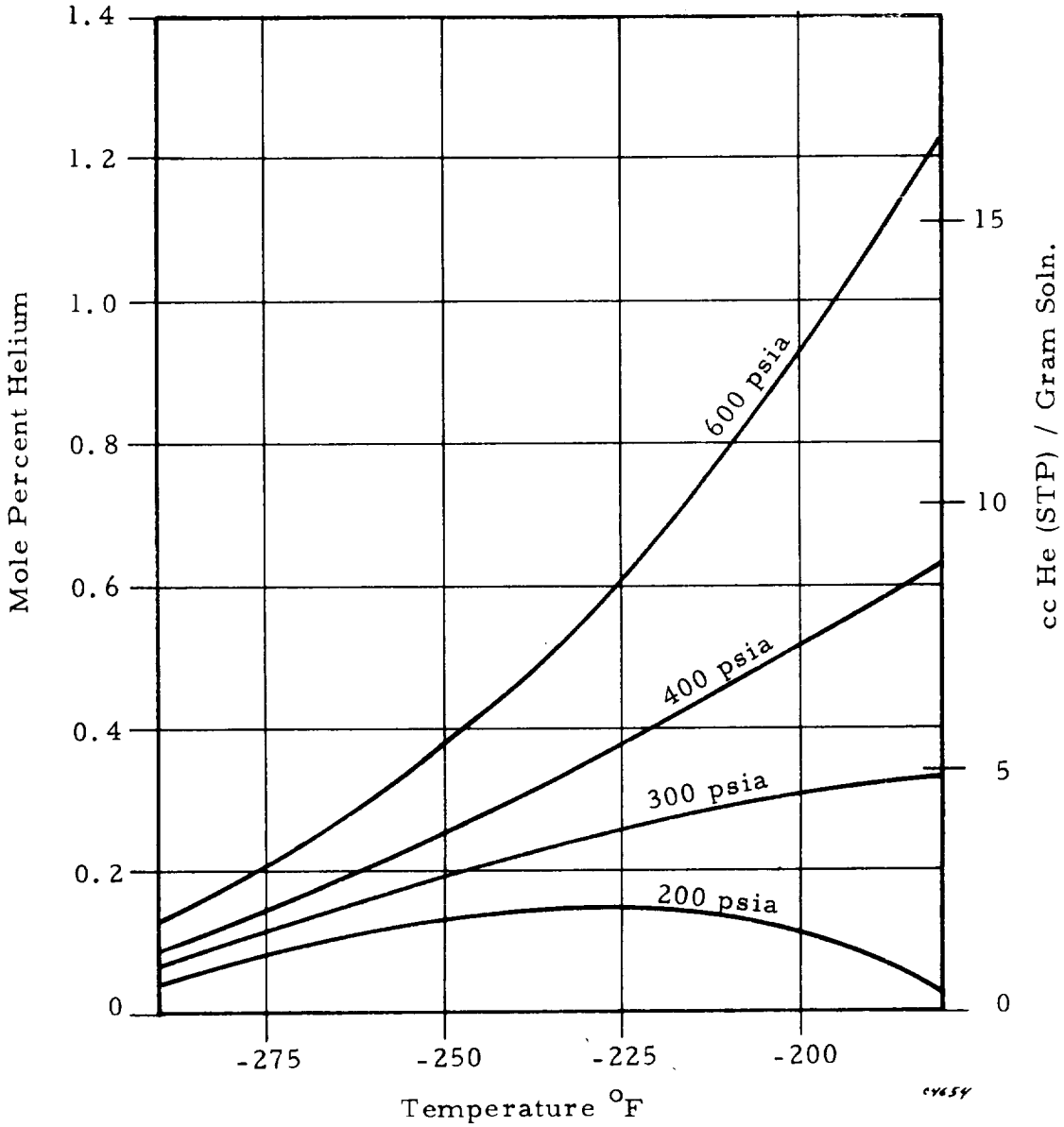

Figure IV-88. Isobaric Temperature – Composition Diagram for the System Liquid Methane-Helium

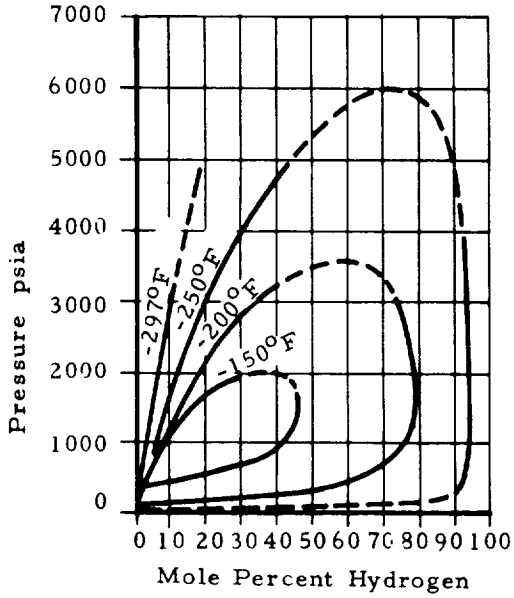

Figure IV-89. Isothermal Pressure - Composition Diagram for the Binary System Methane-Hydrogen

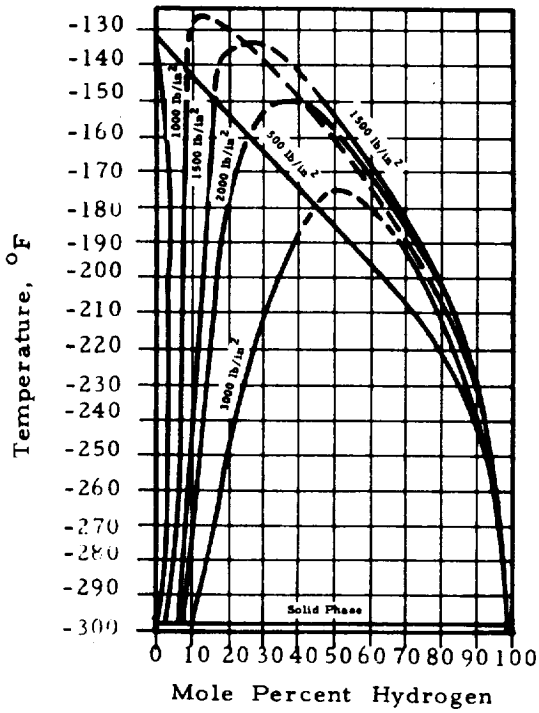

Figure IV-90. Isobaric Temperature - Composition Diagram for the Binary System Methane-Hydrogen

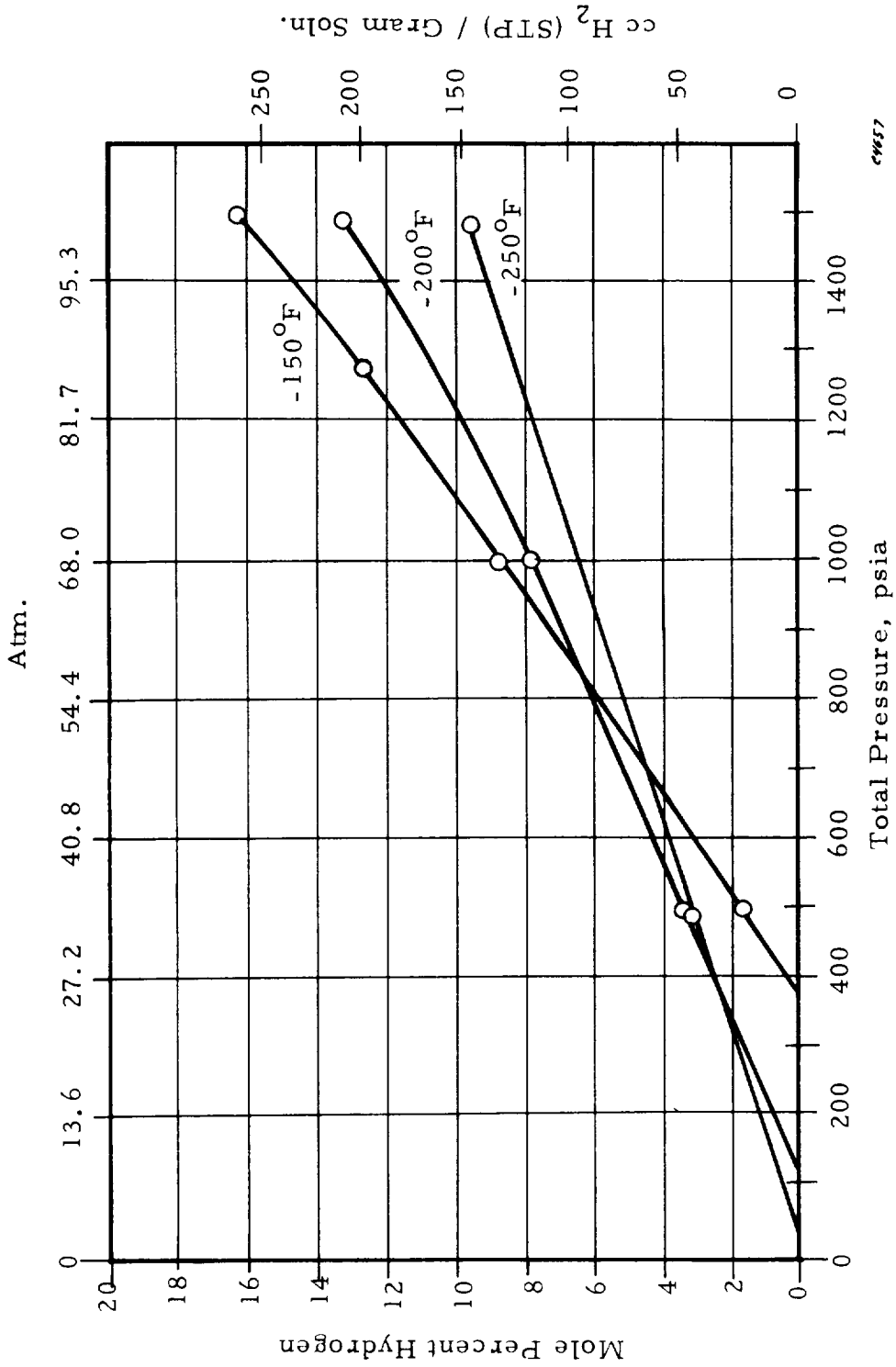

Figure IV-91. Isothermal Pressure – Composition Diagram For the System Liquid Methane-Hydrogen

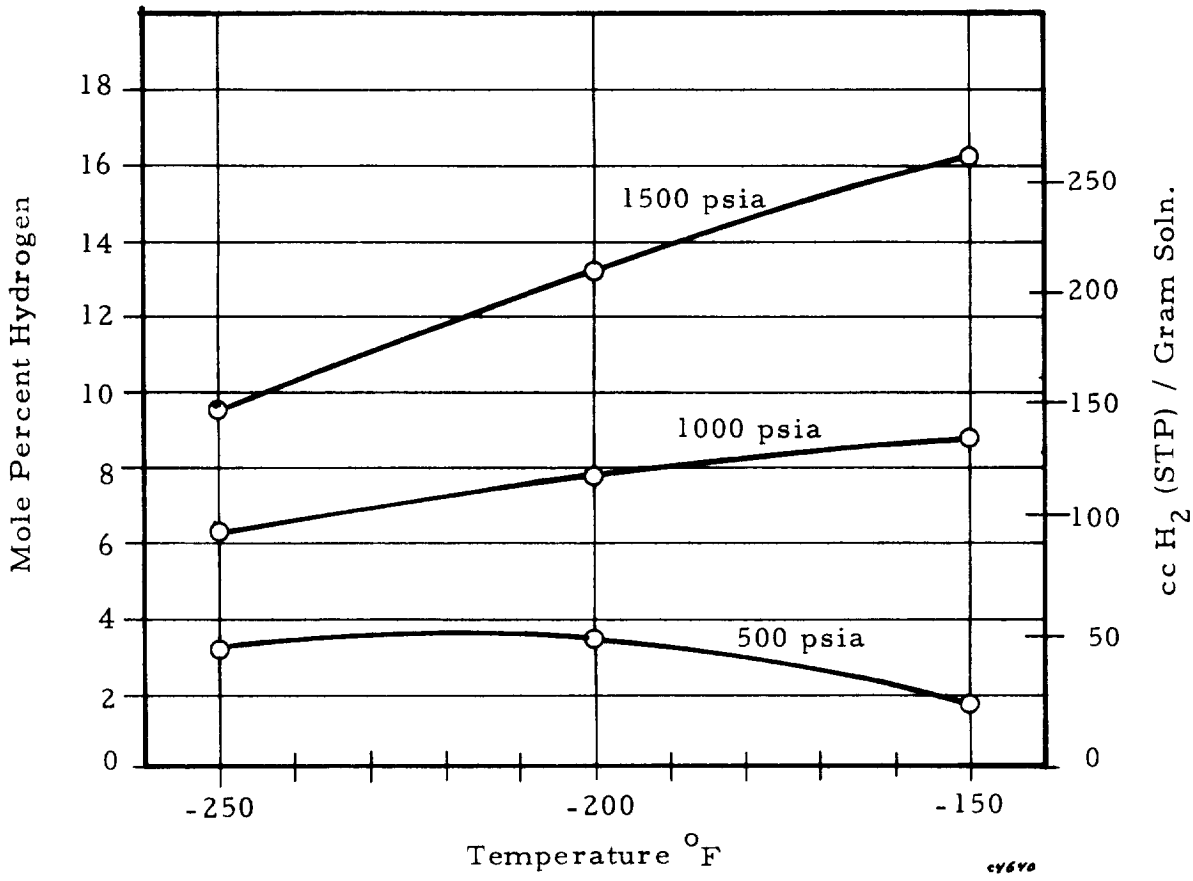

Figure IV-92. Isobaric Temperature – Composition Diagram For the System Liquid Methane-Hydrogen

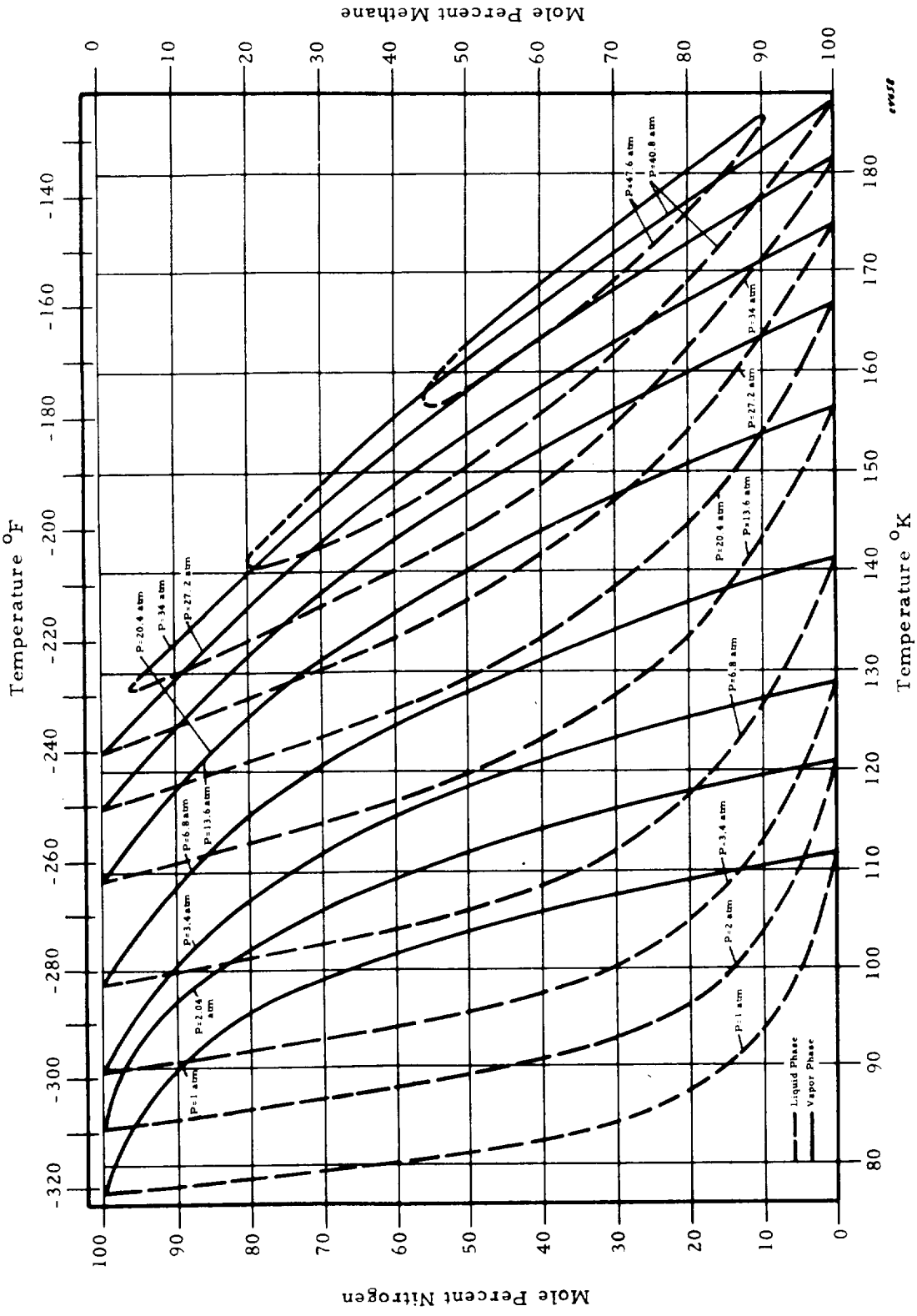

Figure IV-93. Isobaric Equilibrium Composition Diagram for the System Methane-Nitrogen

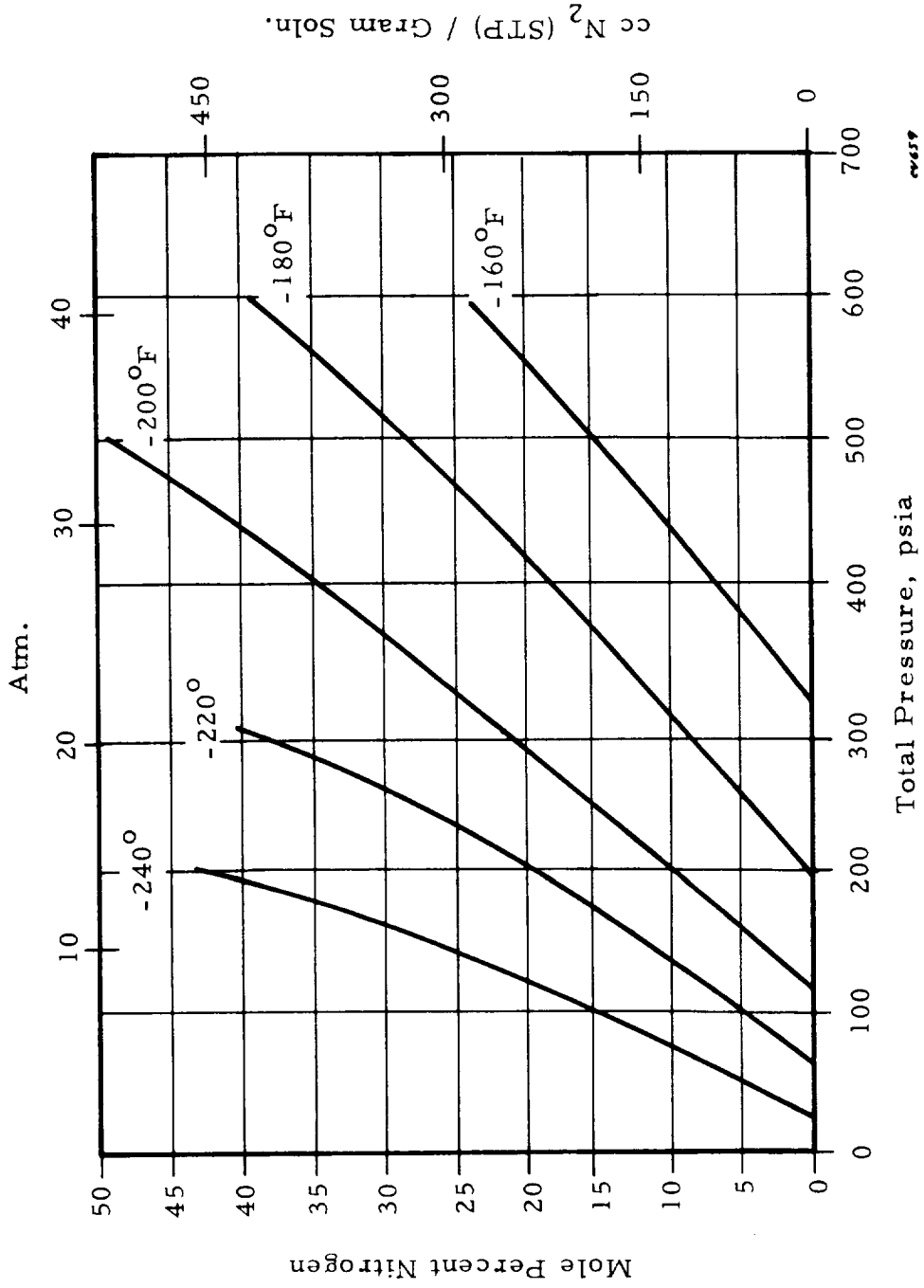

Figure IV-94. Isothermal Pressure – Composition Diagram For the System Liquid Methane-Nitrogen

24. Monomethylhydrazine-Helium

See Section 25.

25. Monomethylhydrazine-Nitrogen

Solubility data for these systems have been reported (Reference 71) at pressures of about 15 and 30 psia in the temperature range from -4°F to 77°F. The available data are summarized in Table IV-27. (N. B. The pressures given in this Table are partial pressures of the pressurant gas, not total system pressures.)

The systems monomethylhydrazine-helium and monomethylhydrazine-nitrogen have also been investigated at total pressures of 300 and 700 psia over the temperature range from 20°F to 175°F (References 38 and 39). Isobaric solubility plots for these systems are presented in Figures IV-95 and IV-96. Isothermal pressure-composition diagrams have been plotted from this data and are shown in Figures IV-97 and IV-98.

More recent work (Reference 31) on the solubility of helium in monomethylhydrazine is in essential agreement with that cited above.

26. Monomethylhydrazine Hydrate-Helium

Figure IV-99 gives the available solubility data for helium in monomethylhydrazine hydrate (References 51 and 83). The corresponding isothermal plots constructed from these data appear in Figure IV-100.

27. Pentaborane-Helium

The solubility of helium in pentaborane has been determined at total pressures of 500 to 1500 psig and over the temperature range of 86° to 303°F (Reference 83). Isothermal and isobaric solubility plots have been constructed from this data and are shown in Figures IV-101 and IV-102.

It should be noted, in the use of this data, that there may be some uncertainty in these results because of decomposition of the pentaborane. These reactions, which produce hydrogen, become appreciable above about 200°F. For this reason the isothermal diagram has been plotted only to 200°F.

TABLE IV-27

SOLUBILITIES OF ARGON, HELIUM AND NITROGEN IN LIQUID MONOMETHYLHYDRAZINE

Temp. °F	Argon		Helium		Nitrogen	
	P(a) psia	Mole % x10³	P(a) psia	Mole % x10³	P(a) psia	Mole % x10³
-4.0	16.41	16.65	12.15	1.15	14.38	6.48
	29.58	29.75	29.15	3.12	29.45	13.39
32.0	17.17	18.59	16.82	2.04	16.24	8.34
	29.90	32.60	31.53	4.18	29.19	15.02
77.0	17.16	21.00	16.56	2.78	15.54	9.78
	29.66	36.40	30.30	5.41	30.65	19.46

(a) P = Partial pressure of pressurant gas.

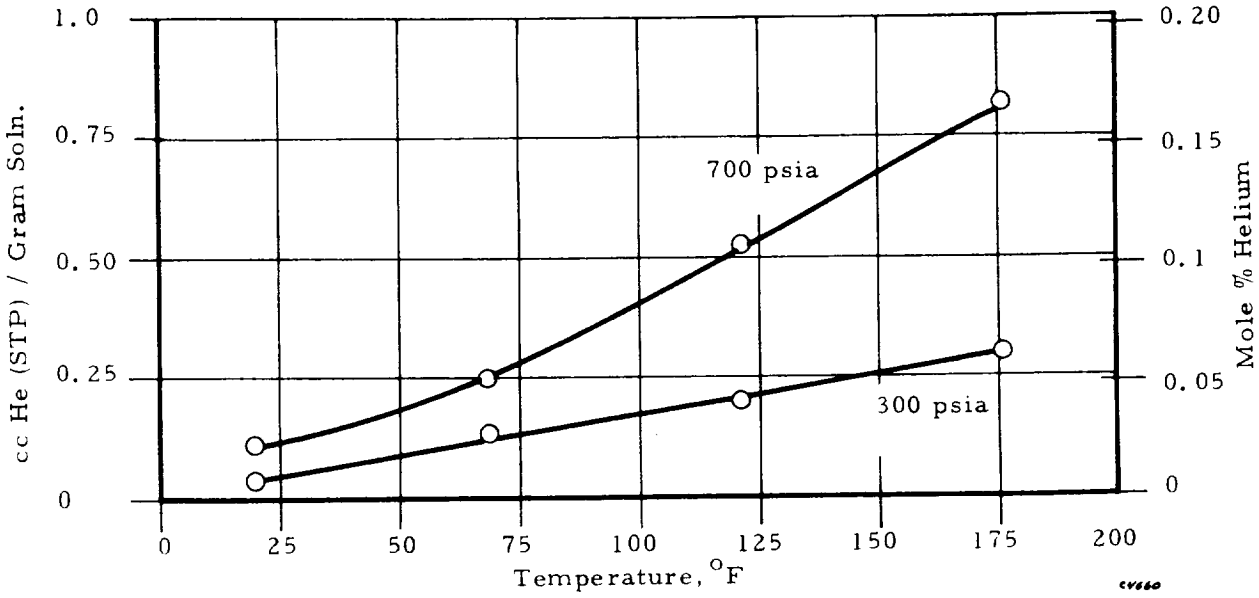

Figure IV-95. Isobaric Temperature-Composition Diagram for the System Liquid Monomethylhydrazine-Helium

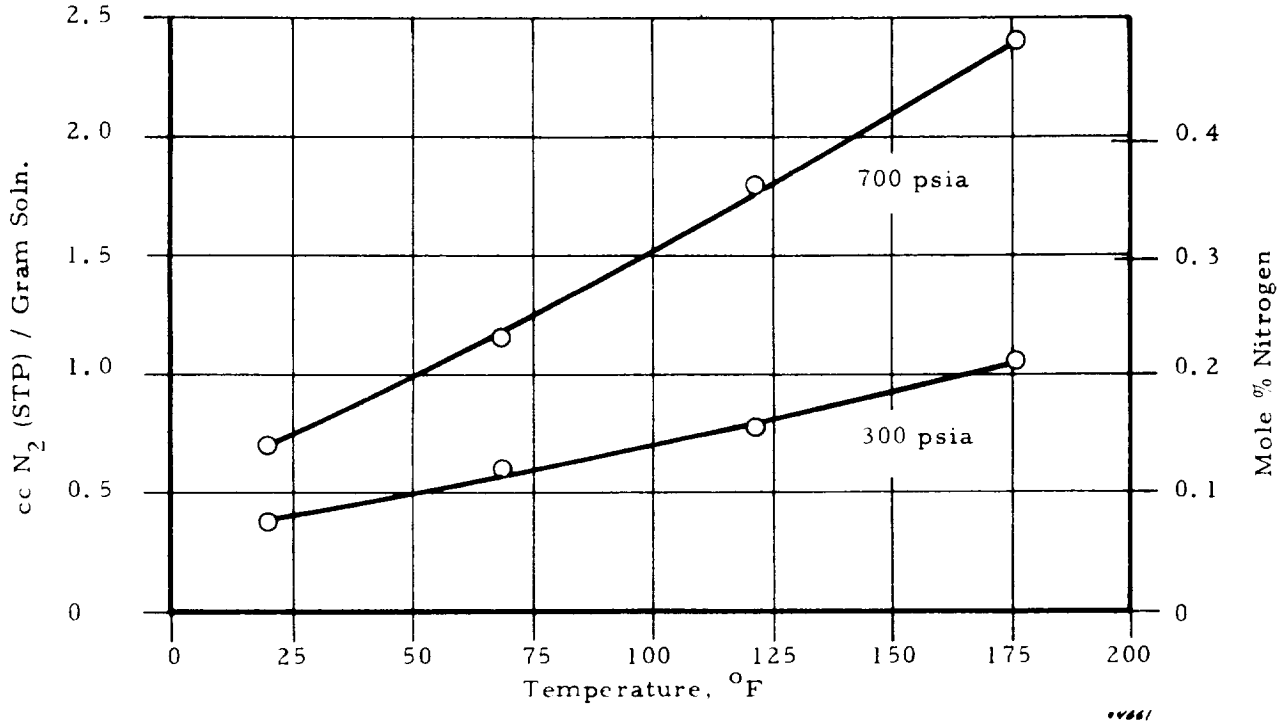

Figure IV-96. Isobaric Temperature-Composition Diagram for the System Liquid Monomethylhydrazine-Nitrogen

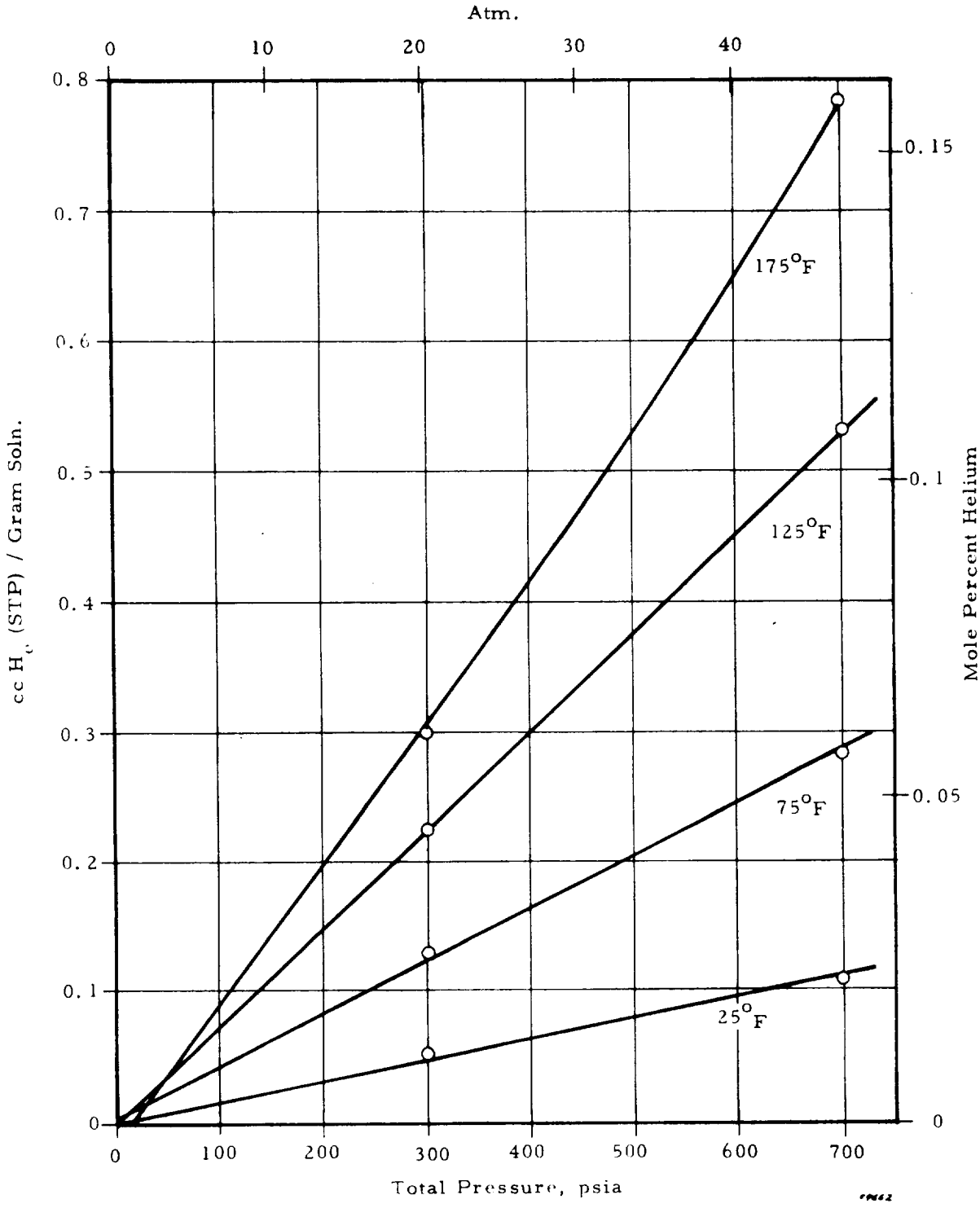

Figure IV-97. Isothermal Pressure–Composition Diagram for the System Liquid Monomethylhydrazine-Helium

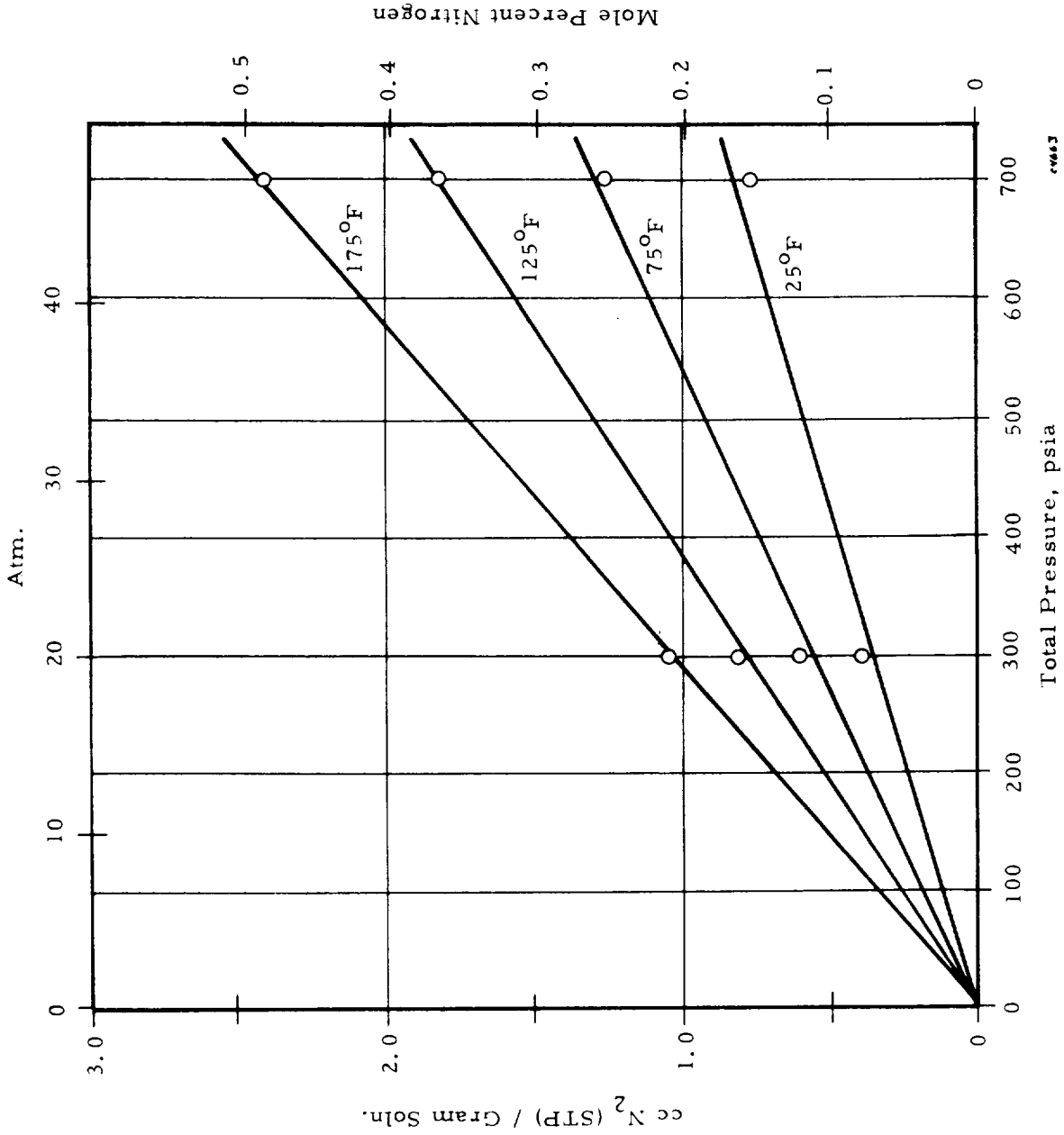

Figure IV-98. Isothermal Pressure-Composition Diagram for System Liquid Monomethylhydrazine-Nitrogen

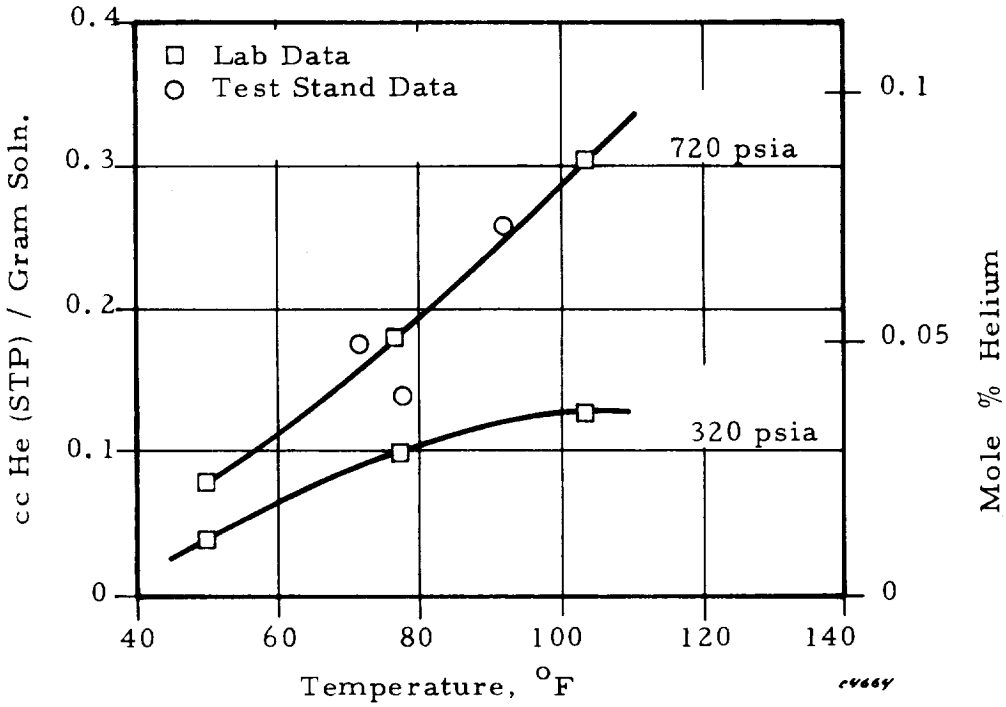

Figure IV-99. Isobaric Temperature-Composition Diagram for the System Liquid Monomethylhydrazine Hydrate-Helium.

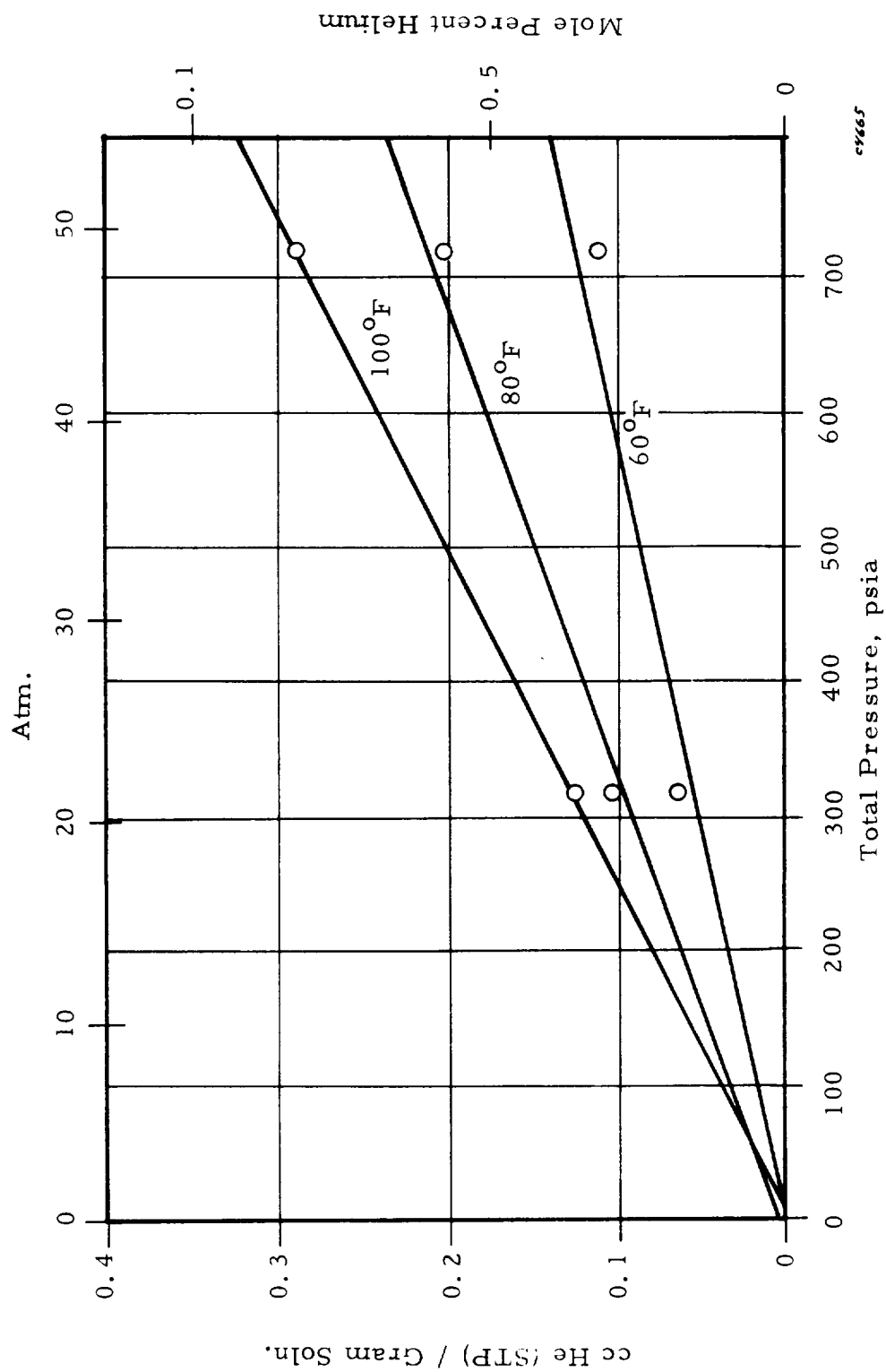

Figure IV-100. Isothermal Pressure – Composition Diagram For the System Liquid Monomethylhydrazine Hydrate-Helium

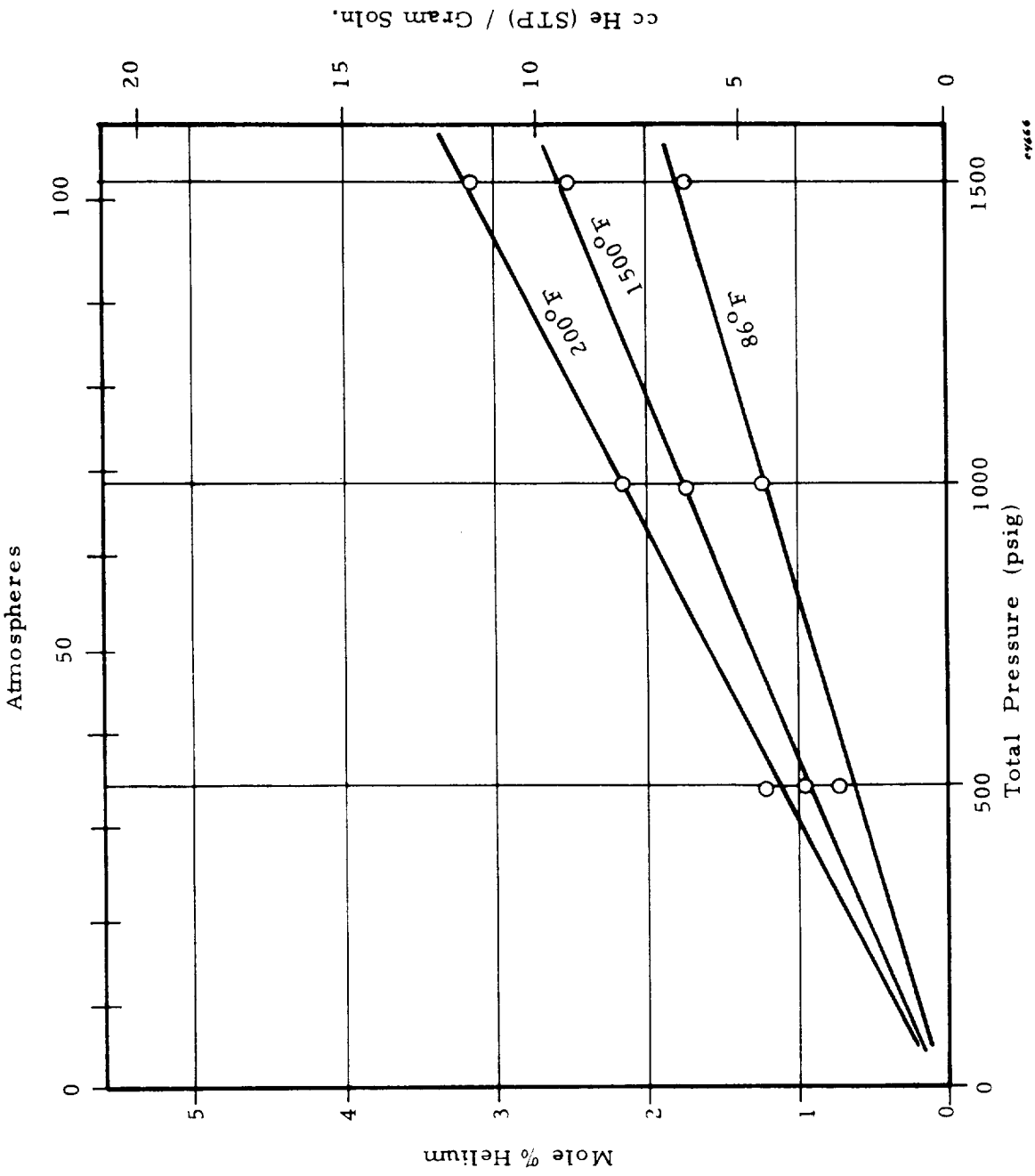

Figure IV-101. Isothermal Pressure-Composition Diagram for the System Liquid Pentaborane-Helium

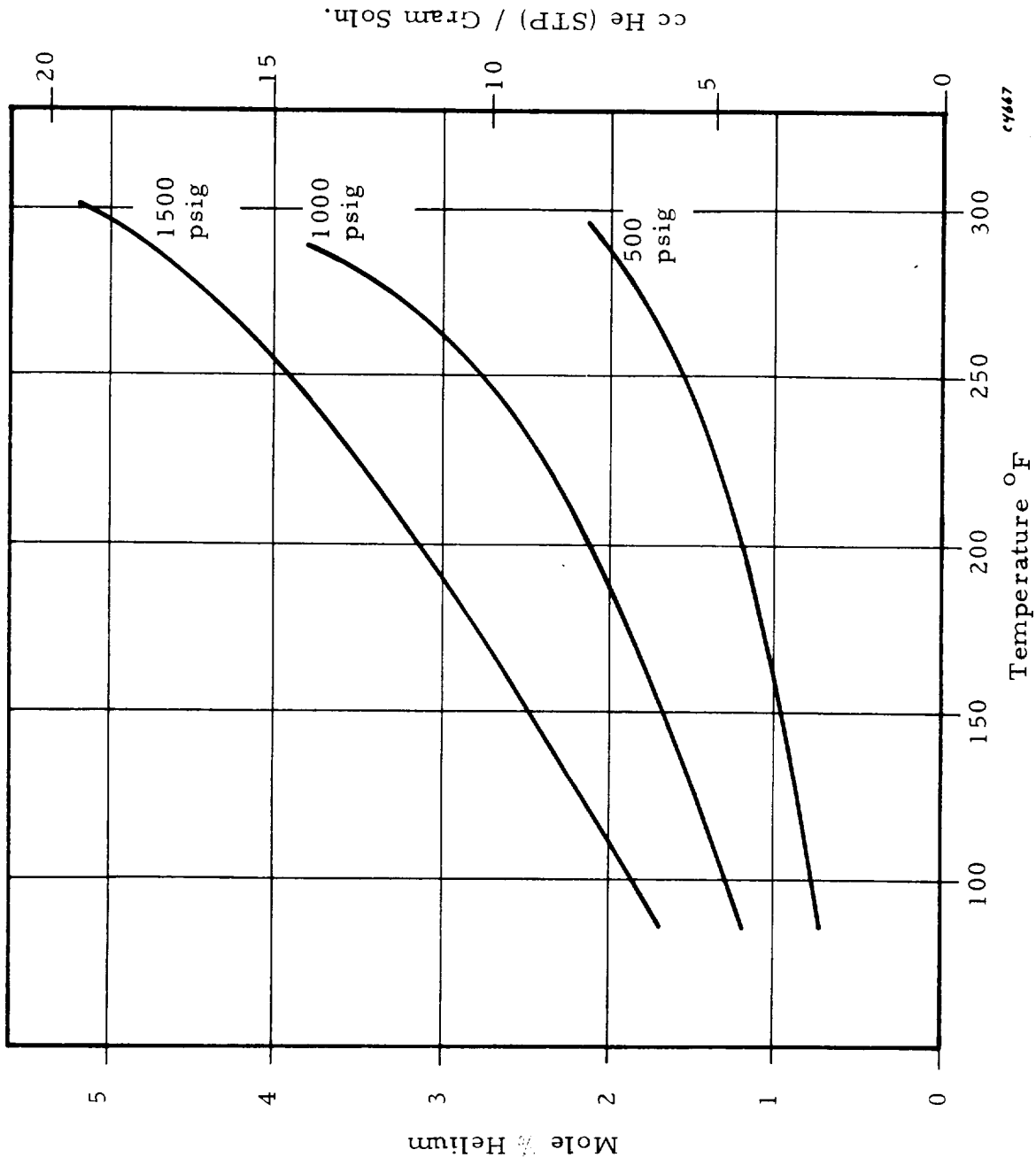

Figure IV-102. Isobaric Temperature-Composition Diagram for the System Liquid Pentaborane-Helium.

28. Pentaborane-Hydrogen

The solubility of hydrogen in pentaborane has been determined at total pressures of 500 to 1500 psig and over the temperature range of 86° to 303°F (Reference 83). Isothermal and isobaric solubility plots have been constructed from this data and are shown in Figures IV-103 and IV-104.

It should be noted, in the use of this data, that there may be some uncertainty in these results because of decomposition of the pentaborane. These reactions, which produce hydrogen, become appreciable above about 200°F. For this reason the isothermal diagram has been plotted only to 200°F.

29. Pentaborane-Nitrogen

The solubility of nitrogen in pentaborane has been determined at total pressures of 500 to 1500 psig and over the temperature range of 86° to 303°F (Reference 83). Isothermal and isobaric solubility plots have been constructed from this data and are shown in Figures IV-105 and IV-106.

It should be noted, in the use of this data, that there may be some uncertainty in these results because of decomposition of the pentaborane. These reactions, which produce hydrogen, become appreciable above about 200°F. For this reason the isothermal diagram has been plotted only to 200°F.

30. Propane-Helium

See Section 31.

31. Propane-Nitrogen

The solubilities of helium and nitrogen in liquid propane were measured by Astropower Laboratory for this Design Guide, under Contract NAS7-548. The solubility data for these two systems are tabulated in Table IV-28; experimental details may be found in Reference 46. The results reported in the table are obtained from duplicate analyses for two successive samples; agreement of these values within experimental error was accepted as indication that solution equilibrium had been attained.

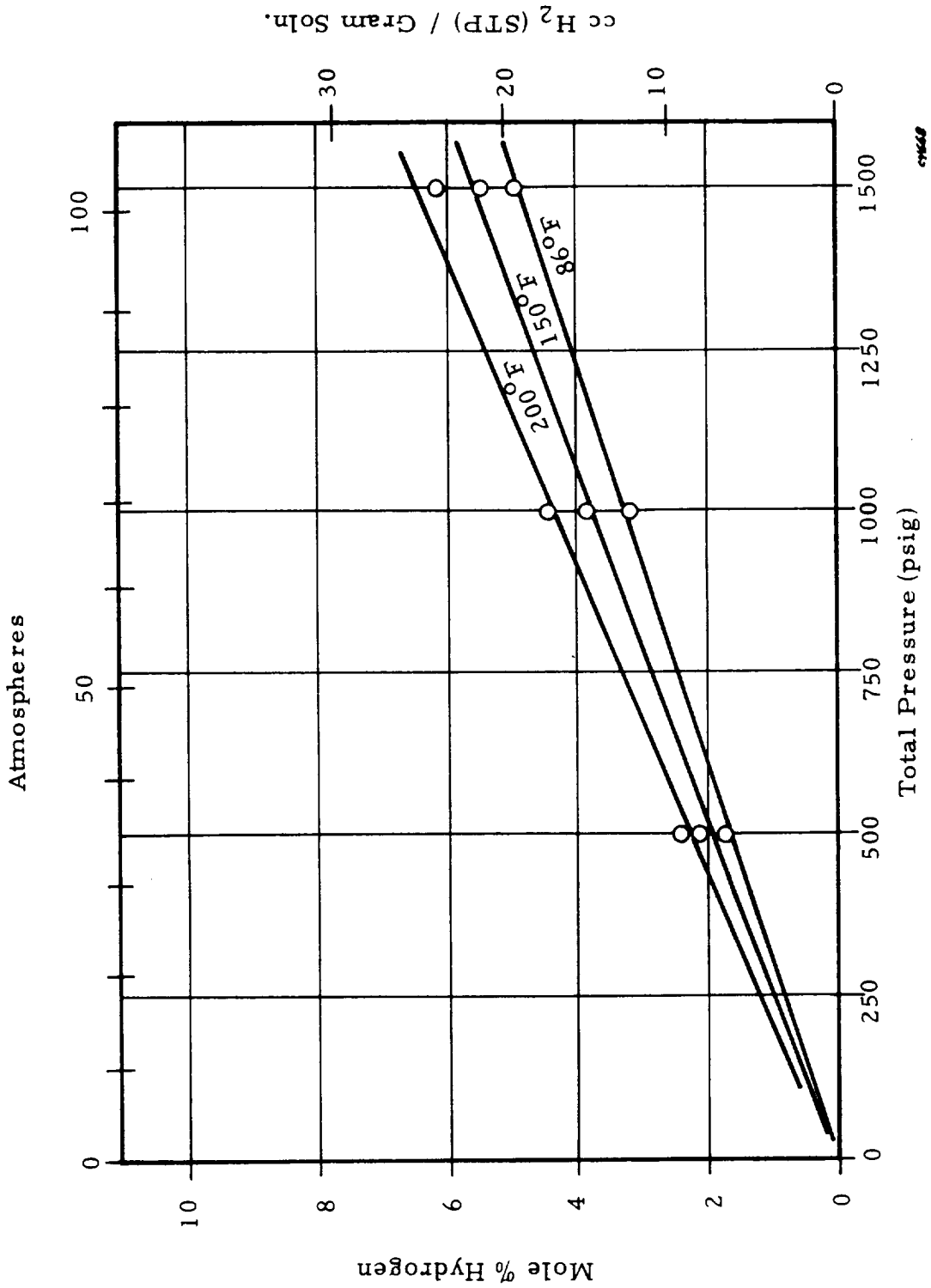

Figure IV-103. Isothermal Pressure-Composition Diagram for the System Liquid Pentaborne-Hydrogen.

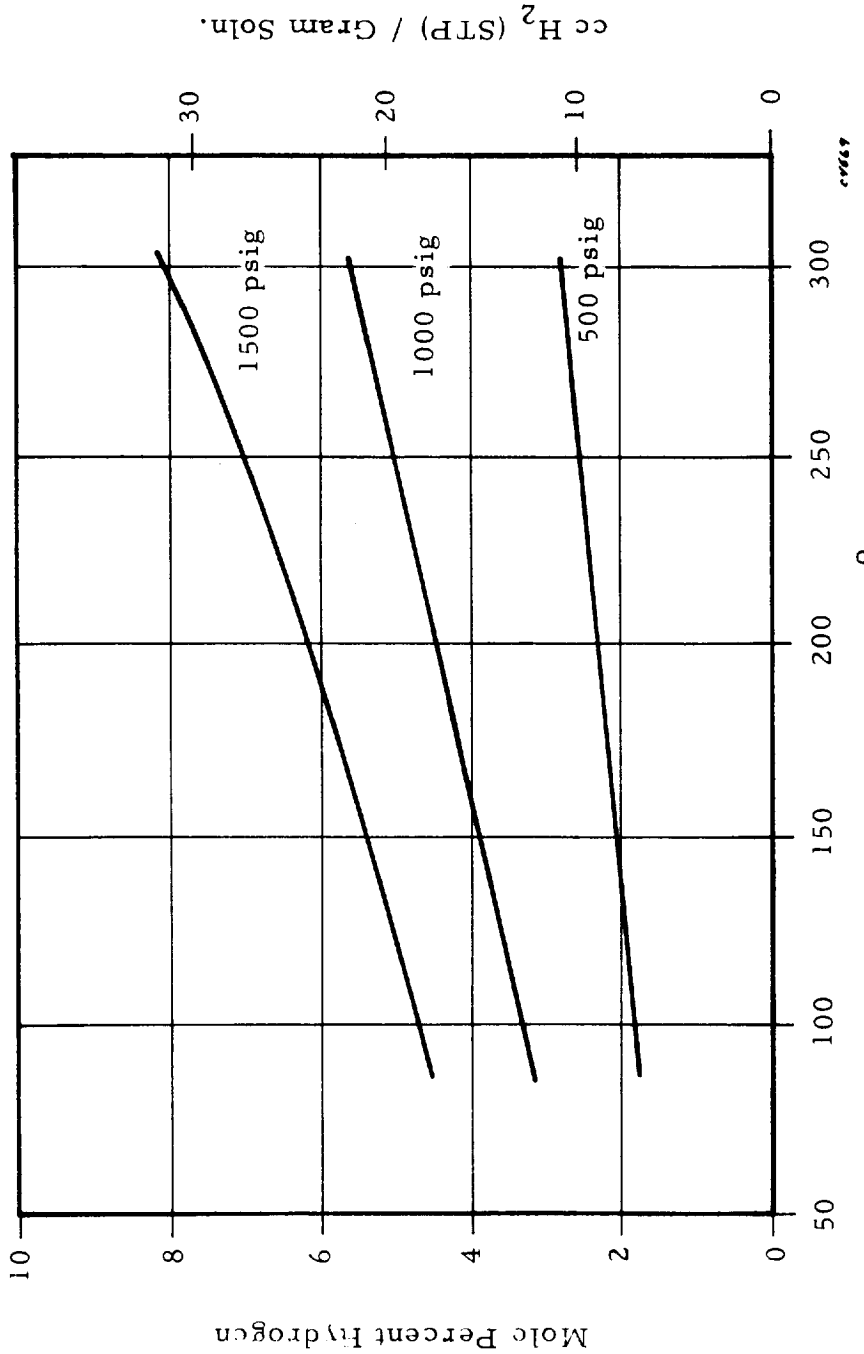

Figure IV-104. Isobaric Temperature – Composition Diagram For the System Liquid Pentaborane-Hydrogen

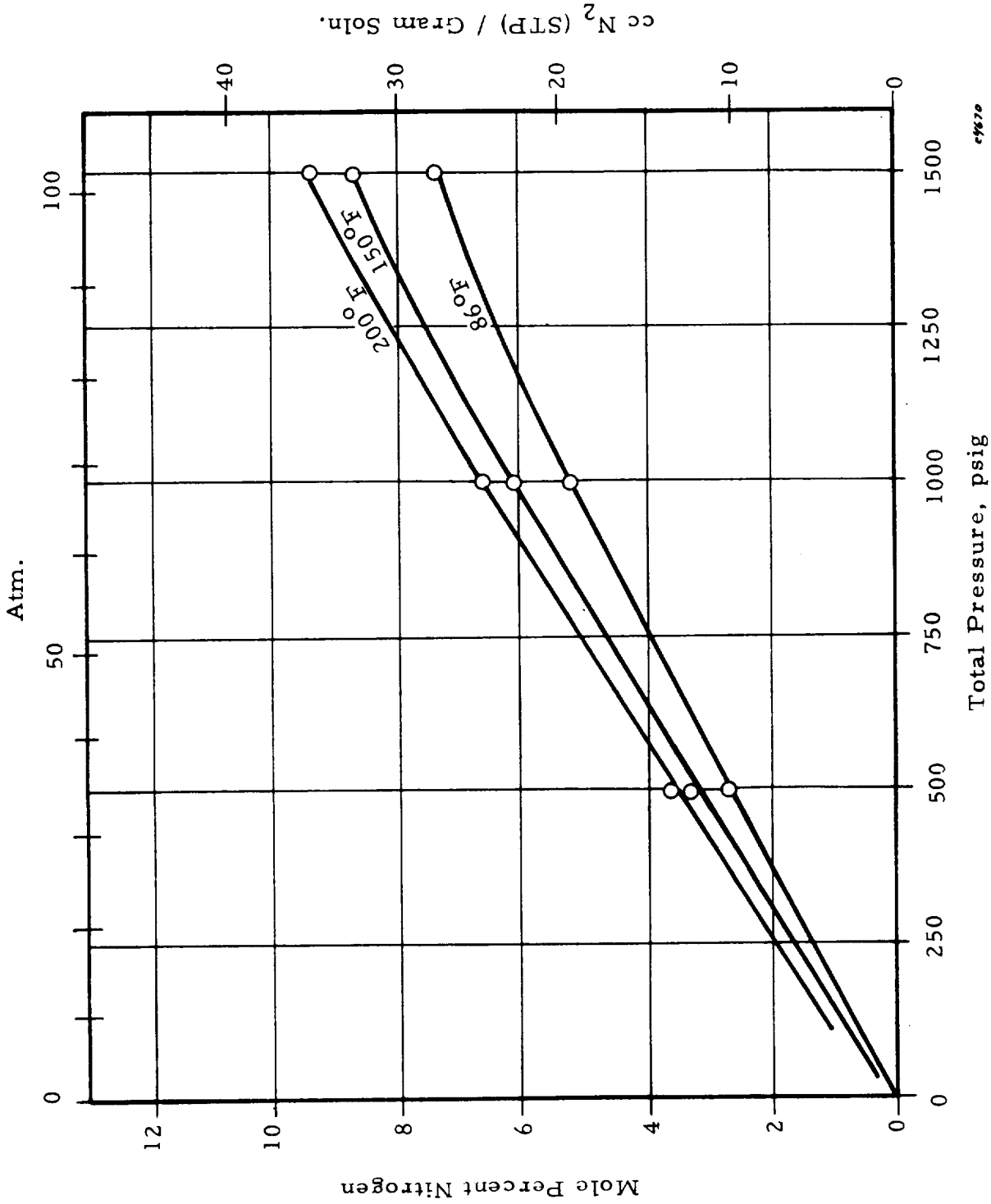

Figure IV-105. Isothermal Pressure – Composition Diagram For the System Liquid Pentaborane-Nitrogen

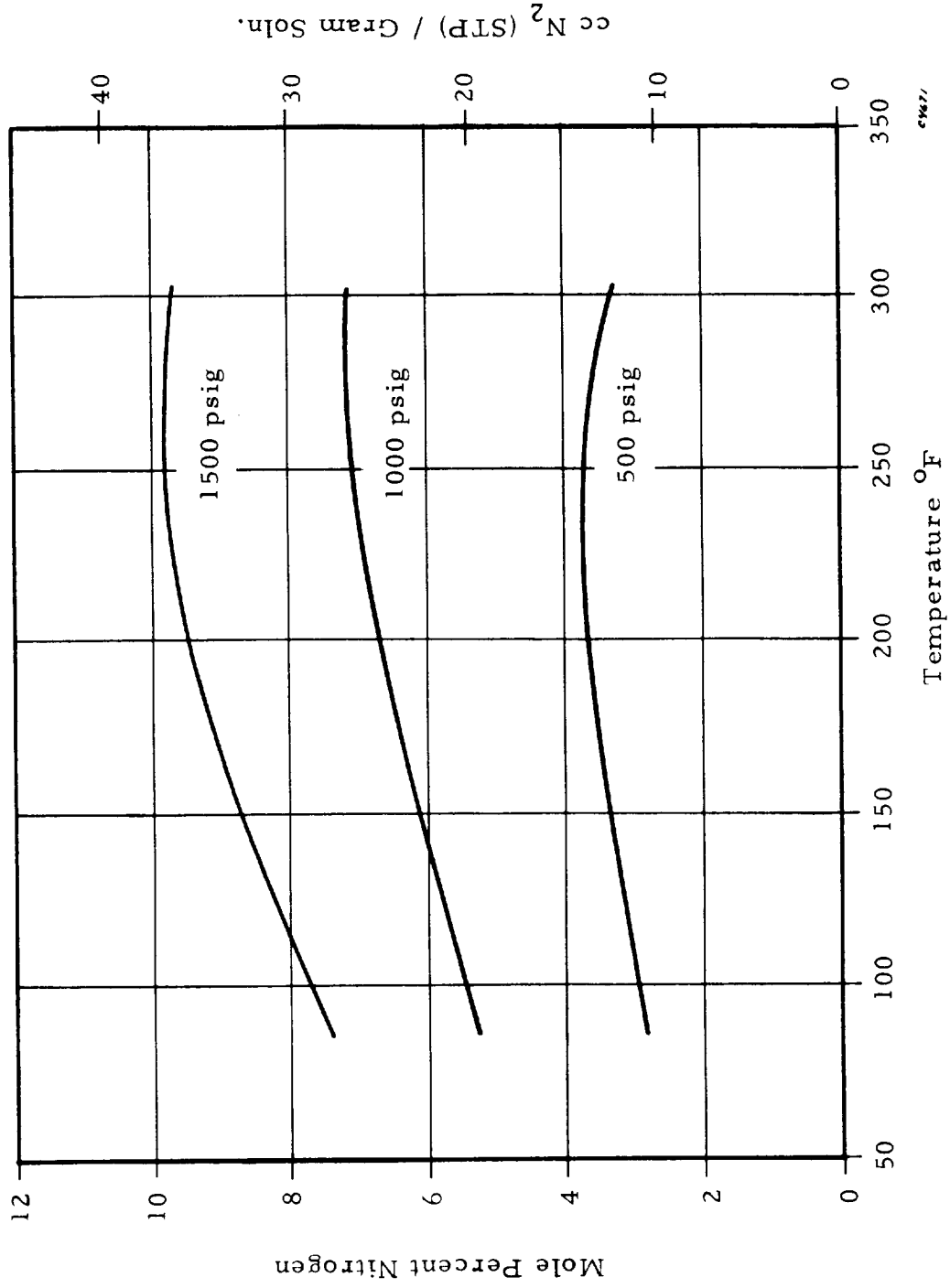

Figure IV-106. Isobaric Temperature – Composition Diagram For the System Liquid Pentaborane-Nitrogen

TABLE IV-28

SOLUBILITY OF HELIUM AND NITROGEN IN LIQUID PROPANE

Test Temperature °F	Vapor Pressure of Propellant psia(a)	Mole Percent Concentration			
		Helium		Nitrogen	
		300 psia	700 psia	300 psia	700 psia
-150	0.1	0.099	0.226	4.97	11.2
-100	3.4	0.205	0.412	4.07	10.6
-50	13.5	0.312	0.711	4.01	10.6
0	41	0.432	1.11	3.44	9.73

(a) Reference 84.

These data are presented as isothermal pressure-composition and isobaric temperature-composition plots in Figures IV-107, IV-108, IV-109, and IV-110. Additional isobars at 150 and 500 psia have been constructed for each system by interpolation.

32. Propane-Hydrogen

The data for this system has been presented by Katz et al (Reference 69) and Sage et. al. (Reference 85). The complete experimental data obtained by Katz is given in Table IV-29 in terms of the equilibrium constants K^* for both components, between the two phases. The combined data of both investigators is given in Figure IV-111 as an isothermal plot of liquid phase composition versus pressure over the temperature range of -300° to 75°F and pressure range of 250 to 8000 psia. Selected data from Table IV-29 (Reference 69) has been used to construct isothermal and isobaric solubility diagrams showing the liquid range below 2000 psia (Figures IV-112 and IV-113). The isothermal curves of Figure IV-112 have been extrapolated to zero hydrogen concentration using propane vapor pressure data from Reference 92.

---

*K_A = mole percent A in vapor/mole percent A in liquid.

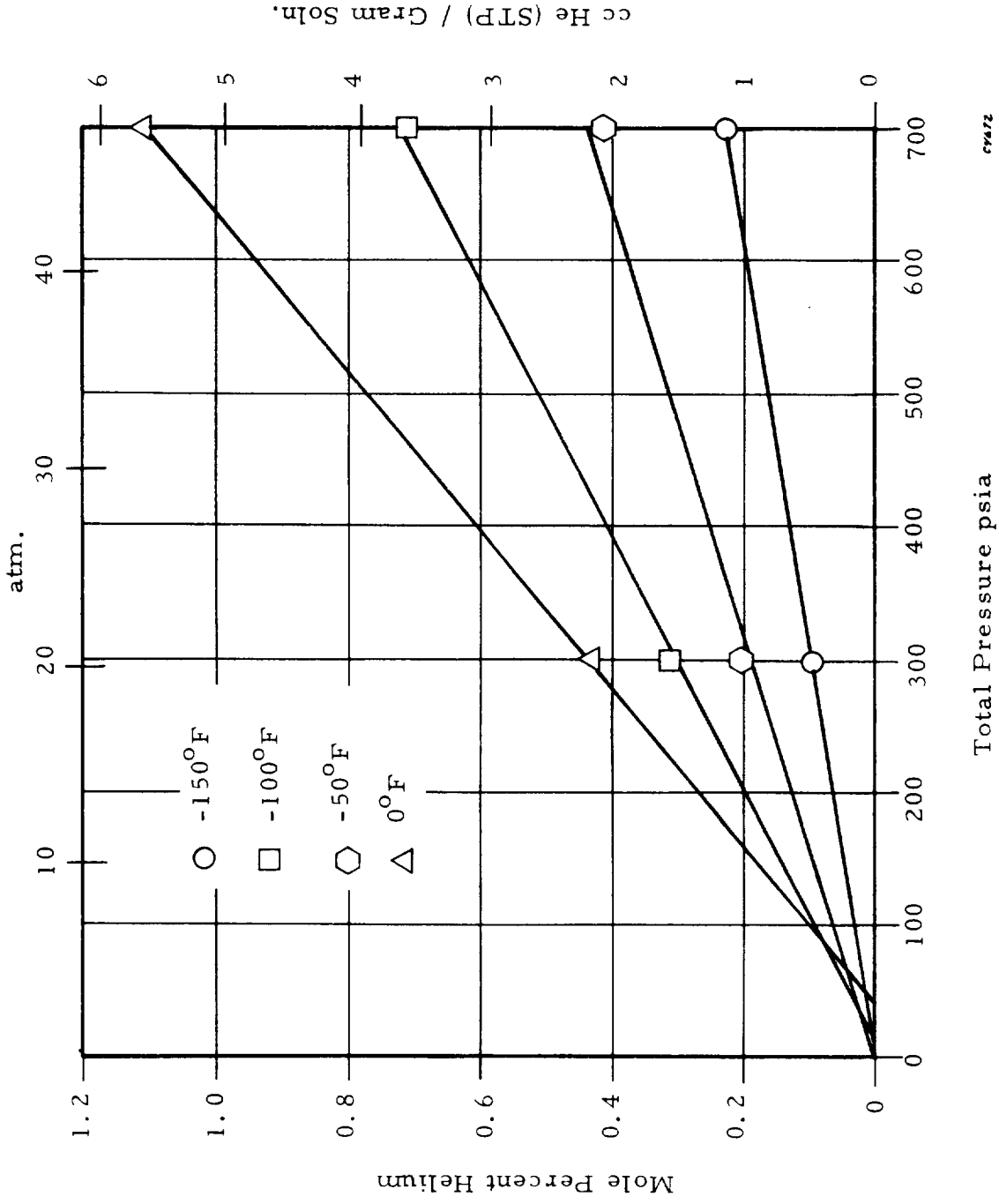

Figure IV-107. Isothermal Pressure-Composition Diagram For The System Liquid Propane-Helium.

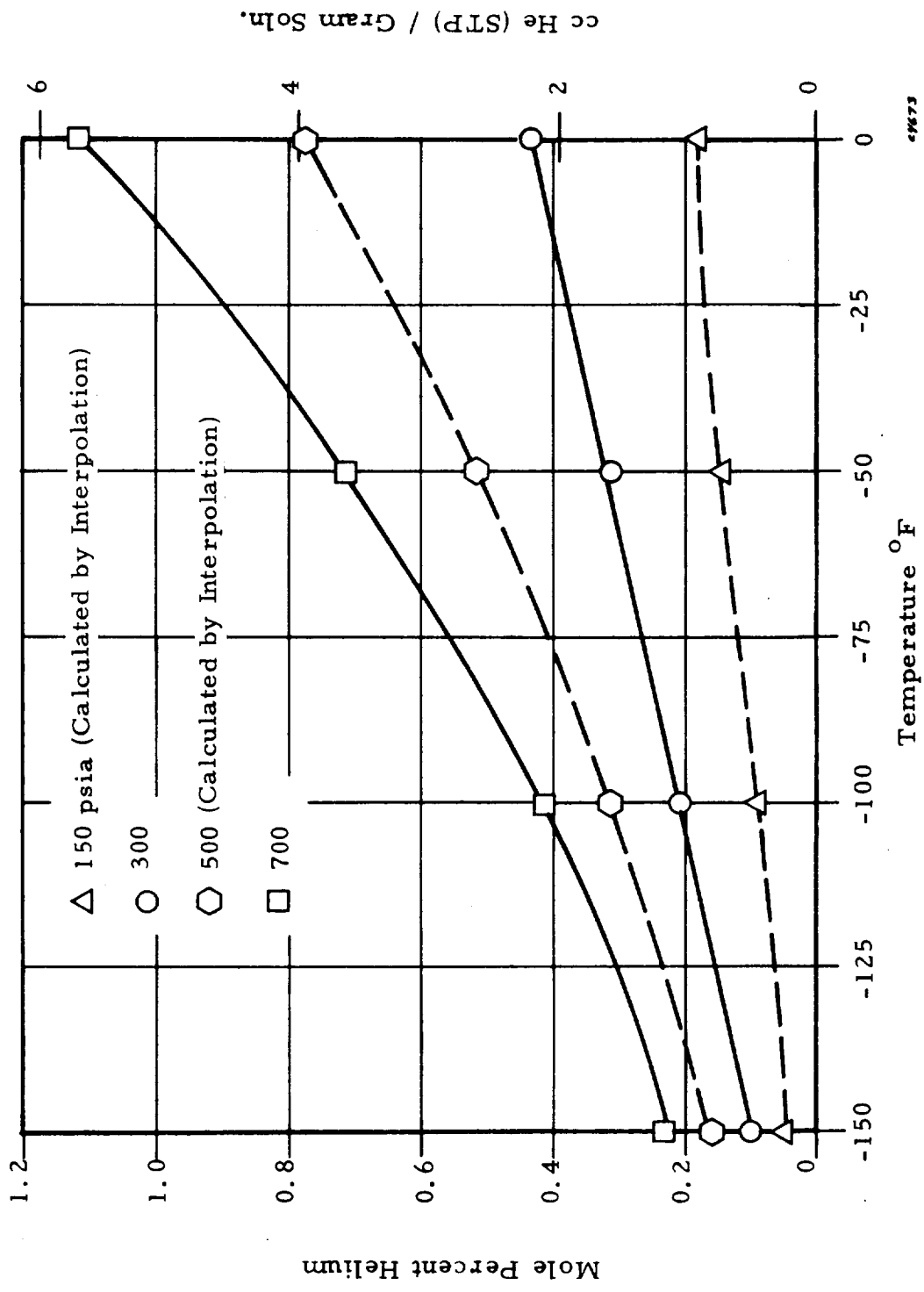

Figure IV-108. Isobaric Temperature-Composition Diagram For The System Liquid Propane-Helium.

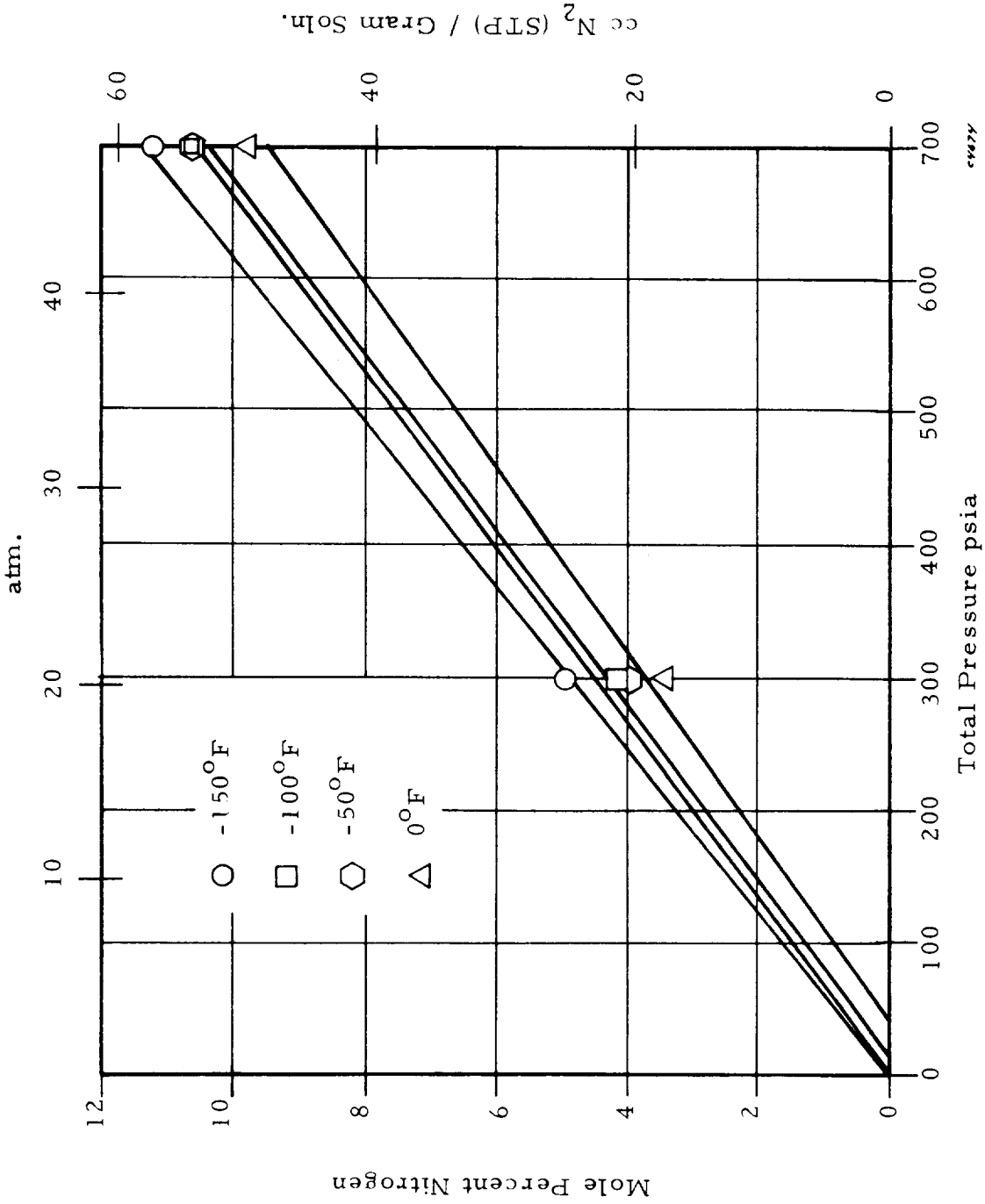

Figure IV-109. Isothermal Pressure-Composition Diagram For The System Liquid Propane-Nitrogen.

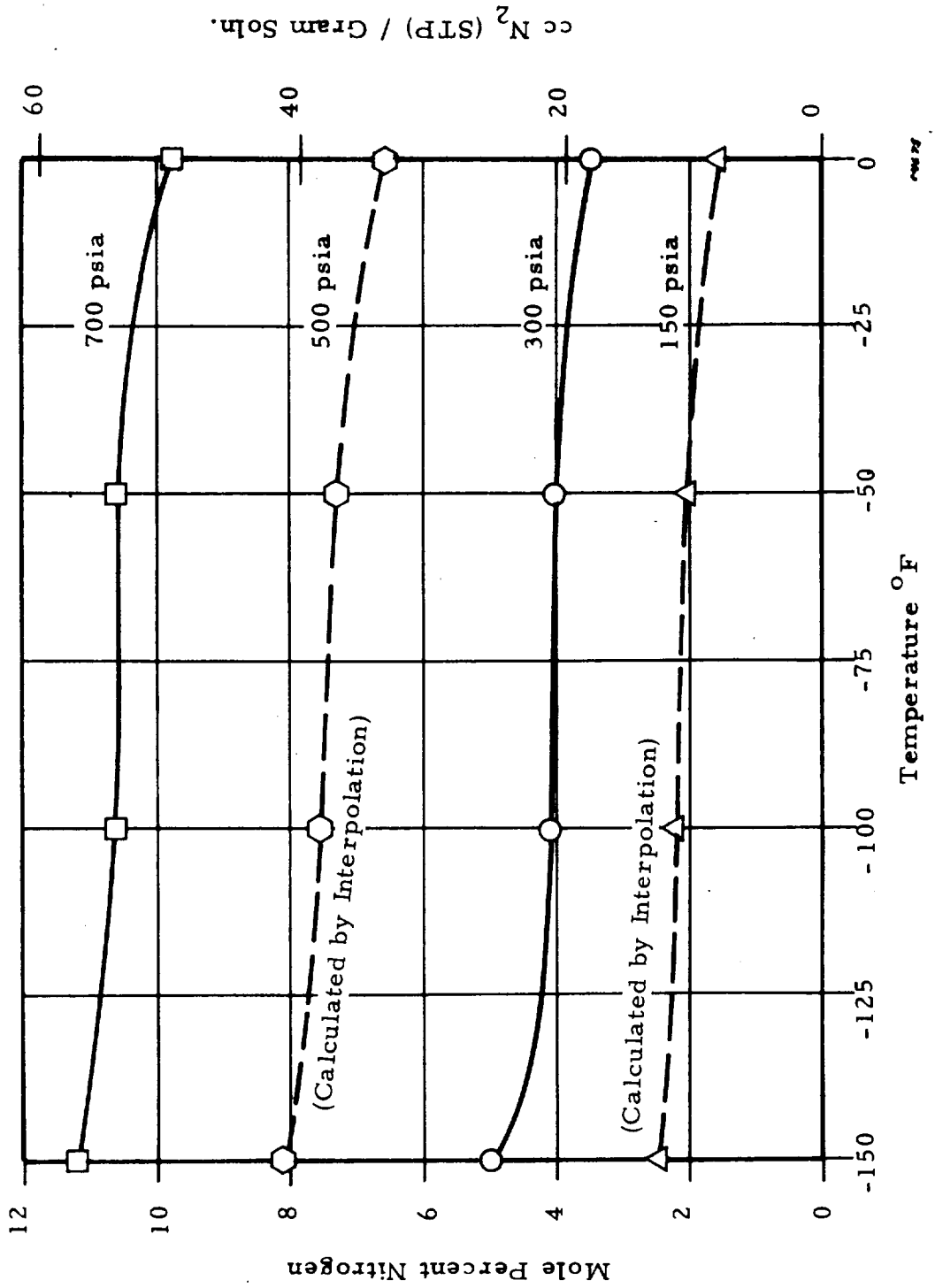

Figure IV-110. Isobaric Temperature-Composition Diagram For The System Liquid Propane-Nitrogen

TABLE IV-29

LIQUID-VAPOR EQUILIBRIUM CONSTANTS FOR THE SYSTEM PROPANE-HYDROGEN

Temp. °F	Total Pressure, psia					
	250	500	1000	2000	4000	8000
+75 KH_2	52.0	26.0	13.2	6.85	3.62	1.825
KC_3H_8	0.592	0.348	0.212	0.149	0.144	0.264
+50 KH_2	60.8	30.4	15.3	7.85	4.15	2.27
KC_3H_8	0.415	0.233	0.144	0.103	0.0977	0.151
0 KH_2	78.4	39.4	19.8	10.1	5.40	3.00
KC_3H_8	0.175	0.0952	0.0621	0.0476	0.0427	0.0629
-50 KH_2	100	51.0	26.0	13.3	6.95	3.95
KC_3H_8	0.0600	0.0336	0.0220	0.0184	0.0180	0.0275
-100 KH_2	123	63.8	32.9	16.9	9.08	5.11
KC_3H_8	0.0180	0.00992	0.00710	0.00590	0.00638	0.0111
-150 KH_2	158	82.0	43.6	22.5	12.1	7.00
KC_3H_8	0.00338	0.00198	0.00133	0.00108	0.00141	0.00324
-200 KH_2	214	114	61.3	33.3	18.6	10.8
-250 KH_2	330	177	96.1	55.5	32.3	19.5
-300 KH_2	664	366	204	120	71.9	45.7

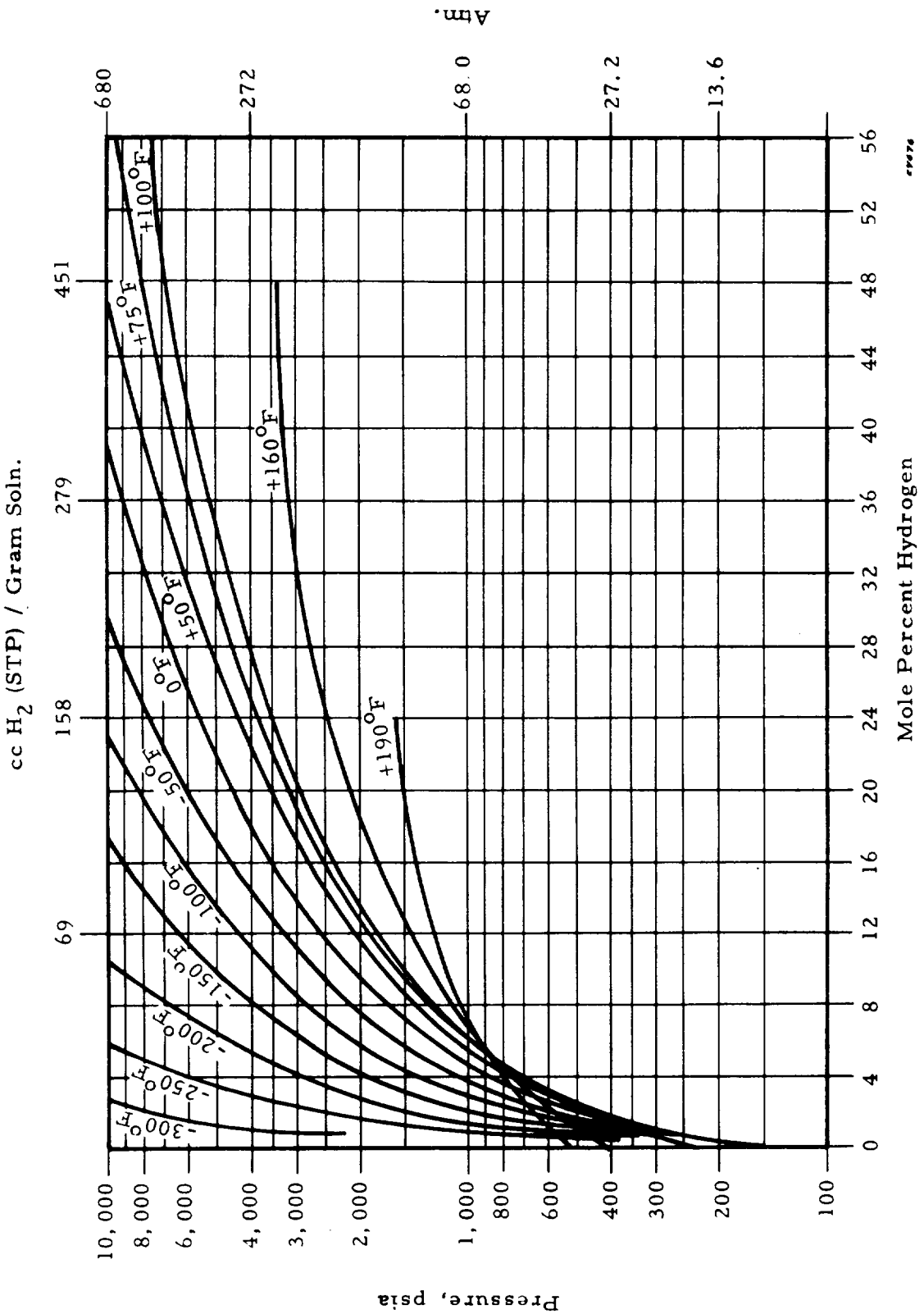

Figure IV-111. Isothermal Pressure-Composition Diagram for the System Liquid Propane-Hydrogen

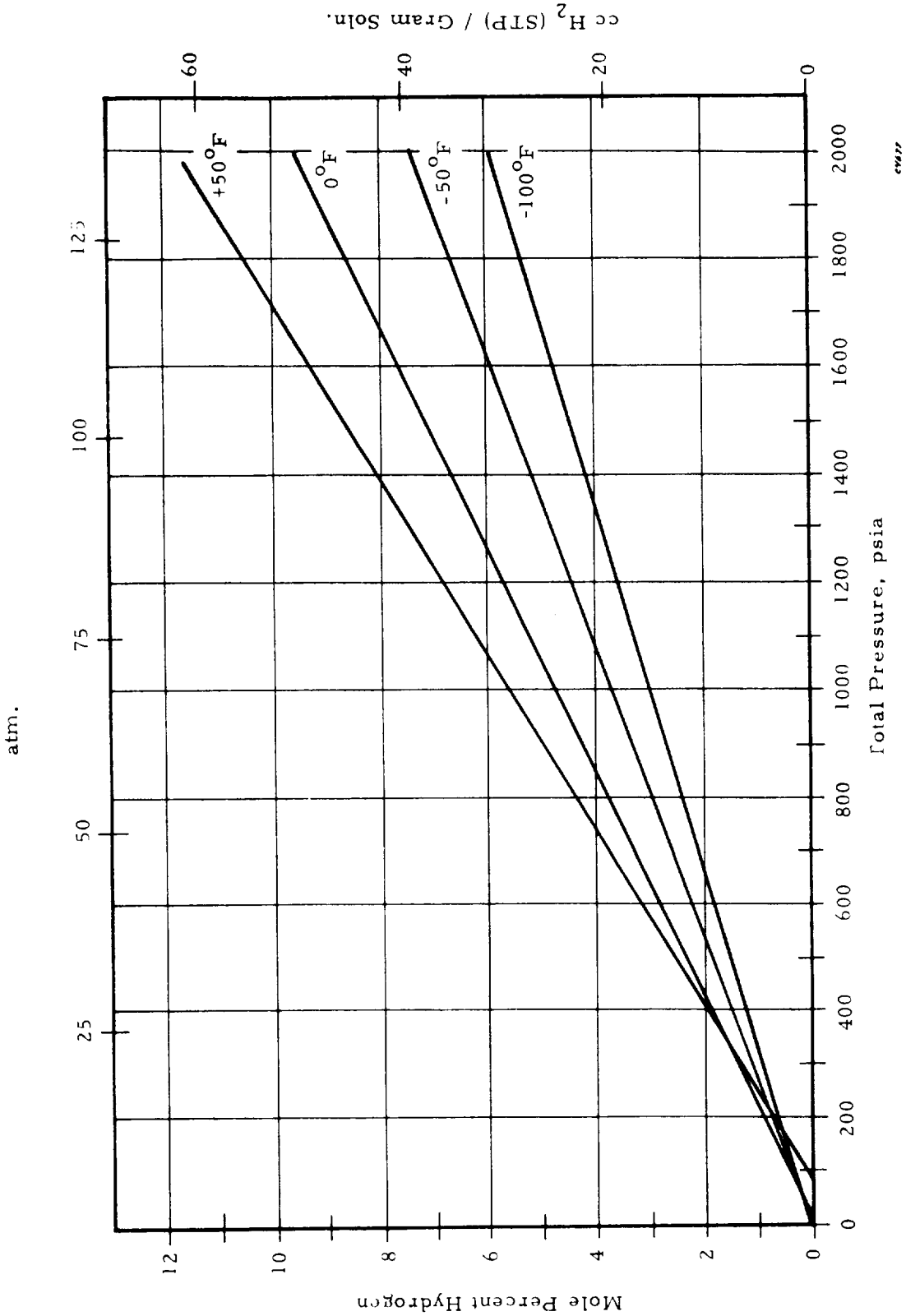

Figure IV-112. Isothermal Pressure-Composition Diagram for the System Liquid Propane-Hydrogen

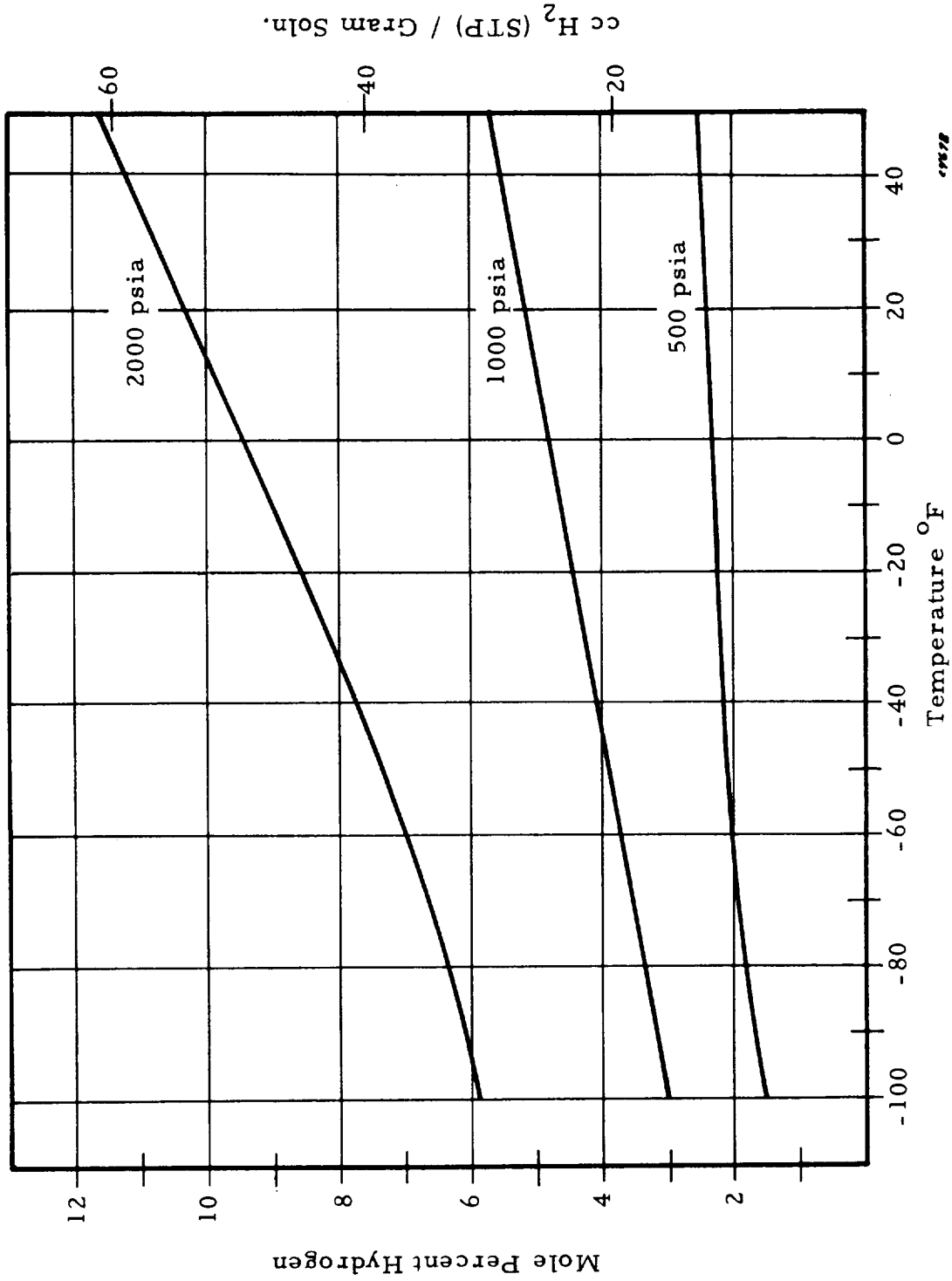

Figure IV-113. Isobaric Temperature – Composition Diagram For the System Liquid Propane-Hydrogen

33. Trimethylborane-Helium

See Section 34.

34. Trimethylborane-Nitrogen

The solubilities of both helium and nitrogen in liquid trimethylborane were measured by Astropower Laboratory for this Design Guide, under Contract NAS7-548. The solubility data for these two systems are tabulated in Table IV-30; experimental details may be found in Reference 46. The results reported in the table are obtained from duplicate analyses for two successive samples; agreement of these values within experimental error was accepted as indication that solution equilibrium had been attained.

TABLE IV-30

SOLUBILITY OF HELIUM AND NITROGEN IN LIQUID TRIMETHYLBORANE

Test Temperature °F	Vapor Pressure of Propellant psia(a)	Mole Percent Concentration			
		Helium		Nitrogen	
		300 psia	700 psia	300 psia	700 psia
-100	1	0.196	0.416	3.98	8.67
-50	3	0.323	0.746	3.68	8.44
0	16	0.467	1.16	3.73	8.23
+50	40	0.689	1.68	3.51	9.06

(a) Reference 86.

These data are presented as isothermal pressure-composition and isobaric temperature-composition plots in Figures IV-114, IV-115, IV-116, and IV-117. Additional isobars at 150 and 500 psia have been constructed for each system by interpolation.

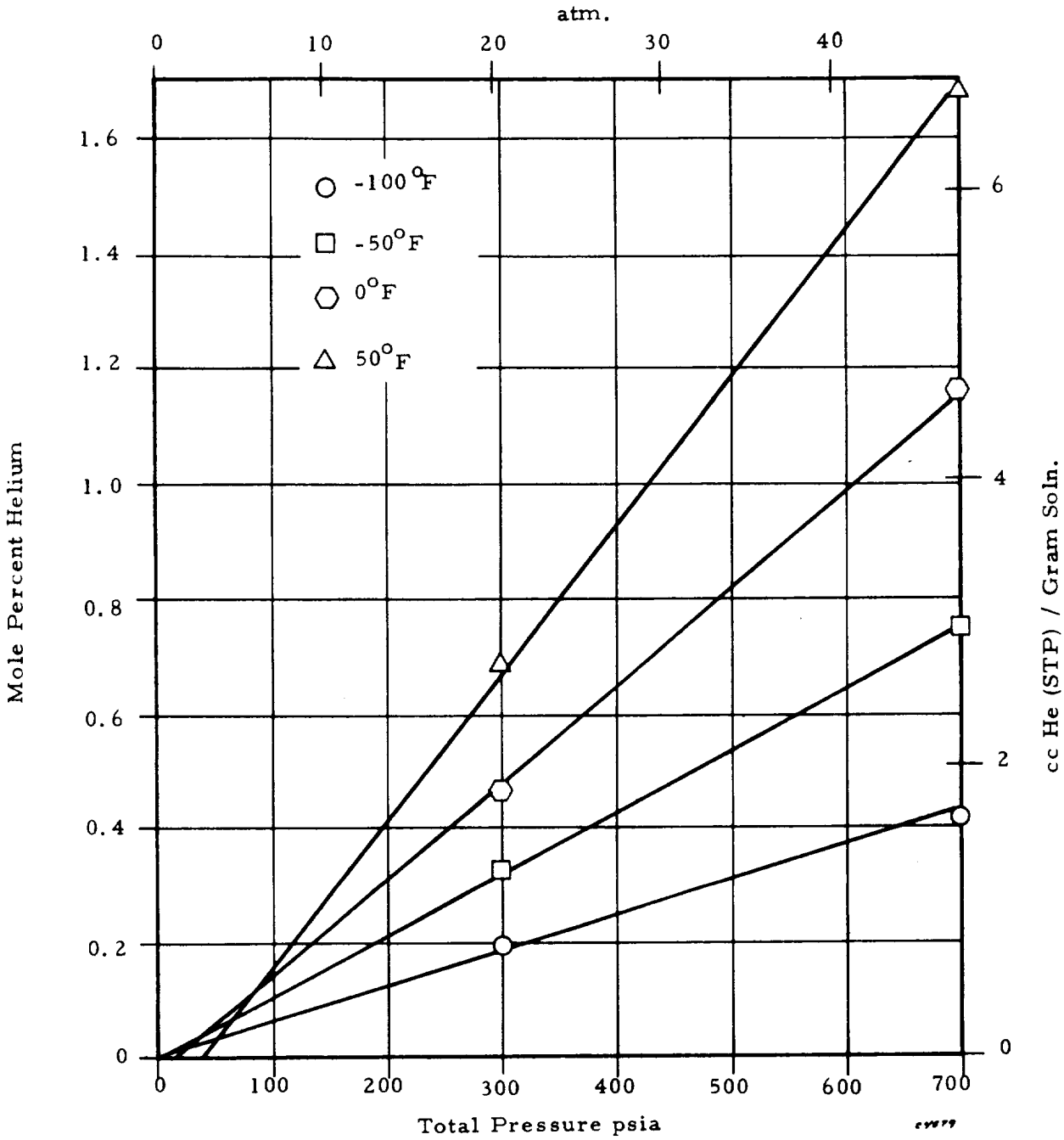

Figure IV-114. Isothermal Pressure-Composition Diagram for the System Liquid Trimethylborane-Helium

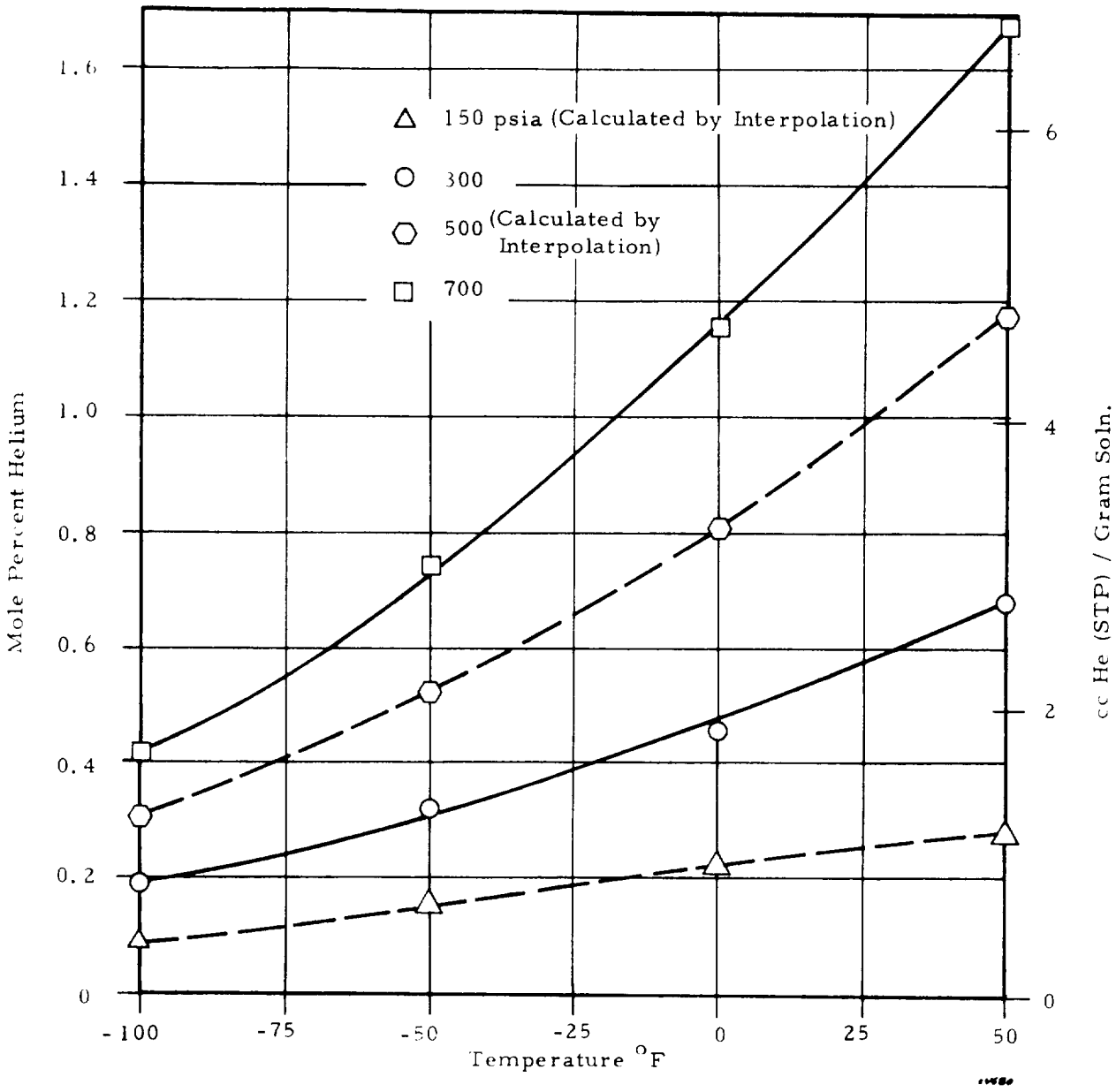

Figure IV-115. Isobaric Temperature-Composition Diagram for the System Liquid Trimethylborane-Helium

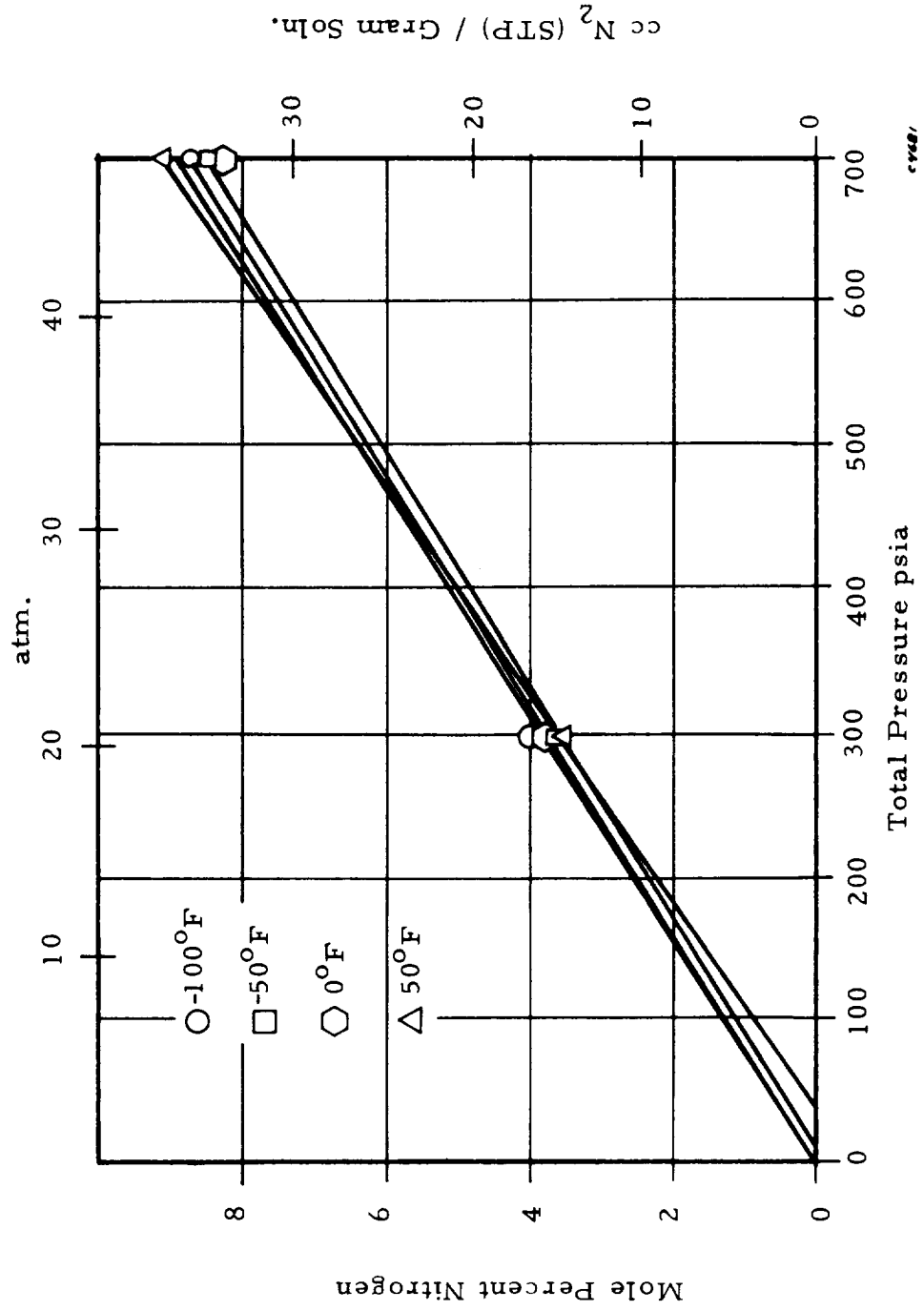

Figure IV-116. Isothermal Pressure-Composition Diagram For The System Liquid Trimethylborane-Nitrogen.

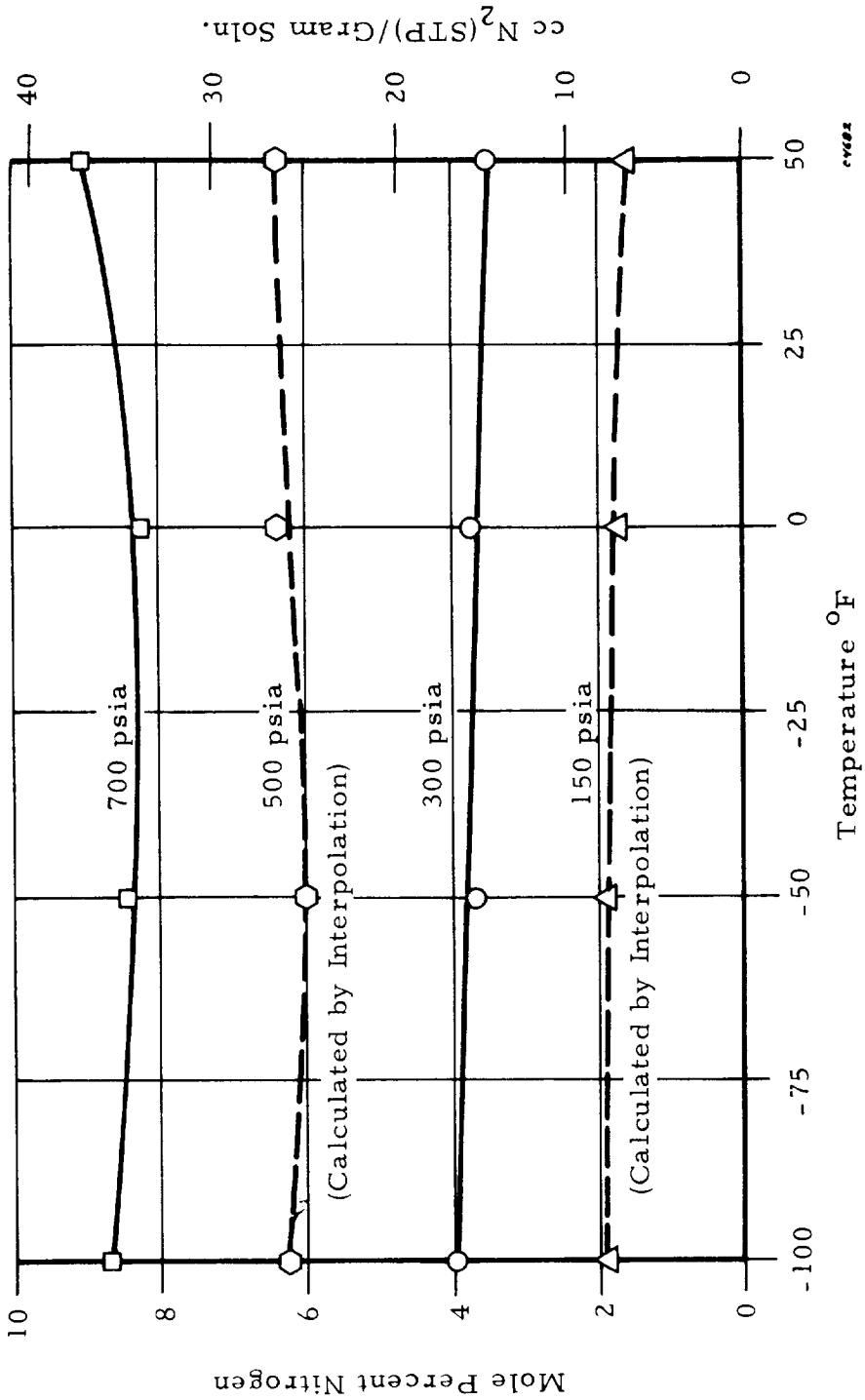

Figure IV-117. Isobaric Temperature – Composition Diagram for the System Liquid Trimethylborane-Nitrogen

35. Unsymmetrical Dimethylhydrazine (UDMH)-Argon

See Section 37.

36. Unsymmetrical Dimethylhydrazine (UDMH)-Helium

See Section 37.

37. Unsymmetrical Dimethylhydrazine (UDMH)-Nitrogen

Solubility data for these three systems have been reported (Reference 71) at pressures of about 15 and 30 psia, and in the temperature range from -4°F to +86°F. The data are summarized in Table IV-31.

TABLE IV-31

SOLUBILITIES OF ARGON, HELIUM, AND NITROGEN IN LIQUID UNSYMMETRICAL DIMETHYLHYDRAZINE

Temp °F	Argon		Helium		Nitrogen	
	$p^{(a)}$ psia	Mole % x 10^3	$p^{(a)}$ psia	Mole % x 10^3	$p^{(a)}$ psia	Mole % x 10^3
-4.0	14.23	62.43	17.22	5.83	18.12	36.64
	28.58	125.2	29.90	10.03	28.95	58.44
32.0	17.03	76.35	20.11	9.19	14.70	32.59
	29.24	131.0	33.08	15.51	19.52	43.48
					30.44	68.08
68.0	14.09	65.84	21.15	12.53	17.03	42.70
	25.97	121.5	32.56	19.81	28.29	71.30

(a) Partial pressure of the pressurant gas in the vapor phase.

(N. B. Pressures are given as partial pressures of the pressurant gas, not total system pressures.)

Additional data for the solubilities of helium and nitrogen in unsymmetrical dimethylhydrazine (UDMH) at moderate pressures are given in Table IV-32. These data are from Reference 87.

TABLE IV-32

SOLUBILITY OF HELIUM AND NITROGEN IN UDMH

Pressurizing Gas	Temperature (°F)	Solubility (wt%)	Final Gas Pressure (psia)
Helium	77.0	0.007 ± 0.005	79.2
	57.1	0.008 ± 0.005	79.9
Nitrogen	81.0	0.0*	76.4
	37.4	0.0*	69.1

*These reported values of zero are believed low; further test data are required.

The systems UDMH-helium and UDMH-nitrogen have been studied at the higher pressure range of 300-700 psia (References 38 and 39). Isobaric solubility plots are shown in Figures IV-118 and IV-119. Isothermal pressure-composition diagrams have been plotted from this data and are presented in Figures IV-120 and IV-121.

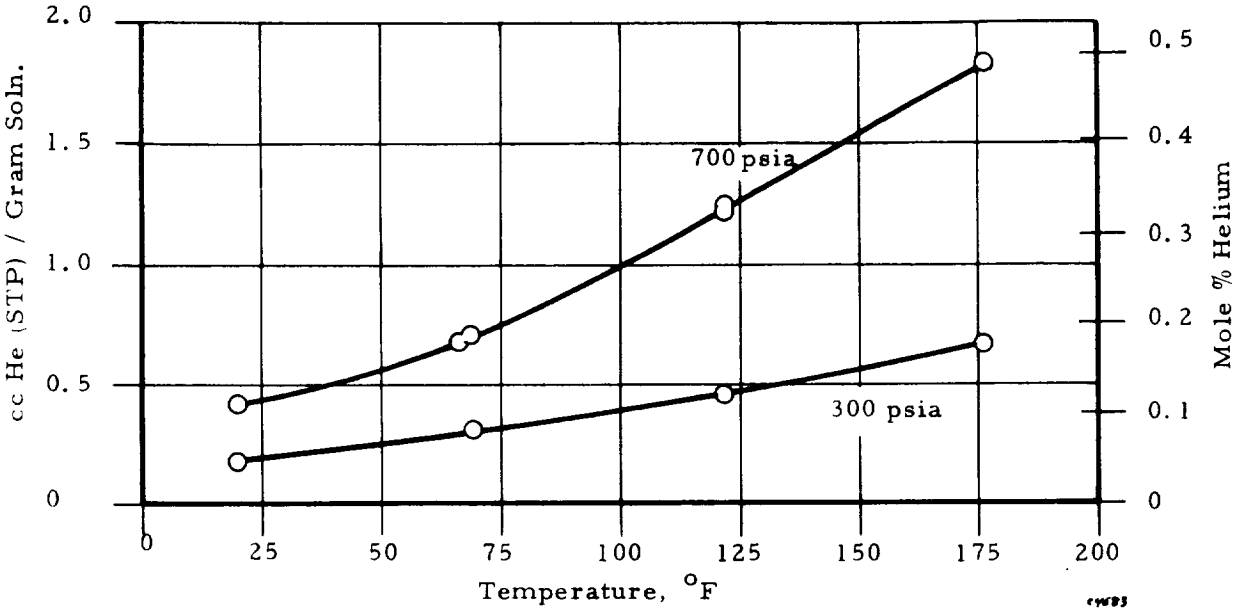

Figure IV-118. Isobaric Temperature-Composition Diagram for the System Liquid UDMH-Helium

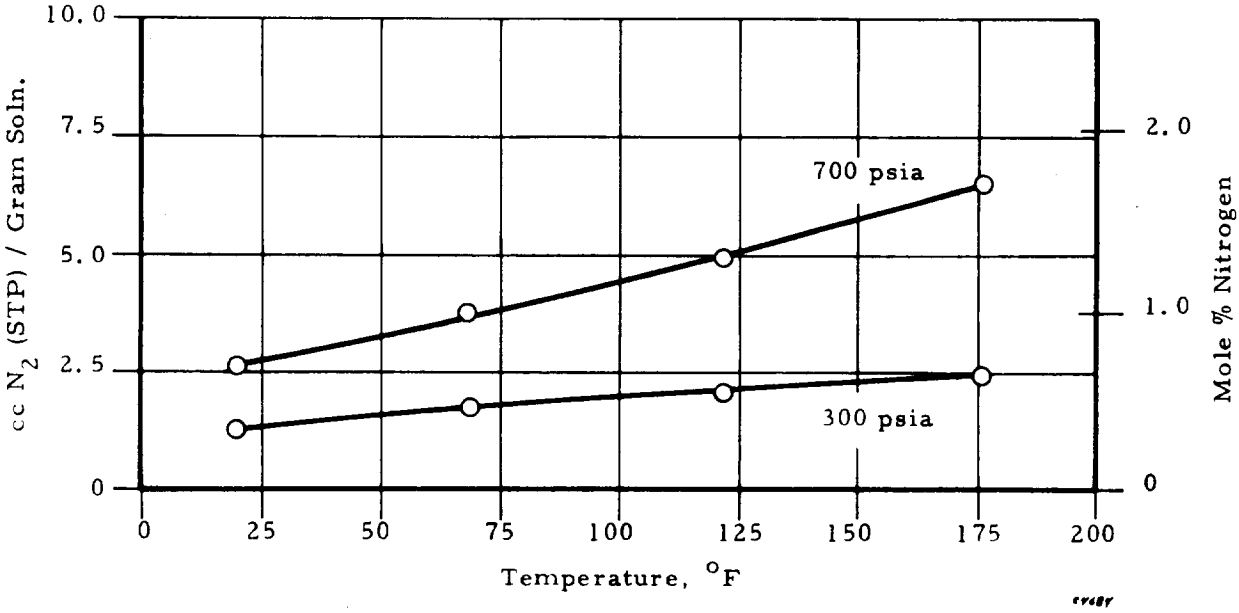

Figure IV-119. Isobaric Temperature-Composition Diagram for the System Liquid UDMH-Nitrogen

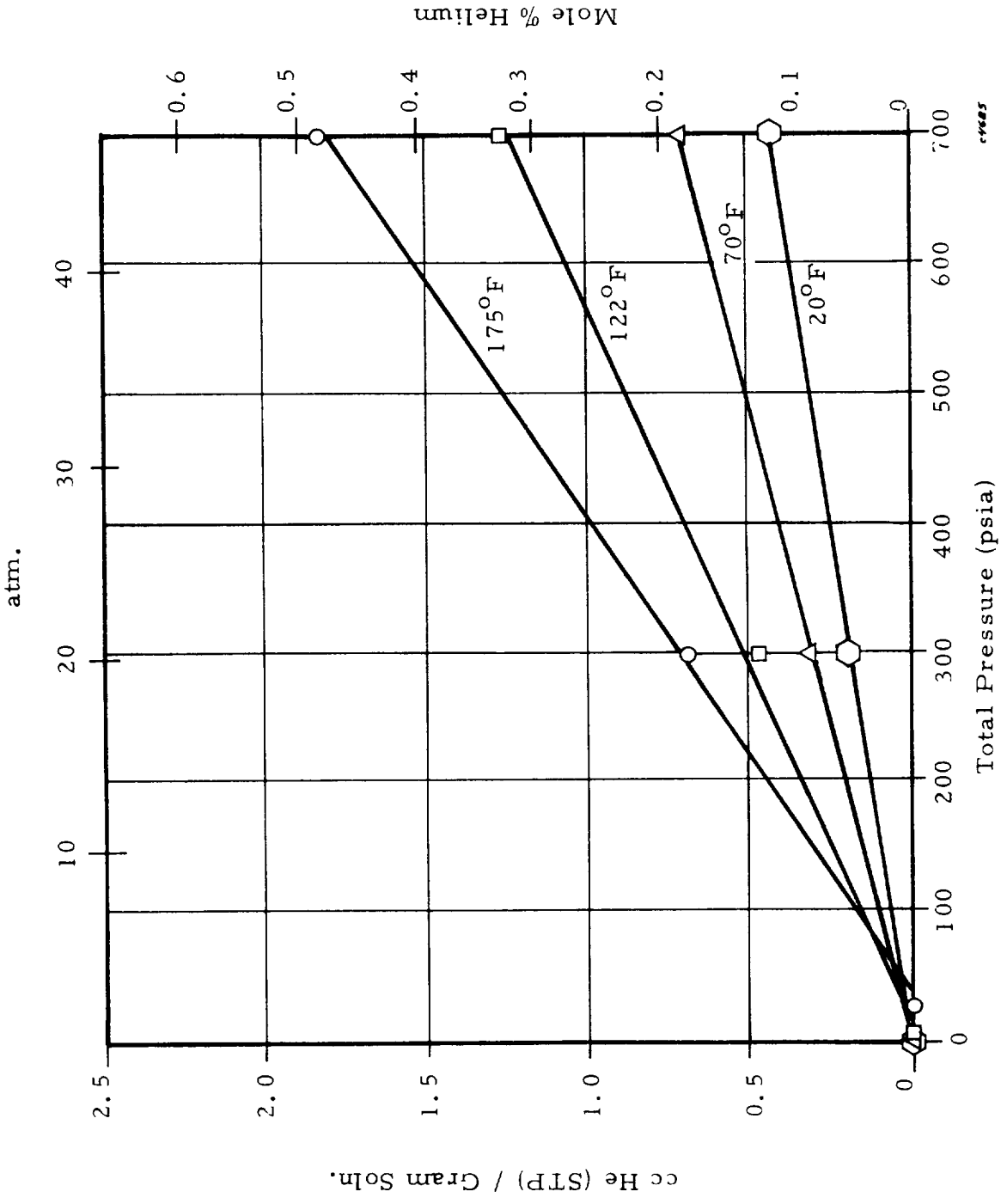

Figure IV-120. Isothermal Pressure-Composition Diagram for the System Liquid UDMH - Helium.

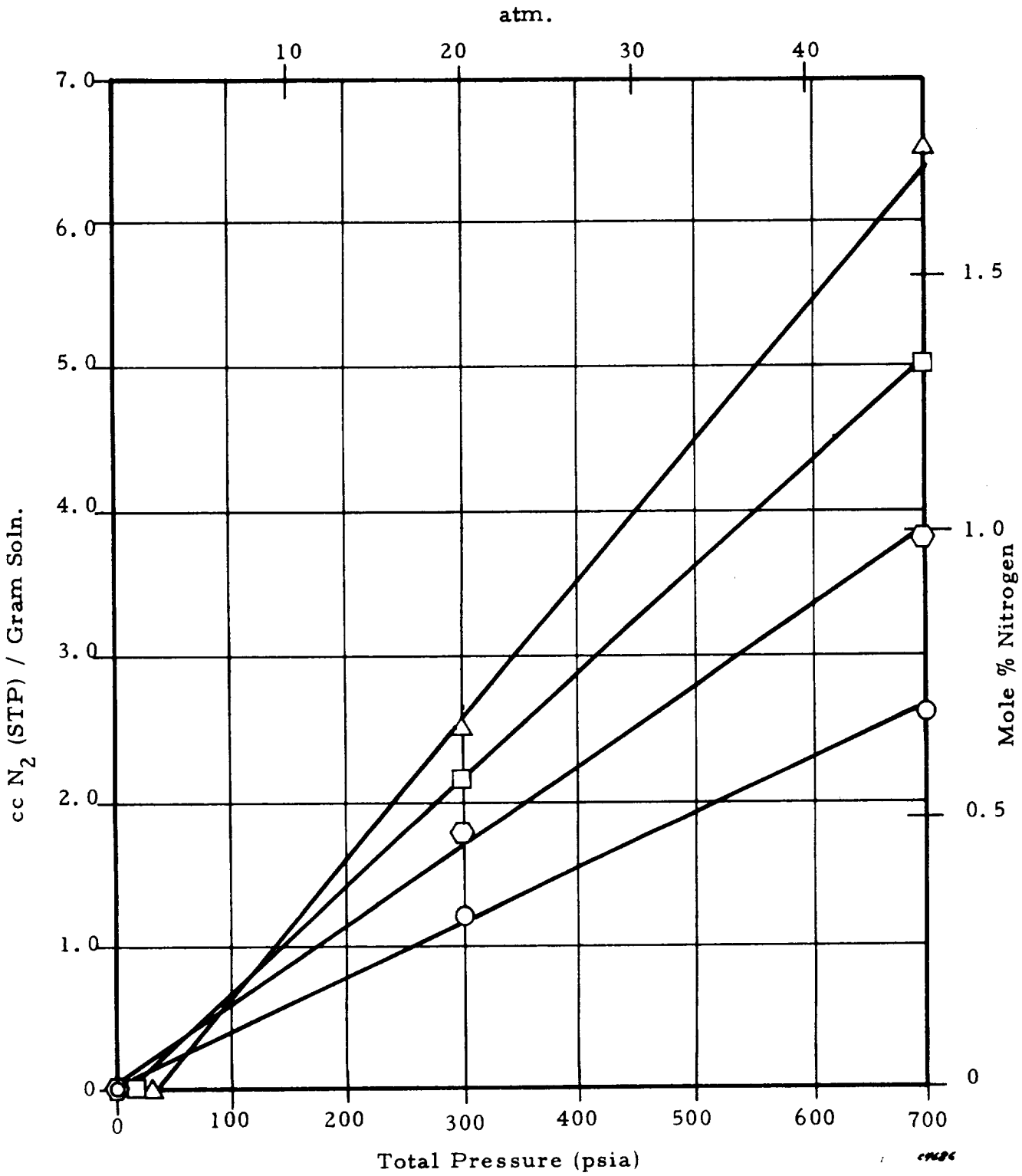

Figure IV-121. Isothermal Pressure - Composition Diagram for the System Liquid UDMH-Nitrogen.

V. REFERENCES

1. B. F. Dodge and A. K. Dunbar, J. Am. Chem. Soc., 49, 591 (1927).

2. S. Greenfield, "Dilution of Cryogenic Liquid Propellants During Pressurized Transfer," Advances in Cryogenic Engineering (K. D. Timmerhaus, Editor), Vol. 3, p. 136, Plenum Press, Inc., N. Y. (1960).

3. D. C. Bowersock, R. W. Gardner, and R. C. Reid, "Pressurized Transfer of Cryogenic Liquids," Advances in Cryogenic Engineering (K. D. Timmerhaus, Editor), Vol. 4, p. 342, Plenum Press, Inc., N. Y. (1960).

4. W. L. Ent, "Investigation of Contamination of Missile Oxygen Due to Nitrogen Pressurization During Loxing," Interim Report, Air Products, Inc. (16 June 1960), Allentown, Pa. (WADD Contract AF 33(616)-6730).

5. R. Battino and H. L. Clever, Chem. Rev. 66, 395-463 (1966).

6. J. H. Hildebrand and R. L. Scott, "The Solubility of Nonelectrolytes," 3rd Edition, Reinhold Publishing Co., N. Y. (1950).

7. S. Glasstone, "Textbook of Physical Chemistry," 2nd Edition, Van Nostrand, N. Y. (1946).

8. C. McKinley, "Phase Equilibria," Cryogenic Technology, Chapter 4, edited by R. W. Vance, John Wiley and Sons, N. Y. (1963).

9. B. S. Kirk, W. T. Ziegler, and J. C. Mullins, "A Comparison of Methods of Predicting Equilibrium Gas Phase Compositions in Pressurized Binary Systems Containing an Essentially Pure Condensed Phase," Advances in Cryogenic Engineering (K. D. Timmerhaus, Editor), Vol. 6, p. 413, Plenum Press, Inc., N. Y. (1961).

10. F. P. Stein, L. C. Claitor, and J. M. Geist, "A Study of the Phase Equilibria of the Hydrogen-Carbon Monoxide-Propane System at Low Temperatures," Advances in Cryogenic Engineering (K. D. Timmerhaus, Editor), Vol. 7, p. 106, Plenum Press, Inc., N. Y. (1962).

11. G. M. Wilson, "Vapor-Liquid Equilibria, Correlation by Means of a Modified Redlich-Kwong Equation of State," Advances in Cryogenic Engineering (K. D. Timmerhauss, Editor), Vol. 9, p. 168, Plenum Press, Inc., N. Y. (1964).

12. W. B. Streett, R. E. Sonntag, and G. J. Van Wylen, J. Chem. Phys., 40, 1390 (1964).

13. R. E. Sonntag, G. J. Van Wylen, and R. W. Cairn, Jr., J. Chem. Phys. 41, 2399 (1964).

14. J. M. Prausnitz and R. D. Gunn, Am. Inst. Chem. Eng. J., 4, 430 (1958).

15. J. M. Prausnitz and A. L. Myers, Am. Inst. Chem. Eng. J., 9, 5 (1963).

16. J. J. M. Beenakker and F. H. Varekamp, "Equation of State of Hydrogen and its Isotopes below 20°K," Bull. Intern. Inst. Refrig., Annexe 1956 -2, 189-194.

17. G. Thomaes and R. Van Steenwinkel, Rev. Sci. Instr., 31, 825 (1960).

18. F. Kurata and P. Kohn, Petrol. Processing, 11, No. 12, 57 (1956).

19. D. White, T. Rubin, P. Camky, and H. L. Johnston, J. Phys. Chem., 64, 1607 (1960).

20. W. H. Mueller, T. W. Leland, Jr., and R. Kobayashi, Am. Inst. Chem. Eng. J., 7, 267 (1961).

21. R. Byrne and G. Thodos, Am. Inst. Chem. Eng. J., 7, 185 (1961).

22. L. C. Nelson and E. F. Obert, Trans. ASME, 76, 1057 (1954).

23. "Absorption Symposium" collection of articles by various authors, Ind. Eng. Chem., 16, 1215-1240 (1924).

24. W. K. Lewis and W. G. Whitman, Ind. Eng. Chem., 16, 1215 (1924). See also W. G. Whitman, Chem. Met. Eng., 29, 146 (1923).

25. H. G. Becker, Ind. Eng. Chem., 16, 1220 (1924).

26. H. S. Davis and G. S. Crandall, J. Am. Chem. Soc., 52, 3757 (1930).

27. W. V. Hanks and W. H. McAdams, Ind. Eng. Chem., 21, 1034 (1929).

28. W. F. Adeny and H. G. Becker, Sci. Proc. Roy, Dublin Soc., 15, 609 (1919).

29. M. M. Calvert, McDonnell Douglas Astronautics Co., Internal Report MP 30, 393, January 30, 1964.

30. J. H. Robson, Astropower Laboratory, McDonnell Douglas Astronautics Co. unpublished data, March 1968.

31. B. Basse, "MMH and N_2O_4 Saturation with Helium," The Marquardt Corp. Test Departmental Procedure No. 7169, March 8, 1968.

32. J. Perman, J. Chem. Soc., 67, 868 (1895).

33. W. G. Whitman and D. S. Davis, Ind. Eng. Chem., 16, 1233 (1924).

34. P. S. Epstein and M. S. Plesset, J. Chem. Phys., 18, 1505 (1950).

35. V. G. Magorien, Hydraulics and Pneumatics, 21, (6), 104 (1968).

36. A. Maimoni, Am. Inst. Chem. Eng. J., 7, 371 (1961).

37. W. W. Akers and L. S. Eubanks, "Vapor-Liquid Equilibria in the System Hydrogen-Nitrogen-Carbon Monoxide," Advances in Cryogenic Engineering (K. D. Timmerhaus, Editor), Vol. 3, p. 275, Plenum Press, Inc., N. Y. (1960).

38. R. L. Beegle, Jr., D. L. Quick and W. J. Flaherty, "Measurement of Helium and Nitrogen Solubility in Nitrogen Tetroxide, Monomethyl-hydrazine and Aerozine-50," Aerojet-General Corp., Appendix to Report LM 0696-03-7, May 2, 1966. See also, succeeding Report No. LM 0696-03-08, June 1966.

39. "Pressurization Systems Design Guide," Aerojet-General Corp., Report 2736, Contract NAS7-169, Second revision, July 1966, Vol. II B, NASA CR-80315, Section VII-D.

40. B. F. Dodge, Chemical Engineering Thermodynamics, McGraw-Hill, N. Y. (1944).

41. W. B. Kay, Ind. Eng. Chem., 30, 459 (1938).

42. J. P. Kuenen, "Theorie der Verdampfung und Verflüssigung von Gemischen, and der Fraktionierte Destillation," J. A. Barth, Leipzig (1906).

43. A. S. Levens, "Nomography," Second Edition, John Wiley and Sons Inc., New York (1959).

44. W. E. De Vaney, B. J. Dalton and J. C. Mecks, Jr., J. Chem. Eng. Data, 8, 473 (1963).

45. F. F. Kharakhorin, Zhur. Lekh. Fiz., 10, 1533 (1940).

46. "Liquid Propellant Gas Absorption Study," Final Technical Report, Contract NAS7-548, McDonnell Douglas Corporation, Report DAC-60510-F2, July 1968.

47. "Liquid Propellant Manual," Chemical Propellant Information Agency, John Hopkins University, Silver Springs, Maryland, January 1963.

48. O. Ruff and H. Krug, Z. anorg. allgem. Chem., 190, 270 (1930).

49. O. Ruff and W. Menzel, Z. anorg. allgem. Chem., 217, 85 (1934).

50. H. W. Schmidt, "Fluorine and Fluorine-Oxygen Mixtures in Rocket Systems," p. 40, NASA SP-3037, Sci. and Tech. Information Division National Aeronautics and Space Administration, Washington, D. C., 1967.

51. Jet Propulsion Laboratory Report No. 37-35, Vol. I, Space Programs Summary, September 30, 1965 (Confidential).

52. E. T. Chang and N. A. Gokcen, J. Phys. Chem., 70, 2394 (1966).

53. Air Force Ballistic Missile Division, "Storable Propellant Data for the Titan II Program," Bell Aerosystems Co., Programs Report, AFBMD TR-61-55, June 1961. See also: "Titan II Storable Propellant Handbook," Revision B, March 1963, AD No. 400748.

54. L. Pierce and E. Pace, J. Chem., Phys., 23, 551 (1955).

55. R. E. Dodd and P. L. Robinson, "Experimental Inorganic Chemistry," p. 241, Elsevier Publishing Co., New York (1954).

56. R. N. Herring and P. L. Barrick, "Gas-Liquid Equilibrium Solubilities for the Helium Oxygen System," International Advances in Cryogenic Engineering (K. D. Timmerhaus, Editor), p. 151, Plenum Press Inc., N. Y. (1965).

57. "Handbook of Chemistry and Physics," 44th ed., p. 2446, The Chemical Rubber Publishing Co., Cleveland, Ohio, 1962.

58. R. B. Stewart and J. S. Johnson, Editors, "A Compendium of the Properties of Materials at Low Temperatures (Phase II), Report 60-56, Part IV, by the National Bureau of Standards, Cryogenic Engineering Laboratory, Boulder, Colorado, for the Aeronautical Systems Division, AFSC, USAF, Wright-Patterson Air Force Base, Ohio, December 1961.

59. G. T. Armstrong, J. M. Goldstein, and D. E. Roberts, J. Res. Nat. Bur. Stand., 55, 265 (1955).

60. M. L. Sagenkahn and H. L. Fink, Pennsylvania State College, OSRD Report 4493 (1944).

61. A. H. Crockett, Proc. Roy. Soc. London, A239, 76 (1957).

62. J. Hilsenrath et. al., National Bureau of Standards, Circ. 564 (1955).

63. R. E. Dodd and P. L. Robinson, "Experimental Inorganic Chemistry," p. 217, Elsevier Publishing Co., New York (1954).

64. A. Kennedy and C. B. Colburn, J. Am. Chem. Soc., 80, 5004 (1958).

65. "Storable Propellant Handbook," Bell Aerosystems Co., AFFTC TR-61-32 (June 1961).

66. B. S. Yaffe, "Diborane, Space Storable Fuel," Callery Chemical Co., Callery, Pennsylvania, 1962.

67. J. H. Hu and G. E. MacWood, J. Phys. Chem., 60, 1483 (1956).

68. "International Critical Tables," 1st ed., Vol. III, p. 217 (1928).

69. R. B. Williams and D. L. Katz, Ind. Eng. Chem., 46, 2512 (1954).

70. "Handbook of Chemistry and Physics," op. cit., p. 2507.

71. E. T. Chang, N. A. Gokcen and T. M. Posten, J. Phys. Chem., 72, 638 (1968).

72. R. E. Sonntag, R. W. Crain, Jr., W. B. Streett and G. J. Van Wylen, "Liquid-Vapor Equilibrium in the System Hydrogen-Helium," Final Report, University of Michigan, Ann Arbor, Accession No. N 64-29214, NASA Contract No. NAS8-5256 (June 1964).

73. C. K. Heck and M. J. Hiza, Am. Inst. Chem. Eng. J., 13, 593 (1967).

74. B. S. Kirk and W. T. Ziegler, "International Advances in Cryogenic Engineering," (K. D. Timmerhaus, Editor), Vol. 10, p. 160, Plenum Press, New York (1965).

75. A. L. Benham and D. L. Katz, Am. Inst. Chem. Eng. J., 3, 33 (1957).

76. A. L. Benham, D. L. Katz, and R. B. Williams, Am. Inst. Chem. Eng. J., 3, 236 (1957).

77. O. T. Bloomer and J. D. Parent, "Methane Nitrogen Phase Equilibria," Gas Technol. Res. Bull., No. 17 (1952).

78. O. T. Bloomer and J. D. Parent, Chem. Engr. Progr. Symposium 49, No. 6, 11-24 (1953).

79. O. T. Bloomer and K. N. Rao, Inst. Gas Technol. Research Bull., No. 18, 1-22 (1952).

80. M. R. Cines, J. T. Roach, R. J. Hogan, and C. H. Roland, Methane Nitrogen Phase Equilibria Program, A. I. Ch. E., Atlantic City, New Jersey (December 24, 1961).

81. M. R. Cines, T. T. Roach, R. J. Hogan, and C. H. Roland, Chem. Engr. Progr. Symposium 49, No. 6, 1-10 (1953).

82. S. P. Vango, Jet Propulsion Laboratory Technical Report, 32-1236, Calif. Inst. Tech., Pasadena, Calif. (April 1968).

83. J. P. Cherenko, "Physical Properties of Liquid Pentaborane," Callery Chemical Co., Callery, Pennsylvania, May 1961.

84. "Handbook of Chemistry and Physics," op. cit., p. 2508.

85. W. L. Burriss, N. T. Hsu, H. H. Reaver, and B. D. Sage, Ind. Eng. Chem., 45, 210 (1953).

86. A. Stock, "Hydrides of Boron and Silicon," Cornell University Press, Ithaca, New York (1933).

87. Bell Aerosystems Report, Table 76, AFFTC TR 60-61, May 19, 1961.

88. Elliot Ring (editor), "Rocket Propellant and Pressurization Systems," Prentice Hall Inc., Englewood Cliffs, New Jersey (1964).

89. "Design Guide for Pressurized Gas Systems," Vol. II, I. I. T. Research Institute, Chicago, Illinois (March 1966).

90. R. A. Guereca et. al., "Thermophysical Properties of Selected Gases Below 300°K," Bureau of Mines, Inf. Circ. IC 8317 (1967).

91. "Handbook of Chemistry and Physics," op. cit., pp. 990 and 2397.

92. Matheson Gas Data Book, 4th ed., Matheson Co. Inc., Herst Litho Inc., New York (1966).